UAB LIBRARIES
The University of Alabama at Birmingham

University of Alabama at Birmingham
UAB Digital Commons

All ETDs from UAB

UAB Theses & Dissertations

2015

Caenorhabditis Elegans Sperm Chemotaxis

Hieu Dinh Hoang
University of Alabama at Birmingham

Follow this and additional works at: https://digitalcommons.library.uab.edu/etd-collection

Recommended Citation

Hoang, Hieu Dinh, "Caenorhabditis Elegans Sperm Chemotaxis" (2015). *All ETDs from UAB*. 1944.
https://digitalcommons.library.uab.edu/etd-collection/1944

This content has been accepted for inclusion by an authorized administrator of the UAB Digital Commons, and is provided as a free open access item. All inquiries regarding this item or the UAB Digital Commons should be directed to the UAB Libraries Office of Scholarly Communication.

CAENORHABDITIS ELEGANS SPERM CHEMOTAXIS

by

HIEU D. HOANG

MICHAEL A. MILLER, CHAIR
BRADLEY K. YODER
CHENBEI CHANG
JIANBO WANG
JIM COLLAWN
KENT KEYSER

A DISSERTATION

Submitted to the graduate faculty of The University of Alabama at Birmingham,
in partial fulfillment of the requirements for the degree of
Doctor of Philosophy

BIRMINGHAM, ALABAMA

2015

CAENORHABDITIS ELEGANS SPERM CHEMOTAXIS

HIEU D. HOANG

GRADUATE PROGRAM IN
CELL MOLECULAR AND DEVELOPMENTAL BIOLOOGY

ABSTRACT

Survival of animal species depends on fertilization, the union of an egg and a sperm. The sperm's ability to find an egg quickly allows it to pass on male genetic material. It is challenging to record sperm targeting or guidance efficiency and motility *in utero*. We use the *Caenorhabditis elegans* model organism to study sperm guidance, primarily because its epidermis is transparent, allowing the observation of live fluorescent sperm in the hermaphrodite uterus. Using genome-editing techniques, genetic analyses, fluorescent microscopy, and mass spectrometry, we aim to address the following two questions: how hermaphrodites regulate sperm motility in the uterus, and how males respond to hermaphrodite cues.

Chapter one gives a general introduction about fertilization, factors affecting fertilization, and sperm motility. Next, background on sperm guidance in externally and internally fertilizing species is given. Given the difficulty of observing sperm *in utero* in mammals, *Caenorhabditis elegans* provides a powerful model system to study sperm guidance. Recent findings suggest that prostaglandin-like lipids derived from *C. elegans* oocytes may be sperm chemoattractants. An introduction to prostaglandins, their diverse roles, their synthesis, and receptors is provided. Then background is presented on the

potential impact of environment on fertility and sperm guidance. Finally, the *C. elegans* sensory nervous system, which is used to sense environmental cues, is discussed.

In chapter two, we use genetics, liquid chromatography, and electrospray ionization tandem mass spectrometry (LC-MS/MS) to investigate prostaglandin metabolism in *C. elegans* hermaphrodites. Our results show that *C. elegans* oocytes or their precursors produce more than ten structurally related F-series prostaglandins (PGFs), which function redundantly to promote sperm targeting. PGFs are derived from omega-3 and omega-6 polyunsaturated fatty acids (PUFAs). Specifically, PGF1 stereoisomers are derived from dihomo-gamma-linolenic acid (DGLA), PGF2 stereoisomers are derived from arachidonic acid (AA) and omega-3-arachidonic acid (O3AA), and PGF3 stereoisomers are derived from eicosapentaenoic (EPA) acid. Genetic ablation of omega-3 PUFA synthesis causes a compensatory increase in production of PGFs derived from omega-6 PUFAs. *C. elegans* PGF synthesis occurs independent of cyclooxygenase (COX) enzymes, which initiate PGF synthesis in mammals. COX-independent PGFs containing different stereochemical configurations than PGF2α are found in mouse tissues. Finally, we identify an evolutionarily conserved cytochrome P450 enzyme that negatively regulates PGF synthesis.

In chapter three, we use genome-editing and transgenic techniques, fluorescence microscopy, quantitative RT-PCR, and RNAseq to investigate the role of a G-protein coupled receptor (GPCR) subfamily in sperm guidance. We show that at least three candidate chemoreceptor GPCRs called SRB-13, SRB-16, and SRB-5 are essential in males to promote efficient sperm guidance. These SRB subfamily chemoreceptors act in at least two parallel pathways. The GOA-1 $G\alpha_{i/o}$ protein appears to be a common downstream component required for sperm guidance. *srb* mutant sperm are activated and

motile, but do not efficiently target the fertilization site and thus, appear of poor quality. Surprisingly, SRB chemoreceptors are not expressed in sperm. Instead, they (e.g. SRB-13 and SRB-16) are expressed in male head neurons, including amphid sensory neurons that perceive environmental cues. SRB-13 is specifically expressed in the cilia of ASI and ASK amphid sensory neurons, whereas SRB-16 is expressed in cell bodies and dendrites of ASH, ASI, ASK, and AWB amphid sensory neurons. SRB-16 is also expressed in I1 pharyngeal interneurons, pm4 and pm5 pharyngeal muscles, and other unidentified male neurons. Expressing *srb-16* in neurons rescues the *srb-16* null mutant sperm guidance defect. Similarly, expressing *srb-13* in sensory neurons rescues the *srb-13* null mutant defect. RNAseq studies suggest that SRB-13 and SRB-16 regulate spermatogenic gene transcription, possibly by modulating a neuroendocrine pathway(s). Together, these data support the unexpected model that male SRB chemoreceptors couple environmental information to sperm quality.

Chapter four ends the thesis by discussing additional published and unpublished data, as well as discussing remaining outstanding questions. Experimental evidence is provided that COX knockout mice synthesize PGFs. These data were published in a collaborative study with Dr. Katherine McKnight. Unpublished data document efforts to identify enzymes essential for PGF synthesis. The thesis ends with a model for the mechanisms controlling sperm guidance (a.k.a. chemotaxis) and concluding remarks on the power of the *C. elegans* model for generating endless exciting questions.

DEDICATION

To my parents, Bieu D. Hoang and Thao T. Phan, who gave life to me and cared for me all my life; my wife, Anh N. Do, who care for me until the day I die and I her; my daughter, ThaoVi D. Hoang, who will hopefully become another researcher, but not a professional singer; and my other relatives in California, who helped me set foot on U.S. soil, fed me, housed me, medicated me when I was sick, and gave me opportunities for a better education and brighter future. I am especially thankful to my aunts Huyen Phan, My Phan, Mo Ba, my uncles Hoa Nguyen, Dieu Phan, and my cousins Van Phan, Chuong Nguyen, Hanh Ngo, Linh Nguyen, Tran Phan, Cuong Phan, Loan Chieu, Phuong Phan, Tri Nguyen. Next, I want to especially thank my mentor, Michael A. Miller, and other lab members, Sung Min Han, Pauline Cottee, Wes Edmonds, Jessica Schultz, Tim Cole, Sejin Lee, Youfeng Young, who have given me the most nurturing learning environment, wonderful advice, and been my most supportive friends.

ACKNOWLEDGEMENTS

I want to thank my mentor, Dr. Michael A. Miller for his brilliant guidance and kind encouragements. Whenever my experiments failed repeatedly, I sought counsel from Michael, who always gave me relief with an alternative hypothesis, alternative strategy, or sometimes with gentle encouragement to tackle the problems again. Michael's expertise in experimental design and writing is superb. I regret that I did not attempt to learn as much as possible early on. I also thank Michael for bringing many games to lab to make the working environment much more fun. The fun from the games must have ligated my SRB-like GPCRs in my sensory neurons, which triggered a neuroendocrine mechanism to affect transcription of metabolic genes that allow me to work more efficiently. I am sure that this mechanism is conserved between *C. elegans* males and me.

Other lab members have also been very kind to me all the way. I learned a lot of my molecular techniques from Dr. Sung Min Han, Dr. Pauline Cottee, Dr. Sejin Lee, and Dr. YouFeng Yang. Dr. Sung Min Han is still teaching me new techniques from his lab at Yale. Sung Min is also a very smart and kind scientist. His comments helped improve my first and last chapters of this thesis. Dr. Jonathan Wes Edmonds taught me a lot about lipid extraction in worms. Dr. Jeevan Prasain and Ray Moore from UAB TMPL mass spectrometry have taught me a lot about mass spectrometry, so that I can understand and analyze my data. Dixon Dorand and Wes taught me how to perform the sperm guidance assays. I am also very grateful to Nan Travis, the CMDB coordinator, who helped me

with all the paper work every step of the way. I am also grateful to the CDIB departmental staff, who have been kind and supportive to me.

I am very thankful to Drs. Yoder, Collawn, Chang, Wang, and Keyser, who were very supportive and helpful during my training. They have also given much good advice, helping me focus and work towards my goals.

I am also grateful of my previous undergraduate professors, who introduced Biology to me and encouraged me to ask many questions. I typically asked 15-20 questions per class meeting. I thank Professor Elisabeth Stauble and Professor Jack Baker. They are both very inspiring and kind educators, who enjoyed my sometimes annoying curiosity. I am very glad that I took Biology courses with them at Evergreen Valley Community College, CA. Otherwise, I may have become a Math teacher and missed all the fun of biological research.

I am also very grateful to my wife Anh N. Do, who is also a wonderful mom. She has double-shifted in taking care of our baby ThaoVi so that I could spend more time preparing this thesis. She is a wonderful person and I don't know what I would do without her.

TABLE OF CONTENTS

LIST OF TABLES

Table Page

A HETEROGENEOUS MIXTURE OF F-SERIES PROSTAGLANDINS PROMOTES SPERM GUIDANCE IN THE *CAENORHABDITIS ELEGANS* REPRODUCTIVE TRACT

A GPCR CIRCUIT IN MALE SENSORY NEURONS MODULATES SPERM PERCEPTION OF THE OVIDUCT

DISCUSSION

LIST OF FIGURES

Figure Page

INTRODUCTION

A HETEROGENEOUS MIXTURE OF F-SERIES PROSTAGLANDINS PROMOTES SPERM GUIDANCE IN THE CAENORHABDITIS ELEGANS REPRODUCTIVE TRACT

A GPCR CIRCUIT IN MALE SENSORY NEURONS MODULATES SPERM PERCEPTION OF THE OVIDUCT

DISCUSSION

LIST OF ABBREVIATIONS

AA	Arachidonic acid
ASH	Amphid single ciliated neuron H
ASI	Amphid single ciliated neuron I
ASK	Amphid single ciliated neuron K
AWB	Amphid winged ciliated neuron B
cAMP	Cyclic adenosine monophosphate
COX	Cyclooxygenase
CYP	Cytochrome P450
DGLA	Dihomo gamma linolenic acid
EPA	Eicosapentaenoic
GPCR	G-protein coupled receptor
IFT	Intraflagellar transport
LC-MS/MS	Liquid chromatography and tandem mass spectrometry
MRM	Multiple reaction monitoring
O3AA	Omega-3-Arachidonic acid
PG	Prostaglandin
PGD	D-series prostaglandin
PGE	E-series prostaglandin
PGF	F-series prostaglandin
PGG	G-series prostaglandin
PGH	H-series prostaglandin
PUFA	Polyunsaturated fatty acid
SRB	Serpentine receptor B

CHAPTER 1

INTRODUCTION

The evolution of multicellularity is among the early natural inventions that bestowed organisms with a competitive advantage. It allowed organisms to have more complex and specialized body plans. Notably, it allowed organisms to become much larger than single-celled rivals, tipping the balance of predator and prey (Campbell and Reece, 2005). On the other hand, cells from a multicellular organism need to function together, harmoniously and synchronously. Therefore, cell-cell communication is of major importance (Niklas and Newman, 2013). Abnormal communication, as seen in autoimmune diseases, often leads to reduced survival (Gurke et al., 2008; Harizi et al., 2008; Zamaria, 2004). The union of sperm and egg cells during fertilization is crucial to the evolutionary success of animal species. An important type of intercellular communication occurs between eggs and sperm. These mechanisms are thought to help motile sperm find immotile oocytes, thereby increasing fertilization frequency. This thesis will focus on sperm and egg communication mechanisms important for modulating sperm motility.

Sperm Motility and Its Importance in Fertilization

Fertilization is the union of an egg and a sperm. Much of what is known about sperm comes from studies in mammalian species. Mammalian sperm have a single flagellum composed of a connecting piece, a mid-piece, a principal piece, and an end piece (Fawcett, 1975). The connecting piece is the junction between the flagellum and the sperm head from where the remnant of the centriole extends to form a dynein and microtubule-based axoneme that runs the full length of the flagellum. In the mid-piece, the axoneme is surrounded by nine outer dense fibers and enclosed by a sheath of mitochondria. In the principal piece, the axoneme is surrounded by two columns of fibrous sheaths and seven outer dense fibers. In the end piece, the axoneme is surrounded only by plasma membrane. In this system, the axoneme is the motor that drives motility while the dense fibers and fibrous sheaths provide structural support, and the mitochondria sheath provide the necessary fuel to run the motor (Clermont et al., 1990; Fawcett, 1975; Turner, 2006).

Mammalian sperm are capable of two modes of motility: activated motility and hyperactivated motility. Activated motility, which occurs early in the journey toward the oocytes, is characterized by symmetrical beating with low amplitude, which allows sperm to move through regions of the reproductive tract with low viscosity. Hyperactivated motility occurs later and is characterized by asymmetrical beating with high amplitude which allows sperm to move through the oviductal region containing high viscosity and penetrate the zona pellucida (Turner, 2006).

C. elegans sperm are not flagellated. Round non-motile spermatids are activated inside the hermaphrodite uterus and become motile by extending a single pseudopod (Figure 2) (L'Hernault, 2006; Smith, 2006). *C. elegans* sperm are almost devoid of an actin

cytoskeleton. Instead, major sperm protein (MSP) polymerization is required for pseudopod formation and function (Nelson et al., 1982). The *C. elegans* genome contains at least 28 transcribed *msp* genes, which function redundantly to promote sperm motility (Smith, 2006). ATP supplied from mitochondria is required for assembly of MSP fibers that are responsible for propelling the membrane at the leading edge of the pseudopod forward (Miao et al., 2003; Smith, 2006). Tyrosine phosphatase activity indirectly promotes MSP disassembly, driving membrane retraction at the trailing edge (Smith, 2006). An intracellular pH gradient in the pseudopod is thought to drive MSP filament assembly and disassembly (Italiano et al., 1999).

Sperm motility is important for fertilization. Average sperm velocity in ejaculates is a predictor of fertilization success in a variety of species including Atlantic salmon, chicken, red deer, mallard, and human (Birkhead et al., 1999; Denk et al., 2005; Donnelly et al., 1998; Donoghue, 1999; Gage et al., 2004; Malo et al., 2005). In humans, higher *in vitro* sperm motility values correlate with shorter time to pregnancy (Buck-Louis et al., 2014a). On the other end of the spectrum, failure to complete capacitation and motility hyperactivation results in male infertility in bulls and humans (Kirichok et al., 2006; Lessard et al., 2011; Lishko et al., 2011; Munire et al., 2004; Shukla et al., 2012).

Sperm motility is also important for fertilization in *C. elegans*. Hermaphrodite-derived sperm are constantly displaced by oocytes that enter the spermatheca, the site of fertilization. They depend on their motility to constantly craw back to the spermatheca (Ward and Carrel, 1979). Male-derived sperm enter the hermaphrodite uterus through the vulva. Motility is required for sperm to travel across many fertilized embryos slowly move in the opposite direction (Figures 1-2) (Smith, 2006). Male-derived sperm use their larger size and superior motility to displace hermaphrodite-derived sperm from the spermatheca.

Therefore, offspring from hermaphrodites mated to males are primarily male sperm-derived (LaMunyon and Ward, 1998; Ward and Carrel, 1979).

Sperm Guidance in Externally Fertilizing Species

Much of our knowledge on how motile sperm find oocytes comes from studies in externally fertilizing marine species (Guerrero et al., 2010; Kaupp et al., 2008). Red abalone (*Haliotis rufescens*) oocytes release amino acid L-tryptophan to attract sperm, whereas mollusk (*Sepia officinalis*), sea urchin (*Arbacia punctulata*), and starfish (*Asterias amurensis*) oocytes release small peptides called sepsap, resact, or asterosap, respectively, to attract species-specific sperm (Bohmer et al., 2005; Himes et al., 2011; Kaupp et al., 2003; Nishigaki et al., 1996; Riffell et al., 2002; Ward et al., 1985; Zatylny et al., 2002). Sea squirt (*Ciona intestinalis* and *Ciona savignyi*) oocytes utilize a sulfated steroid as a sperm guiding signal (Yoshida et al., 2002). The guidance cues are essential to fertilization as oocytes of those species are only fertile for a short time (Garbers et al., 1986; Riffell et al., 2002; Ward et al., 1985).

On the sperm end, resact binds to its sea urchin sperm receptor, a guanylyl cyclase, to increase sperm intracellular concentration of cyclic guanosine monophosphate (cGMP) and stimulate sperm metabolism and motility (Bentley et al., 1986; Garbers et al., 1986; Ramarao and Garbers, 1985; Shimomura et al., 1986). Similarly, asterosap induce a fast and transient increase in cGMP and a subsequence increase in calcium concentration in starfish sperm to modulate sperm motility (Matsumoto et al., 2003). However, it is not clear how the sperm of red abalone, mollusk, and sea squirt sense the egg-derived chemoattractants.

In the African-clawed frog (*Xenopus laevis*), oocytes release a 21-kDa cysteine-rich protein called allurin to attract sperm (Olson et al., 2001; Xiang et al., 2004; Xiang et al., 2005). Allurin binds to the mid-piece of sperm, where mitochondria are concentrated, and stimulates sperm motility in an external calcium-dependent manner (Burnett et al., 2011; Tholl et al., 2011). However, it is not clear how sperm sense allurin and react to it at the molecular level.

Sperm Guidance in Internally Fertilizing Species

Much less is known about sperm motility in internally fertilizing species. It has been postulated that mammalian sperm respond to chemotactic cues within the oviduct. However, no *bona fide* mammalian sperm chemoattractant has been identified. *In vitro* assays suggest that a component(s) in human follicular fluid attracts sperm (Ralt et al., 1991; Ralt et al., 1994; Villanueva-Diaz et al., 1990). Despite decades of efforts, the identity(s) of human sperm chemoattractant(s) is still not clear. Sperm chemoattraction is much less understood in mammals because of the technical difficulty of recording sperm motility *in utero*, and the importance of capacitation and hyperactivation in the reproductive tract (Cohen-Dayag et al., 1995; Jaiswal and Eisenbach, 2002). This limitation makes it hard to investigate sperm guidance mechanism(s) in mammals.

Caenorhabditis elegans as a Model System to Study Sperm Chemoattraction

C. elegans has been developed as an animal model to study sperm guidance *in utero.* The transparent epidermis allows imaging vitally stained sperm, as they crawl across

fertilized embryos in live hermaphrodites (Figure 1) (Edmonds et al., 2011; Edmonds et al., 2010; Kubagawa et al., 2006; McKnight et al., 2014). This feature, together with a wealth of available genetic and molecular techniques, gives *C. elegans* compelling advantages to discover mechanisms that regulate sperm motility within the oviduct (Riddle et al., 1997).

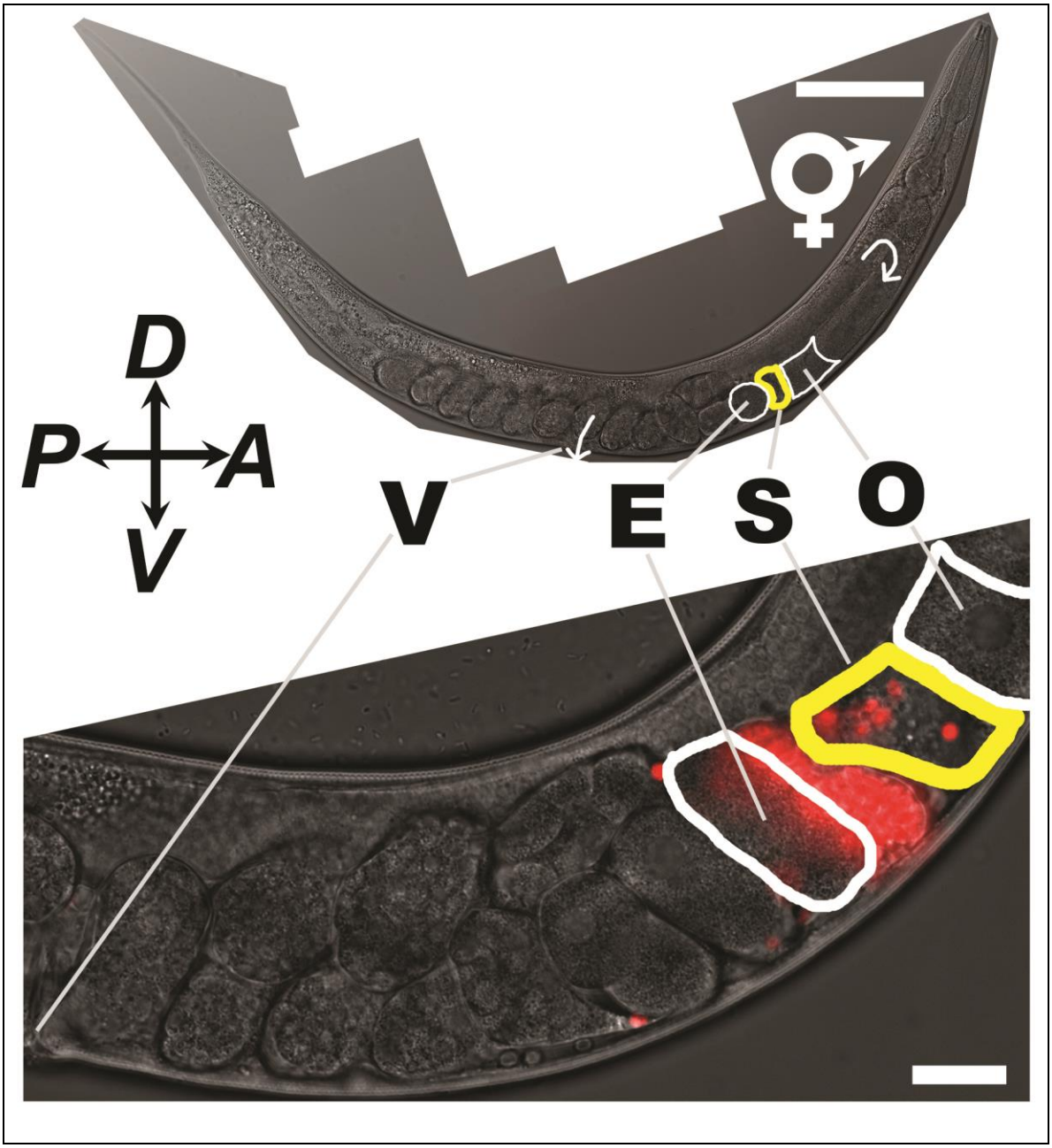

Figure 1. Live sperm imaging *in utero* of wild-type adult *C. elegans* hermaphrodite

The x-axis is Anterior (*A*) – Posterior (*P*) axis. The y-axis is Dorsal (*D*) – Ventral (*V*) axis. V, vulva – the site of sperm entry and embryo exit from the uterus. E, newly fertilized embryo. S, spermatheca – the site of fertilization and sperm storage. O, mature oocyte. The upper Differential Interference Contrast (DIC) image of a whole mount of wild-type (N2) worm. The lower image is of the merged image of DIC channel and TRITC channel of 1 uterus arm of a wild-type (N2) hermaphrodite mated to a CMXROS mitotracker-stained (Invitrogen) wild-type males (*fog-2(q71)*). Red dots represent individual live sperm in a live hermaphrodite gonad. Upper arrow indicates the flow of developing oocytes. Lower arrow indicates a late stage embryo exiting the uterus through the vulva. Upper scale bar, 100 um. Lower scale bar, 20 um.

C. elegans is a hermaphroditic species with rare, but important occurrence of males (Brenner, 1974; Cutter et al., 2009; Cutter and Payseur, 2003; Stewart and Phillips, 2002). The genome of *C. elegans* hermaphrodites includes 5 pairs of autosomes and a pair of X chromosomes. The male counterpart has 5 pairs of autosomes and only 1 X chromosome (Kelly et al., 2002; Miller et al., 1988). XO male progeny can be generated from XX hermaphrodites by rare chromosomal non-disjunction events (Miller et al., 1988) Alternatively, male mating increases the incidence of XO males, as male sperm displace hermaphrodite sperm from the spermatheca due to their larger size and probably better motility (LaMunyon and Ward, 1998; Ward and Carrel, 1979).

The presence of males in the population is important because male mating is the only natural means of genetic outcrossing (Anderson et al., 2010; Ward and Carrel, 1979). Male mating can help slow homozygosity and reduce the negative impact of inbreeding,

which can help the organism better survive a changing environment (Anderson et al., 2010; Cutter and Payseur, 2003; Stewart and Phillips, 2002).

Males make and store non-motile round spermatids in the seminal vesicle (Figure 7) (L'Hernault, 2006). During mating, males transfer their spermatids and seminal fluid into the uterus of hermaphrodites (L'Hernault and Roberts, 1995). Spermatids are quickly activated and break radial symmetry by extending a single pseudopod (Figure 2) (L'Hernault and Roberts, 1995; Smith, 2006). Polymerization and depolymerization of various Major Sperm Proteins (MSPs) drive pseudopod formation and motility (Italiano et al., 1999; Nelson et al., 1982; Roberts and King, 1991; Roberts and Ward, 1982; Sepsenwol et al., 1989). Activated male sperm uses the pseudopod to crawl over newly fertilized embryos toward the spermatheca, where they wait to fertilize ovulating eggs (Figure 1) (Smith, 2006).

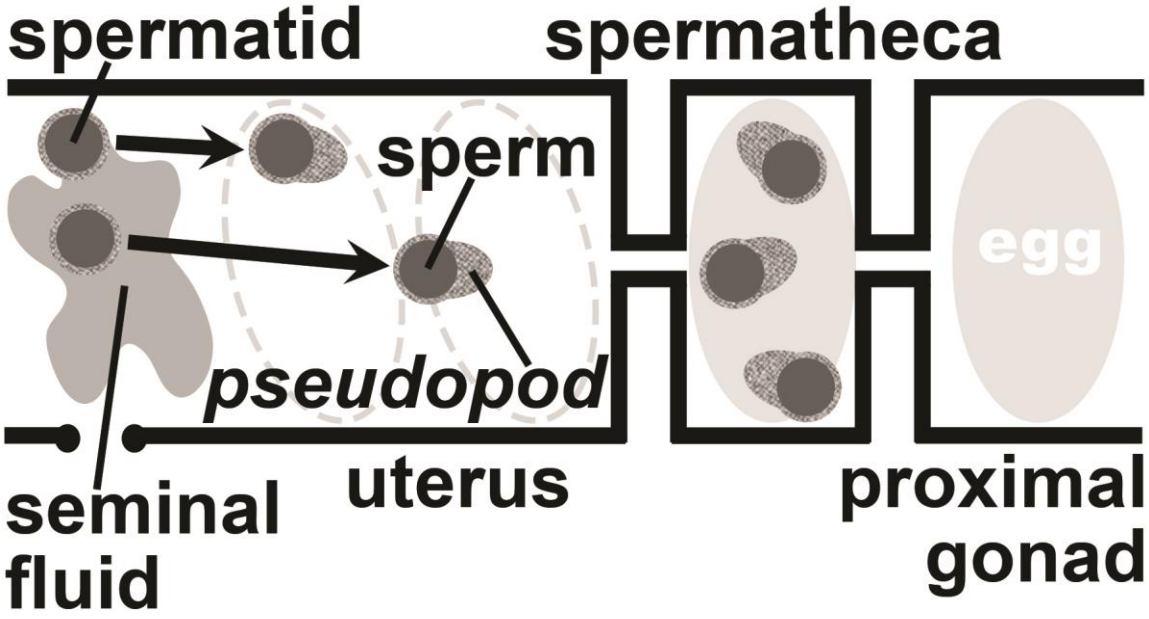

Figure 2. Illustration of *C. elegans* male sperm activation *in utero*

During mating, spermatids and seminal fluid are injected into a hermaphrodite uterus through an opening in the middle of the uterus called vulva. An unknown factor(s), likely a protease, in seminal fluid help activate spermatids. Activated sperm extend a single pseudopod and become motile. Maturing oocytes ovulate into the spermatheca. Activated sperm crawl to the right to unite with the maturing oocytes within the spermatheca. Fertilized eggs are pushed into the uterus, outlined with broken gray lines, and eventually out through the vulva.

Oocyte-Derived Sperm Chemoattractant(s)

Our laboratory previously showed that *C. elegans* oocytes convert 18 or 20-carbon poly unsaturated fatty acid(s) (PUFAs) into prostaglandin-like molecules resembling PGF2α (Edmonds et al., 2010; Kubagawa et al., 2006). PUFA synthesis and transport into oocytes are required for sperm guidance (Edmonds et al., 2010; Kubagawa et al., 2006). Synthetic PGFs (e.g. PGF2α) promote sperm motility (Edmonds et al., 2010). However, the PUFA metabolic pathways and prostaglandin products that promote sperm guidance *in vivo* are not well understood.

Prostaglandins and Their Roles in Mammals

Prostaglandins (PGs) are oxygenated derivatives of 20-carbon PUFAs including arachidonic acid (AA) and eicosapentaenoic acid EPA (Figure 3) (Funk, 2001; Rowley et al., 2005). Examples of structures of PUFAs and F-series prostaglandins are shown in Figures 3 and 4, respectively.

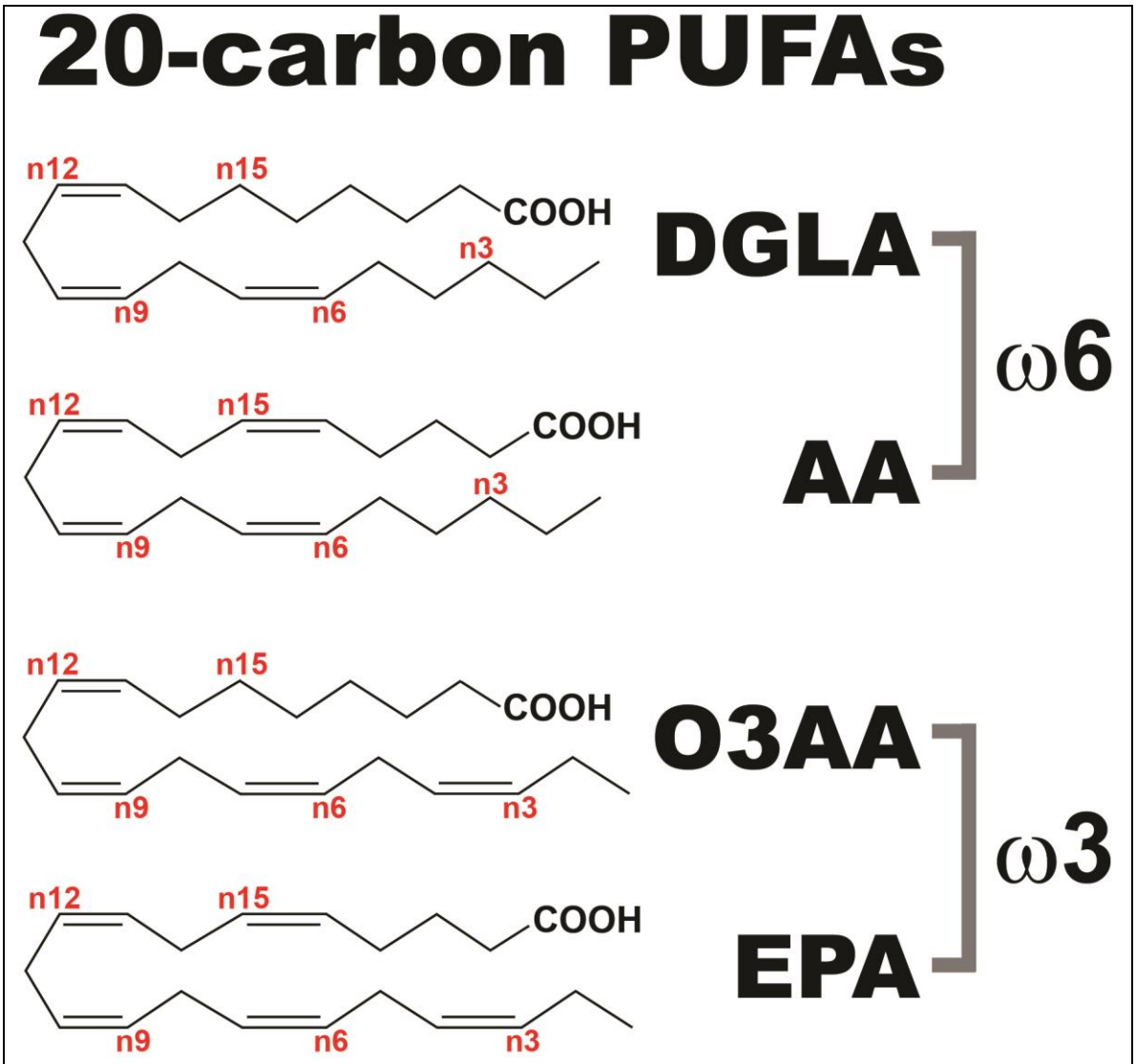

Figure 3. Structures of selected ω3 and ω6 twenty-carbon PUFAs

The red numbers label the carbon position from the non-carboxylated (or omega) end. For example, n3 labels the 3rd carbon from the omega end and n6 labels the 6th carbon from the omega end. ω3 and ω6 PUFAs have their first double bonds in between the 3rd and 4th or

the 6th and 7th carbons, respectively. PUFA, polyunsaturated fatty acid; AA, arachidonic acid; DGLA, Dihomo gamma linolenic acid; O3AA, omega-3-arachidonic acid; EPA, Eicosapentaenoic.

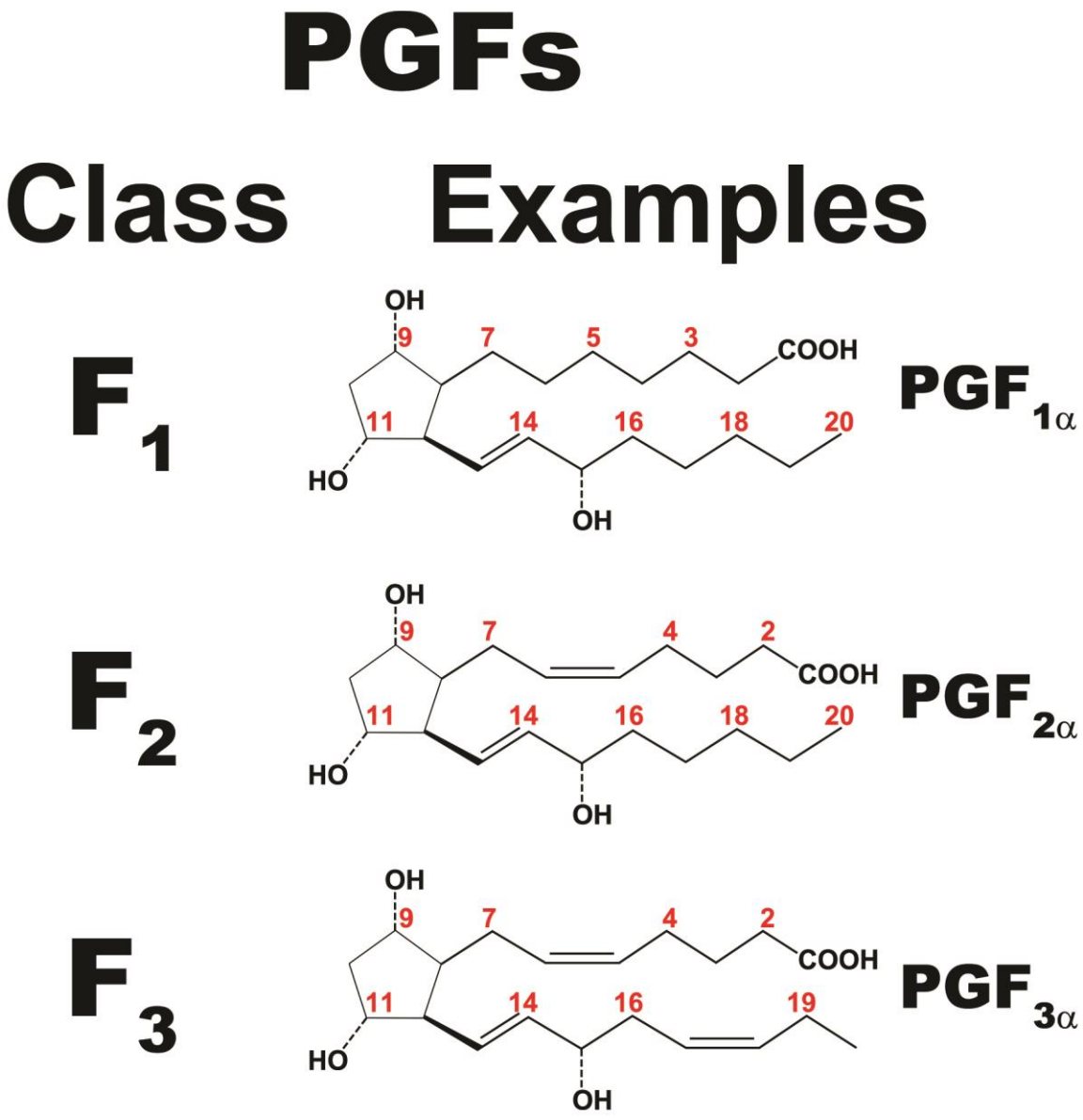

Figure 4. PGF classification and structures

Prostaglandins F_1, F_2, and F_3 classes differ by the numbered of double bonds in the side chains. PGF_1 class has the least and PGF_3 has the most. The red numbers indicate the

carbon positions on the hydrocarbon chain that a chemical group is on. e.g. the 3 hydroxyl groups are at carbon 9, 11, and 15.

In mammals, prostaglandins are important locally acting hormones that play many roles in development and physiology (Rowley et al., 2005). PGD2 and E2 regulate sleep-wake cycle, and PGE2 influences thermoregulation of the central nervous system (Dubois et al., 1998; Hayaishi, 2000). PGI2 causes vascular smooth muscle cells to dilate and therefore, indirectly affects thermoregulation and kidney function. PGF2α causes uterine smooth muscle cells to contract during parturition (Funk, 2001). PGE2 acts in neurons to promote pain sensation and may play a role in oocyte maturation and ovulation (Barbera-Cremades et al., 2012; Harvey et al., 2004; Marei et al., 2014).

PGs also play roles in inflammation and diseases. PGD2 activates lung epithelial cells to induce allergic asthma and lung inflammation (Claar et al., 2015; Han et al., 2010). PGI2 promotes platelet declumping, while PGD2 regulates trafficking of Th2 and memory T lymphocytes (Ahmed et al., 2011; Moncada and Vane, 1979; Xue et al., 2014). PGE2 activates osteoclasts to favor bone reabsorption, and promotes colorectal cancer cell growth (Han et al., 2010; Shibata-Nozaki et al., 2011; Zhang et al., 2015). These studies highlight a subset of known roles for PGs in mammals.

Mammalian Prostaglandin Synthesis

In mammals, PGs are synthesized from free AA. Most AA in cells is bound to phospholipids or triglycerides. Phospholipase A2 enzymes liberate AA from phospholipids. The first and also rate-limiting step in PG synthesis is catalyzed by

cyclooxygenase enzymes (COX). Mammals have two COX homologs in the genome, *Cox-1* and *Cox-2* (Funk, 2001; Rowley et al., 2005; Simmons et al., 2004). AA is committed to enter the pathway when COX-1 and COX-2 cyclize linear AA to form a cyclic endoperoxide-containing intermediate called PGG2 (Hamberg et al., 1974). COX then converts a hydroperoxyl group in PGG2 to a hydroxyl group to form PGH2 (Smith and Lands, 1972). PGH2 is rapidly converted into PGE2, PGD2, PGI2, and PGF2α by different isomerases and oxidoreductases (Simmons et al., 2004). PGI2 is unstable and quickly converted into 6-keto PGF1α, a stable metabolite (Figure 5) (Funk, 2001). COX enzymes are found in mammals and more primitive animals such as corals, but not in nematodes, arthropods, and many other invertebrates (Koljak et al., 2001; Rowley et al., 2005; Tootle and Spradling, 2008).

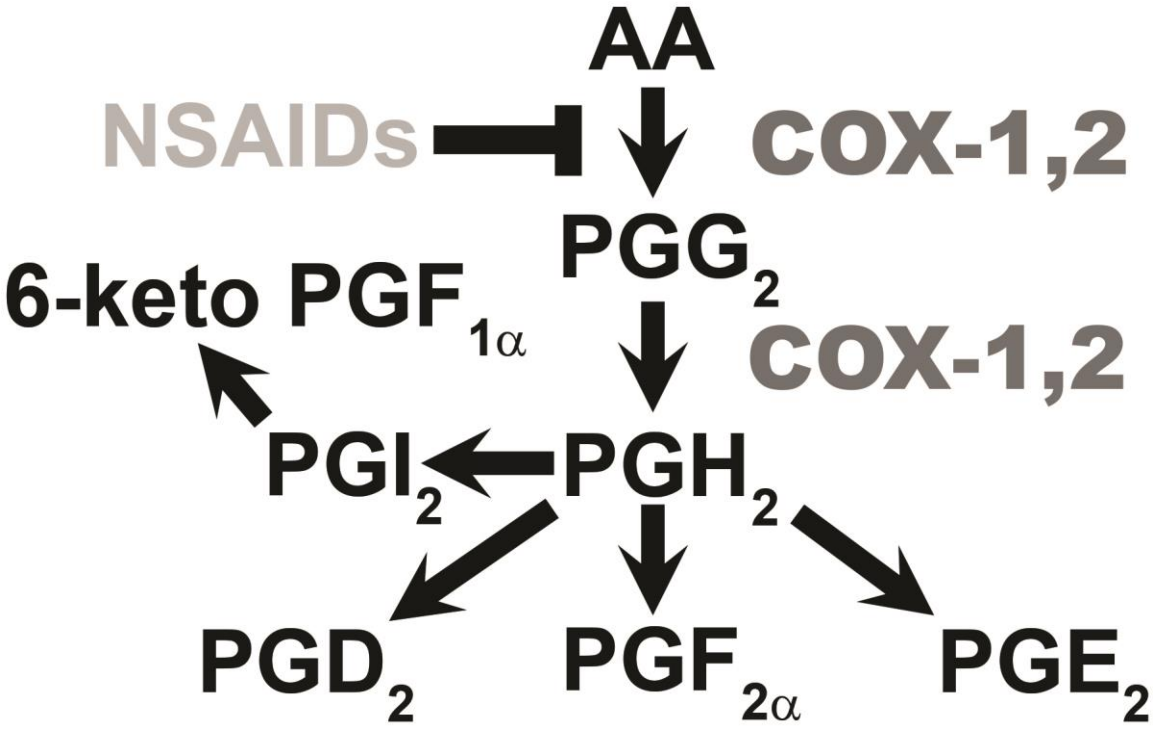

Figure 5. Cyclooxygenase-dependent prostaglandin synthesis pathway in mammals

AA, arachidonic acid; NSAIDs, nonsteroidal anti-inflammatory drugs; COX, cyclooxygenase. Conversion of PGH_2 to other PGs require different enzymes. 6-keto PGF1 is a stable metabolite of PGI_2.

Prostaglandin Receptors in Mammals

Based on previous mammalian studies, PGF receptors in mouse, rat, cow, and human belong to the G-protein coupled receptor (GPCR) class of molecules (Abramovitz et al., 1994; Kiriyama et al., 1997; Kitanaka et al., 1994; Sakamoto et al., 1994; Sugimoto et al., 1994). Most of the GPCR receptors are at the plasma membrane, although some localize to the nuclear envelope (Bhattacharya et al., 1999; Bhattacharya et al., 1998). In human and mouse, PGD2 has two receptors, DP1 and DP2. PGE2 has four receptors, EP1, EP2, EP3, and EP4. PGF2α and PGI2 each have one receptor, FP and IP, respectively (Funk, 2001). PGs can activate their GPCR receptors at nanomolar concentrations. Once activated, IP, DP1, EP2, and EP4 receptors signal through $G\alpha_s$ to increase intracellular cyclic AMP (cAMP). Activated EP_3 acts through $G\alpha_i$ to decrease intracellular cAMP. Activated EP1and FP signal via $G\alpha_q$ to increase intracellular calcium (Funk, 2001). Thus, PGs act through different GPCRs to signal distinct downstream G protein effectors.

PG receptors can also be nuclear receptors. PPARγ nuclear receptors have been shown to bind 15-deoxy-delta-12,14-PGJ_2, a dehydration product of PGD_2 (Kliewer et al., 1995; Yu et al., 1995). PGI_2 can also bind PPARδ, though such ligation requires micromolar concentrations of the PG ligands (Gupta et al., 2000).

Environmental and Fertilization

Human activities in recent centuries have threatened biodiversity with assertions of a sixth mass extinction (Barnosky et al., 2011; Ceballos and Ehrlich, 2002; Hughes et al., 1997; Pereira et al., 2010; Pimm et al., 1995; Wake and Vredenburg, 2008; Young et al., 2014). Human activities change species habitats. Mankind competes with animals for resources, breaking up their habitats into increasingly smaller areas, releasing adverse chemicals (e.g. endocrine-disrupting contaminants), and altering global climate. Together, these changes appear to render many animals unfit for survival (Barnosky et al., 2011; Dirzo and Raven, 2003; Hoffmann et al., 2010; Vredenburg et al., 2010). However, the mechanisms by which environment impacts species survival are not well understood. In particular, there are few established links between environmental conditions and fertilization.

In humans, at least 80 million couples world-wide suffered from infertility (Ombelet and Campo, 2007). In the United States alone, 6.7 million women have impaired fecundity, and 7.4 millions have used infertility services costing the economy billions of dollars in direct cost and an enormous loss of work time due to treatment procedures (Martine et al., 2013). Moreover, the rate of pregnancy for U.S. women continues to drop (Curtin et al., 2013). In developing countries, infertility can result in severe psychological, cultural, and economic disadvantages (Asemota and Klatsky, 2015). Environmental conditions have been proposed to disturb reproductive processes. For example, endocrine-disrupting contaminants have been implicated in negatively affecting female infertility

(Mittendorf and Herbst, 1994). However, more studies are needed to assess the environmental impact on fertility and the underlying mechanisms.

Men exposed to phthalate have a 20% reduction in fecundity, which is thought to be mediated by oxidative stress (Buck-Louis et al., 2014b; Guo et al., 2014). Phthalate is an additive to plastics or vinyl to increase flexibility. It is commonly present in hundreds of consumer products (Guo et al., 2014). Polychlorinated biphenyls, a common compound in pesticides, is found to reduce human sperm motility (Hauser, 2006). Components of cigarette smoke also decrease sperm motility (Kunzle et al., 2003; Zenzes et al., 1999). However, whether toxic compounds in the environment are responsible for a significant number of infertility cases is controversial. Importantly, the underlining molecular mechanisms that effect male fertility are not known.

Recent studies in *C. elegans* hermaphrodites document a clear mechanistic link between environment and sperm function (McKnight et al., 2014). Environmental cues such as pheromones and bacterial-derived molecules provide hermaphrodites with information on future resource availability (Bargmann, 2006; Schackwitz et al., 1996). These cues act on GPCRs in ASI or ASK sensory neurons (Ludewig and Schroeder, 2013). When conditions are favorable for reproduction, ASI neurons secrete a TGF-β ligand called DAF-7 (Inoue and Thomas, 2000a, b). DAF-7 functions as a neuroendocrine factor that stimulates PGF synthesis in the ovary, thereby increasing sperm velocity and providing sperm with positional information (McKnight et al., 2014). In unfavorable conditions, DAF-7 transcription is repressed, impairing sperm motility and fertilization efficiency (McKnight et al., 2014). Thus, environmental perception by hermaphrodite roundworms plays a critical role in reproductive success.

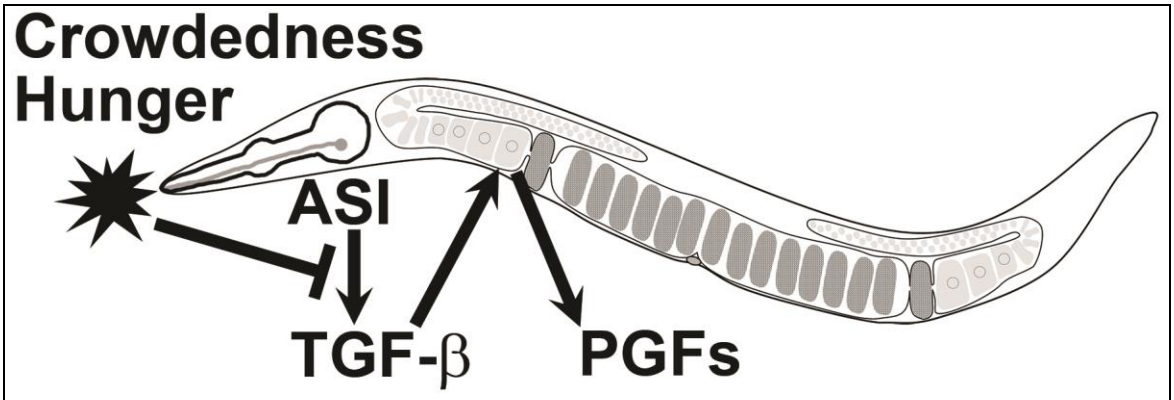

Figure 6. Model of environmental control of hermaphrodite fertility based on McKnight et al., 2014

Under normal well-fed conditions, hermaphrodite ASI sensory neurons release TFG-β (DAF-7) to act on interneurons and oocyte precursors to promote production of PGFs, which in turn increase sperm targeting efficiency. Under excessively crowded conditions, ,increased ascaroside pheromone concentration sensed by ASI sensory neurons decreases DAF-7 expression. Consequently, PGF production and sperm targeting efficiency decrease.

The *C. elegans* Sensory Nervous System

C. elegans senses their environment through ciliated sensory neurons. The hermaphrodite nervous system includes three hundred and two neurons and fifty-six glial cells, an equivalent of 37% of all somatic cells (White et al., 1986). The neurons belong to one hundred and eighteen morphologically unique classes. Asymmetric division gives rise to almost all neurons (Hobert, 2010; White et al., 1986). Of these neurons, sixty-one are

sensory neurons (Inglis et al., 2007). Of these, thirty-two are predicted to be chemosensory neurons because their dendrites are open to the outside (Ward et al., 1975; Ware et al., 1975). Chemosensory neurons come in bilateral pairs, including amphid, phasmid, and inner labial neurons (Hall and Russell, 1991; Ward et al., 1975; White et al., 1986). Twelve pairs of amphid neurons (ADF, ADL, AFD, ASE, ASG, ASH, ASI, ASJ, ASK, AWA, AWB, AWC) have their cell bodies located near the anterior part of the terminal pharyngeal bulb, sending dendrites anteriorly through side openings near the lip. These amphid sensory neurons also send axons to the nearby nerve ring to make connections with interneurons (Figure 7) (Bargmann, 2006; Inglis et al., 2007). Phasmid neuron cell bodies are posterior to the worm anus (Hall and Russell, 1991). Inner labial neurons are arranged in set of 6 symmetrical cells, and their cell bodies are more anterior than amphid cell bodies (Ward et al., 1975; Ware et al., 1975). Males have an additional 52 ciliated sensory neurons, the majority of which are in the tail ray/hook to sense the hermaphrodite vulva and modulate male mating behavior (Inglis et al., 2007; Peden and Barr, 2005; Sulston et al., 1980). Other male specific neurons include 4 CEM (DL/DR/ VL/VR) neurons, which are predicted to be involved in chemotaxis and male attraction (Sulston et al., 1980; White et al., 2007).

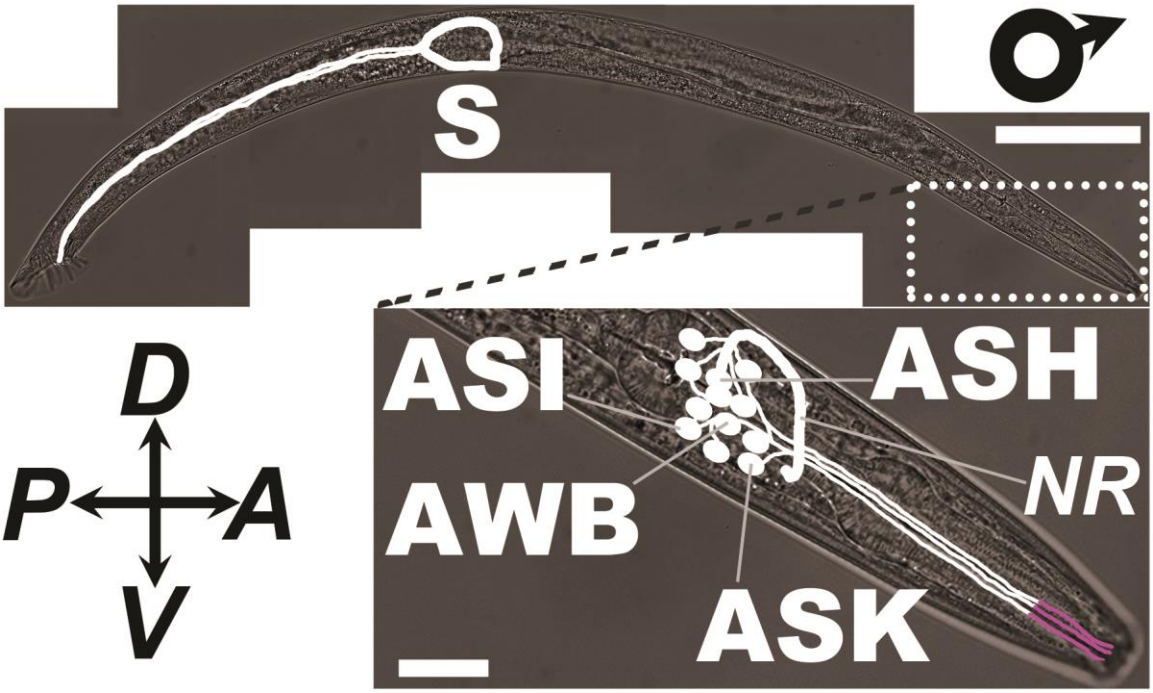

Figure 7. Anatomy of a male *C. elegans* worm illustrating the sperm storage compartment and amphid sensory neurons

The x-axis is Anterior (*A*) – Posterior (*P*) axis. The y-axis is Dorsal (*D*) – Ventral (*V*) axis. The upper DIC image depict a whole male worm. S, seminal vesicle – the site of spermatid storage. NR, nerve ring. The lower image depicts an enlargement of the male head to illustrate the shape and positions the 12 amphid sensory neuron cell bodies and dendrites. The terminal end of the dendrite are sensory (primary) cilia which are illustrated as pink terminals. Only 4 of the cell bodies (relevant to Chapter 3 results) are labeled with names. ASH, amphid single ciliated neuron H. ASI, amphid single ciliated neuron I. ASK, amphid single ciliated neuron K. AWB, amphid winged neuron B. ASH, ASI, and ASK neurons have linear cilia whereas AWB neurons have branched cilia. Upper scale bar, 100 um. Lower scale bar, 20 um.

Cilia in *C. elegans*

The only ciliated cells in *C. elegans* are sensory neurons. Cilia are non-motile microtubule-based organelles at the end of dendritic processes of sensory neurons (Inglis et al., 2007). Cilia are composed of a basal body (i.e. transition zone) with a circular array of doublet microtubules, a middle segment with 9 microtubule doublets, and a distal segment with 9 microtubule singlets (Perkins et al., 1986; Ward et al., 1975; Ware et al., 1975). Intact cilia structure and function are required for chemosensation and osmotic avoidance (Bargmann et al., 1993; Lewis and Hodgkin, 1977; Perkins et al., 1986; Ward, 1973). For example, slight truncation of cilia by deficiency in BBS-7 and BBS-8, which function to stabilize intraflagellar transport (ITF) particle subcomplexes A and B, results in a defect in iso-amyl alcohol and acetone chemosensation (Blacque et al., 2004). Similarly, localization of a known chemoreceptor *odr-10* to the tip of cilia of AWA amphid sensory neurons is required for its function in sensing diacetyl ligand (Dwyer et al., 1998; Sengupta et al., 1996). Thus, sensory neurons contain chemoreceptors in their ciliated endings that recognize extracellular cues and require IFT for function.

C. elegans Olfactory Receptor

About 1280 genes in the *C. elegans* genome encode for olfactory receptor candidates based on their homology with mammalian rhodopsin olfactory receptors (Robertson and Thomas, 2006). These genes are grouped into families whose names start with *Serpentine Receptor* (e.g. *Serpentine Receptor A* (*sra*), *Serpentine Receptor B* (*srb*), *Serpentine Receptor D* (*srd*), etc.) (Figure 8) (Chen et al., 2005; Robertson, 1998, 2001;

Stein et al., 2003; Thomas et al., 2005; Troemel et al., 1995). Some members of serpentine receptor families are expressed in sensory neurons, where they mediate olfaction, nociception, and pheromone sensing (Hilliard et al., 2004; Jansen et al., 1999; Jansen et al., 2002; Roayaie et al., 1998). For instance, *odr-10*, a member of the *serpentine receptor* STR family, is expressed in the ciliary endings of AWA amphid sensory neuron pair and is required to detect diacetyl, a volatile diketone organic compound (Robertson and Thomas, 2006; Sengupta et al., 1996). Similarly, *srbc-64* and *srbc-66*, two members of the *serpentine receptor* BC family, are expressed in ASK amphid sensory neuron, and are required to detect dauer pheromones called ascarosides (Fielenbach and Antebi, 2008; Kim et al., 2009).

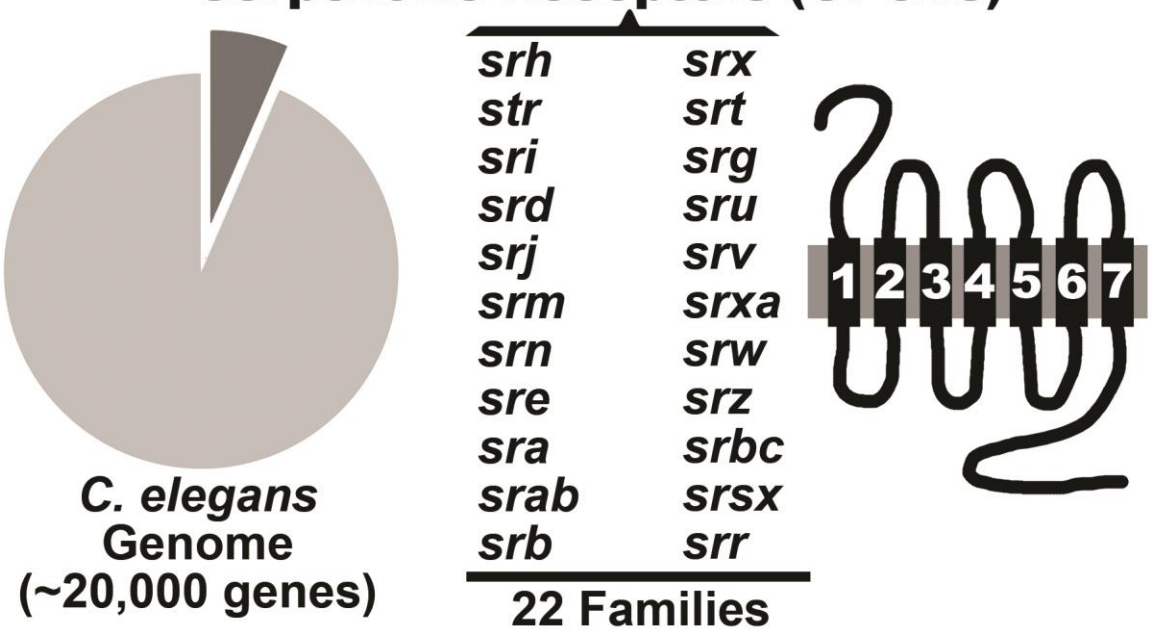

Figure 8. Chemosensory serpentine receptors in *C. elegans*

C. elegans devote 6-7% of its protein-coding genes to code for chemosensory GPCRs called serpentine receptors. They are divided into 22 families based on homology. A schematic of GPCR structure is shown on the right.

When looking for genes required in males for efficient sperm targeting to oocytes, we found a deletion mutation (*ok3126*) in *srb-13* gene that causes a sperm distribution defect. *srb-13* lies in a genomic locus tightly clustered with six other *srb* genes (Figure 9). However, not much is known about the function of any member of the *srb* family. Understanding the roles of SRB-13 and other clustered chemoreceptors is the goal of chapter 3.

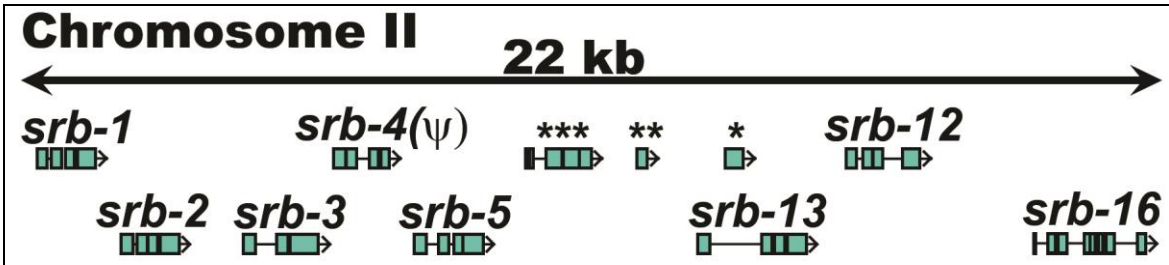

Figure 9. **Diagram of *srb* genes cluster on *C. elegans* Chromosome II**

Cyan boxes represent coding exons. All the elements are up to scale. The gene structure, deletion size and location are up to scale. Genes of interest are labeled with names whereas other genes are labeled with asterisks. * & **, two major sperm protein (MSP) coding genes, *msp-45* & *F58A6.9*, respectively; ***, *C27D6.11*, a gene with unknown function. *srb-4* is a pseudogene. This diagram is modified and adapted from thesis chapter 3.

In brief, results from the studies described in chapter two of this thesis will help identify metabolic pathways required to produce sperm guidance cues in *C. elegans*

hermaphrodites. In Chapter three, the focus is on males. A subfamily of chemosensory receptors is identified that are required in males to promote efficient sperm guidance. These receptors function in ciliated sensory neurons, where they are postulated to couple environmental information to sperm quality. Together, these studies help delineate the molecular pathways that this roundworm species uses to control sperm motility. The results have broad implications for fertilization in internally fertilizing animals, as well as for basic biology of prostaglandins.

CHAPTER 2

A HETEROGENEOUS MIXTURE OF F-SERIES PROSTAGLANDINS PROMOTES SPERM GUIDANCE IN THE *CAENORHABDITIS ELEGANS* REPRODUCTIVE TRACT

by

HIEU D. HOANG, JEEVAN K. PRASAIN, DIXON DORAND, MICHAEL A. MILLER

PLoS Genet 9(1): e1003271. doi:10.1371/journal.pgen.1003271

Copyright

2013

by

PLoS Genetics and authors

The work is under Creative Commons Attribution License (CCAL) and therefore requires no permission for modification or reprint

Format adapted and errata corrected for dissertation

Abstract

The mechanisms that guide motile sperm through the female reproductive tract to oocytes are not well understood. We have shown that *Caenorhabditis elegans* oocytes synthesize sperm guiding F-series prostaglandins from polyunsaturated fatty acid (PUFA) precursors provided in yolk lipoprotein complexes. Here we use genetics and electrospray ionization tandem mass spectrometry to partially delineate F-series prostaglandin metabolism pathways. We show that omega-6 and omega-3 PUFAs, including arachidonic and eicosapentaenoic acids are converted into more than 10 structurally related F-series prostaglandins, which function collectively and largely redundantly to promote sperm guidance. Disruption of omega-3 PUFA synthesis triggers compensatory up-regulation of prostaglandins derived from omega-6 PUFAs. *C. elegans* F-series prostaglandin synthesis involves biochemical mechanisms distinct from those in mammalian cyclooxygenase-dependent pathways, yet PGF2α stereoisomers are still synthesized. A comparison of F-series prostaglandins in *C. elegans* and mouse tissues reveals shared features. Finally, we show that a conserved cytochrome P450 enzyme, whose human homolog is implicated in Bietti's Crystalline Dystrophy, negatively regulates prostaglandin synthesis. These results support the model that multiple cyclooxygenase-independent prostaglandins function together to promote sperm motility important for fertilization. This cyclooxygenase-independent pathway for F-series synthesis may be conserved.

Author Summary

A fundamental question in cell and developmental biology is how motile cells find their target destinations. One of the most important cell targeting mechanisms involves the sperm and oocyte, which unite during fertilization to produce the next generation of offspring. We have been using the nematode *C. elegans* to delineate these mechanisms. Our prior studies have shown that oocytes secrete F-series prostaglandins that stimulate sperm motility. Prostaglandins are widespread signaling molecules derived from polyunsaturated fatty acids or PUFAs. Mammals are not capable of synthesizing PUFAs and must receive them in the diet. *C. elegans* was not thought to synthesize prostaglandins because the genome lacks cyclooxygenases, enzymes that catalyze the rate-limiting step in mammalian prostaglandin synthesis. Here we show that *C. elegans* oocytes synthesize a heterogenous mixture of structurally related F-series prostaglandins derived from different PUFA classes, including the enantiomer of PGF2α. These prostaglandins function collectively and redundantly to guide sperm to the fertilization site. Our results indicate that F-series prostaglandins can be synthesized independent of cyclooxygenase enzymes. This novel pathway may be evolutionarily conserved. Evidence is emerging that prostaglandins regulate sperm motility in the female reproductive tract of humans.

INTRODUCTION

The union of oocyte and sperm, known as fertilization, is paramount to the survival of animal species (Evans and Florman, 2002; Gadella and Evans, 2011; Han et al., 2010; Marcello et al., 2013). Oocytes tend to be large stationary cells filled with nutrients to support early embryonic development. Sperm, on the other hand, are smaller mobile cells capable of sensing their environment and responding with changes in motility. Sperm have a relatively simple job – find an oocyte and provide it with a second set of chromosomes. While much has been learned about sperm motility in aquatic species (Guerrero et al., 2010; Kaupp et al., 2008), the mechanisms that guide sperm to oocytes in internally fertilizing animals are less well understood. These guidance mechanisms are likely crucial for reproductive success (Chang and Suarez, 2010; Eisenbach and Giojalas, 2006). Evidence is emerging that lipid signaling molecules, such as steroids and prostaglandins are important regulators of sperm motility in the human female reproductive tract (Brenker et al., 2012; Lishko et al., 2011; Schuetz and Dubin, 1981; Strunker et al., 2011; Teves et al., 2009).

Caenorhabditis elegans is a powerful model to study sperm behavior and fertilization (Han et al., 2010; Kim et al., 2013; L'Hernault, 2009; Marcello et al., 2013; Stanfield and Villeneuve, 2006). Its transparent epidermis allows visualization of sperm distribution and motility in live wild-type and mutant animals (Figure 1A) (Hill and L'Hernault, 2001; Kubagawa et al., 2006; Ward and Carrel, 1979). Sperm velocity, directional velocity toward eggs, and reversal frequency within the reproductive tract can be quantified from time-lapse videos (Edmonds et al., 2010; Kubagawa et al., 2006). Genetic and biochemical analyses have shown that oocytes synthesize F-series

prostaglandins (PGs) from polyunsaturated fatty acids (PUFAs) provided in yolk lipoprotein complexes (Edmonds et al., 2011; Edmonds et al., 2010; Kubagawa et al., 2006). PUFAs are fatty acids with two or more double bonds, which are essential for prostaglandin cyclopentane ring formation (Figure S1) (Funk, 2001). Mutations in PUFA biosynthesis enzymes and predicted prostaglandin synthases cause nonautonomous defects in sperm motility, resulting in inefficient targeting to the site of fertilization and reduced reproductive output (Edmonds et al., 2010; Kubagawa et al., 2006). Introducing nanomolar concentrations of F-series prostaglandins into the uteri of prostaglandin-deficient mutants has an immediate effect on sperm motility (Edmonds et al., 2010). Liquid chromatography coupled to electrospray ionization tandem mass spectrometry (LC-MS/MS) has identified multiple F-series prostaglandins in *C. elegans* extracts (Edmonds et al., 2011; Edmonds et al., 2010). The synthesis of CePGF2, an analog of $PGF_{2\propto}$, is dependent on 20-carbon PUFA synthesis and transport to oocytes (Edmonds et al., 2010). However, the extent to which specific loss of CePGF2 or other prostaglandins affects sperm guidance is not clear. It is also not clear whether *C. elegans* F-series prostaglandins are derived from a single or multiple PUFA precursors.

Mammals lack the desaturase enzymes necessary to convert monounsaturated fatty acids into PUFAs (Burr and Burr, 1929, 1930). A key enzyme in mammalian prostaglandin synthesis is cyclooxygenase or PG G/H synthase, which converts PUFAs into the intermediate PGH (Figure S1) (Vane et al., 1998). There are three prostaglandin classes that are synthesized from distinct PUFA precursors (Bergstrom et al., 1964; Hamberg and Samuelsson, 1967; Wathes et al., 2007) (Figure 1B). The F1 class is derived from dihomo-gamma-linolenic acid (DGLA), a 20-carbon PUFA with three double bonds in the carbon backbone. DGLA is also called 20:3n6, where the third double bond occurs at the n6 or

omega-6 position. The F2 class is derived from arachidonic acid (AA, 20:4n6; Figure S1B) and the F3 class is derived from the omega-3 PUFA eicosapentaenoic acid (EPA, 20:5n3). $PGF_{2\alpha}$ is a member of the F2 class synthesized from AA by the sequential action of cyclooxygenase and PGF synthase (Figure S1) (Funk, 2001; Vane et al., 1998). 11β-$PGF_{2\alpha}$ and 9β-$PGF_{2\alpha}$ stereoisomers are formed from PGD_2 and PGE_2 intermediates, respectively (Watanabe, 2002). In addition, a wide array of F-series prostaglandin isomers is formed via cyclooxygenase-independent mechanisms mediated by free radical-initiated peroxidation (Milne et al., 2008). In most cases, the biological activities of F-series prostaglandins are not known.

The *C. elegans* PUFA biosynthetic pathways have been delineated (Figure 1C) (Watts, 2009; Watts and Browse, 2002). Four fatty acid desaturases encoded by *fat* genes convert monounsaturated fatty acids into omega-3 and omega-6 PUFAs. Here we use mutations in *fat* genes, together with LC-MS/MS, to delineate F-series prostaglandin synthesis pathways. We show that multiple F-series prostaglandins, whose formation in large part requires an adult germ line, act collectively to promote sperm guidance. F2 class prostaglandin synthesis does not involve H_2, D_2, and E_2 intermediates that are characteristic of mammalian cyclooxygenase-dependent pathways (Figure S1). We identify a conserved cytochrome P450 enzyme that functions to inhibit prostaglandin metabolism, possibly by diverting their precursors into an alternative pathway(s). Our results support the model that *C. elegans* oocytes secrete a blend of F-series prostaglandins for guiding sperm to the fertilization site.

RESULTS

PUFAs act collectively to promote sperm guidance

To explore the F-series prostaglandin biosynthetic mechanisms important for sperm guidance, we examined *fat* mutants deficient in the synthesis of specific PUFAs classes (Figure 1C). Two quantitative assays were used to evaluate sperm guidance. In both assays, wild-type males are stained with MitoTracker CMXRos dye, which brightly labels sperm (Kubagawa et al., 2006). Stained males are mated to unstained mutant or control hermaphrodites and separated. The first assay measures sperm distribution within the uterus one hour after mating, using three defined zones (Figure 1A). In controls, over 90% of sperm move around developing embryos to the fertilization site, called the spermatheca in an hour (Figure 2). The second assay uses time-lapse imaging to directly measure sperm velocity, directional velocity, and reversal frequency within the uterus immediately after mating. Sperm in control uteri move with an average velocity of 8.6 microns per minute, rarely reversing direction. Average directional velocity toward the spermatheca is less than average velocity as sperm migrate around embryos blocking their path (Table 1, line 1).

First, wild-type males were mated to *fat-1(wa9)* and *fat-4(wa14)* mutant hermaphrodites. *fat-1(wa9)* mutants have undetectable EPA (20:5n3) and omega-3 AA (20:4n3), but have elevated AA (20:4n6) levels relative to the wild type (Kahn-Kirby et al., 2004; Watts and Browse, 2002). On the other hand, *fat-4(wa14)* mutants have undetectable EPA and AA, but have elevated omega-3 AA levels (Kahn-Kirby et al., 2004; Watts and Browse, 2002). Minor sperm motility defects are evident from sperm distribution and time-lapse imaging assays, but a large percentage of sperm are still able to target the spermatheca (Figure 2 and Table 1, lines 2 and 3). These data raise the possibility that DGLA, which is still synthesized in both *fat-1* and *fat-4* mutants, is the key precursor for sperm guiding prostaglandins.

To test whether or not DGLA is essential, we compared sperm guidance values in *fat-3(wa22)* mutants to *fat-1(wa9) fat-4(wa14)* double mutants. *fat-3(wa22)* mutants contain abundant 18:3n3 (linolenic acid, ALA), but trace amounts of 20:3n3 and undetectable DGLA (20:3n6), AA, omega-3 AA, and EPA (Watts and Browse, 2002). On the other hand, *fat-1(wa9) fat-4(wa14)* double mutants contain abundant DGLA with undetectable AA, omega-3 AA, and EPA (Kahn-Kirby et al., 2004; Watts and Browse, 2002). Surprisingly, the sperm guidance values in both mutant strains were similar, albeit significantly less than controls (Figure 2 and Table 1, lines 1, 4, and 5; $P < 0.001$). Sperm in both strains have similar directional velocity, although there are differences in velocity and reversal frequency (Table 1, lines 4 and 5). These data indicate that DGLA is not essential for sperm guidance, but it may have a modulatory or partially redundant role.

Finally, we measured sperm guidance in the healthiest 1-2 day old adult *fat-2(wa17)* mutants, avoiding those mutants with considerable pleiotropy. *fat-2* encodes a Δ12 fatty-acyl desaturase that converts monounsaturated fatty acids into PUFAs. *fat-2(wa17)* mutants contain reduced levels of all PUFAs, although approximately 5% Δ12 desaturase activity persists in this strain that is sufficient for prostaglandin synthesis (Edmonds et al., 2010; Watts and Browse, 2002). The sperm guidance defects in *fat-2* mutants are more severe than *fat-3(wa22)* mutants and *fat-1(wa9) fat-4(wa14)* double mutants (Figure 2 and Table 1, lines 4, 5, and 6). Furthermore, the defects are similar to *rme-2(b1008)* mutants, which fail to transport PUFAs to oocytes and *glp-4(bn2)* mutants, which lack oocytes (Table 1, lines 6, 7, and 8) (Beanan and Strome, 1992; Grant and Hirsh, 1999; Kubagawa et al., 2006). The trend from *fat* mutant data is that sperm guidance defects inversely correlate with total PUFA content. We conclude that loss of single PUFA classes does not

have major effects on sperm guidance. Sperm guidance defects depend on the extent to which PUFA classes are collectively eliminated.

F-series prostaglandins are synthesized from distinct PUFA pools

A collective requirement for PUFA synthesis could have multiple interpretations. One model is that F-series prostaglandins are synthesized from multiple PUFA classes. A non-mutually exclusive alternative is that worms compensate for loss of a PUFA class by up-regulating prostaglandin synthesis from another class. In both models, prostaglandins from different PUFAs must have largely redundant functions. These (and additional) models were tested through LC-MS/MS analyses of wild-type and *fat* mutant lipid extracts. Mammals synthesize F1, F2, and F3 class prostaglandins from DGLA, AA, and EPA, respectively (Figure 1B and Figure S1). To test whether wild-type worm extracts contained these classes, we used LC-MS/MS operated in multiple reaction monitoring (MRM) mode. In MRM, the parent ion to decomposition (product) ion mass transition is specified, providing excellent specificity and sensitivity. The F1 prostaglandins are detected with mass transition *m/z* 355/311, the F2 class with transition *m/z* 353/193, and the F3 class with transition *m/z* 351/193 or 351/191 (Kingsley et al., 2005; Masoodi and Nicolaou, 2006; Murphy et al., 2005). We found that wild-type extracts contained multiple isomers of each class (Figure 3A). Comparing the collision-induced decomposition (CID or MS/MS) patterns of these prostaglandins to their corresponding chemically synthesized $PGF_{1\alpha}$, $PGF_{2\alpha}$, or $PGF_{3\alpha}$ standards shows extensive similarities (Figure 4 and Tables 2 and 3). Key shared decomposition features include the loss of 44 Da ($-C_2H_4O$) from the parent ion followed by two 18 Da losses ($-2x\ H_2O$), and the presence of the *m/z* 193 ion in the F2 and F3 series (Figure 1B) (Murphy et al., 2005).

One of the two most abundant worm F1 isomers (CePGF1) has a chromatography retention time (RT) that is indistinguishable from $PGF_{1\alpha}$ (Figure 3). Their CID patterns are nearly identical, with the exception of minor ions at *m/z* 157 and 223 (Figure 4). We have previously shown that CePGF2 and $PGF_{2\alpha}$ have indistinguishable chromatography RTs and nearly identical CID patterns (Edmonds et al., 2010). In contrast, the $PGF_{3\alpha}$ RT is several seconds shorter than the closest worm F3 class prostaglandin at RT = 11.33 (Figure 3). While the CID patterns of $PGF_{3\alpha}$ and this prostaglandin are similar, there are more differences than in F1 and F2 classes (Figure 4). One key difference is the abundance of product ion *m/z* 193, which is thought to derive from C14-C15 cleavage and methyl terminus side chain loss (Figure 1B) (Murphy et al., 2005). This product ion is less abundant in the closest eluting worm F3 prostaglandin compared to $PGF_{3\alpha}$. Another difference is the product ion *m/z* 167, which is not found in $PGF_{3\alpha}$. Therefore, *C. elegans* F3 class prostaglandins are likely to have a significant structural difference relative to $PGF_{3\alpha}$. These data indicate that worms synthesize an array of F1, F2, and F3 class prostaglandins, including CePGF1 and CePGF2.

Next, we examined F-series prostaglandins in *fat-1(wa9)* mutants, *fat-4(wa14)* mutants, and *fat-1(wa9) fat-4(wa14)* double mutants. There are several important features of the data. First, all three mutant strains lack EPA and F3 class prostaglandins (Figure 3A). Second, *fat-1(wa9)* mutants with elevated AA levels have elevated CePGF2 and a second $PGF_{2\alpha}$ analog, called CePGF2b (Figure 3A-3B). Both CePGF2 and CePGF2b are absent in *fat-4(wa14)* mutants and *fat-1(wa9) fat-4(wa14)* double mutants that lack AA (Figure 3A-3B). Third, *fat-4* mutants with elevated omega-3 AA levels have elevated levels of several F2 class isomers (Figure 3A). These prostaglandins are also found in wild-type

extracts at lower abundance. Finally, *fat-1(wa9) fat-4(wa14)* double mutants with elevated DGLA have elevated F1 class prostaglandins, including CePGF1 (Figure 3A). Taken together, these data strongly support the model that *C. elegans* extracts contain F1, F2, and F3 class prostaglandins derived from 20:3, 20:4, and 20:5 PUFA precursors, respectively. We conclude that prostaglandin synthesis is regulated in part by precursor abundance.

fat-3(wa22) mutants and *fat-1(wa9) fat-4(wa14)* double mutants have similar sperm guidance defects, yet different PUFA content. We previously showed that *fat-3* is required for CePGF2 synthesis, but F1 and F3 class members were not analyzed (Edmonds et al., 2010). A re-examination of *fat-3(wa22)* mutant extracts using LC-MS/MS shows that CePGF1, CePGF2, CePGF2b, and all F3 class prostaglandins are largely absent in *fat-3* mutants (Figure S2A). However, several potential F-series prostaglandins are found, perhaps derived from trace levels of 20:3n3 found in *fat-3(wa22)* extracts (Watts and Browse, 2000). Overall, the total 20-carbon prostaglandin level in *fat-3* mutants is lower than the level in *fat-1 fat-4* double mutants. As *fat-3* mutants have approximately 12-fold higher 18:3n3 (ALA) than the wild type (Watts and Browse, 2000), we hypothesized that 18:3n3 might serve as a substrate for prostaglandin synthesis. The 18-carbon $PGF_{2\alpha}$ metabolite 2,3-Dinor 11β $PGF_{2\alpha}$ has a chromatography RT of 10.7 min, so we predicted a prostaglandin derived from 18:3n3 might have a similar RT (Table 3). An 18:3n3 F-series prostaglandin should have parent ion mass *m/z* 327, which is 28 Da lighter ($-C_2H_4$) than $PGF_{1\alpha}$. LC-MS/MS identified a putative F-series prostaglandin at RT = 10.9 min with considerable similarity to $PGF_{1\alpha}$, including loss of 44 Da from the parent ion followed by two 18 Da losses (Figure S2B). MRM using mass transition *m/z* 327/283 shows that this compound and at least one other compound are strongly up-regulated in *fat-3* mutants

relative to the wild type (Figure S2C). These data add further support to the model that multiple precursors can generate F-series prostaglandins and precursor abundance influences synthesis.

F-series prostaglandins have redundant functions in sperm guidance

The current data provide evidence that F-series prostaglandins have redundant functions. Consistent with this possibility, microinjecting nanomolar concentrations of $PGF_{2\alpha}$ or $PGF_{3\alpha}$ into the uteri of *fat-2(wa17)* or *rme-2(b1008)* mutants has an immediate and similar effect on sperm velocity (Edmonds et al., 2010). To further test this model, we supplemented the diets of wild-type, *fat-3(wa22)* mutant, and *fat-1(wa9) fat-4(wa14)* double mutant hermaphrodites with AA or EPA. Whereas *fat-2* and *fat-3* mutants convert AA into EPA, *fat-1(wa9) fat-4(wa14)* double mutants cannot (Kahn-Kirby et al., 2004; Kubagawa et al., 2006; Watts and Browse, 2002). We found that AA or EPA supplementation rescued the sperm guidance defects of *fat-2* mutants, *fat-3* mutants, and *fat-1 fat-4* double mutants (Figures 2, 5, and 6; $P < 0.001$). In these experiments, the NA22 bacteria used as a food source do not accumulate PUFAs to high levels (< 5% of total membrane lipids), resulting in modest dietary intake (Kubagawa et al., 2006). We have not yet developed methods to measure prostaglandins in supplementation experiments. The data, together with previous and published data, strongly support the hypothesis that F-series prostaglandins derived from different precursors function redundantly to promote sperm guidance.

F-series prostaglandins are not synthesized from D- or E-series intermediates

We next sought to investigate the mechanism by which F-series prostaglandins are synthesized from PUFA precursors. In the mammalian cyclooxygenase-dependent pathway for F2 class prostaglandin synthesis, PGH_2, PGD_2, and PGE_2 are intermediates of $PGF_{2\propto}$, 11β $PGF_{2\propto}$, and 9β $PGF_{2\propto}$ (Figure S1) (Funk, 2001; Watanabe, 2002). To test whether worm extracts contain these intermediates, we used MRM with mass transition *m/z* 351/189, which detects PGD_2, PGE_2, and PGH_2 in the low picomolar range. Several peaks of low abundance were identified in wild-type extracts (Figure 3A). If these peaks represent PGD_2, PGE_2, and PGH_2 isomers, then *fat-1* loss should increase their levels because *fat-1* mutants contain elevated AA and CePGF2. However, this was not the case. The minor peaks observed in wild-type extracts with mass transition *m/z* 351/189 are eliminated in *fat-1* mutants, *fat-4* mutants, and *fat-1 fat-4* double mutants (Figure 3A). This pattern indicates that these compounds likely require EPA, but not AA for synthesis. In addition, CID of parent ions *m/z* 351 at RT = 11.4 min and 12.6 min in wild-type extracts shows similarity to F3 class prostaglandins, with the exception of the minor product ion *m/z* 189 (data not shown). Thus, these compounds are not AA-derived PGD_2, PGE_2, or PGH_2 analogs. These data indicate that worms either do not synthesize PGD_2, PGE_2, and PGH_2 analogs or their concentrations are below the level of detection.

We have previously identified predicted prostaglandin D, E, and F synthases that are required for sperm guidance (Edmonds et al., 2010). *gst-4* and *R11A8.5* encode glutathione S-transferase enzymes related to PGD and PGE synthases, respectively (Edmonds et al., 2010). *gst-4* mutants have more severe sperm guidance defects than the mild defects observed in *R11A8.5* mutants (Edmonds et al., 2010). To test whether these enzymes are essential for F-series prostaglandin synthesis, we conducted LC-MS/MS on *gst-4* and *R11A8.5* null mutant extracts. In four independent trials, we consistently

observed a 25-75% reduction in F1, F2, and F3 prostaglandins in *gst-4* null mutants compared to the wild type (Figure S3). *R11A8.5* null mutants had a more complex pattern, with elevated levels of some prostaglandins and reduced levels of others (Figure S3). Null mutations are not currently available for the predicted PGF synthases *Y39G8B.2* and *C35D10.6*. These data indicate that *gst-4* and *R11A8.5* are not essential for F-series prostaglandin synthesis. Instead, they appear to have modulatory roles.

CePGF2 consists predominantly of ent-$PGF_{2\propto}$

Although *C. elegans* lacks cyclooxygenase enzymes, our data strongly support the hypothesis that CePGF2 is synthesized from AA. Furthermore, the CID of CePGF2 is almost identical to $PGF_{2\propto}$ (Figure 4). The product ions *m/z* 309 and 193 are characteristic of the $F_{2\propto}$ cyclopentane ring (Murphy et al., 2005). The loss of 44 Da ($-C_2H_4O$) from the parent ion followed by two 18 Da losses ($-2x\ H_2O$), together with the presence of abundant ion *m/z* 193, further indicates the compound has three hydroxyl groups at the C9, C11, and C15 positions (Figure 1B). There is no product ion *m/z* 115 that is abundant in $PGF_{2\propto}$ isomers with a hydroxyl group at the C5 position (Waugh et al., 1997). There are sometimes a few differences in minor product ions of unknown composition between $PGF_{2\propto}$ and CePGF2 from wild-type extracts. However, the CePGF2 decomposition pattern from *fat-1* mutant extracts, which have increased CePGF2 concentration, is almost identical to $PGF_{2\propto}$ (Figure 4). Minor differences between CePGF2 and $PGF_{2\propto}$ spectra could be due to low concentration and co-eluting compounds. We conclude that CePGF2 has chemical

composition $C_{20}H_{34}O_5$ with an $F_{2\propto}$ cyclopentane ring and hydroxyl groups at positions C9, C11, and C15.

Structural differences in similar compounds often cause changes in chromatographic retention. For example, the RTs of $PGF_{2\propto}$ and $PGF_{3\propto}$ differ by 34 seconds, although the only structural difference is an additional double bond at C17 in $PGF_{3\propto}$ (Figure 1B). Given that CePGF2 and $PGF_{2\propto}$ have indistinguishable retention times, we asked whether $PGF_{2\propto}$ stereoisomers are resolved in our HPLC program. The C-OH bonds at C9, C11, and C15, the C-C bonds at C8 and C12, and the C=C bonds at C5 and C13 can be in different conformations. We analyzed by LC-MS/MS a series of chemically synthesized $PGF_{2\propto}$ stereoisomers that included conformation changes at the C5, C8, C9, C11, and C15 positions. With the exception of the $PGF_{2\propto}$ enantiomer (ent- $PGF_{2\propto}$), all other stereoisomers were separated (Table 3). The RT differences relative to $PGF_{2\propto}$ ranged from 7 seconds for 5-*trans* $PGF_{2\propto}$ to 30 seconds for 9β $PGF_{2\propto}$. Similar changes were observed with several $PGF_{1\propto}$ and $PGF_{3\propto}$ stereoisomers in reverse-phase chromatography (Table 3). It is noteworthy that CePGF1, CePGF2, $PGF_{1\propto}$, $PGF_{2\propto}$, and ent-$PGF_{2\propto}$ elute together and the CID patterns of ent-$PGF_{2\propto}$ and $PGF_{2\propto}$ are identical (Figure 3 and Table 3). These results indicate that CePGF2 is $PGF_{2\propto}$, a co-eluting stereoisomer such as ent-$PGF_{2\propto}$, or a racemic mixture. To distinguish between these possibilities, we developed a normal phase chiral LC-MS/MS method operated in MRM mode (mass transition 353/193) to separate $PGF_{2\propto}$ and ent-$PGF_{2\propto}$. When *fat-1(wa9)* mutant extract, which contains abundant CePGF2 (Figure 3), was analyzed by chiral LC-MS/MS, the predominant isomer eluted with the same retention time as the ent-$PGF_{2\propto}$ standard (Figure S4). These results strongly support the hypothesis that CePGF2 consists predominantly of ent-$PGF_{2\propto}$.

Similarly, CePGF1 may be the enatiomer of $PGF_{1\propto}$. Nuclear Magnetic Resonance spectroscopic studies will be necessary for absolute confirmation.

The adult germ line is essential for F-series prostaglandin synthesis

We have previously shown that CePGF2 synthesis requires the RME-2 low-density lipoprotein receptor, which transports PUFAs from the intestine to oocytes (Edmonds et al., 2010; Kubagawa et al., 2006). These experiments were conducted with extracts from mixed stage worm cultures. To evaluate the extent to which F-series prostaglandins are synthesized in the adult germ line, we synchronized mass worm cultures from wild-type and *glp-4(bn2)* mutant hermaphrodites. *glp-4(bn2)* is a temperature sensitive mutation that prevents germ cell proliferation and differentiation at the restrictive temperature (25 ºC) (Beanan and Strome, 1992). We extracted prostaglandins from 1-2 day adult wild-type and *glp-4(bn2)* hermaphrodites raised at 25 ºC. As shown in Figure 7, multiple F2 and F3 class prostaglandins are present in the extracts, including CePGF2 and CePGF2b. The F1 series could not be evaluated because synchronization limits culture size, restricting the number of LC-MS/MS analyses that can be conducted. CePGF2 is less abundant in 1-2 day old adults relative to mixed stage cultures (Figure 3B and 7B). *glp-4(bn2)* mutant adults lacking germ cells and oocytes have severely reduced levels of F2 and F3-series prostaglandins compared to wild-type adults (Figure 7A). CePGF2 was reduced by about 75% (Figure 7B; $P < 0.001$). We conclude that the adult germ line is required to synthesize multiple F-series prostaglandins.

A cytochrome P450 enzyme influences germline prostaglandin metabolism

A major remaining question is how F-series prostaglandins are metabolized. Identifying genes required non-autonomously for sperm guidance should provide insight into the pathway(s). In a prior RNAi screen for these genes, we identified *H02I12.8* (also called *cyp-31A2)* (Kubagawa et al., 2006). This gene and its paralog *cyp-31A3* encode class 4 cytochrome P450 enzymes most closely related to CYP4V2 (Benenati et al., 2009). Given that *cyp-31A2* and *cyp-31A3* mRNAs share approximately 92% identity in their coding regions, RNAi might affect both gene products. Previous studies have shown that these two enzymes act redundantly to promote formation of the egg permeability barrier following fertilization (Benenati et al., 2009; Olson et al., 2012). To test whether *cyp-31A2* and *cyp-31A3* are required for sperm guidance, we analyzed their deletion mutants. *cyp-31A2(tm2711)* and *cyp-31A3(tm3224)* single mutants are both fertile with no obvious oogenesis defects. However, wild-type sperm fail to target the spermatheca efficiently in the mutants (Figure 8A; $P < 0.001$). Similar results are observed in *emb-8* RNAi hermaphrodites ($P < 0.001$). *emb-8* encodes a homolog of NADPH cytochrome P450 reductase, which provides electrons for cytochrome P450s. Sperm velocity in *cyp-31A2(tm2711)* mutants is not significantly different than velocity in the wild type ($P > 0.30$), but directional velocity is decreased (Table 1, lines 1 and 9; $P < 0.05$). Similar results were previously reported using RNAi (Kubagawa et al., 2006). These results indicate that cytochrome P450 function is required for sperm guidance.

To investigate the mechanism, we conducted LC-MS/MS analysis of *cyp-31A2(tm2711)* mutant extracts. MRM in three independent trials showed that F1, F2, and F3 class prostaglandins were consistently elevated in the mutant strain compared to the wild type (Figure 8B). LC-MS analysis in the mass range *m/z* 315-360 did not show global elevation of PUFA-derived compounds, demonstrating specificity for F-series

prostaglandins (data not shown). Therefore, *cyp-31A2* is not essential for prostaglandin synthesis. A feature of class 4 cytochrome P450s is the ability to hydroxylate PUFAs and prostaglandins at the C19 and C20 positions (Hsu et al., 2007). We considered the possibility that *cyp-31A2* is required to form hydroxylated F-series prostaglandins. However, no evidence of these compounds can be been found using LC-MS/MS (Figure S5). MRM with mass transition *m/z* 369/193, which detects 19-hydroxy $PGF_{2\propto}$ and 20-hydroxy $PGF_{2\propto}$ standards, fails to detect these metabolites in wild-type extracts or *fat-1(wa17)* mutant extracts with elevated CePGF2. Similar results were observed using MRM with mass transition *m/z* 367/193, which detects hydroxylated $PGF_{3\propto}$ (Figure S5). We conclude that CYP-31A2 negatively regulates F-series prostaglandin metabolism, likely by affecting a process common to F1, F2, and F3 classes. The increased prostaglandin levels in *cyp-31A2* mutants could be due to continued synthesis in fertilized eggs (see Discussion).

C. elegans and mouse tissues contain similar F-series prostaglandin profiles

CePGF1 and CePGF2 appear to be identical to or co-eluting stereoisomers of $PGF_{1\propto}$ and $PGF_{2\propto}$, respectively. However, genetic, biochemical, and pharmacological evidence shows that their biosynthesis is cyclooxygenase-independent (Edmonds et al., 2010). In mammals, $PGF_{2\propto}$, ent-$PGF_{2\propto}$, and other stereoisomers can be formed independent of cyclooxygenase via free radical-initiated peroxidation (Milne et al., 2008; Yin et al., 2007a). To determine which F-series prostaglandin isomers are synthesized in healthy mammalian tissues, we extracted lipids from adult wild-type mouse liver, heart, kidney, and lung. LC-MS/MS analysis indicates that these extracts contain abundant $PGF_{1\propto}$

and $PGF_{2\propto}$, which co-elute (Figure 9). The lung is particularly rich in these prostaglandins. On the other hand, $PGF_{3\propto}$ could only be detected in lung extracts, perhaps reflecting the low abundance of omega-3 PUFAs in the mouse diet. In *C. elegans*, multiple prostaglandin isomers are synthesized from DGLA and AA independent of cyclooxygenase. We found that mouse tissues also contain putative $PGF_{1\propto}$ and $PGF_{2\propto}$ isomers, but of relatively low abundance (Figure 9). LC-MS/MS and CID of lung extracts support the view that these compounds are indeed F-series isomers (data not shown). The RTs of these isomers are in many cases identical to the RTs of *C. elegans* isomers. We conclude that extracts from healthy *C. elegans* and mouse tissues contain at least two and perhaps more F-series prostaglandin isomers in common. These results raise the interesting possibility that mammals can synthesize $PGF_{1\propto}$ and $PGF_{2\propto}$ stereoisomers independent of cyclooxygenase enzymes.

DISCUSSION

For fertilization to occur, sperm must sense the environment within the female reproductive tract and locate an oocyte that has recently completed meiotic maturation and ovulation. We have been using *C. elegans* to delineate the mechanisms that guide sperm to maturing oocytes (Edmonds et al., 2011; Edmonds et al., 2010; Kubagawa et al., 2006; Whitten and Miller, 2007). Results from this study and previous studies support the following model. In the intestine, dietary fats are converted into PUFAs and incorporated into yolk lipoprotein complexes (Kubagawa et al., 2006). Yolk is secreted into the pseudocoelom and flows to the gonad, where it is endocytosed into oocytes by the RME-2 low-density lipoprotein receptor (Grant and Hirsh, 1999). Yolk provides oocytes with 20-

carbon PUFAs that are converted into at least 10 structurally related F-series prostaglandins, independent of cyclooxygenase enzymes. DGLA, AA, and EPA are major precursors for F1, F2, and F3 classes, respectively, that include $PGF_{1\propto}$ and $PGF_{2\propto}$ stereoisomers. Conserved glutathione S-transferase and cytochrome P450 enzymes modulate oocyte F-series prostaglandin metabolism, although the biochemical mechanisms are not yet clear.

F-series prostaglandins secreted into the reproductive tract function collectively and partially redundantly to promote sperm velocity and directional motility toward the spermatheca. Prostaglandins provide positional information to sperm that allow them to locate and maintain their place in the spermatheca, despite the obstruction of passing fertilized eggs. As maturing oocytes enter the spermatheca during ovulation, they are immediately fertilized. The CYP-31A2 enzyme acts following fertilization to inhibit prostaglandin synthesis and secretion, ensuring that sperm are not attracted to developing embryos. Endocrine signals such as insulin, as well as signals from somatic gonadal cells transduced by gap junctions regulate oocyte prostaglandin metabolism (Edmonds et al., 2011; Edmonds et al., 2010; Whitten and Miller, 2007). Together, these mechanisms help couple nutritional status and oocyte development to reproductive output. New evidence supporting this model is discussed below.

F-series prostaglandin synthesis from multiple precursors

LC-MS/MS analyses of wild-type and *fat* mutant extracts provide strong evidence that F-series prostaglandins can be synthesized from DGLA, O3AA, AA, and EPA. The concentrations of CePGF1 and CePGF2 in wild-type extracts are similar, although absolute levels of CePGF1 were not determined. The concentrations of F3 class prostaglandins are

difficult to estimate because appropriate standards are not available. Given the abundance of EPA in wild-type hermaphrodites and yolk (Kubagawa et al., 2006; Watts and Browse, 2002), the F3 prostaglandins are likely the most abundant. Precursor levels appear to have a profound impact on prostaglandin synthesis and signaling. For example, *fat-1* mutants have approximately 13-fold higher AA levels relative to the wild type (Kahn-Kirby et al., 2004; Watts and Browse, 2002). We found that CePGF2 levels increase by over three fold, helping to compensate for F3 class prostaglandin loss. LC-MS/MS analysis also detected a putative F-series prostaglandin(s) derived from 18:3n3 in *fat-3* mutants. However, F-series prostaglandins derived from 18:3 or 18:4 were not identified in wild-type extracts. These results reveal unexpected complexity in the mechanisms that couple PUFA homeostasis to prostaglandin synthesis. A mutant strain completely deficient in prostaglandin synthesis has not been identified. Hence, the extent to which prostaglandins regulate development, immunity, and reproduction is not known.

A key feature of prostaglandin synthesis in *C. elegans* is the absence of cyclooxygenase enzymes (Edmonds et al., 2010). The *C. elegans* genome does not encode cyclooxygenase homologs. Furthermore, drugs that inhibit cyclooxygenase activity do not affect sperm motility (Edmonds et al., 2010). In this study, we show that *C. elegans* extracts contain $PGF_{1\propto}$ and $PGF_{2\propto}$ stereoisomers, but not key PGH_2, PGD_2, and PGE_2 intermediates of cyclooxygenase-dependent pathways. These data provide compelling evidence that $PGF_{1\propto}$ and $PGF_{2\propto}$ are synthesized using a cyclooxygenase-independent mechanism. Prostaglandins can be synthesized via a non-enzymatic mechanism mediated by free radical-initiated peroxidation (Milne et al., 2008). However, free radical-initiated peroxidation generates a nonselective mixture of prostaglandin stereoisomers, including 8-

iso $PGF_{2\propto}$ and 8-iso PGE_2 that are undetectable in *C. elegans*. Free radicals could play a role in worm prostaglandin synthesis, but it seems likely that enzymes are involved. The enantiomeric form of $PGF_{2\propto}$, which is not formed by cyclooxygenase and cannot be distinguished from $PGF_{2\propto}$ using standard LC-MS/MS or immunoassays, is the major F2 class prostaglandin in human urine (Yin et al., 2007b) and *C. elegans* extracts. An attractive possibility is that F-series prostaglandins can be formed by a conserved, yet undiscovered mechanism that does not involve cyclooxygenases.

F-series prostaglandins function redundantly

We show that sperm guidance defects depend on the extent to which PUFA classes are collectively eliminated. As each PUFA class with at least three double bonds can serve as a precursor for prostaglandin synthesis, the data support the model F-series prostaglandins function collectively and partially redundantly. Indeed, supplementation of *fat-2(wa17)* mutants, *fat-3(wa22)* mutants, and *fat-1(wa9) fat-4(wa14)* mutants with either AA or EPA largely rescues the sperm guidance defects. Similar results were observed when *fat-2(wa17)* mutants were supplemented with linoleic acid, AA, and EPA and sperm motility was analyzed by time-lapse video microscopy (Kubagawa et al., 2006). Microinjecting AA into *fat-2* mutant gonads rescues the sperm distribution defect (Kubagawa et al., 2006). Finally, microinjecting nanomolar concentrations of $PGF_{2\alpha}$ or $PGF_{3\alpha}$ into the uteri of *fat-2(wa17)* or *rme-2(b1008)* mutants has an immediate and similar effect on sperm velocity (Edmonds et al., 2010). These results provide strong evidence that F2 or F3 class prostaglandins are sufficient for sperm guidance, yet neither class is essential.

F1 class prostaglandins and prostaglandins derived from 18:3n3 are also likely to function redundantly with F2 and F3 classes. In *fat-1 fat-4* double mutants, the F1 prostaglandins appear to partially compensate for the absence of F2 and F3 classes. Similarly, 18:3n3-derived prostaglandins appear to partially compensate for 20-carbon prostaglandin loss in *fat-3* mutants. Thus, there appears to be tremendous flexibility in the mechanisms that synthesize prostaglandins and transduce their signals. Collective function explains the low abundance of individual prostaglandin isomers in wild-type extracts (relative to mammalian tissues). Why such flexibility and redundancy exists in an animal that generates its own omega-3 and omega-6 PUFAs is not clear, but perhaps it provides a buffer against dietary or genetic changes.

The cytochrome P450 CYP-31A2 in sperm guidance

CYP-31A2 is a class 4 cytochrome P450 that is most similar to human CYP4V2, which is implicated in the retinal disease Bietti's Crystalline Dystrophy (Li et al., 2004). This enzymatic class has a well characterized function in hydroxylating fatty acids, particularly at the omega-1 and omega-2 positions (Hsu et al., 2007). Recombinant human CYP4V2 has been shown to hydroxylate EPA and docosahexaenoic acid (Nakano et al., 2012). In *C. elegans*, RNAi of CYP-31A1/A2/A3 together causes a reduction in hydroxylated EPA metabolites synthesized from microsomes (Kulas et al., 2008). We were unable to detect hydroxylated forms of F-series prostaglandins in mixed stage wild-type extracts. Thus, potential substrates for CYP-31A2 are EPA and other PUFAs. LC-MS/MS analysis of *cyp-32A2* null mutants indicates that F1, F2, and F3 class prostaglandins are elevated by up to 2-fold. These data support the idea that CYP-32A2 down-regulates prostaglandin synthesis. Time-lapse imaging of sperm motility in *cyp-32A2* null mutants

and RNAi hermaphrodites is consistent with a gain of signaling activity, as sperm velocity is unaffected (Kubagawa et al., 2006). *cyp-32A2* might act together with or in parallel to *cyp-31A3*, which is also required for sperm guidance.

An interesting possibility is that CYP-31A2 functions to down-regulate prostaglandin synthesis in fertilized eggs. Continued prostaglandin production in embryos might disturb positional information (i.e. the maintenance of a gradient in the uterus), a model supported by sperm guidance data. Consistent with this model, RNAi mosaic studies suggest that CYP-31A2 acts in the germ line, not the somatic gonad (Kubagawa et al., 2006). In addition to sperm guidance, CYP-31A2 promotes formation of the permeability barrier in fertilized eggs (Olson et al., 2012). This barrier is thought to consist of long chain fatty acids conjugated to sugars and prevents the entry and exit of small molecules (< 3,000 Da) (Olson et al., 2012). Hence, CYP-31A2 might act after fertilization to divert PUFAs away from prostaglandin synthesis to permeability barrier formation. The permeability barrier could also prevent prostaglandins from being secreted into the extracellular environment.

Prostaglandins as conserved sperm guidance cues?

Outside of aquatic species, little is known regarding the mechanisms that guide sperm to oocytes. Human sperm are thought to receive multiple signals that guide them to cumulus-enclosed oocytes, which lie in the highly arborized lumen of the oviduct (Eisenbach and Giojalas, 2006; Lishko et al., 2012; Teves et al., 2009). Recent studies have documented that progesterone and prostaglandins bind to CatSper (Brenker et al., 2012; Lishko et al., 2011; Strunker et al., 2011), a sperm Ca^{2+} channel implicated in hyperactivation and chemotaxis (Quill et al., 2001; Ren et al., 2001). $PGF_{1\propto}$ and PGE_1

activate CatSper at physiological concentrations, suggesting that these interactions are functional (Brenker et al., 2012; Lishko et al., 2011). Although the role of prostaglandins is not entirely clear, they are synthesized by cumulus-oocyte complexes and affect sperm motility *in vitro* (Aitken and Kelly, 1985; Gottlieb et al., 1988; Schuetz and Dubin, 1981). Thus, an attractive scenario is that prostaglandins provide positional information to both human and worm sperm. While there are obvious differences between *C. elegans* and human reproductive systems, it is possible that some molecular features are shared. Delineating shared versus divergent mechanisms should lead to better understanding of those that are fundamental to animal reproduction.

In summary, we show that a heterogeneous mixture of structurally related F-series prostaglandins promotes sperm guidance in *C. elegans*. Prostaglandin synthesis does not involve conventional cyclooxygenase pathways, yet $PGF_{1\propto}$ and $PGF_{2\propto}$ stereoisomers are still generated. Furthermore, conserved enzymes such as cytochrome P450s regulate prostaglandin synthesis. The *C. elegans* model could provide unanticipated insight into the mechanisms and actions of prostaglandins, which are among the most widespread and important signaling molecules in metazoans.

MATERIALS AND METHODS

C. elegans strains, culture, and RNA-mediated interference

C. elegans were maintained at 20°C, unless otherwise indicated, and fed with NA22 *E. coli* bacteria, as previously described (Edmonds et al., 2010; Kubagawa et al., 2006). The *fog-2(q71)* strain was used for males. The following strains were used: *N2* Bristol (wild type), BX24 [*fat-1(wa9) IV*], BX26 [*fat-2(wa17) IV*], BX30 [*fat-3(wa22) IV*], BX17 [*fat-4(wa14) IV*], BX52 [*fat1(wa9) fat-4(wa14) IV*], SS104 [*glp-4(bn2) I*], *cyp-31A2(tm2711) IV, cyp-*

31A3(tm3224) IV, and CB4108 [*fog-2(q71) V*]. The *cyp-31A2(tm2711)* and *cyp-31A3(tm3224)* mutants were provided by the Japanese National Bioresource Project. The *cyp-31A2(tm2711)* strain was backcrossed to the wild type three times. RNAi was performed by the feeding method (Timmons and Fire, 1998). HT115 bacterial strains were obtained from the feeding library (Kamath and Ahringer, 2003) and sequenced for verification. Wild-type and *glp-4(bn2)* mutant hermaphrodites were grown at 16°C and synchronized to the L1 stage using an egg preparation with minor modifications (Porta-de-la-Riva et al., 2012). The larva were shifted to 25°C and cultured for 2-3 days. For prostaglandin analyses, strains were grown on up to sixty-five 150 mm seeded plates, as previously described (Edmonds et al., 2011; Edmonds et al., 2010). Cultures were supplemented with concentrated bacteria as needed to prevent starvation. Worms were washed off plates with M9 buffer, collected in polypropylene tubes, and stored at -80°C for lipid extraction. Tissue was weighed to ensure that equal amounts were analyzed.

Sperm guidance assays

MitoTracker Red CMXRos (Invitrogen) was used to stain *fog-2(q71)* males, as previously described (Edmonds et al., 2010; Kubagawa et al., 2006). Briefly, about 150 male worms were transferred to a watch glass with 300 µl M9 buffer. Three microliters of a 1 mM MitoTracker CMXRos solution in DMSO was added to the worm solution and mixed. Males were incubated in the dark for 2-3 hours and then transferred to a seeded plate. After 20 minutes, the males were transferred again to a fresh plate and allowed to recover overnight at 16°C. 10-20 ~2 day old adult hermaphrodites were anesthetized with 0.1% tricaine and 0.01% tetramisole hydrochloride in M9 buffer for 30 minutes (McCarter et al.,

1999). The anesthetized hermaphrodites were transferred to a plate containing an ~1 cm drop of bacteria with 50-75 stained males. After 30 minutes of mating, the hermaphrodites were separated from the males and transferred to a fresh seeded plate. To directly observe sperm motility, mated hermaphrodites were mounted immediately onto a 2% agarose pad for time-lapse fluorescence microscopy. DIC and fluorescence images were taken every 30 seconds. Directional velocity toward the spermatheca was measured by creating a straight line through the uterus from the vulva to the spermatheca. The distance traveled along this line from the beginning of a sperm trace to the end was divided by time. Positive values indicate movement toward the spermatheca relative to the starting point. A change in migration direction of greater than 90° within 3 consecutive frames was classified as a reversal. Sperm traces range from a minimum of 2.5 minutes to a maximum of 21 minutes. At least 3 videos from different animals were used for quantification.

To assess sperm distribution, mated hermaphrodites were incubated in the dark for an hour without males and then mounted for microscopy. The reproductive tract was divided into 3 zones, as shown in Figure 1A. Zone 3 was defined as the region spanning the center of the spermatheca plus 50 microns toward the vulva. In cases where large sperm aggregations were adjacent to the spermatheca, zone 3 was expanded to include the entire aggregation. Zones 1 and 2 were defined by measuring the distance from the zone 3 border to the vulva and dividing this region in half. AxioVision software was used to measure distances. A two sample T-test was used to test for significance.

PUFA supplementation

AA or EPA containing plates were prepared as previously described (Kubagawa et al., 2006). Briefly, PUFAs were added slowly to cooled media containing 0.1% NP-40. The

final PUFA concentration was 200 µM. Plates were kept in the dark at room temperature for 24 hours and then seeded with NA22 *E. coli* bacteria. Plates were incubated in the dark at room temperature for 3 days. NA22 bacteria accumulate PUFAs in their lipids at ranges from 1-5% (Kubagawa et al., 2006).

Lipid extraction

For lipid extraction, 2.0 grams of synchronized adult worms or 6.0 grams of mixed-staged worms were used. Hydrophilic lipids were extracted from frozen worm pellets using a liquid-liquid extraction technique (Golovko and Murphy, 2008). Briefly, frozen worms were resuspended with 12 ml of ice cold acetone/saline containing 0.005% butylated hydroxytoluene (BHT) to prevent oxidation. Worms were evenly dispersed into twelve 5 ml self-standing plastic tubes for use in the Bullet Blender 5 homogenizer (Next Advance). 0.7-0.8 ml of 0.5 mm diameter Ceria stabilized zirconium oxide beads were added to each tube and the Bullet Blender was set to speed 8 for 2-4 minutes. Homogenization efficiency was checked on a microscope slide. The homogenates were evenly transferred to four 10 ml conical glass tubes. The beads were washed with 4 ml of 1:2 acetone/saline containing BHT and the wash solution was evenly transferred into the four 10 ml glass tubes. These tubes were centrifuged at 4°C in a clinical centrifuge for 10 minutes at 1000 RCF. The supernatants were transferred to four clean 10 ml conical glass tubes. An equivalent volume of hexane was added to each tube and the tubes were vortexed for 30 seconds. The glass tubes were then centrifuged at 4°C for 10 minutes at 1000 RCF. The upper hexane phase and white debris in the interphase were removed. The lower aqueous phase was acidified to pH 3.5 using 2M formic acid. An equal volume of chloroform was added to each tube.

Next, the tubes were vortexed for 30 seconds and centrifuged at 4°C for 10-15 minutes at 1000 RCF. The lower organic phases from four 10 ml glass tubes were transferred to a clean 15 ml conical tube. The extract was flushed with nitrogen gas and stored at -20°C for at least 24 hours. Next, the aqueous top layer was removed and the organic phase containing prostaglandins was evaporated in a Teflon-lined capped ½-Dram glass vial under a gentle stream of nitrogen gas. The dried lipids were stored at -20°C for up to 2 weeks. For mass spectrometry analysis, the dried extract was dissolved in 200 µl of 80% methanol. For the synchronized adult preps containing 2 grams tissue, the dried extracts were dissolved in 60 µl of 80% methanol to increase prostaglandin concentration.

Mouse heart, lung, kidney, and liver were dissected from eight month old black 6 mice (C57BL/6J). The tissue was immediately frozen in a dry ice bath and stored at -80°C. The tissue weights were 0.50 g heart, 0.41 g lung, 1.04 g kidney, and 1.79 g liver. Liquid/liquid extraction was performed as described above with the following exception: 0.8 ml of 2.0 mm diameter Ceria stabilized zirconium oxide beads and Bullet Blender speed 9 (5 min) were used for homogenization.

Chromatography and Mass spectrometry

LC-MS/MS analyses of commercial standards and tissue extracts were performed as previously described (Edmonds et al., 2011; Edmonds et al., 2010) using a system consisting of a Shimadzu Prominence HPLC with a refrigerated auto sampler (Shimadzu Scientific Instruments, Inc., Columbia, MD) and an API 4000 (Applied Biosystems/MDS Sciex, Concord, Ontario, Canada) triple quadrupole mass spectrometer. The chromatographic separation was performed on a Synergy hydro RP-C18 column pre-

equilibrated with 0.1% formic acid. The mobile phase consists of 0.1% formic acid [A] and acetonitrile containing 0.1% formic acid [B] and was pumped at a flow rate of 0.2 ml/min. The gradient started with 10% B and went up to 80% B from 0-11 min, 80-100% B from 11-14 min and returned back to 10% B at 16 min. The column effluent was introduced into the mass spectrometer using an ESI interface operating in negative ion mode. Nitrogen was used as a nebulizer and curtain gas (CUR = 10). The collision gas, collision energy and temperature were set at 10, -35 eV and 600°C, respectively. The LC-MS/MS system was controlled by BioAnalyst 1.4.2 software. For comparative analysis of different strains, the extracts and standards were run consecutively.

To determine CePGF2 concentration, a stock solution of $PGF_{2\alpha}$ (1 µg/ml in 80% MeOH) was serially diluted with the same solvent to obtain 1000, 100, 10, 1, 0.1 ng/ml concentrations. The samples were analyzed by the MRM method. The standard curve exhibited excellent linearity in the range of concentration 0.1-1000 ng/ml with a correlation coefficient >0.99. Average CePGF2 concentration was calculated from three MRM analyses using two independent sample extractions.

Separation of $PGF_{2\alpha}$ stereoisomers that co-elute in reverse-phase liquid chromatography was achieved by following a previously published method with modification (Yin et al., 2007b). Separation was carried out on a ChiralPak AD-H column (4.6 mm x 250 mm, 5 m, Chiral Technologies, Exton, PA) with 12.5% ethyl alcohol and 12.5% isopropyl alcohol in hexane containing 0.1% formic acid at 1 ml/min. MRM was carried out in atmospheric pressure chemical ionization (APCI) negative ion mode with mass transition *m/z* 353/193. The instrument conditions were optimized with the collision gas, collision energy and temperature were set at 10, -35 eV and 450°C, respectively.

ACKNOWLEDGMENTS

We thank Inga Kadish, Ulrika Beitnere, and Thomas van Groen for help with mouse dissections, Sung Min Han and Se-Jin Lee for comments on the manuscript, and Ray Moore for technical support. We also thank the UAB Targeted Metabolomics and Proteomics Laboratory, the *Caenorhabditis* Genetics Center, and the Japanese National Bioresource Project.

REFERENCES

1. Evans JP, Florman HM (2002) The state of the union: the cell biology of fertilization. Nat Cell Biol 4 Suppl: s57-63.

2. Marcello MR, Singaravelu G, Singson A (2013) Fertilization. Adv Exp Med Biol 757: 321-350.

3. Gadella BM, Evans JP (2011) Membrane fusions during mammalian fertilization. Adv Exp Med Biol 713: 65-80.

4. Han SM, Cottee PA, Miller MA (2010) Sperm and oocyte communication mechanisms controlling C. elegans fertility. Dev Dyn 239: 1265-1281.

5. Kaupp UB, Kashikar ND, Weyand I (2008) Mechanisms of sperm chemotaxis. Annu Rev Physiol 70: 93-117.

6. Guerrero A, Wood CD, Nishigaki T, Carneiro J, Darszon A (2010) Tuning sperm chemotaxis. Biochem Soc Trans 38: 1270-1274.

7. Chang H, Suarez SS (2010) Rethinking the relationship between hyperactivation and chemotaxis in mammalian sperm. Biol Reprod 83: 507-513.

8. Eisenbach M, Giojalas LC (2006) Sperm guidance in mammals - an unpaved road to the egg. Nat Rev Mol Cell Biol 7: 276-285.

9. Lishko PV, Botchkina IL, Kirichok Y (2011) Progesterone activates the principal Ca2+ channel of human sperm. Nature 471: 387-391.

10. Strunker T, Goodwin N, Brenker C, Kashikar ND, Weyand I, et al. (2011) The CatSper channel mediates progesterone-induced Ca2+ influx in human sperm. Nature 471: 382-386.

11. Teves ME, Guidobaldi HA, Unates DR, Sanchez R, Miska W, et al. (2009) Molecular mechanism for human sperm chemotaxis mediated by progesterone. PloS One 4: e8211.

12. Brenker C, Goodwin N, Weyand I, Kashikar ND, Naruse M, et al. (2012) The CatSper channel: a polymodal chemosensor in human sperm. EMBO J 31: 1654-1665.

13. Schuetz AW, Dubin NH (1981) Progesterone and prostaglandin secretion by ovulated rat cumulus cell-oocyte complexes. Endocrinology 108: 457-463.

14. L'Hernault SW (2009) The genetics and cell biology of spermatogenesis in the nematode C. elegans. Mol Cell Endocrinol 306: 59-65.

15. Stanfield GM, Villeneuve AM (2006) Regulation of sperm activation by SWM-1 is required for reproductive success of C. elegans males. Curr Biol 16: 252-263.

16. Kim S, Spike C, Greenstein D (2013) Control of Oocyte Growth and Meiotic Maturation in Caenorhabditis elegans. Adv Exp Med Biol 757: 277-320.

17. Hill KL, L'Hernault SW (2001) Analyses of reproductive interactions that occur after heterospecific matings within the genus Caenorhabditis. Dev Biol 232: 105-114.

18. Kubagawa HM, Watts JL, Corrigan C, Edmonds JW, Sztul E, et al. (2006) Oocyte signals derived from polyunsaturated fatty acids control sperm recruitment in vivo. Nat Cell Biol 8: 1143-1148.

19. Ward S, Carrel JS (1979) Fertilization and sperm competition in the nematode Caenorhabditis elegans. Dev Biol 73: 304-321.

20. Edmonds JW, Prasain JK, Dorand D, Yang Y, Hoang HD, et al. (2010) Insulin/FOXO signaling regulates ovarian prostaglandins critical for reproduction. Dev Cell 19: 858-871.

21. Edmonds JW, McKinney SL, Prasain JK, Miller MA (2011) The gap junctional protein INX-14 functions in oocyte precursors to promote C. elegans sperm guidance. Dev Biol 359: 47-58.

22. Funk CD (2001) Prostaglandins and leukotrienes: advances in eicosanoid biology. Science 294: 1871-1875.

23. Burr GO, Burr MM (1929) A new deficiency disease produced by the rigid exclusion of fat from the diet. J Biol Chem 82: 345-367.

24. Burr GO, Burr MM (1930) On the nature and role of the fatty acids essential for nutrition. J Biol Chem 86: 587-621.

25. Vane JR, Bakhle YS, Botting RM (1998) Cyclooxygenases 1 and 2. Annu Rev Pharmacol Toxicol 38: 97-120.

26. Wathes DC, Abayasekara DR, Aitken RJ (2007) Polyunsaturated fatty acids in male and female reproduction. Biology of reproduction 77: 190-201.

27. Bergstrom S, Danielsson H, Klenberg D, Samuelsson B (1964) The enzymatic conversion of essential fatty acids into prostaglandins. J Biol Chem 239: PC4006-4008.

28. Hamberg M, Samuelsson B (1967) On the mechanism of the biosynthesis of prostaglandins E-1 and F-1-alpha. J Biol Chem 242: 5336-5343.

29. Watanabe K (2002) Prostaglandin F synthase. Prostaglandins Other Lipid Mediat 68-69: 401-407.

30. Milne GL, Yin H, Morrow JD (2008) Human biochemistry of the isoprostane pathway. J Biol Chem 283: 15533-15537.

31. Watts JL (2009) Fat synthesis and adiposity regulation in Caenorhabditis elegans. Trends Endocrinol Metab 20: 58-65.

32. Watts JL, Browse J (2002) Genetic dissection of polyunsaturated fatty acid synthesis in Caenorhabditis elegans. Proc Natl Acad Sci U S A 99: 5854-5859.

33. Kahn-Kirby AH, Dantzker JL, Apicella AJ, Schafer WR, Browse J, et al. (2004) Specific polyunsaturated fatty acids drive TRPV-dependent sensory signaling in vivo. Cell 119: 889-900.

34. Grant B, Hirsh D (1999) Receptor-mediated endocytosis in the Caenorhabditis elegans oocyte. Mol Biol Cell 10: 4311-4326.

35. Beanan MJ, Strome S (1992) Characterization of a germ-line proliferation mutation in C. elegans. Development 116: 755-766.

36. Murphy RC, Barkley RM, Zemski Berry K, Hankin J, Harrison K, et al. (2005) Electrospray ionization and tandem mass spectrometry of eicosanoids. Anal Biochem 346: 1-42.

37. Masoodi M, Nicolaou A (2006) Lipidomic analysis of twenty-seven prostanoids and isoprostanes by liquid chromatography/electrospray tandem mass spectrometry. Rapid Commun Mass Spectrom 20: 3023-3029.

38. Kingsley PJ, Rouzer CA, Saleh S, Marnett LJ (2005) Simultaneous analysis of prostaglandin glyceryl esters and prostaglandins by electrospray tandem mass spectrometry. Anal Biochem 343: 203-211.

39. Watts JL, Browse J (2000) A palmitoyl-CoA-specific delta9 fatty acid desaturase from Caenorhabditis elegans. Biochem Biophys Res Commun 272: 263-269.

40. Waugh RJ, Morrow JD, Roberts LJ, 2nd, Murphy RC (1997) Identification and relative quantitation of F2-isoprostane regioisomers formed in vivo in the rat. Free Radic Biol Med 23: 943-954.

41. Benenati G, Penkov S, Muller-Reichert T, Entchev EV, Kurzchalia TV (2009) Two cytochrome P450s in Caenorhabditis elegans are essential for the organization of eggshell, correct execution of meiosis and the polarization of embryo. Mech Dev 126: 382-393.

42. Olson SK, Greenan G, Desai A, Muller-Reichert T, Oegema K (2012) Hierarchical assembly of the eggshell and permeability barrier in C. elegans. J Cell Biol 198: 731-748.

43. Hsu MH, Savas U, Griffin KJ, Johnson EF (2007) Human cytochrome p450 family 4 enzymes: function, genetic variation and regulation. Drug Metab Rev 39: 515-538.

44. Yin H, Gao L, Tai HH, Murphey LJ, Porter NA, et al. (2007) Urinary prostaglandin F2alpha is generated from the isoprostane pathway and not the cyclooxygenase in humans. The Journal of biological chemistry 282: 329-336.

45. Whitten SJ, Miller MA (2007) The role of gap junctions in Caenorhabditis elegans oocyte maturation and fertilization. Dev Biol 301: 432-446.

46. Yin H, Gao L, Tai HH, Murphey LJ, Porter NA, et al. (2007) Urinary prostaglandin F2alpha is generated from the isoprostane pathway and not the cyclooxygenase in humans. J Biol Chem 282: 329-336.

47. Li A, Jiao X, Munier FL, Schorderet DF, Yao W, et al. (2004) Bietti crystalline corneoretinal dystrophy is caused by mutations in the novel gene CYP4V2. Am J Hum Genet 74: 817-826.

48. Nakano M, Kelly EJ, Wiek C, Hanenberg H, Rettie AE (2012) CYP4V2 in Bietti's Crystalline Dystrophy: Ocular Localization, Metabolism of omega-3-Polyunsaturated Fatty Acids, and Functional Deficit of the p.H331P Variant. Mol Pharmacol 82: 679-686.

49. Kulas J, Schmidt C, Rothe M, Schunck WH, Menzel R (2008) Cytochrome P450-dependent metabolism of eicosapentaenoic acid in the nematode Caenorhabditis elegans. Arch Biochem Biophys 472: 65-75.

50. Lishko PV, Kirichok Y, Ren D, Navarro B, Chung JJ, et al. (2012) The control of male fertility by spermatozoan ion channels. Annu Rev Physiol 74: 453-475.

51. Ren D, Navarro B, Perez G, Jackson AC, Hsu S, et al. (2001) A sperm ion channel required for sperm motility and male fertility. Nature 413: 603-609.

52. Quill TA, Ren D, Clapham DE, Garbers DL (2001) A voltage-gated ion channel expressed specifically in spermatozoa. Proc Natl Acad Sci U S A 98: 12527-12531.

53. Aitken RJ, Kelly RW (1985) Analysis of the direct effects of prostaglandins on human sperm function. J Reprod Fertil 73: 139-146.

54. Gottlieb C, Svanborg K, Eneroth P, Bygdeman M (1988) Effect of prostaglandins on human sperm function in vitro and seminal adenosine triphosphate content. Fertil Steril 49: 322-327.

55. Timmons L, Fire A (1998) Specific interference by ingested dsRNA. Nature 395: 854.

56. Kamath RS, Ahringer J (2003) Genome-wide RNAi screening in Caenorhabditis elegans. Methods 30: 313-321.

57. Porta-de-la-Riva M, Fontrodona L, Villanueva A, Ceron J (2012) Basic Caenorhabditis elegans methods: synchronization and observation. J Vis Exp: e4019.

58. McCarter J, Bartlett B, Dang T, Schedl T (1999) On the control of oocyte meiotic maturation and ovulation in Caenorhabditis elegans. Dev Biol 205: 111-128.

59. Golovko MY, Murphy EJ (2008) An improved LC-MS/MS procedure for brain prostanoid analysis using brain fixation with head-focused microwave irradiation and liquid-liquid extraction. J Lipid Res 49: 893-902.

FIGURES

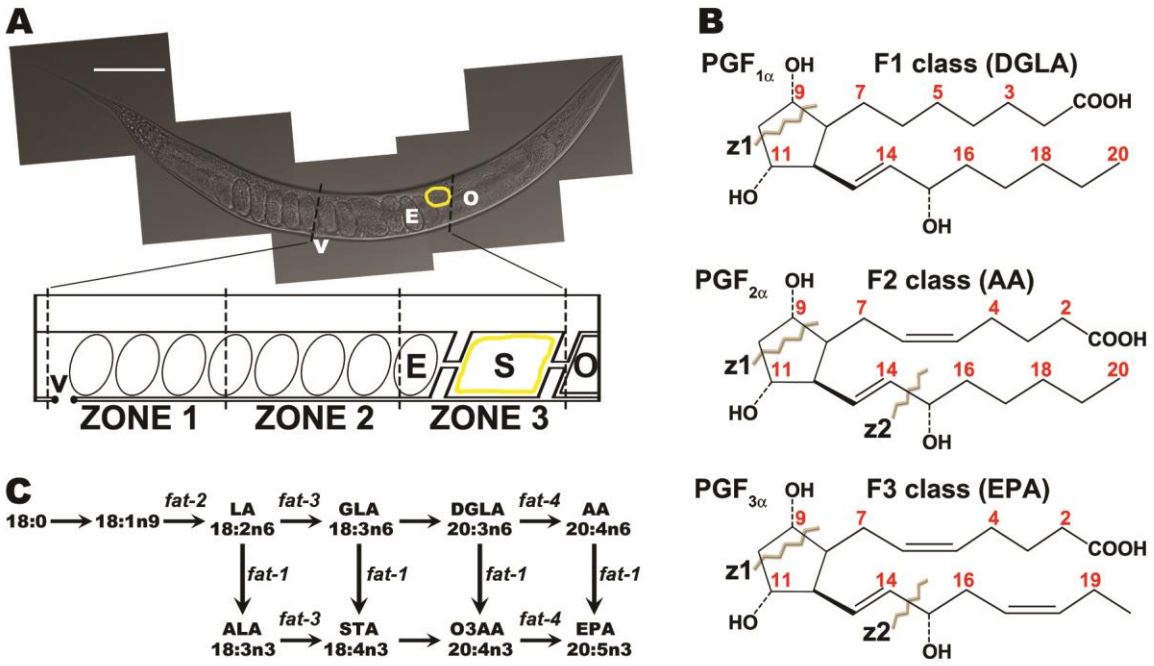

Figure 1. *C. elegans* gonad, F-series prostaglandin structures, and PUFA metabolism pathways.

(A) The *C. elegans* hermaphrodite reproductive tract. A differential interference contrast (DIC) image of an adult hermaphrodite is shown above with a diagram of half the uterus below. Males inject sperm through the vulva (V) into the uterus. Sperm become motile by extending a pseudopod and crawl around fertilized embryos (E) toward the spermatheca (S, yellow outline). Oocytes (O) enter the spermatheca during oocyte maturation and ovulation. The uterus is divided into 3 zones for quantification of sperm distribution. Scale bar, 0.1 mm.

(B) Human F-series prostaglandin structures showing carbon numbering and important energy-induced cleavage sites characteristic of F-series prostaglandins. z1 cleavage causes loss of 44 Da from the parent ion and z2 cleavage, together with methyl terminal loss, generates the product ion *m/z 193*. Prostaglandin precursors for each class are shown in

parentheses.

(C) Diagram of *C. elegans* PUFA synthesis pathways. Δ9 and Δ12 desaturase activities generate substrates for the n3 desaturase FAT-1, the Δ6 desaturase FAT-3, and the Δ5 desaturase FAT-4 (Watts, 2009). Fatty acids are abbreviated as in 20:4n6, which has 20 carbons with four double bonds, the first occurring at the n6 position. LA, linoleic acid; ALA, linolenic acid; GLA, γ-linolenic acid; STA, stearidonic acid; DGLA, dihomo-γ-linolenic acid; O3AA, omega-3 arachidonic acid; AA, arachidonic acid; EPA, eicosapentaenoic acid.

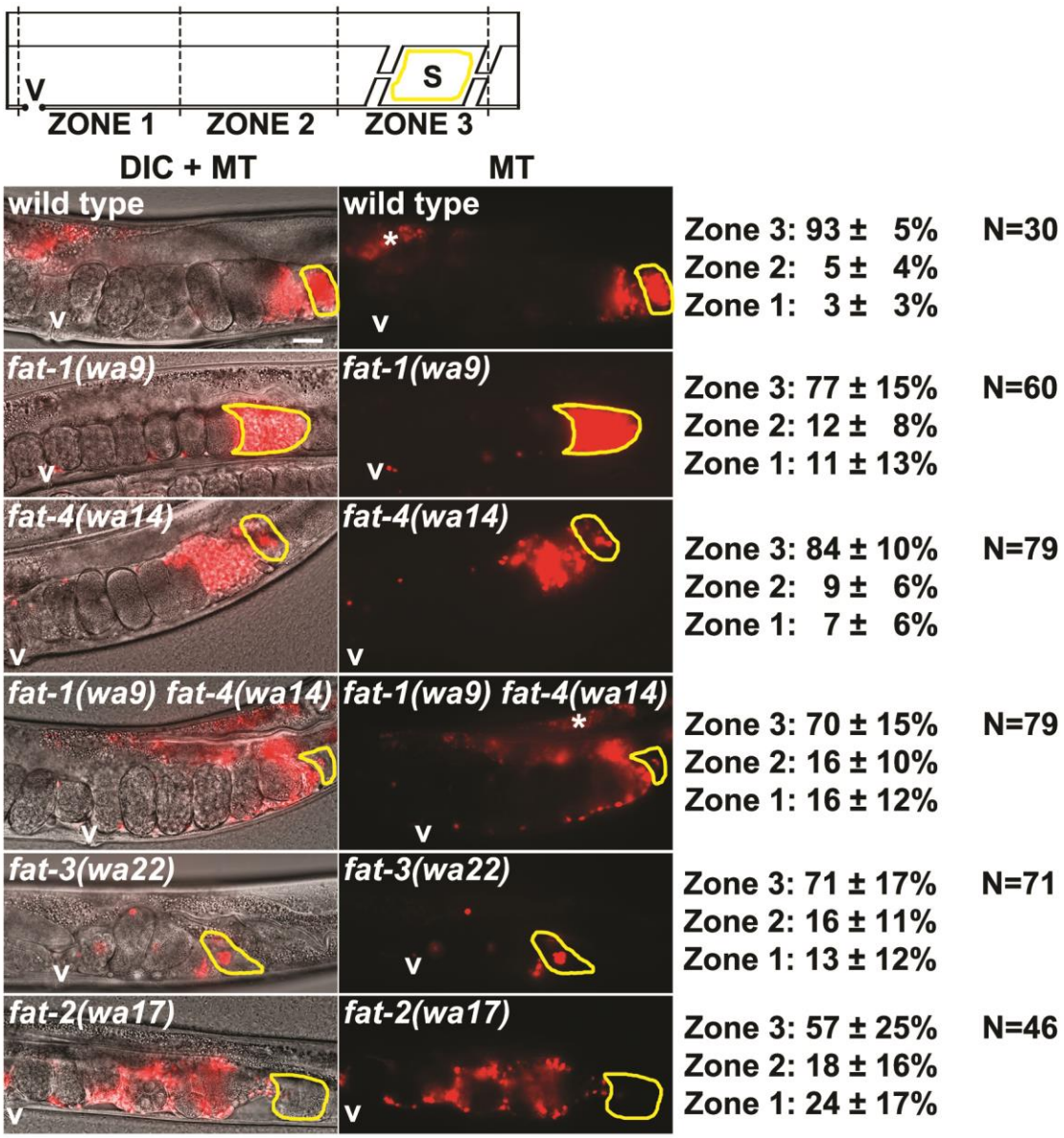

Figure 2. Sperm guidance in wild-type and *fat* mutant hermaphrodites.

Uterine sperm distribution 1 hr after mating wild-type or mutant hermaphrodites to wild-type males. A representative image is shown to the left and average zone distribution ± standard deviation is to the right. The spermatheca (S) is outlined in yellow. Asterisks indicate nonspecific gut autoflourescence. *fat-2* and *fat-3* mutants have reduced distance from vulva to spermatheca relative to the wild type, a feature that may influence

distribution values. MT, MitoTracker channel; N, number of gonads scored; V, vulva. Scale bar, 20 μm. See Materials and Methods for zone definitions.

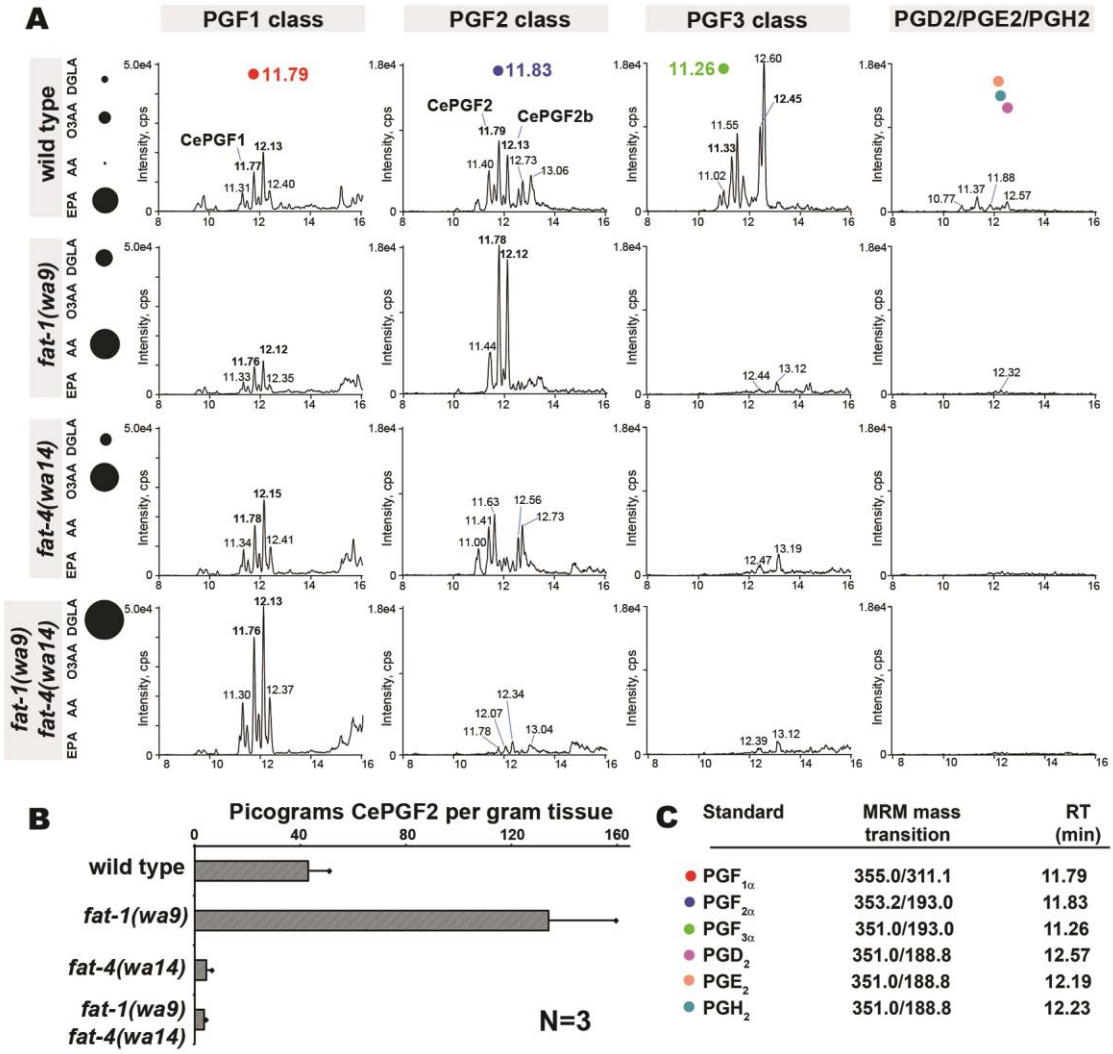

Figure 3. Prostaglandins in wild-type and *fat* mutant extracts.

(A) MRM chromatograms of wild-type and *fat* mutant extracts. Liquid chromatography retention time (min) is shown on the X-axis and for selected prostaglandin isomers. Bolded retention times indicate prostaglandin isomers shown in Figure 4. Prostaglandin standard retention times are shown at the top. The dot diagram to the left indicates relative PUFA levels in the corresponding strains (Kahn-Kirby et al., 2004). DGLA, dihomo-γ-linolenic acid; O3AA, omega-3 arachidonic acid; AA, arachidonic acid; EPA, eicosapentaenoic acid;

cps, counts per second.

(B) CePGF2 quantification in wild-type and *fat* mutant extracts. Error bars are SD.

(C) Summary of MRM mass transitions and retention times for chemically synthesized standards. RT, retention time.

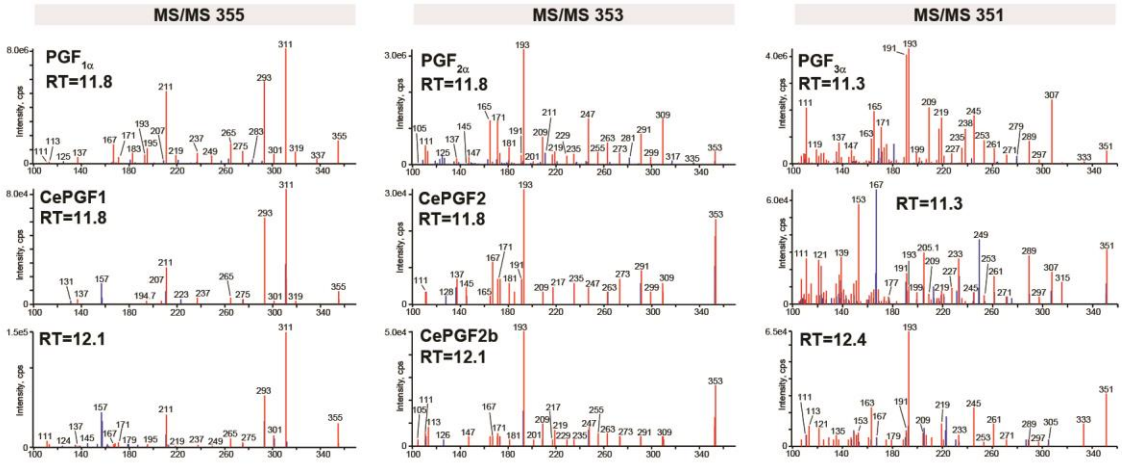

Figure 4. Collision induced decomposition patterns of selected *C. elegans* and human prostaglandins.

LC-MS/MS of authentic standards (top) compared to selected *C. elegans* prostaglandins highlighted in Figure 3A. Red color indicates ions shared by the standard and an unknown prostaglandin. Blue color indicates ions that are not shared. *m/z* is on the X-axis. *C. elegans* MS/MS data are from *fat-1(wa9) fat-4(wa14)* mutant extracts (F1 class), *fat-1(wa9)* extracts (F2 class), and wild-type extracts (F3 class). RT, retention time.

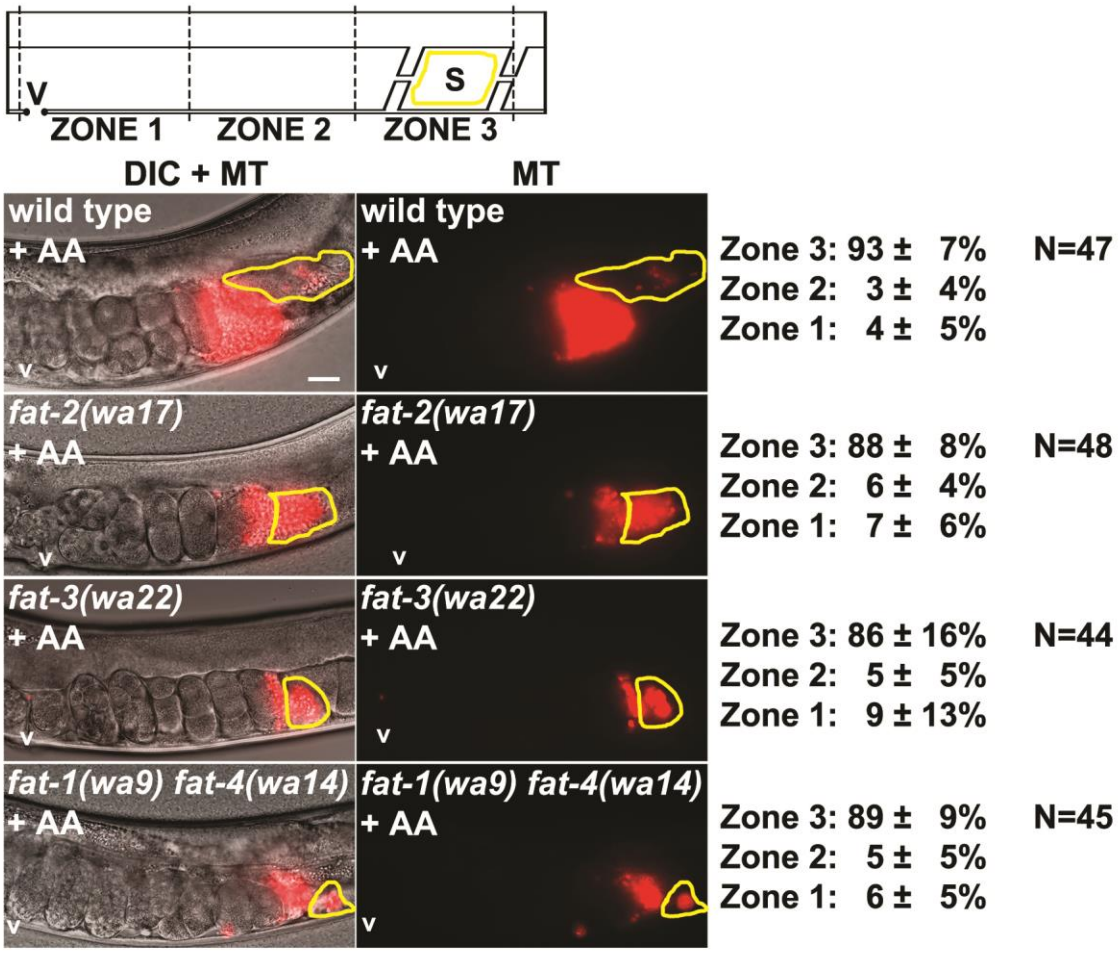

Figure 5. Effect of AA supplementation on sperm guidance in wild-type and *fat* mutant hermaphrodites.

Sperm distribution 1 hr after mating AA supplemented wild-type or mutant hermaphrodites to non-supplemented wild-type males. A representative image is shown to the left and average zone distribution ± standard deviation is to the right. See Figure 2 for sperm distribution in non-supplemented *fat* mutants. The spermatheca (S) is outlined in yellow. V, vulva; MT, MitoTracker channel; N, number of gonads scored. Scale bar, 20 µm.

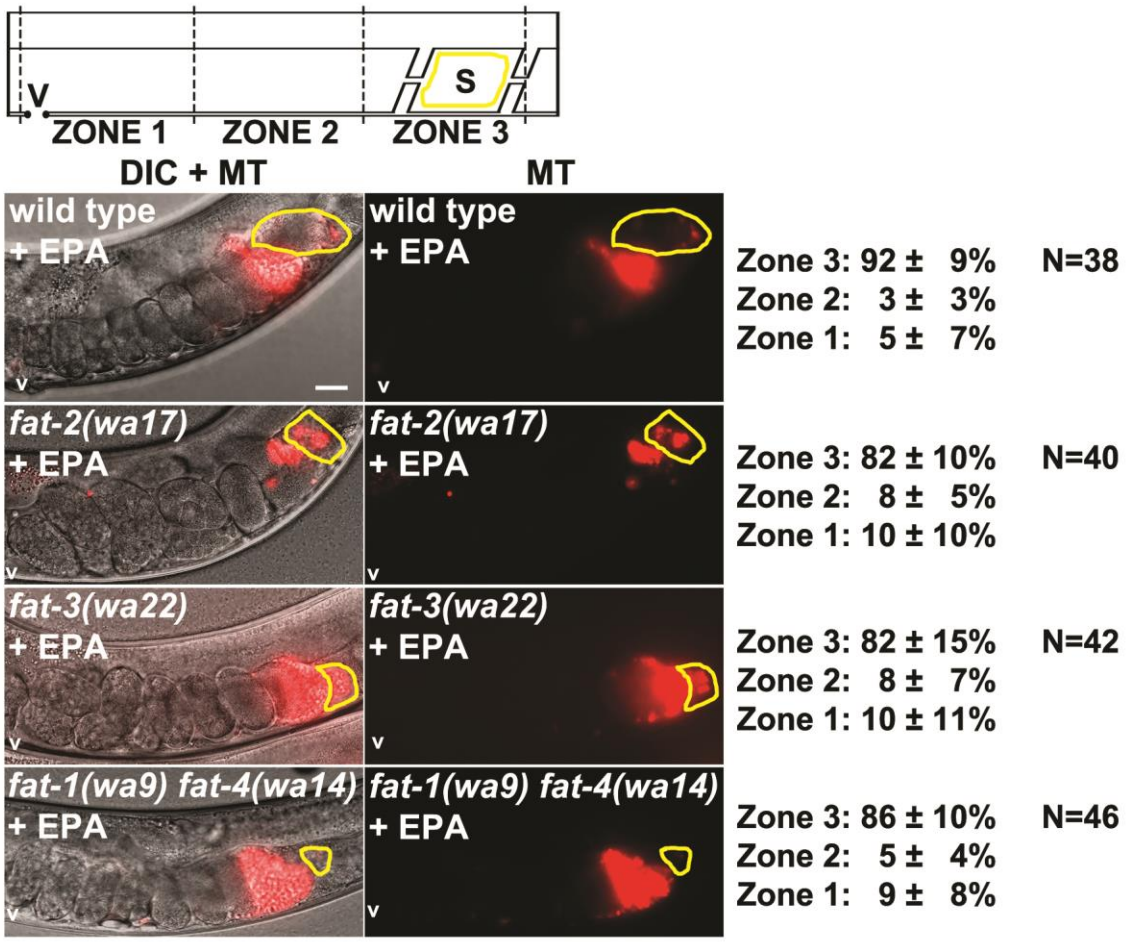

Figure 6. Effect of EPA supplementation on sperm guidance in wild-type and *fat* mutant hermaphrodites.

Sperm distribution 1 hr after mating EPA supplemented wild-type or mutant hermaphrodites to non-supplemented wild-type males. A representative image is shown to the left and average zone distribution ± standard deviation is to the right. See Figure 2 for sperm distribution in non-supplemented *fat* mutants. The spermatheca (S) is outlined in yellow. V, vulva; MT, MitoTracker channel; N, number of gonads scored. Scale bar, 20 µm.

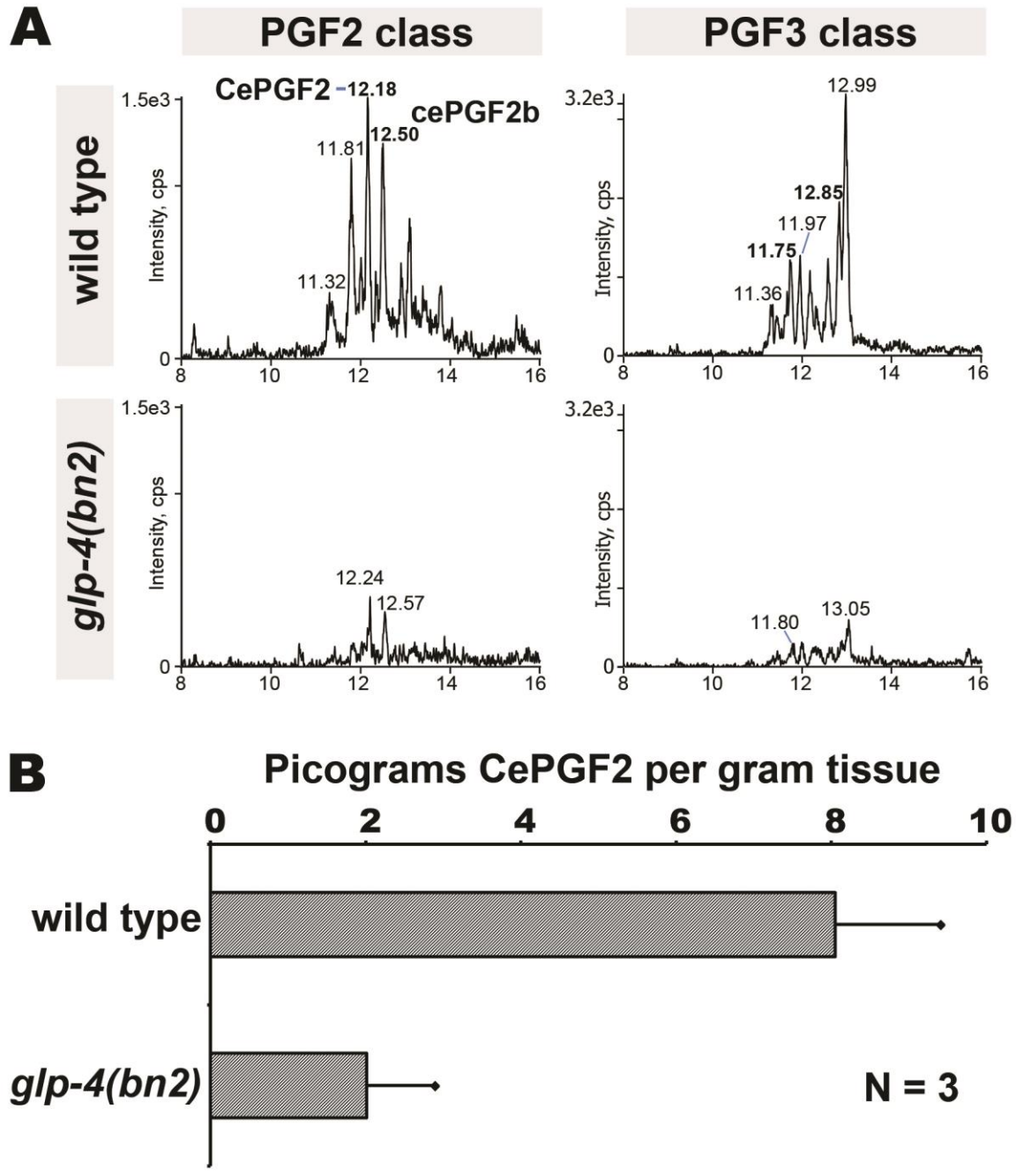

Figure 7. Prostaglandins in adult wild type and germline-deficient *glp-4* mutants.

(A) MRM chromatograms of synchronized 1-2 day adult wild-type and *glp-4(bn2)* mutants. The F2 class was detected with mass transition *m/z* 353/193 and the F3 class was detected with mass transition *m/z* 351/193. Liquid chromatography retention time (min) is shown on the X-axis and for selected prostaglandin isomers. Cps, counts per second.

(B) CePGF2 quantification in wild-type and *glp-4* mutant extracts. Error bars are SD.

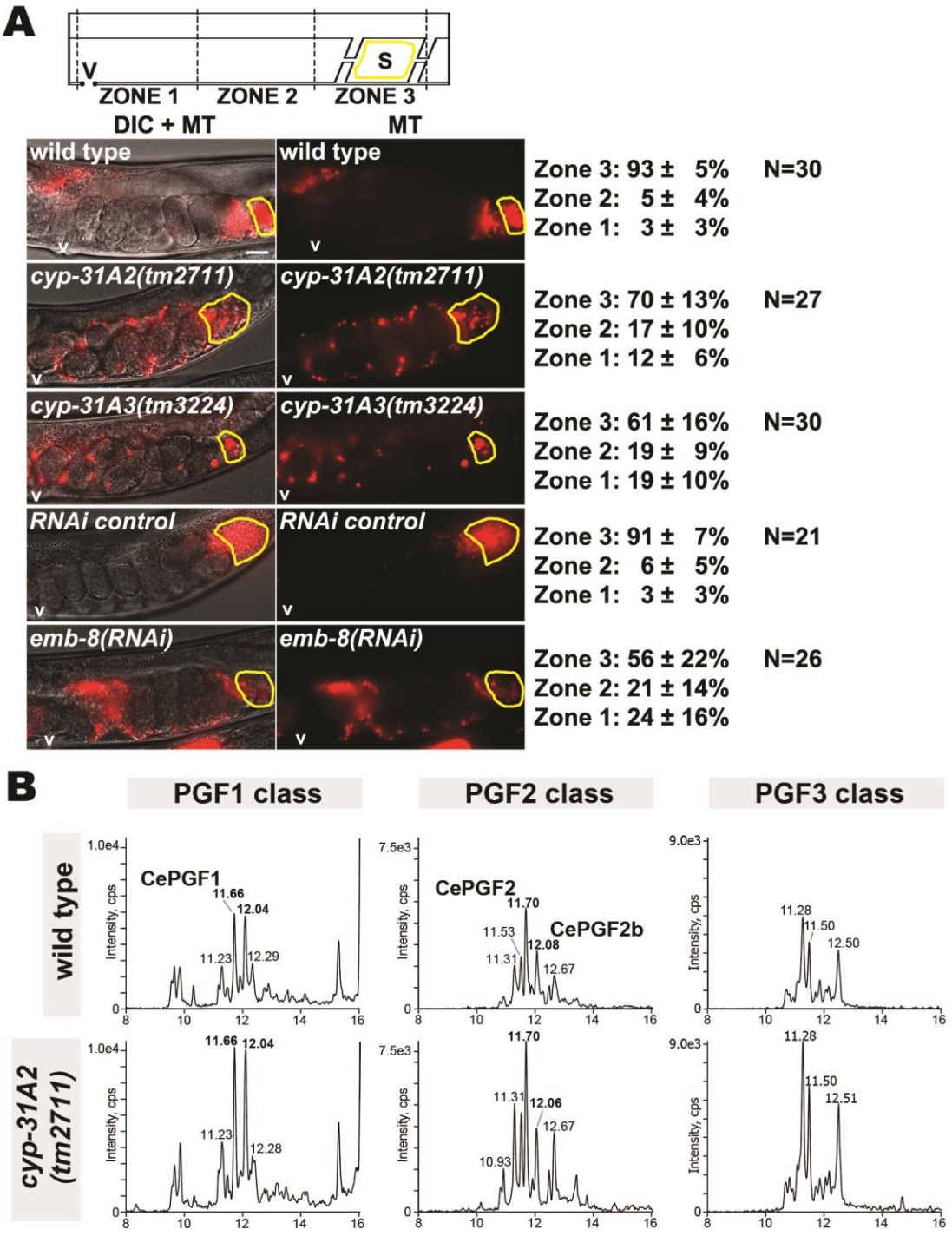

Figure 8. Effect of cytochrome P450 enzymes on sperm guidance and prostaglandin metabolism.

(A) Sperm distribution 1 hr after mating wild-type or mutant hermaphrodites to wild-type males. A representative image is shown to the left and average zone distribution ± standard

deviation is to the right. The spermatheca (S) is outlined in yellow. V, vulva; MT, MitoTracker channel; N, number of gonads scored. Scale bar, 20 μm.

(B) MRM chromatograms of wild-type and *cyp-32A2(tm2711)* mutants. The F1 class was detected with mass transition *m/z* 355/311, the F2 class was detected with mass transition *m/z* 353/193, and the F3 class was detected with mass transition *m/z* 351/191. Liquid chromatography retention time (min) is shown on the X-axis and for selected prostaglandin isomers. Cps, counts per second.

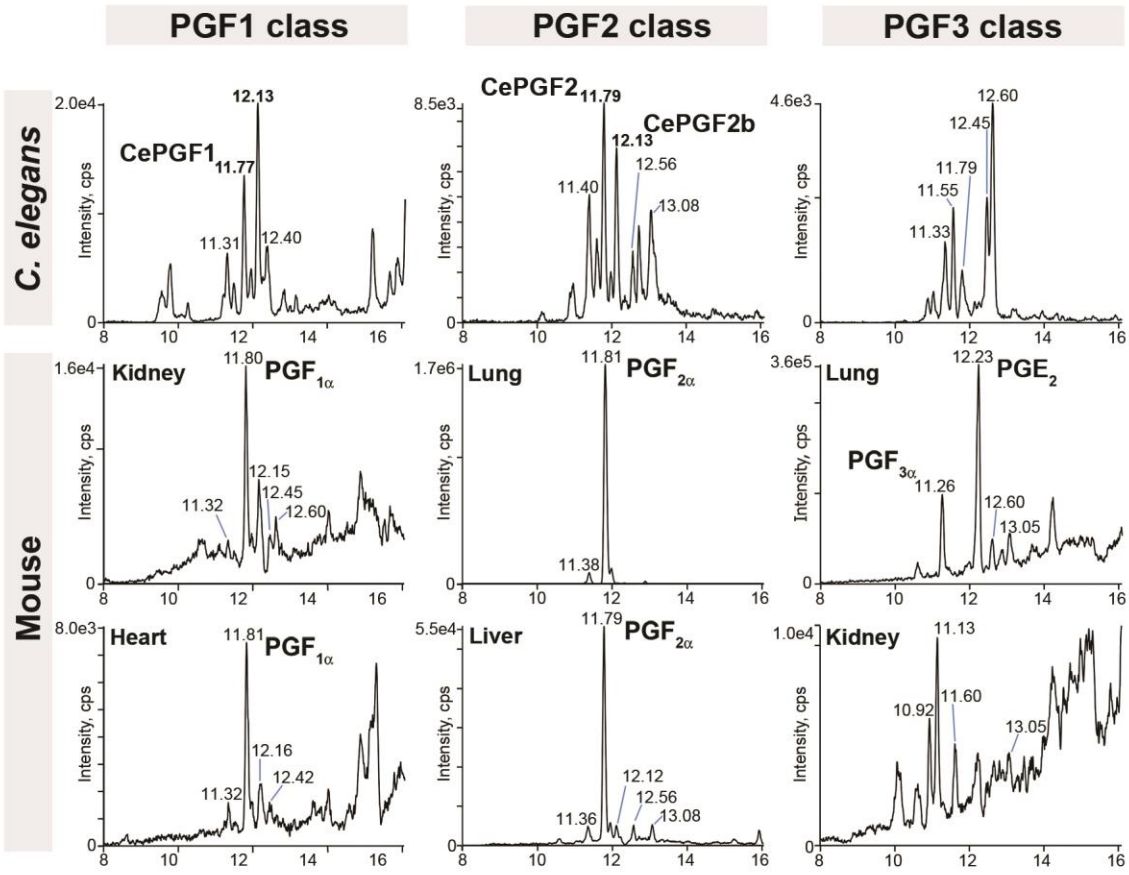

Figure 9. F-series prostaglandins in *C. elegans* and mouse tissues.

MRM chromatograms comparing F-series prostaglandins in *C. elegans* and mouse tissue extracts. The F1 class was detected with mass transition *m/z* 355/311, the F2 class was detected with mass transition *m/z* 353/193, and the F3 class was detected with mass transition *m/z* 351/193. Liquid chromatography retention time (min) is shown on the X-axis and for selected prostaglandin isomers. Cps, counts per second. The *C. elegans* MRM chromatograms are from Figure 3A. The mouse lung is extremely rich in PGE_2, which was detectable with mass transition *m/z* 351/193.

SUPPLEMENTARY FIGURES

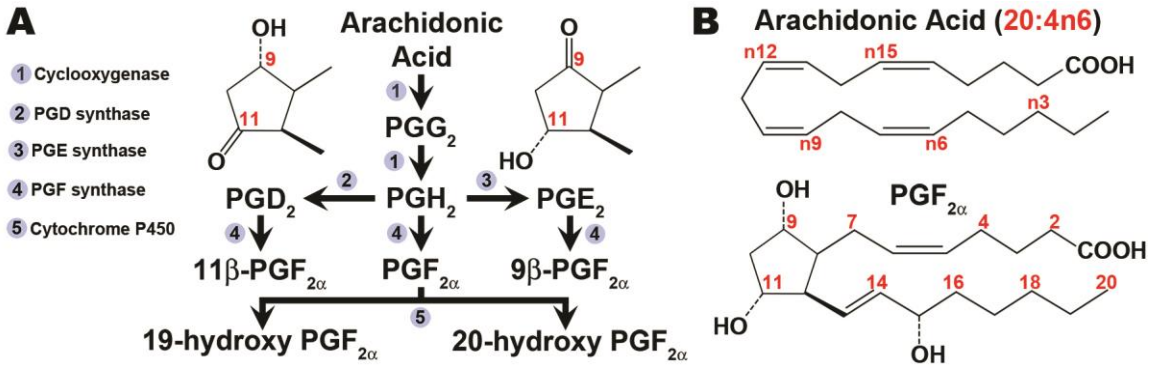

Figure S1. Mammalian F2 class prostaglandin synthesis.

(A) Cyclooxygenase-dependent pathways.

(B) Structures of arachidonic acid and $PGF_{2\alpha}$.

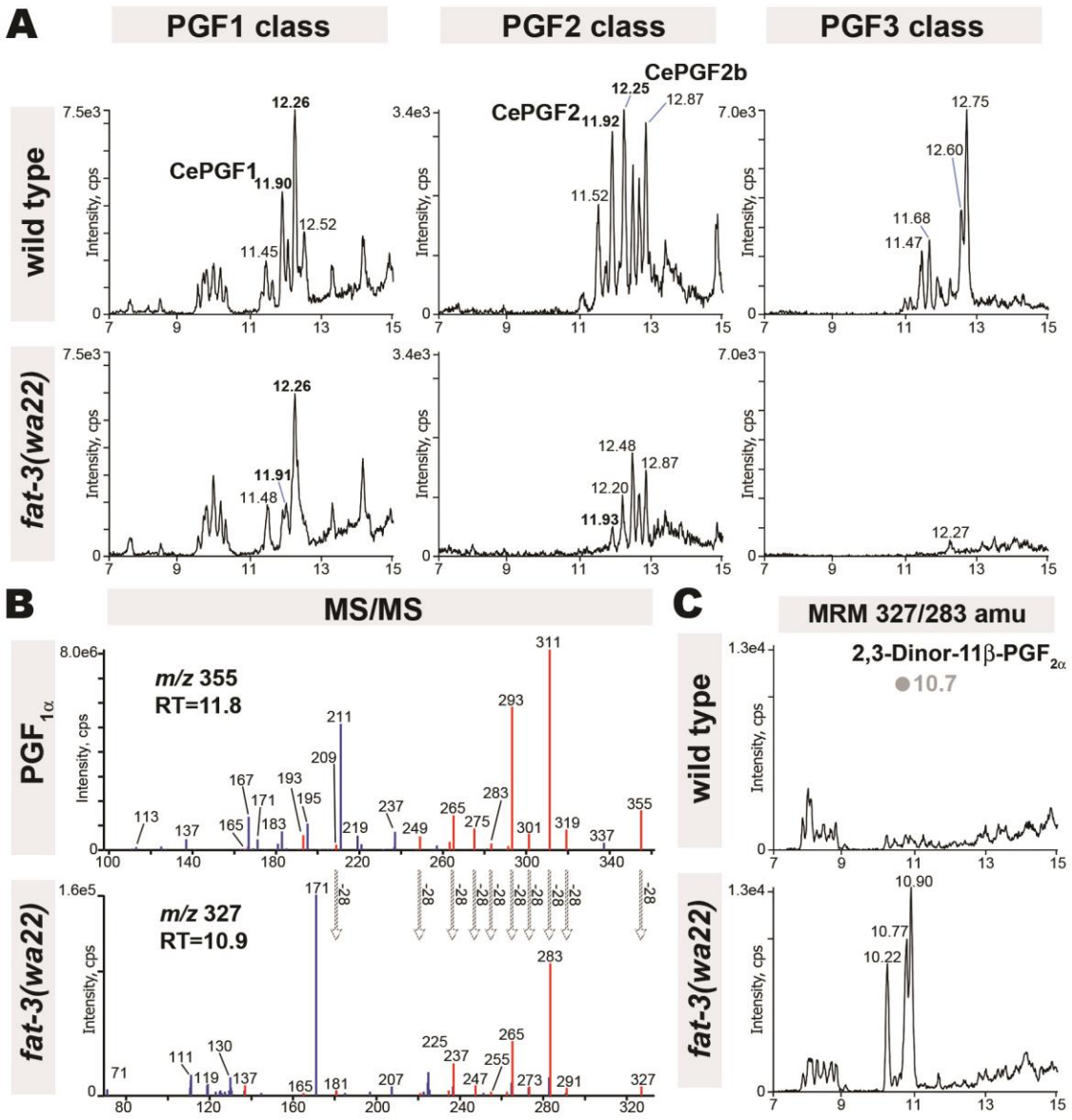

Figure S2. Prostaglandins in *fat-3* mutant.

(A) MRM chromatograms of wild-type and *fat-3(wa22)* mutant extracts. The F1 class was detected with mass transition *m/z* 355/311, the F2 class was detected with mass transition *m/z* 353/193, and the F3 class was detected with mass transition *m/z* 351/193. Liquid chromatography retention time (min) is shown on the X-axis and for major prostaglandin isomers. Cps, counts per second.

(B) LC-MS/MS of chemically synthesized $PGF_{1\alpha}$ compared to a putative F-series prostaglandin derived from 18:3n3 in *fat-3* mutant extracts. Red color indicates ions shared by the standard and the unknown prostaglandin, after subtracting the mass difference between DGLA and 18:3n3 (28 Da). Blue color indicates ions that are not shared. *m/z* is on the X-axis.

(C) MRM chromatograms of wild-type and *fat-3(wa22)* mutant extracts using the mass transition *m/z* 327/283. 2,3-Dinor-11β-$PGF_{2\alpha}$ is an 18-carbon $PGF_{2\alpha}$ metabolite.

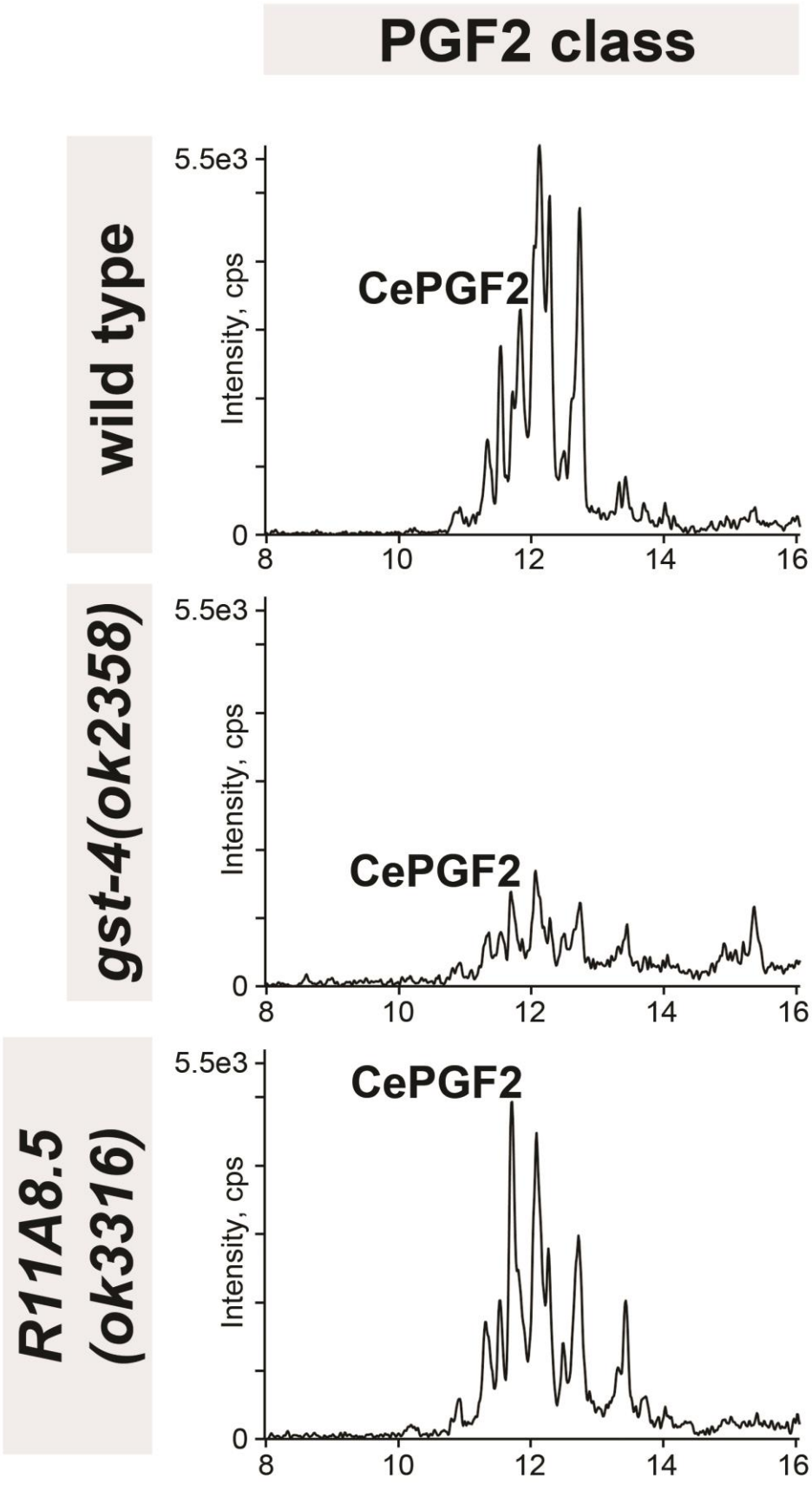
PGF2 class
wild type
gst-4(ok2358)
R11A8.5 (ok3316)
CePGF2
CePGF2
CePGF2
Intensity, cps
Intensity, cps
Intensity, cps
5.5e3
0
8
10
12
14
16

Figure S3. F2 class prostaglandins in *gst-4(ok2358)* and *R11A8.5(ok3316)* mutant extracts.

MRM chromatograms using the mass transition *m/z* 353/193. *gst-4* and *R11A8.5* encode glutathione S-transferases with sequence similarities to PGD and PGE synthases, respectively. Liquid chromatography retention time (min) is shown on the X-axis and for major prostaglandin isomers. Cps, counts per second.

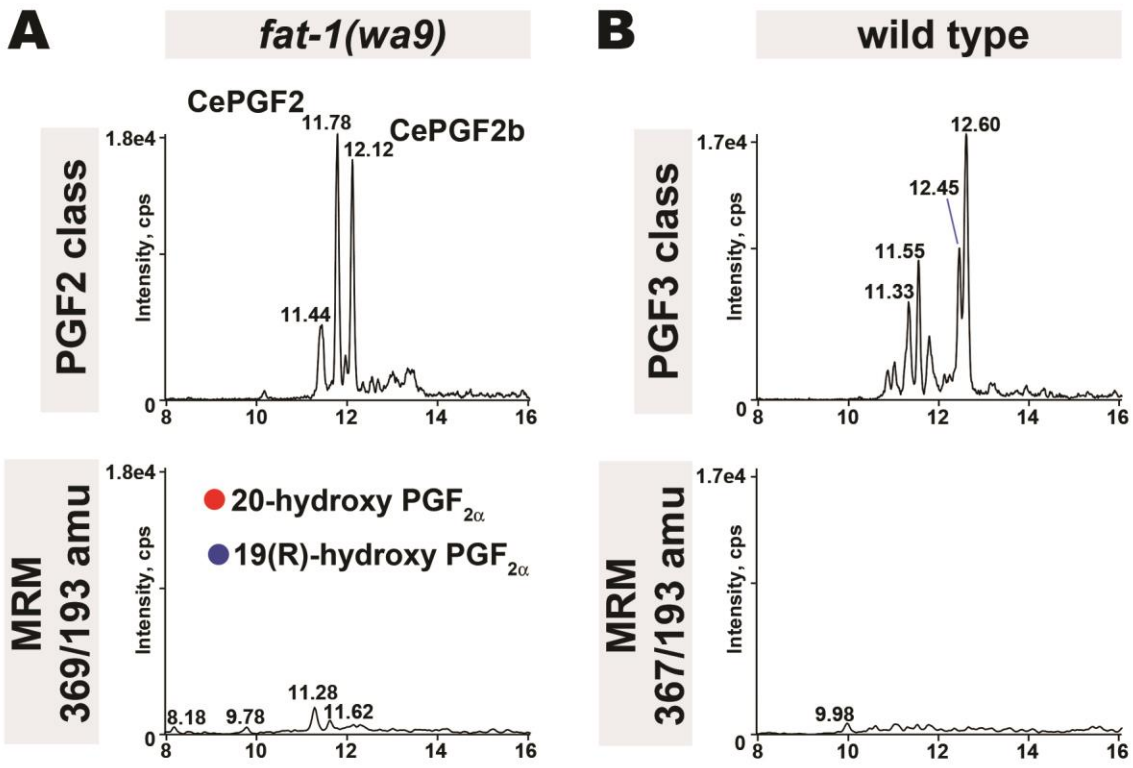

Figure S4. The $PGF_{2\alpha}$ enantiomer co-elutes with the predominant F2 class prostaglandin in *fat-1* mutant extracts using chiral chromatographic separation.

Normal phase chiral LC-APCI-MS/MS chromatograms operated in MRM with mass transition *m/z* 353/193. Chromatograms of chemically synthesized standards (top) and mixed staged *fat-1(wa9)* mutant extract (bottom) are shown.

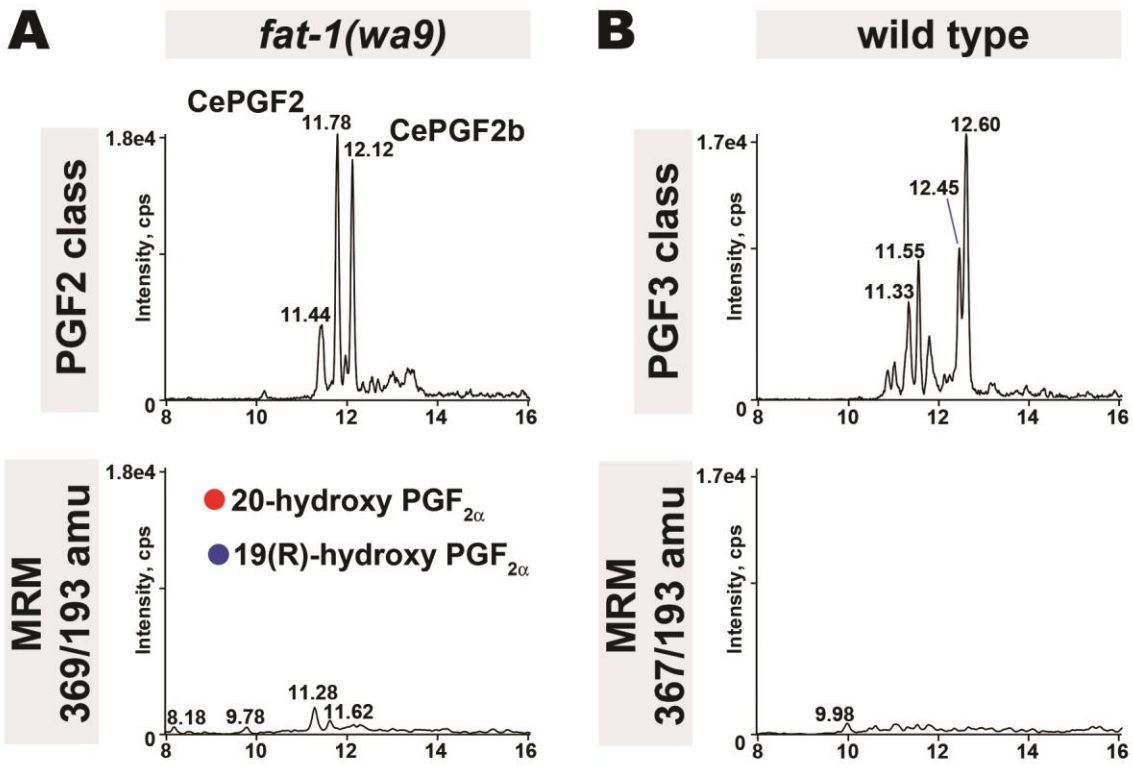

Figure S5. Absence of hydroxylated F-series prostaglandins in wild-type worm extracts.

(A) MRM chromatograms of mixed staged *fat-1(wa9)* mutant extracts. The mass transition *m/z* 353/193 was used to detect F2 class prostaglandins and mass transition *m/z* 369/193 was used to detect hydroxylated forms, such as 20-hydroxy $PGF_{2\alpha}$. Liquid chromatography retention time (min) is shown on the X-axis and for major prostaglandin isomers. The retention times for 20-hydroxy $PGF_{2\alpha}$ and 19-hydroxy $PGF_{2\alpha}$ are 9.13 min and 9.19 min, respectively. Cps, counts per second.

(B) MRM chromatograms of mixed staged wild-type extracts. The mass transition *m/z* 351/193 was used to detect F3 class prostaglandins and mass transition *m/z* 367/193 was used to detect hydroxylated forms. Cps, counts per second.

TABLES

Table 1. Sperm motility values in wild-type and mutant hermaphrodite uteri.

Description	Average Velocity (μm/min)	Average Directional Velocity (μm/min)	Reversal Frequency (rev/hr)	N
1. Wild type*	8.62 ± 0.60	4.28 ± 0.78	1.8	88
2. *fat-1(wa9)*	7.97 ± 0.51	2.50 ± 0.70	9.3	42
3. *fat-4(wa14)*	6.50 ± 0.33	2.08 ± 0.54	5.9	60
4. *fat-1(wa9) fat-4(wa14)*	5.68 ± 0.35	2.74 ± 0.48	5.7	55
5. *fat-3(wa22)**	3.84 ± 0.31	2.16 ± 0.42	2.5	49
6. *fat-2(wa17)**	3.85 ± 0.22	0.47 ± 0.30	8.1	94
7. *rme-2(b1008)***	3.68 ± 0.28	0.45 ± 0.32	9.5	75
8. *glp-4(bn2)***	3.43 ± 0.25	-0.23 ± 0.25	16.2	79
9. *cyp-31A2(tm2711)*	7.63 ± 0.84	2.04 ± 1.07	3.5	26

The average velocity, average directional velocity toward the spermatheca, and average reversal frequency were determined for wild-type sperm within the uterus (Zone 2) of wild-type and mutant hermaphrodites. Value ± standard error of the mean is shown.

* Includes new data and published data from Kubagawa et al (2006) (Kubagawa et al., 2006).

** Published data from Kubagawa et al (2006) for reference (Kubagawa et al., 2006).

Table 2. LC-MS/MS data summary for chemically synthesized F-series prostaglandin standards.

Name	RT (min)*	$[M-H]^-$ *m/z*	Key product ions in CID (MS/MS)
PGD_2	12.56	351	315, 271, 233, 203, 189
PGE_2	12.23	351	333, 315, 271, 235, 189, 175, 109
PGH_2	12.23	351	333, 315, 271, 235, 217, 189, 175, 113, 109
$PGF_{1\alpha}$	11.83*	355	337, 319, 311, 301, 293, 275, 265, 249, 237, 211, 195
8-iso $PGF_{1\alpha}$	11.34	355	337, 319, 311, 293, 275, 265, 249, 237, 219, 211, 183
9β-$PGF_{1\alpha}$	11.36	355	337, 319, 311, 301, 293, 275, 265, 237, 211,183, 167
8-iso 9β-$PGF_{1\alpha}$	11.44	355	337, 319, 311, 293, 275, 265, 219, 211, 183
9β, 11β-$PGF_{1\alpha}$	11.99	355	337, 319, 311, 301, 293, 275, 265, 237, 219, 211, 183
$PGF_{2\alpha}$	11.73*	353	335, 317, 309, 291, 273, 263, 247, 209, 193, 171, 165
ent-$PGF_{2\alpha}$	11.71	353	335, 317, 309, 291, 273, 247, 209, 193, 191, 171, 165
11β $PGF_{2\alpha}$	11.48	353	335, 317, 309, 291, 273, 247, 209, 193, 173, 165, 111
15(R)-$PGF_{2\alpha}$	11.89	353	335, 317, 309, 291, 273, 247, 209, 193, 191, 171, 165
8-iso $PGF_{2\alpha}$	11.31	353	335, 307, 309, 291, 273, 247, 209, 193, 181, 171, 165
5-trans $PGF_{2\alpha}$	11.60	353	335, 317, 309, 291, 273, 247, 209, 193, 171, 165, 111
8-iso 15(R)-$PGF_{2\alpha}$	11.39	353	335, 317, 309, 291, 273, 263, 247, 209, 193, 171, 165
9β-$PGF_{2\alpha}$	11.22	353	335, 317, 309, 291, 273, 255, 247, 193, 173, 171, 165
$PGF_{3\alpha}$	11.26	351	333, 315, 307, 289, 271, 245, 219, 209, 193, 191, 165
8-iso $PGF_{3\alpha}$	10.83	351	333, 315, 307, 289, 271, 245, 219, 209, 193, 191, 171
2,3-Dinor-11β-$PGF_{2\alpha}$	10.67	325	261, 245, 227, 219, 173, 163, 153, 145, 137, 113, 107
19(R)-hydroxy $PGF_{2\alpha}$	9.19	369	351, 333, 325, 315, 307, 263, 235, 209, 193, 171, 165
20-hydroxy $PGF_{2\alpha}$	9.13	369	351, 333, 325, 315, 307, 263, 209, 193, 181, 171, 165

Retention time (RT), parent ion mass ($[M-H]^-$), and key product ion masses are shown for prostaglandin (PG) standards.

* Isomers within each prostaglandin class (i.e. $PGF_{2\alpha}$ isomers) were run together and RTs are directly comparable. PGF_1 and PGF_2 classes were run on different days and a slight RT shift is observed. For example, the RTs for $PGF_{1\alpha}$ and $PGF_{2\alpha}$ are indistinguishable when run together.

Table 3. LC-MS/MS data for selected *C. elegans* F-series prostaglandins.

Name	RT (min)	$[M-H]^-$ m/z	Key product ions in CID (MS/MS)
Class 1	11.24	355	319, 311, 301, 293, 275, 265, 249, 219, 211, 179, 157
CePGF1*	11.70	355	319, 311, 301, 293, 275, 265, 237, 223, 211, 195, 157
Class 1	11.85	355	311, 301, 293, 237, 195, 193, 183, 179, 157, 153
Class 1*	12.08	355	311, 301, 293, 275, 265, 211, 195, 167, 157
Class 1	12.31	355	337, 319, 311, 293, 275, 265, 187, 179, 157, 153
CePGF2*	11.73	353	309, 291, 273, 263, 247, 209, 193, 171, 167, 137
CePGF2b*	12.09	353	309, 291, 273, 263, 255, 247, 219, 209, 193, 171, 113
Class 3*	11.34	351	315, 307, 289, 275, 249, 205, 193, 191, 167, 153, 139
Class 3	11.90	351	307, 289, 263, 249, 193, 191, 185, 147, 137, 115, 109
Class 3*	12.51	351	333, 289, 271, 261, 245, 223, 193, 191, 163
Class 3	12.62	351	289, 271, 245, 223, 219, 201, 193, 183, 149, 113, 107

Retention time (RT), parent ion mass ($[M-H]^-$), and key product ion masses are shown. CID data are from wild-type, *fat-1(wa9)* mutant, or *fat-1(wa9) fat-4(wa14)* double mutant extracts. Prostaglandins derived from omega-3 AA are not shown.

* MS/MS data are shown in Figure 4.

CHAPTER 3

A GPCR CIRCUIT IN MALE SENSORY NEURONS MODULATES SPERM PERCEPTION OF THE OVIDUCT

by

HIEU D. HOANG, MICHAEL A. MILLER

In preparation for submission to *Development*

Format adapted and errata corrected for dissertation

ABSTRACT

Fertilization is the union of egg and sperm. The more efficient sperm are at finding eggs within the oviduct, the better their chance of passing on genetic material to the next generation. In *Caenorhabditis elegans*, developing eggs secrete lipid signaling molecules called F-series prostaglandins to guide sperm toward them. However, little is known about how sperm perceive these guidance cues. In this paper, we identify at least four related G protein-coupled receptors (GPCRs), including SRB-13, SRB-16, and SRB-5 predicted chemoreceptors, as well as downstream Gα GOA-1 that are required in males to promote efficient sperm guidance within the oviduct. Non-cell autonomous function of the SRB GPCRs in sperm guidance is supported by multiple lines of evidence. First, *srb* genes are not expressed in sperm. Instead, they are expressed in male head neurons, including sensory neurons. Second, transgenic and genome-editing methods demonstrate that SRB-13 functions in male sensory neurons, most likely pheromone-sensing ASK neurons to promote sperm guidance. Finally, global mRNA sequencing analysis suggest that the SRB GPCRs modulate a neuroendocrine mechanism affecting cytoskeletal and metabolic gene transcription during spermatogenesis. Thus, environmental cues perceived by the male nervous system may have unanticipated effects on sperm quality and fertilization.

KEY WORDS: SRB-13, SRB GPCRs, ASI, ASK, Sperm guidance

INTRODUCTION

In the past five hundred years, human activities have been associated with extinction of many species and the dwindling population of others (Barnosky et al., 2011; Ceballos and Ehrlich, 2002; Hughes et al., 1997; Pereira et al., 2010; Pimm et al., 1995;

Wake and Vredenburg, 2008; Young et al., 2014). Barnosky et al. projected that if the now-endangered species (5-20%) soon become extinct, we will lose 75% of species of birds, mammals, and amphibians in about 240 to 540 years (Barnosky et al., 2011; Hoffmann et al., 2010). That degree of loss in biodiversity could be devastating to human society (Aminov, 2010; Fleming, 1929; Lambert, 2005; Ribeiro et al., 2009; Rokaya et al., 2014; Wells, 1952). Humans alter their surrounding environments, competing with animals for food and other resources, fragmenting their habitats, adding non-native invasive species and pathogens, and changing the global climate (Barnosky et al., 2011; Dirzo and Raven, 2003; Hoffmann et al., 2010; Vredenburg et al., 2010). Most animals and to some extent humans now have to face the challenge of rapidly adapting to altered environments (Dorman et al., 2015; Kullberg et al., 2015; Moghadam and Zimmer, 2014; Piggott et al., 2015; Rivetti et al., 2014; Vinagre et al., 2015). Changing environment is thought to affect multiple biological processes including reproduction (Chiba and Roy, 2011; Cinner et al., 2013; Gibbons et al., 2000; Huey et al., 2009; Jenkins et al., 2014; Negro-Vilar, 1993; Punjabi et al., 2013; Quinn et al., 2014; Ribeiro et al., 2009). However, the molecular mechanisms underlying the effect of environment on reproduction are not clear.

Sperm motility is an important factor for fertilization success (Pizzari and Parker, 2009). In mammals, post-copulation sperm undergo capacitation and motility hyperactivation allowing sperm to detach from the wall of the oviduct, to move in the lumen of the oviduct, and to penetrate the mucus substances and the zona pellucida of the oocyte (Kupker et al., 1998; Suarez, 2008; Suarez and Ho, 2003). In red deer, *Cervus elaphus*, Atlantic salmon, mallard, and human, ejaculates with higher average sperm velocity have higher fertilization success (Birkhead et al., 1999; Denk et al., 2005; Donnelly et al., 1998; Donoghue, 1999; Gage et al., 2004; Malo et al., 2005). Failure to

complete capacitation and motility hyperactivation have been reported as a cause of male infertility (Lessard et al., 2011; Munire et al., 2004). Sperm motility in poultry ejaculates have been regarded as an important natural and artificial selection trait (Etches, 1996).

Sperm chemoattraction is well-known in several marine species that externally fertilize. Oocytes of the mollusk *Sepia officinalis*, sea urchin *Arbacia punctulata*, and starfish *Asterias amurensis* release small peptides called sepsap, resact, or asterosap, respectively, to attract species-specific sperm (Bohmer et al., 2005; Himes et al., 2011; Kaupp et al., 2003; Nishigaki et al., 1996; Ward et al., 1985). L-tryptophan and a sulfated steroid were also identified as sperm chemoattractants in red abalone *Haliotis rufescens* and sea squirt *Ciona intestinalis* (Yoshida et al., 2002; Zatylny et al., 2002). In an externally fertilizing vertebrate species, the African clawed frog *Xenopus laevis*, the oocytes release a cysteine-rich protein called allurin, which is thought to attract sperm (Olson et al., 2001; Xiang et al., 2004; Xiang et al., 2005). In humans, follicular fluid appears to contain unknown sperm chemoattractant(s), when assessed using *in vitro* assays (Ralt et al., 1991; Ralt et al., 1994; Villanueva-Diaz et al., 1990). Sperm chemoattraction is much less understood in mammals due to the difficulty of measuring sperm motility *in utero*, and the importance of capacitation and hyperactivation processes occurring in the oviduct (Cohen-Dayag et al., 1995; Jaiswal and Eisenbach, 2002).

C. elegans is an androdioecious nematode species with hermaphrodites and rare males (Brenner, 1974; Cutter and Payseur, 2003; Stewart and Phillips, 2002). Because *C. elegans* hermaphrodites cannot mate to each other, outcrossing of new gene mutations must rely on mating with males (Anderson et al., 2010; Ward and Carrel, 1979). Mating with males can help slow the tendency to converge towards homozygosity and mitigate the impact of inbreeding depression (Anderson et al., 2010; Cutter and Payseur, 2003; Stewart

and Phillips, 2002). Moreover, male mating increases the frequency of males in the population, as male sperm outcompete hermaphrodite sperm due to its larger size and probably better motility (LaMunyon and Ward, 1998; Ward and Carrel, 1979).

The male gonad produces and stores non-motile round spermatids in the seminal vesicle (L'Hernault, 2006). After entering the hermaphrodite uterus (i.e. oviduct) together with male-derived seminal fluid during mating, spermatids are activated and become motile spermatozoa by means of extending a single pseudopod (L'Hernault and Roberts, 1995). Sperm pseudopod formation and movement depend on the polymerization and depolymerization of various Major Sperm Proteins (MSPs) across an intracellular pH gradient (Italiano et al., 1999; Nelson et al., 1982; Roberts and King, 1991; Roberts and Ward, 1982; Sepsenwol et al., 1989). Male sperm then crawl over fertilized eggs towards the spermatheca, where they wait for ovulating eggs. Male sperm also displace hermaphrodite-derived sperm from the spermatheca (L'Hernault, 2006).

C. elegans is a powerful animal model system to study sperm chemoattraction because sperm motility within the oviduct can be measured in live animals (Edmonds et al., 2011; Edmonds et al., 2010; Hoang et al., 2013; Kubagawa et al., 2006; McKnight et al., 2014). We have previously shown that oocytes secrete F-series prostaglandins (PGFs) that function redundantly to promote sperm guidance to the spermatheca (Edmonds et al., 2010; Hoang et al., 2013; Kubagawa et al., 2006). Prostaglandins (PGs) are important lipid signaling molecules characterized by a cyclopentyl ring bearing two hydrocarbon side chains (Funk, 2001). In mammals, PGs are derived from 20-carbon polyunsaturated fatty acids (PUFAs) such as dihomo-gamma -linolenic acid (DGLA), arachidonic acid (AA), and eicosapentanoic acid (EPA) (Funk, 2001). In *C. elegans*, PGFs are also derived from the same PUFAs although the PG metabolic pathway is different (Hoang et al., 2013).

Moreover, PGs bind to and activate a human sperm calcium channel called CatSper, which is implicated in sperm hyperactivation and chemotaxis (Brenker et al., 2012; Lishko et al., 2011; Publicover et al., 2008; Strunker et al., 2011; Suarez, 2008). Studies of *C. elegans* sperm guidance are providing novel insight into PG metabolism and function.

C. elegans hermaphrodites respond to pheromones in the external environment by stimulating sperm motility within the oviduct (McKnight et al., 2014). A TGF-β signaling pathway mediates this neuroendocrine response by promoting ovarian PGF synthesis (McKnight et al., 2014). Here we provide strong evidence that *C. elegans* males also modulate motility parameters of their sperm. We identify a set of chemosensory receptors, including *Serpentine Receptors B 13* (*srb-13*) and *16* (*srb-16)* that are expressed in male sensory neurons. Genetic knockout of these receptors, as well as the downstream $G\alpha_{i/o}$ homolog *goa-1* causes impaired sperm motility within the oviduct. In particular, SRB-13 is expressed in ciliated endings on amphid sensory neurons in the male nose, where it functions to promote sperm guidance. RNA sequencing suggests that *srb* chemoreceptors modulate the transcriptional program of spermatogenic genes involved in cytoskeletal and metabolic regulation. Our data suggest that males and hermaphrodites manipulate sperm motility behavior within the oviduct, but in response to different environmental cues. This study supports the unexpected idea that sperm quality is under environmental control.

RESULTS

srb-13 is required in males to promote efficient sperm guidance

We have previously found that a deletion in the predicted gene *srb-13* (allele *ok3126*, which will be referred to as *srb-13Δ1* from hereon) causes abnormal sperm

distribution within the hermaphrodite uterus one hour after mating (Edmonds et al., 2010). The predicted *srb-13* gene structure consists of four exons. However, the *msp-45* gene lies within its first intron, suggesting that *msp-45* might be included in *srb-13* transcripts. Sequencing cDNA derived from male *srb-13* mRNA shows that the *srb-13* gene produces 2 transcripts, one corresponded to the full-length coding sequence and the other corresponded to an alternative spliced form, missing exon 2 (supplementary material Fig. S1). Neither transcript contained *msp-45*. The *srb-13* 3'UTR is 57 bp in length (supplementary material Fig. S1). The *srb-13Δ1* mutation deletes a part of exon 3, most of exon 4, and renders the remaining downstream coding sequence out of frame (Fig. 2). Thus, *srb-13* encodes a GPCR expressed in males.

To identify male GPCRs important for sperm guidance, we measured sperm distribution in the uterus one hour after mating mutant males to wild-type hermaphrodites. Mutations in ten GPCR genes were evaluated including *srb-13* (Table 1). Only the *srb-13Δ1* mutation causes significant sperm guidance defects (Table 1). We found that the percentage of *srb-13Δ1* mutant sperm at zone 3 of the wild-type hermaphrodite uterus averaged 66%, lower than that of wild-type sperm ($p<0.000001$) (Fig. 1; Table 1). To confirm that *srb-13* is essential for sperm guidance, we create a second deletion in *srb-13* using the MOSDEL technique (Frokjaer-Jensen et al., 2010). The *xm1* allele (referred to as *srb-13Δ2* from hereon) deletes exon 1 and 2, and most of exon 3 (supplementary material Fig. S2). The *srb-13Δ2* mutation causes similar sperm distribution defects as the *srb-13Δ1* mutation (Fig. 1). These results indicate that SRB-13 is essential for sperm targeting efficiency within the uterus (i.e. oviduct).

***srb-16* and *srb-5* are also required in males for sperm guidance**

Seven different *srb* class chemoreceptor genes (including *srb-13* but excluding *srb-4* pseudogene) are clustered within a 22 kb stretch of DNA on chromosome II (Fig. 2). This chromosomal region was previously shown to contain a high percentage of genes influencing fertility (Miller et al., 2004). Clustered *srb* genes encode GPCRs ranging from 17% to 75% percent identity (Fig. 2). To test whether other clustered *srb* genes are essential for sperm guidance, we mated *srb-16(gk774)* and *srb-5(tm5831)* mutant males, referred to as *srb-16Δ and srb-5Δ* from here on, to wild-type hermaphrodites. The percentage of sperm from *srb-16Δ* and *srb-5Δ* males at zone 3 averaged 67% ($p<0.000001$ compared to wild type sperm) and 69% ($p<0.000001$ compared to wild type sperm), respectively (Fig. 1). These data implicate the role of *srb-16* and *srb*-5 in sperm guidance, in addition to the role of *srb*-13. *srb* mutant males appear healthy and are fertile, provided sperm reach the spermatheca. Wild-type sperm efficiently target the spermatheca in *srb-13* or *srb-16* mutant hermaphrodites (supplementary material Fig. S3), suggesting that the sperm guidance defects are not due to general sickness. Together, these data support the model that *srb-5*, *srb-13,* and *srb-16* play specific roles in males to promote efficient sperm guidance.

Next, we wanted to test whether or not these *srb* chemoreceptors function in common or parallel genetic pathways. Given the close physical proximity of the genes, genome-editing methods were necessary to generate mutant lines lacking multiple genes. First we used MOSDEL to delete a 6.8kb region containing *srb-13, srb- 12,* and *srb-16* coding sequences (allele *xm3,* referred to as *srb-13,12,16Δ* from hereon) (supplementary material Fig. S4) (Frokjaer-Jensen et al., 2010). We confirmed the loss of *srb-13*, *srb-12*,

and *srb-16* coding sequences using PCR (supplementary material Fig. S4). The percentage of sperm from *srb-13,12,16Δ* males found in zone 3 averaged 49%, lower than sperm from *srb-13*$^{\Delta 1}$ ($p<0.0002$), *srb-13*$^{\Delta 2}$ ($p<0.0002$), or *srb-16*$^{\Delta}$ ($p<0.0001$) mutants (Fig. 1). These data suggest that either *srb-12* or *srb-16* acts in parallel to *srb-13*.

We similarly created an *srb-2*, *srb-3*, and *srb-5* triple deletion mutation using MOSDEL (supplementary material Fig. S5) (Frokjaer-Jensen et al., 2010). The generated allele is named *xm2*, referred to as *srb-2,3,5Δ* from hereon (supplementary material Fig. S5). We confirmed the loss of *srb-2*, *srb-3*, and *srb-5* coding sequences by PCR (supplementary material Fig. S5). The percentage of sperm from *srb-2,3,5Δ* males distributed in zone 3 averaged 61%, lower than *srb-5Δ* mutant sperm ($p<0.02$) (Fig. 1). Therefore, *srb-2* or *srb-3* may also play a role in sperm guidance. We conclude that multiple male *srb* GPCRs function in at least two parallel pathways to promote sperm targeting in the oviduct.

goa-1($G\alpha_{i/o}$) and *egl-30* ($G\alpha_q$) regulate sperm guidance

We hypothesized that SRB class GPCRs transmit signals via G-proteins such as Gα. The *C. elegans* genome contain one ortholog of each of the mammalian Gα protein family: *gsa-1* ($G\alpha_s$), *goa-1* ($G\alpha_{i/o}$), *egl-30* ($G\alpha_q$), and *gpa-12* ($G\alpha_{12/13}$), as well as 18 other unclassified $G\alpha_{i/o}$–like coding genes (Cuppen et al., 2003; Jansen et al., 1999). We tested whether mutations in *gsa-1* ($G\alpha_s$), *goa-1* ($G\alpha_{i/o}$), and *egl-30* ($G\alpha_q$) affect sperm guidance (Fig. 3). Gain of function (gof) mutations of *egl-30* and *gsa-1* were used because loss of function (lof) mutations cause embryonic lethality (Brundage et al., 1996). The percentage of *gsa-1*^{gof} mutant sperm distributed in zone 3 averaged 87%, similar to that of wild-type

sperm. In contrast, the percentage of *egl-30*^{gof} and *goa-1*^{lof} mutant perm distributed in zone 3 averaged 49% ($p<0.000001$ compared to wild-type sperm) and 53% ($p<0.000001$ compared to wild-type sperm), respectively. Therefore, both *goa-1* ($G\alpha_{i/o}$) and *egl-30* ($G\alpha_q$) play roles in males to promote sperm targeting.

Sperm from *srb* mutant males have abnormal motility

After insemination into the uterus, male sperm become activated for motility, then respond to PGF guidance cues by increasing velocity and directional velocity toward the spermatheca. Time-lapse images of *srb* mutant sperm in the wild-type hermaphrodite oviduct show that all *srb* mutant sperm are motile and therefore, must have been activated. The mutant sperm are also capable of fertilizing oocytes because *srb* mutant hermaphrodites are fertile and mutant males produce outcross progeny. Spermatid size of *srb-13Δ2* and *srb-13,12,16Δ* males is not different than controls (data not shown), yet srb mutant sperm target the spermatheca with reduced efficiency. To understand why mutant sperm target the spermatheca less efficiently, we looked at sperm motility characteristics, such as average velocity and reversal frequency (Table 2). Compared to wild-type sperm, *srb-13Δ1* sperm have normal average velocity and more than 2-fold higher reversal frequency (Table 2). In contrast, *srb-16Δ* sperm have reduced average velocity ($p<0.00001$) and slightly increased reversal frequency (Table 2). Sperm from *srb-5Δ, srb-13,12,16Δ,* and *srb-2,3,5Δ* males also move with abnormal motility parameters (Table 2). The motility parameters from *srb* mutant sperm are consistent with an inefficient response to PGF guidance cues. We conclude that *srb* GPCRs are not essential for sperm activation or motility, but are essential for efficient motility responses.

srb genes are not expressed in sperm

We have shown that *srb-13*, *srb-16*, *srb-5*, and *srb-2* or *srb-3* are required in males for efficient sperm guidance. One simple mechanistic explanation would be that these *srb* genes are expressed in sperm where they help perceive PGF guidance cues (Edmonds et al., 2010; Hoang et al., 2013; Kubagawa et al., 2006). To test this hypothesis, we compared mRNA expression in gonads undergoing spermatogenesis to those not, using quantitative polymerase chain reaction (qPCR). The gonads of *fem-3(q20)* mutant hermaphrodites undergo continuous spermatogenesis in the absence of oogenesis at non-permissive temperature of 25^{o}C. In contrast, the germline of *glp-4(bn2)* mutants produce neither sperm nor oocytes at 25^{o}C (Ahringer and Kimble, 1991; Beanan and Strome, 1992). Two genes known to be expressed in sperm, *spe-9* and *spe-11*, were used as positive controls (Browning and Strome, 1996; Putiri et al., 2004; Royal et al., 1997; Singson et al., 1998; Zannoni et al., 2003). All qPCR reactions were ran in quadruplicate, and *cdc-42* (a house keeping gene) was used as a reference gene.

We found that *spe-9* and *spe-11* transcripts are enriched, as expected, by more than 250 fold in *fem-3* mutants compared to *glp-4* mutants (Fig. 4). However, none of the *srb* genes are enriched in spermatogenesis by qPCR (Fig. 4). These data support the hypothesis that SRB GPCRs are not expressed in sperm.

To determine the true expression pattern of *srb-13* and *srb-16*, we used homologous recombination to knock-in tdTomato to their respective genomic loci, before the stop codons (supplementary material Fig. S6-S7) (Friedland et al., 2013; Frokjaer-Jensen et al., 2010). The generated knock-in alleles are named *xm4* and *xm10*, and referred to as *srb-13*$^{\mathrm{KI}tdTomato}$, and *srb-16*$^{\mathrm{KI}tdTomato}$ from hereon (supplementary material Fig. S6-S7). *srb-*

13$^{\text{KI}tdTomato}$ and *srb-16*$^{\text{KI}tdTomato}$ mutant males were mated to wild-type hermaphrodites to test whether the tdTomato tag compromised *srb-13* or *srb*-16 function. The *srb-13*$^{\text{KI}tdTomato}$ and *srb-16*$^{\text{KI}tdTomato}$ mutant sperm distribution in zone 3 averaged 86% and 89%, similar to wild-type sperm, indicating that addition of tdTomato to SRB-13 or SRB-16 C-terminus does not compromise protein function (supplementary material Fig. S6-S7).

In *srb-13*$^{\text{KI}tdTomato}$ *and srb-16*$^{\text{KI}tdTomato}$ mutant hermaphrodites, we failed to detect *srb-13* or *srb-16* expression in the spermatheca, which contains the sperm, Moreover, we failed to detect expression in gonads of *srb-13*$^{\text{KI}tdTomato}$ *and srb-16*$^{\text{KI}tdTomato}$ mutant males (Fig. 5). As a positive control, we knocked tdTomato into the *spe-9* gene, which encodes a receptor expressed in sperm (Fig. 4) (Friedland et al., 2013; Putiri et al., 2004; Singson et al., 1998). The generated mutant named *xm14*, referred to as *spe-9*$^{\text{KI}tdTomato}$ from hereon (supplementary material Fig. S8), is fertile, indicating SPE-9 function is not disrupted (Putiri et al., 2004; Singson et al., 1998). Endogenous *spe-9* expression is detected in the spermatheca of *spe-9*$^{\text{KI}tdTomato}$ mutant hermaphrodites (Fig. 5). Taken together, these results demonstrate that *srb* genes are not expressed in sperm.

srb-13 is expressed in cilia of ASI and ASK amphid sensory neurons in males

To determine where *srb* genes are expressed, we first examined *srb* transcriptional reporters (promoter::GFP fusions) expressed from extrachromosomal arrays. Reporters for *srb-3*, *srb-5*, *srb-12*, *srb-13*, and *srb-16* predicted promoters show expression in a variety of male head neurons that send dendrites anteriorly toward the mouth (supplementary material Fig. S9-S13). By labeling all sensory neurons in *srb-13p::GFP* males with a far-red fluorescent membrane tag called DiD (see MATERIALS AND METHODS), we found that the predicted *srb-13* promoter drives GFP expression in 3 pairs of amphid sensory

neurons, Amphid Single-ciliated neuron I, ASI, Amphid Single-ciliated neuron K, ASK, and Amphid Wing neuron B, AWB, exclusively (Fig. 6).

Next, we looked at endogenous *srb-13* expression from *srb-13*$^{KI tdTomato}$ males. Fluorescence is detected in a few sensory cilia-like structures near the anterior tip of the mouth (Fig. 7). The SRB-13 fusion protein shows expression in two cilia basal body-like structures (white arrows) and two cilia axoneme-like rays (white diamond) (Fig. 7). We also found endogenous *srb-13* expression in a few cytoplasmic puncta located near the nerve ring. The positions are consistent with relative positions of ASI or ASK neuron cell bodies and may represent trafficking populations (Fig. 7).

To confirm that *srb-13* is expressed in sensory cilia, we transiently expressed a pan-sensory cilia marker (*osm-6p::dyf-11::GFP*) in *srb-13*$^{KI tdTomato}$ mutant male worms (Fig. 8). We found GFP and tdTomato co-localization in a pair of sensory cilia-like ray (Fig. 8). These results support the idea that SRB-13 is expressed in sensory cilia. These cilia are likely to belong to ASI and ASK neurons, which contain a single linear cilium, rather than AWB neuron, which contain a branched cilium.

srb-16 is expressed in multiple head neurons

Next, we examined SRB-16 expression. By labeling all sensory neurons in *srb-16p::GFP* males with DiD (see MATERIALS AND METHODS), we found that the predicted *srb-16* promoter drives GFP expression in 4 pairs of amphid sensory neurons, Amphid Single-ciliated neuron H, ASH, Amphid Single-ciliated neuron I, ASI, Amphid Single-ciliated neuron K, ASK, and Amphid Wing neuron B, AWB (Fig. 9). We also found GFP expression in pm4 and pm5 pharyngeal muscle triplets, and unidentified neurons (Fig. 9).

In *srb-16*$^{KI tdTomato}$ males, we found endogenous SRB-16 expression in pm4 and pm5 pharyngeal muscles, I1 interneuron neuron pair (cell bodies and dendrites), and 4 neurons probably representing the 4 amphid sensory neurons ASH, ASI, ASK, and AWB (Fig. 10; supplementary material Fig. S14).

To check if *srb-16* is expressed in sensory cilia, we expressed the pan-sensory cilia marker (*osm-6p::dyf-11::GFP*) in *srb-16*$^{KI tdTomato}$ males. In contrast to SRB-13, we failed to find co-localization of tdTomato and GFP (Fig. 11). We conclude that SRB-16 is expressed in in pm4 and pm5 pharyngeal muscles, I1 interneuron neurons, and amphid sensory neurons ASH, ASI, ASK, and AWB. SRB-16 is largely present in the cell bodies, but not the sensory cilia.

srb-13 and *srb-16* function in neurons to promote sperm guidance

To test whether or not *srb-13* or *srb-16* function in neurons to promote sperm guidance, we overexpressed their cDNAs under the pan-neuronal *unc-119* promoter in null mutant males (Table 3). In three independent transgenic lines, overexpressing *srb-13* in neurons of *srb-13Δ1* mutant males rescued the sperm distribution defect (Table 3). In contrast, driving expression in muscle using the *myo-3* promoter did not affect sperm distribution (Table 3). Similar to *srb-13*, overexpressing *srb-16* pan-neuronally in *srb-16Δ* mutant males rescued the sperm distribution defect in three independent transgenic lines (Table 3). Therefore, *srb-13* and *srb-16* function in male neurons to promote efficient sperm guidance.

srb-13 functions in sensory neurons to promote sperm guidance

We observed endogenous expression of *srb-13* in sensory cilia-like structures (Fig. 7, 8). To confirm that *srb-13* functions in sensory neurons, we overexpressed *srb-13*::*mCherry* under the sensory neuron *osm-6* promoter. As shown in supplementary material Fig. S15, SRB-13::mCherry is expressed in male sensory neurons. Expressing *srb-13* specifically in sensory neurons of *srb-13Δ1* mutant males rescued the sperm guidance defect in two transgenic lines (Table 3). Thus, *srb-13* functions in male sensory neurons to promote efficient sperm guidance.

srb genes influence spermatogenic gene transcription

C. elegans hermaphrodites transmit neuroendocrine signals from sensory neurons to the ovary, influencing gene transcription important for PGF metabolism (McKnight et al., 2014). We hypothesized that SRB chemoreceptors affect gene transcription during spermatogenesis. To test this hypothesis, we sequenced cDNA derived from one-day adult control, *srb-13Δ2,* and *srb-13,12,16Δ* mutant male polyadenylated mRNA transcripts. The rationale is that genes found to change in both *srb-13Δ2* and *srb-13,12,16Δ* are likely to be due to SRB-13 function, whereas those found to change in only *srb-13,12,16Δ* mutants are likely due to the parallel SRB-12/16 pathway.

Compared to control males, roughly 1000 genes are upregulated and about 500 genes are down regulated in either *srb-13Δ2* or *srb-13,12,16Δ* males compared to control males (Fig. 12; SupplRNAseqData.xlsx Excel sheets 1 and 2). To narrow on spermatogenic genes, we filtered them through a list of 1000 genes most abundantly transcribed in purified spermatids (adapted from (Ma et al., 2014); SupplRNAseqData.xlsx Excel sheet 4; Fig. 12). We called the resulted genes sperm-enriched genes. We found sixty five sperm-

enriched genes up-regulated in *srb-13,12,16Δ* males, but not *srb-13Δ2* males (Fig. 12; Table S1; SupplRNAseqData.xlsx Excel sheet 6). Of those, sixteen genes encode for sperm-specific structural proteins (Fig. 13; supplementary material Table S1; SupplRNAseqData.xlsx Excel sheet 6). We also found twelve sperm-enriched genes up-regulated and nineteen down-regulated in both *srb-13Δ2* and *srb-13,12,16Δ* males (Fig. 12; supplementary material Table S1-S2). Of the nineteen down regulated genes, eight genes encode mitochondrial proteins. Seven out of these eight reside in the mitochondrial genome (Fig. 13; supplementary material Table S2; SupplRNAseqData.xlsx Excel sheets 5 and 6). These data support the model that SRB-12/16 primarily suppresses spermatogenic transcription of cytoskeletal genes, whereas SRB-13 promotes spermatogenic transcription of mitochondrial genes. Aside from sperm-enriched genes, we also detected expression changes in genes important for immunity, basement membrane remodeling, and metabolism (supplementary material Fig. S16; SupplRNAseqData.xlsx Excel sheet 3).

DISCUSSION

The survival of animal species depends on fertilization, the union of sperm and egg. Sperm that are able to locate unfertilized eggs more rapidly have a competitive advantage. We have previously shown that *C. elegans* oocytes (or their precursors) convert polyunsaturated fatty acids into a heterogeneous mixture of PGFs that promote sperm motility and guide them to the spermatheca (Hoang et al., 2013). However, not much is known about how sperm perceive PGFs. Here we provide strong evidence that male sensory neurons have an unanticipated effect on sperm motility within the oviduct. Based on the results from this study, we propose the following model. SRB-13 and other clustered SRB chemoreceptors function in male neurons, particularly sensory neurons. These

chemoreceptors directly or indirectly sense cues in the external environment (e.g. male-derived ascaroside, signals within exosome-like vesicles, etc.). In favorable environments, SRB GPCRs initiate signaling via the $G\alpha_{i/o}$ protein GOA-1, triggering a neuroendocrine mechanism(s) affecting gene transcription in developing sperm and other cell types. Changes in spermatogenic gene transcription, including cytoskeletal and metabolic genes produce more competitive sperm, which are better able to perceive PGF guidance cues in the oviduct. These results argue against conventional wisdom that males maximize reproductive success through copious production of competitive sperm. Instead, *C. elegans* males adjust sperm quality to the environment around them. Below, evidence for and implications of this model are discussed.

SRB chemoreceptors and Gα protein coding genes are required in males for sperm guidance

We identified at least three *srb* class chemoreceptors that are required in males to generate efficiently migrating sperm. Two independently made deletions in *srb-13* cause sperm guidance defects. Deletions in *srb-16* and *srb-5* cause similar defects. A large deletion made using MOSDEL removed coding sequences for *srb-2*, *srb-3*, and *srb-5* (the *srb-4* gene is a pseudogene). This deletion causes more severe sperm guidance defects than the *srb-5* deletion, suggesting that either *srb-2* or *srb-3* is also required.

srb mutant males appear healthy, live at least as long as control males, and produce motile sperm capable of fertilization. Moreover, *srb* loss in hermaphrodites does not affect guidance of wild-type sperm. The average spermatid size of *srb* mutant males is not different from control males (data not shown). Importantly, mutations in nine other GPCRs, including in two *sra* genes closely related to *srb* class genes, are not required for efficient

sperm guidance (Table 1; Roberson, 2006). Therefore, *srb* class chemoreceptors have a specific role in promoting efficient sperm guidance within the oviduct.

Seven *srb* class chemoreceptor genes are physically clustered in a 22-kb locus on chromosome II. This small cluster lies within a larger chromosomal region enriched in fertility genes (Miller et al., 2004). While the significance of this clustered organization is not known, new genome editing methods have greatly facilitated their functional characterization.

The *srb* chemoreceptors could function in a common pathway or independent pathways. Three lines of evidence support the latter model. First, sperm motility values are different in *srb-13* mutants relative to *srb-5* or *srb-16* mutants (see below). Second, multi-gene deletions in *srb-13,12,16Δ* or *srb-2,3,5Δ* males have more severe sperm guidance defects than single *srb-5, srb-13,* or *srb-16* mutants. Similarly, mutations in downstream Gα proteins have more severe sperm guidance defects than single *srb* mutants. Third, *rb-13* is expressed in sensory cilia whereas srb-16 is expressed in the cell bodies of sensory neurons. Therefore, there should be at least two parallel pathways in which individual *srb* genes function to promote sperm guidance.

Chemosensory GPCRs can transmit signals through downstream Gα proteins. Indeed, we identified a loss of function mutation in *goa-1* $G\alpha_{i/o}$ and a gain of function mutation in *egl-30* $G\alpha_q$. The sperm guidance defect of *goa-1*^{lof} mutant males is as severe as *srb-13,12,16Δ* and *srb-2,3,5Δ* males, suggesting that GOA-1 is a common downstream effectors of parallel SRB pathways. Furthermore, *egl-30*^{gof} mutant males have similar sperm guidance defects as *goa-1*^{lof} mutant males, in agreement with the known antagonistic roles of *egl-30* and *goa-1* in egg laying, locomotion, pharyngeal pumping, vulva

development, neuronal migration, and motor neuron acetylcholine release (Trent et al., 1983; Brundage et al., 1996; Lackner et al., 1999; Miller et al., 1999; Kindt et al., 2002; Moghal et al., 2003; Mendel et al., 1995; Ségalat et al., 1995; Fraser et al., 2000; Miller and Rand, 2000; Sawin et al., 2000; van Swinderen et al., 2001; Keane and Avery 2003; Nurrish et al., 1999). In the case of acetylcholine release from motor neurons, *goa-1* acts upstream to negatively regulate *egl-30* (Lackner et al., 1999; Miller et al., 1999; Nurrish et al., 1999). It remains to be determined whether *goa-1* also act upstream of *egl-30* in promoting sperm guidance.

SRB GPCRs promote efficient sperm motility within the oviduct

Deficient ovarian PGF synthesis causes sperm to move with reduced velocity, little directional velocity, and high reversal frequency. These sperm motility defects result in inefficient sperm targeting to the spermatheca. However, inefficient sperm targeting can also be caused by other factors such as impaired sperm activation. To investigate the basis of *srb* mutant sperm distribution abnormalities, we conducted time-lapse microscopy on wild-type hermaphrodites mated to *srb* mutant male sperm. These videos show that sperm become activated after insemination, but have altered motility parameters compared to control sperm.

Some *srb* mutant sperm (e.g. *srb-16Δ*, *srb-5Δ*) move slower than control sperm. Other srb mutant sperm (e.g. *srb-13Δ1*) reverse direction more frequently. Multiple *srb* GPCR losses result in combinatorial defects, consistent with the existence of parallel pathways affecting distinct sperm properties. The *srb* mutant sperm motility parameters are consistent with an impaired ability to respond to prostaglandin signals. However, further work is needed to test this model. Genetic epistasis study can be performed by

mating *srb* mutant males to hermaphrodites deficient in prostaglandins. If *srb* genes are essential for PGF function, sperm motility in the double mutants should be similar to single mutants.

SRB chemoreceptors likely function in male sensory neurons

qPCR and tdTomato tagged knock-in strategies demonstrate that *srb* genes are not expressed in sperm. The predicted promoters of *srb-2*, *srb-3*, *srb-5*, *srb-12*, and *srb-16* drive expression in sensory neuron-like cells in hermaphrodites and males. Particularly, *srb-13* appears expressed exclusively in three pairs of male sensory neurons (ASI, ASK, and AWB), and *srb-16* appears expressed in four pairs of male sensory neurons (ASH, ASI, ASK, and AWB). *srb-13* is expressed in the cilia of what appears to be ASI and/or ASK sensory neurons. Functional rescue experiments clearly show that *srb-13* is required in male sensory neurons. Future studies are needed to test whether SRB-13 acts in ASI, ASK, or both.

Although we failed to see endogenous SRB-16 in sensory cilia, *srb-16* is found primarily in the cell bodies of ASH, ASI, ASK, and AWB amphid sensory neuron pairs. Therefore, these expression data suggest that *srb-13* and *srb-16* work in common sensory neurons. *srb-16* is also expressed in cell bodies and dendrites of I1 interneuron pair, pm4 and pm5 pharyngeal muscle triplets, and unidentified head neurons. Although *srb-16* functions in neurons to promote sperm guidance, more work is needed to determine the specific neuron type(s).

Notably, *srb-13* and *srb-16* are both expressed in ASI and ASK sensory neurons. ASI and ASK have been known to promote chemotaxis (e.g. to lysisne) (Bargmann and Horvitz, 1991). ASK and ASI also have antagonistic roles in sensing and responding to

pheromones called ascarosides. Specifically, ASK promotes local food search behavior during early starvation, dauer, and male-specific sexual attraction, while ASI suppresses these responses (Bargmann and Horvitz, 1991; Gray et al., 2005; Kim et al., 2009; Schackwitz et al., 1996; Srinivasan et al., 2008; White and Jorgensen, 2012). Therefore, *srb-13* chemoreceptor gene expression and function in ASK or ASI sensory neurons suggest that SRB-13 is a pheromone receptor.

What are ligands of SRB-13 or other SRB chemoreceptors?

The serpentine receptors SRBC-64 and SRBC-66 are expressed in hermaphrodite ASK chemosensory neurons, where they recognize ascaroside #2 and #3 pheromones (Kim et al., 2009). Two other serpentine receptors SRG-36 and SRG-37 are expressed in ASI chemosensory neurons and are redundant receptors to ascaroside #5 pheromone (McGrath et al., 2011). The presence of SRB-13 or possibly other SRB chemoreceptors in male ASI or ASK cilia suggest that they also perceive ascarosides. A wide variety of ascaroside structures have been identified, with males and hermaphrodites synthesizing different types (Izrayelit et al., 2012; Srinivasan et al., 2008; von Reuss et al., 2012). One possibility is that ligands are hermaphrodite-derived. Previously, Srinivasan et al. reported that *C. elegans* males sense a blend of three different hermaphrodite-derived ascaroside #2, #3, and #4 pheromones (Srinivasan et al., 2008).

A second possibility is that the ligands are male-derived. The presence of other males might signal the male gonad to make more competitive sperm. Males are known to produce male-enriched ascaroside #10 to attract hermaphrodites in a population-density dependent manner (Izrayelit et al., 2012). Alternatively, male ciliated sensory neurons release extracellular vesicles that induce male mating behavior (Wang et al., 2014). Further

experiments are needed to determine whether SRB GPCRs are essential for perceiving ascaroside #10, other ascarosides, or unknown factors.

SRB GPCRs regulate gene transcription during spermatogenesis

How might SRB GPCRs in male sensory neurons affect sperm? We have recently shown in hermaphrodites that sensory neurons modulate expression of neuroendocrine signals such as DAF-7 TGF-β. DAF-7 transmits signals to developing oocytes, resulting in altered gene transcription (McKnight et al., 2014). To test whether male SRB GPCRs regulates spermatogenic gene transcription, we conducted transcriptome sequencing. We found a large number of sperm-enriched genes altered in *srb-13Δ2* males *srb-13,12,16Δ* males, including numerous genes exclusively expressed in sperm. Of the sixty five sperm-enriched genes up-regulated in *srb-13,12,16Δ* males alone, sixteen encode for sperm structural components (e.g. MSP, SSP, etc.). The other large sperm gene class is mitochondrial genes. We speculate that SRB GPCRs modulate the expression of cytoskeletal and metabolic genes, thereby making sperm more competitive and better at locating and maintaining position nearest to unfertilized eggs in the oviduct.

CONCLUSIONS

In summary, we have shown that SRB-13, SRB-16, SRB-15 and SRB-2 or SRB-3 chemoreceptors, as well as the downstream Gα GOA-1 function in male neurons to promote efficient sperm guidance. Gα EGL-30 also plays a role. We propose that these GPCRs initiate neuroendocrine transduction mechanisms that alter spermatogenic gene transcription, thereby coupling sperm quality to environmental status. This study and future

studies on this topic can help us better understand the impact of environmental changes on animal fertility and species survival.

MATERIALS AND METHODS

C. elegans strains

C. elegans were maintained at 20°C, unless otherwise indicated, and fed with NA22 *E. coli* bacteria, as previously described (Edmonds et al., 2010; Kubagawa et al., 2006). The *fog-2(q71)* strain was used for males. The following strains provided by Caenorhabditis Genetics Center (CGC) were used: N2 Bristol (wild type hermaphrodites), CB4108 [*fog-2(q71) V*] (wild-type male), SS104 [*glp-4(bn2) I*], JK816 [*fem-3(q20) IV*], RB2303 [*srb-13(ok3126) II*] (this strain was backcrossed 3 times and put into *fog-2(q71)* background), VC10071 [*srb-16(gk774) II unc-4(e120) II*] (this strain was outcrossed to remove the *unc-4(e120)* background, backcrossed 2 times and put into *fog-2(q71)* background), CG21 [*egl-30(tg26) I; him-5(e1490) V*] (this strain was outcrossed to replace the *him-5(e1490)* by *fog-2(q71)* background), DG1856 [*goa-1(sa734) I*] (this strain was crossed into *fog-2(q71)* background), KG524 [*gsa-1(ce94) I*] (this strain was crossed into *fog-2(q71)* background), BC12286 [*dpy-5(e907) I; sEx12286 [rCes srb-3::GFP + pCeh361]*], BC12285 [*dpy-5(e907) I; sEx12285 [rCes srb-5::GFP + pCeh361]*], BC12003 [*dpy-5(e907) I; sEx12003 [rCes srb-12::GFP + pCeh361]*], BC14700 [*dpy-5(e907) I; sEx14700 [rCes srb-13::GFP + pCeh361]*], BC14820 [*dpy-5(e907) I; sEx14820 [rCes srb-16::GFP + pCeh361]*]. The *srb-5(tm5831)* mutant were provided by the Japanese National Bioresource Project. The *srb-5(tm5831)* strain was backcrossed 1 time and put into *fog-2(q71)* background. The *srb-13(ttTi4405)* and *srb-2(ttTi4953)* mutants were provided by the NemaGENTAG consortium. The *srb-13(ttTi4405)* and *srb-*

2(ttTi4953) mutants were then crossed into *unc-119(ed3)* mutant background to facilitate positive selection.

Total RNA purification

N2 wild type, *fem-3(q20),* and *glp-4(bn2)* mutant hermaphrodites were grown at 16°C and synchronized to the L1 stage using an egg preparation with minor modifications (Porta-de-la-Riva et al., 2012). The larva were shifted to 25°C and cultured on thirty 150mm seeded plates per genotype for 2–3 days until they reach young adult stage (Edmonds et al., 2010; Hoang et al., 2013). Cultures were supplemented with concentrated bacteria as needed to prevent starvation. The adult worms were checked by inverted stereo scope to make sure that they did not have oocytes. The worms were then washed off plates with M9 and pelleted. Worm were then wash several more times with M9 to remove most bacteria (until the supernatant was clear). Worms were then pelleted and worm paste was transfer into a 5mL poly propylene tube. 1 mL of 0.5mm Zirconium beads (Next Advance) and 1.2mL of Trizol (Invitrogen) was added to each tube and the tubes were stored at -80ºC overnight. *srb-13(ok3126); fog-2(q71)*, *fog-2(q71)*, *srb-13 (xm1); fog-2(q71),* or *srb-13,12,16(xm3); fog-2(q71)* mutant males were purified by a previous published method (Miller, 2006). Briefly, synchronized adult males and hermaphrodites were separated using net with pore size of 35 um because gravid hermaphrodites were much thicker than males, as previously described (Miller, 2006).

The frozen N2 wild-type hermaphrodites or *fem-3(q20)* and *glp-4(bn2)* mutant hermaphrodites (Fig. 4), the frozen *srb-13(ok3126);fog-2(q71)* males (supplementary material Fig. S1), or the frozen *fog-2(q71)* wild-type male, *srb-13 (xm1); fog-2(q71),* or *srb-13,12,16(xm3); fog-2(q71)* mutant males (Fig. 10-12; supplementary material Table

S1-S2; SupplRNAseqData.xlsx) were thawed in their tubes at room temperature and homogenized with Bullet Blender 5© (Next Advance). Worm extracts were then transferred to a 1.6mL tube and spun at 16,000g at 4ºC for 15 minutes to pellet cellular debris. Supernatant was carefully transferred to a new 1.6mL tube leaving behind 100uL. 200uL of chloroform was added and vortexed for 15 seconds. The tube was left standing at room temperature for 2 min and spun at 16,000g at 4ºC for 10 minutes. 500uL of upper aqueous phase was carefully transferred to a new 1.6 mL tube. 500uL of isopropanol was added and the tube was quickly vortexed. The tube was left standing at room temperature for 10 minutes, and then spun at 16,000g at 4ºC for 10 minutes. Supernatant was discarded and 500uL of 70% ethanol was added. The tube was tilted horizontally and rolled slowly briefly. The tube was then spun at 16,000g at 4ºC for 2 minutes. Supernatant was removed and the total RNA pellet was air dried for about 10 minutes until it look transparent. 40-80uL of nuclease free water was added and slowly dissolving the pellet. At the end of 20 minutes waiting, the solution was slowly pipetted up and down to speed up the solvation. RNA concentration was measured by BioDrop©.

Reverse transcription PCR

4ug of total RNA of wild-type (*fog-2(q71)*) males (supplementary material Fig. S1) was used to make cDNA using Cloned AMV 1st strand cDNA synthesis kit (Invitrogen). PCR to amplify *srb-13* coding region was performed using Go-Taq (Promega) and primers *srb-13*P1 and *srb-13*P2 (see sequences in supplementary material table S3).

Quantitative reverse transcription real-time PCR

1ug of total RNA of N2 wild-type hermaphrodites, *fem-3(q20),* or *glp-4(bn2)* mutant hermaphrodites (Fig. 4) was used to make cDNA using Cloned AMV 1st strand cDNA synthesis kit (Invitrogen). qPCR was performed with SYBR green real-time PCR master mix (Life Technologies) and the following primers srb13qpcrF, srb13qpcrR, srb16qpcrF, srb16qpcrR, srb12qpcrF, srb12qpcrR, srb5qpcrF, srb5qpcrR, srb3qpcrF, srb3qpcrR, srb2qpcrF, srb2qpcrR, spe9qpcrF, spe9qpcrR ,spe11qpcrF ,spe11qpcrR ,cdc42qPCRF, cdc42qPCRR (see sequences in supplementary material Table S3).

Transcriptome RNA sequencing

5uL of 200ng/uL total RNA from *fem-3(q20)* and *glp-4(bn2)* mutant worms was sent UAB Heflin center for Next Generation Sequencing on Illlumina platform. Briefly, the quality of the total RNA were assessed using the Agilent 2100 Bioanalyzer followed by 2 rounds of poly A+ selection and conversion to cDNA. The TruSeq library generation kits was used as per the manufacturer's instructions (Illumina, San Diego, CA). Library construction consisted of random fragmentation of the polyA mRNA, followed by cDNA production using random primers. The ends of the cDNA were repaired, A-tailed and adaptors ligated for indexing (up to 12 different barcodes per lane) during the sequencing runs. The cDNA libraries was quantitated using qPCR in a Roche LightCycler 480 with the Kapa Biosystems kit for library quantitation (Kapa Biosystems, Woburn, MA) prior to cluster generation. Clusters was generated to yield approximately 725K-825K clusters/mm^2. Cluster density and quality was determined during the run after the first base addition parameters were assessed. We ran paired end 2X50bp sequencing runs to align the cDNA sequences to the reference genome. For data assessment, TopHat was used to align the raw RNA-Seq fastq reads to the C. elegans WBcel235 genome using the short

read aligner Bowtie (Langmead et al., 2009; Trapnell et al., 2009; Trapnell et al., 2012). TopHat also analyzed the mapping results to identify splice junctions between exons. Cufflinks used the aligned reads from TopHat to assemble transcripts, estimated their abundances and tested for differential expression and regulation (Trapnell et al., 2012; Trapnell et al., 2010). Cuffmerge, which is part of Cufflinks merged the assembled transcripts to a reference annotation and is capable of tracking Cufflinks transcripts across multiple experiments. Finally, Cuffdiff found significant changes in transcript expression, splicing and promoter use.

The levels of all transcript isoforms of each gene were pooled together to represent the level of the gene. The average level of transcripts of each gene in mutant male (*srb-13Δ2* or *srb-13,12,16Δ*) was compared with wild-type counterpart to give fold change. p-values of the gene expression differences between mutant and wild-type samples range from $5.0x10^{-5}$ to $3.3x10^{-3}$, and q-values are all under 0.05.

Molecular Cloning

pXM1, pXM2, and pXM3 (supplementary material Fig. S2,S4-S5) targeting vectors was cloned by Multisite Gateway 3-Fragment system (Invitrogen), where the middle fragment (*unc-119* rescue fragment and coelomocyte GFP marker) came from a pDONR221 called pCFJ66 plasmid (Addgene).

pXM4 (supplementary material Fig. S6) targeting vector was constructed by sequential restriction digest cloning with the following restriction enzymes (in the order of appearance in final vector): HindIII, XbaI, BamHI, SpeI, and ApaI into *myo-3p::mito::GFP* vector from Dr. van de Bliek (Labrousse et al., 1999).

pXM10 (supplementary material Fig. S7), pXM14 (supplementary material Fig. S8), pO6D11GFP (Fig. 7,9), pUS13 (Table 3), pUS16 (Table 3), pOS13 (Table 4), and pMS13 (Table 4) plasmids are constructed by Gibson Assembly (New England Biolab). The backbone pGem5Zf(+) was chosen for its small sequence and Blue-White screening. The backbone was linearized by NotI restriction enzyme (in pXM10, pUS13, and pUS16 plasmids) or by SacI restriction enzyme (pXM14, pO6D11FGP, pOS13, and pMS13 plasmids). Note that the *tdTomato::srb-16 3'UTR::unc-119 rescue fragment* from pXM14 was amplified from pXM10. Note that pOS13, and pMS13 plasmids share 3 construction primers.

Single guide RNAs (sgRNAs) plasmids for tdTomato knock-in into *srb-16* gene (in pSS16 plasmid) and *spe-9* (in pSS9 plasmid) were derived from *PU6::unc-119*_sgRNA plasmid (Addgene ID 46169) and cloned by Gibson Assembly. PCR amplified the entire sgRNA backbone except for 20 bases that belong to *unc-119* gene. The PCR primers also contained overlap that will introduce 20 bp of genomic DNA in 3' UTR of *sbr-16* and *spe-9* genes back into the sgRNA vector.

The transgenes *unc-119p::srb*-13 and *unc-119p::srb-16* (from pUS13 and pUS16 plasmids) are composed of 1204 bp upstream of the start codon of *unc-119* gene and 2725 bp of genomic DNA of *srb-13* gene including 6 bases upstream of the first codon, all exons and introns in between the start and stop codons, and 529 bp downstream of the stop codon (in pUS13 plasmid), or 2317 bp of genomic DNA of *srb-16* gene including 6 bases upstream of the first codon, all exons and introns in between the start and stop codons, and 69 bp downstream of the stop codon (in pUS16 plasmid). pUS13 and pUS16 plasmids were cloned by Gibson Assembly (New England Biolab).

The transgenes (from pOS13 and pMS13 plasmids) are composed of 427 bp upstream of the start codon of *osm-6* gene (in pOS13 plasmid) or 2,385 bp upstream of the start codon of *myo-3* gene (in pMS13 plasmid) and 1,035 bp of the full coding sequence of *srb-13* gene (from cDNA), *mCherry* tag, and *unc-54* 3'UTR amplified from pCFJ90 (Addgene). *srb-13* cDNA was used to avoid potential influence of *srb-13* introns on its expression pattern. The mCherry tag was used to confirm the expression pattern of the transgenes (shown in supplementary material Fig. S16). Gibson assembly (New England Biolab) was used to construct pOS13 and pMS13 plasmids.

Sequences of all vectors created (pXM1, pXM2, pXM3, pXM4, pXM10, pXM14, pSS16, pSS9, pO6D11GFP, pUS13, pUS16, pOS13, and pMS13) are provided in annotated ApE file format. The sequences of the primers used to construct the above plasmids are included in supplementary material Table S3.

Genome-editing using homologous recombination

srb-13Δ2 (supplementary material Fig. S2), *srb-13,12,16Δ* (supplementary material Fig. S4), and *srb-2,3,4,5Δ* (supplementary material Fig. S5) mutants was generated by MOSDEL technique (Frokjaer-Jensen et al., 2010). Briefly, mutant worms containing a *Drosophila* transposon called *Mos1* in or near the gene(s) of interest (obtained from NemaGENETAG consortium) was crossed into *unc-119* loss of function (*ed3* allele) mutant background. The resulting mutant worm is dumpy, uncoordinated, and has less survival fitness so that an *unc-119* rescuing DNA fragment serves as a positive selection marker. When Mos transposase gene was delivered into the worm via injection and expressed, Mos1 transposon was removed creating a double strand break at or near the

gene(s). The worm gonad was also injected with a homologous recombination plasmid (pXM1, pXM3, or pXM2) with left and right homology arms and a positive selection marker (*unc-119* DNA which is composed of 986 bp of *unc-119* promoter, 5' UTR, and start codon from *C. elegans*, 846 bp of coding exons from *C. briggsae,* and 293 bp of 3' UTR from *C. briggsae*) and a non-essential ceolomocyte GFP marker. We later learned from Dr. Christian Frøkjaer-Jensen, the first author of MOSDEL paper (Frøkjaer-Jensen et. al, 2010), that the GFP marker was unessential and its expression in targeted worm is often not seen. If recombination occurred, *unc-119* rescue fragment will replace the gene of interest, rescuing *unc-119* loss of function independent of the presence of extrachromosomal array which is marked by a cocktail of 3 bright mCherry markers. See (Frokjaer-Jensen et al., 2010) for more details.

srb-13$^{\text{KI}tdTomato}$ (supplementary material Fig. S6) mutant was generated similar to the *srb-13*$^{\Delta 2}$ mutant except that the recombination targeting plasmid (pXM4) contains *tdTomato*, 250 bases downstream of *srb-13* stop codon including 57-bp 3'UTR, the same 2-kb *unc-119* rescue fragment, in between the left (2-kb upstream of *srb-13* stop codon) and right homology (2-kb downstream of *srb-13* 3'UTR). pXM4 was cloned by sequential restriction digests.

srb-16$^{\text{KI}tdTomato}$ (supplementary material Fig. S7) and *spe-9*$^{\text{KI}tdTomato}$ (supplementary material Fig. S8) mutant was generated by in a way similar to *srb-13*$^{\text{KI}tdTomato}$ mutant except that CRISPR technique (Friedland et al., 2013) was used to generate a double strand break at about 90 bp downstream of the stop codons of *srb-16* or *spe-9*, respectively. The recombination targeting plasmids (pXM10 and pXM14) were cloned by Gibson assembly.

Phylogenetic tree analysis

The amino acid sequence of the SRB proteins were retrieved from WormBase.org version WS246. The multiple sequence analysis was performed by ClustalW2 web-based tool from the European Bioinformatics Institute at http://www.ebi.ac.uk/Tools/msa/clustalw2/. The phylogenetic tree and the sequence identity matrix were generated as part of the alignment.

Dye-filling with DiD

Dye-filling with DiD (Molecular Probes) was performed as described previously for DiI and DiO with minor modifications (Herman and Hedgecock, 1990; Williams et al., 2010). Briefly, male worms were picked and transfer to M9 buffer. Worm were washed 1 time with M9 to remove bacteria. Worms were incubated with 5mL of DiD stock (2mg/mL) in 1mL of M9 on a slow nurator for 30 minutes. Worms were washed twice with M9 and transferred to a watch glass. Worm were anesthetized with 0.1% tricaine and 0.01% tetramisole hydrochloride in M9 buffer for 30 minutes (McCarter et al., 1999). Then, they are mounted on a 2% agar pad, and confocal analysis was performed on a Nikon 2000U inverted microscope (Melville, KY) outfitted with a PerkinElmer UltraVIEW ERS 6FE-US spinning disk laser apparatus (Shelton, CT) in Yoder lab at University of Alabama at Birmingham. Confocal images were processed with Image J version 1.48 (Wayne Rasband, National Institute of Health).

Sperm guidance assays

MitoTracker Red CMXRos (Invitrogen) was used to stain *fog-2(q71)* males, as previously described (Edmonds et al., 2010; Hoang et al., 2013; Kubagawa et al., 2006). Briefly, about 150 male worms were transferred to a watch glass with 300 µl M9 buffer.

Three microliters of a 1 mM MitoTracker CMXRos solution in DMSO was added to the worm solution and mixed. Males were incubated in the dark for 2–3 hours and then transferred to a seeded plate. After 20 minutes, the males were transferred again to a fresh plate and allowed to recover overnight at 16°C. 10–20~2 day old adult hermaphrodites were anesthetized with 0.1% tricaine and 0.01% tetramisole hydrochloride in M9 buffer for 30 minutes (McCarter et al., 1999). The anesthetized hermaphrodites were transferred to a plate containing a ~1 cm drop of bacteria with 50–75 stained males. After 30 minutes of mating, the hermaphrodites were separated from the males and transferred to a fresh seeded plate. To directly observe sperm motility, mated hermaphrodites were mounted immediately onto a 2% agarose pad for time-lapse fluorescence microscopy. DIC and fluorescence images were taken every 30 seconds. Directional velocity toward the spermatheca was measured by creating a straight line through the uterus from the vulva to the spermatheca. The distance traveled along this line from the beginning of a sperm trace to the end was divided by time. Positive values indicate movement toward the spermatheca relative to the starting point. A change in migration direction of greater than 90° within 3 consecutive frames was classified as a reversal. Sperm traces range from a minimum of 2.5 minutes to a maximum of 15 minutes. At least 4 videos from different animals were used for quantification.

To assess sperm distribution, mated hermaphrodites were incubated in the dark for an hour without males and then mounted for microscopy. The reproductive tract was divided into 3 zones, as shown in Fig. 1. Zone 3 was defined as the region spanning the center of the spermatheca plus 50 microns toward the vulva. In cases where large sperm aggregations were adjacent to the spermatheca, zone 3 was expanded to include the entire aggregation. Zones 1 and 2 were defined by measuring the distance from the zone 3 border

to the vulva and dividing this region in half. AxioVision software was used to measure distances. A two sample, 2-tailed T-test where equal variance was not assumed was used to test for significance.

ACKNOWLEDGMENTS

We thank Dr. Michael Crowley, Dr. David Crossman, and the UAB Finley Sequencing Core Facility for performing RNAseq and bioinformatics analyses. We thank Dawn Landis, Scott Hanke, and Dr. Bradley Yoder for their help imaging cilia, the DiD studies, and providing the tdTomato containing plasmid. We thank Jessica Schultz, Tim Cole, and Matthew Alexander for helpful comments on the manuscript, as well as the Caenorhabditis Genetics Center, Japanese National Bioresource Project, and NemaGENTAG consortium for worm strains. We thank Wormbase.org, Wormbook.org, and Wormatlas.org for making worm knowledge easily accessible.

REFERENCES

Ahringer, J., Kimble, J., 1991. Control of the sperm-oocyte switch in Caenorhabditis elegans hermaphrodites by the fem-3 3' untranslated region. Nature 349, 346-348.

Aminov, R.I., 2010. A brief history of the antibiotic era: lessons learned and challenges for the future. Frontiers in microbiology 1, 134.

Anderson, J.L., Morran, L.T., Phillips, P.C., 2010. Outcrossing and the maintenance of males within C. elegans populations. The Journal of heredity 101 Suppl 1, S62-74.

Bargmann, C.I., Horvitz, H.R., 1991. Chemosensory neurons with overlapping functions direct chemotaxis to multiple chemicals in C. elegans. Neuron 7, 729-742.

Barnosky, A.D., Matzke, N., Tomiya, S., Wogan, G.O., Swartz, B., Quental, T.B., Marshall, C., McGuire, J.L., Lindsey, E.L., Maguire, K.C., Mersey, B., Ferrer, E.A., 2011. Has the Earth's sixth mass extinction already arrived? Nature 471, 51-57.

Beanan, M.J., Strome, S., 1992. Characterization of a germ-line proliferation mutation in C. elegans. Development 116, 755-766.

Birkhead, T.R., Martinez, J.G., Burke, T., Froman, D.P., 1999. Sperm mobility determines the outcome of sperm competition in the domestic fowl. Proceedings. Biological sciences / The Royal Society 266, 1759-1764.

Bohmer, M., Van, Q., Weyand, I., Hagen, V., Beyermann, M., Matsumoto, M., Hoshi, M., Hildebrand, E., Kaupp, U.B., 2005. Ca2+ spikes in the flagellum control chemotactic behavior of sperm. The EMBO journal 24, 2741-2752.

Brenker, C., Goodwin, N., Weyand, I., Kashikar, N.D., Naruse, M., Krahling, M., Muller, A., Kaupp, U.B., Strunker, T., 2012. The CatSper channel: a polymodal chemosensor in human sperm. The EMBO journal 31, 1654-1665.

Brenner, S., 1974. The genetics of Caenorhabditis elegans. Genetics 77, 71-94.

Browning, H., Strome, S., 1996. A sperm-supplied factor required for embryogenesis in C. elegans. Development 122, 391-404.

Brundage, L., Avery, L., Katz, A., Kim, U.J., Mendel, J.E., Sternberg, P.W., Simon, M.I., 1996. Mutations in a C. elegans Gqalpha gene disrupt movement, egg laying, and viability. Neuron 16, 999-1009.

Ceballos, G., Ehrlich, P.R., 2002. Mammal population losses and the extinction crisis. Science 296, 904-907.

Chiba, S., Roy, K., 2011. Selectivity of terrestrial gastropod extinctions on an oceanic archipelago and insights into the anthropogenic extinction process. Proceedings of the National Academy of Sciences of the United States of America 108, 9496-9501.

Cinner, J.E., Huchery, C., Darling, E.S., Humphries, A.T., Graham, N.A., Hicks, C.C., Marshall, N., McClanahan, T.R., 2013. Evaluating social and ecological vulnerability of coral reef fisheries to climate change. PLoS One 8, e74321.

Cohen-Dayag, A., Tur-Kaspa, I., Dor, J., Mashiach, S., Eisenbach, M., 1995. Sperm capacitation in humans is transient and correlates with chemotactic responsiveness to follicular factors. Proceedings of the National Academy of Sciences of the United States of America 92, 11039-11043.

Collet, J., Spike, C.A., Lundquist, E.A., Shaw, J.E., Herman, R.K., 1998. Analysis of osm-6, a gene that affects sensory cilium structure and sensory neuron function in Caenorhabditis elegans. Genetics 148, 187-200.

Cuppen, E., van der Linden, A.M., Jansen, G., Plasterk, R.H., 2003. Proteins interacting with Caenorhabditis elegans Galpha subunits. Comparative and functional genomics 4, 479-491.

Cutter, A.D., Payseur, B.A., 2003. Rates of deleterious mutation and the evolution of sex in Caenorhabditis. Journal of evolutionary biology 16, 812-822.

Denk, A.G., Holzmann, A., Peters, A., Vermeirssen, E.L.M., Kempenaer, B., 2005. Paternity in mallards: effects of sperm quality, and female sperm selection for inbreeding avoidance. Behavioral Ecology 16, 825-833.

Dirzo, R., Raven, P.H., 2003. Global state of biodiversity and loss. Annu. Rev. Environ. Resour. 28, 137-167.

Donnelly, E.T., Lewis, S.E., McNally, J.A., Thompson, W., 1998. In vitro fertilization and pregnancy rates: the influence of sperm motility and morphology on IVF outcome. Fertility and sterility 70, 305-314.

Donoghue, A.M., 1999. Prospective approaches to avoid flock fertility problems: predictive assessment of sperm function traits in poultry. Poultry science 78, 437-443.

Dorman, M., Perevolotsky, A., Sarris, D., Svoray, T., 2015. The effect of rainfall and competition intensity on forest response to drought: lessons learned from a dry extreme. Oecologia.

Edmonds, J.W., McKinney, S.L., Prasain, J.K., Miller, M.A., 2011. The gap junctional protein INX-14 functions in oocyte precursors to promote C. elegans sperm guidance. Developmental biology 359, 47-58.

Edmonds, J.W., Prasain, J.K., Dorand, D., Yang, Y., Hoang, H.D., Vibbert, J., Kubagawa, H.M., Miller, M.A., 2010. Insulin/FOXO signaling regulates ovarian prostaglandins critical for reproduction. Developmental cell 19, 858-871.

Etches, R.J., 1996. Reproduction in poultry. C.A.B International, Oxon.

Fleming, A., 1929. On antibacterial action of culture of Penicillium, with special reference to their use in isolation of B. influenzae. Br. J. Exp. Pathol. 10, 226-236.

Friedland, A.E., Tzur, Y.B., Esvelt, K.M., Colaiacovo, M.P., Church, G.M., Calarco, J.A., 2013. Heritable genome editing in C. elegans via a CRISPR-Cas9 system. Nature methods 10, 741-743.

Frokjaer-Jensen, C., Davis, M.W., Hollopeter, G., Taylor, J., Harris, T.W., Nix, P., Lofgren, R., Prestgard-Duke, M., Bastiani, M., Moerman, D.G., Jorgensen, E.M.,

2010. Targeted gene deletions in C. elegans using transposon excision. Nature methods 7, 451-453.

Funk, C.D., 2001. Prostaglandins and leukotrienes: advances in eicosanoid biology. Science 294, 1871-1875.

Gage, M.J., Macfarlane, C.P., Yeates, S., Ward, R.G., Searle, J.B., Parker, G.A., 2004. Spermatozoal traits and sperm competition in Atlantic salmon: relative sperm velocity is the primary determinant of fertilization success. Current biology : CB 14, 44-47.

Gibbons, J.W., Scott, D.E., Ryan, T.J., Buhlmann, K.A., Tuberville, T.D., Metts, B.S., Greene, J.L., Mills, T., Leiden, Y., Poppy, S., Winne, C.T., 2000. The Global Decline of Reptiles, Déjà Vu Amphibians: Reptile species are declining on a global scale. Six significant threats to reptile populations are habitat loss and degradation, introduced invasive species, environmental pollution, disease, unsustainable use, and global climate change. BioScience 50, 653-666.

Gray, J.M., Hill, J.J., Bargmann, C.I., 2005. A circuit for navigation in Caenorhabditis elegans. Proceedings of the National Academy of Sciences of the United States of America 102, 3184-3191.

Harris, T.W., Antoshechkin, I., Bieri, T., Blasiar, D., Chan, J., Chen, W.J., De La Cruz, N., Davis, P., Duesbury, M., Fang, R., Fernandes, J., Han, M., Kishore, R., Lee, R., Muller, H.M., Nakamura, C., Ozersky, P., Petcherski, A., Rangarajan, A., Rogers, A., Schindelman, G., Schwarz, E.M., Tuli, M.A., Van Auken, K., Wang, D., Wang, X., Williams, G., Yook, K., Durbin, R., Stein, L.D., Spieth, J., Sternberg, P.W., 2010. WormBase: a comprehensive resource for nematode research. Nucleic acids research 38, D463-467.

Herman, R.K., Hedgecock, E.M., 1990. Limitation of the size of the vulval primordium of Caenorhabditis elegans by lin-15 expression in surrounding hypodermis. Nature 348, 169-171.

Himes, J.E., Riffell, J.A., Zimmer, C.A., Zimmer, R.K., 2011. Sperm chemotaxis as revealed with live and synthetic eggs. The Biological bulletin 220, 1-5.

Hoang, H.D., Prasain, J.K., Dorand, D., Miller, M.A., 2013. A heterogeneous mixture of F-series prostaglandins promotes sperm guidance in the Caenorhabditis elegans reproductive tract. PLoS genetics 9, e1003271.

Hoffmann, M., Hilton-Taylor, C., Angulo, A., Bohm, M., Brooks, T.M., Butchart, S.H., Carpenter, K.E., Chanson, J., Collen, B., Cox, N.A., Darwall, W.R., Dulvy, N.K., Harrison, L.R., Katariya, V., Pollock, C.M., Quader, S., Richman, N.I., Rodrigues, A.S., Tognelli, M.F., Vie, J.C., Aguiar, J.M., Allen, D.J., Allen, G.R., Amori, G., Ananjeva, N.B., Andreone, F., Andrew, P., Aquino Ortiz, A.L., Baillie, J.E., Baldi, R., Bell, B.D., Biju, S.D., Bird, J.P., Black-Decima, P., Blanc, J.J., Bolanos, F., Bolivar, G.W., Burfield, I.J., Burton, J.A., Capper, D.R., Castro, F., Catullo, G., Cavanagh, R.D., Channing, A., Chao, N.L., Chenery, A.M., Chiozza, F., Clausnitzer, V., Collar, N.J., Collett, L.C., Collette, B.B., Cortez Fernandez, C.F., Craig, M.T., Crosby, M.J., Cumberlidge, N., Cuttelod, A., Derocher, A.E., Diesmos, A.C., Donaldson, J.S., Duckworth, J.W., Dutson, G., Dutta, S.K., Emslie, R.H., Farjon, A., Fowler, S., Freyhof, J., Garshelis, D.L., Gerlach, J., Gower, D.J., Grant, T.D., Hammerson, G.A., Harris, R.B., Heaney, L.R., Hedges, S.B., Hero, J.M., Hughes, B., Hussain, S.A., Icochea, M.J., Inger, R.F., Ishii, N., Iskandar, D.T., Jenkins, R.K., Kaneko, Y., Kottelat, M., Kovacs, K.M., Kuzmin, S.L., La Marca, E., Lamoreux, J.F., Lau, M.W., Lavilla, E.O.,

Leus, K., Lewison, R.L., Lichtenstein, G., Livingstone, S.R., Lukoschek, V., Mallon, D.P., McGowan, P.J., McIvor, A., Moehlman, P.D., Molur, S., Munoz Alonso, A., Musick, J.A., Nowell, K., Nussbaum, R.A., Olech, W., Orlov, N.L., Papenfuss, T.J., Parra-Olea, G., Perrin, W.F., Polidoro, B.A., Pourkazemi, M., Racey, P.A., Ragle, J.S., Ram, M., Rathbun, G., Reynolds, R.P., Rhodin, A.G., Richards, S.J., Rodriguez, L.O., Ron, S.R., Rondinini, C., Rylands, A.B., Sadovy de Mitcheson, Y., Sanciangco, J.C., Sanders, K.L., Santos-Barrera, G., Schipper, J., Self-Sullivan, C., Shi, Y., Shoemaker, A., Short, F.T., Sillero-Zubiri, C., Silvano, D.L., Smith, K.G., Smith, A.T., Snoeks, J., Stattersfield, A.J., Symes, A.J., Taber, A.B., Talukdar, B.K., Temple, H.J., Timmins, R., Tobias, J.A., Tsytsulina, K., Tweddle, D., Ubeda, C., Valenti, S.V., van Dijk, P.P., Veiga, L.M., Veloso, A., Wege, D.C., Wilkinson, M., Williamson, E.A., Xie, F., Young, B.E., Akcakaya, H.R., Bennun, L., Blackburn, T.M., Boitani, L., Dublin, H.T., da Fonseca, G.A., Gascon, C., Lacher, T.E., Jr., Mace, G.M., Mainka, S.A., McNeely, J.A., Mittermeier, R.A., Reid, G.M., Rodriguez, J.P., Rosenberg, A.A., Samways, M.J., Smart, J., Stein, B.A., Stuart, S.N., 2010. The impact of conservation on the status of the world's vertebrates. Science 330, 1503-1509.

Huey, R.B., Deutsch, C.A., Tewksbury, J.J., Vitt, L.J., Hertz, P.E., Alvarez Perez, H.J., Garland, T., Jr., 2009. Why tropical forest lizards are vulnerable to climate warming. Proceedings. Biological sciences / The Royal Society 276, 1939-1948.

Hughes, J.B., Daily, G.C., Ehrlich, P.R., 1997. Population diversity: its extent and extinction. Science 278, 689-692.

Italiano, J.E., Jr., Stewart, M., Roberts, T.M., 1999. Localized depolymerization of the major sperm protein cytoskeleton correlates with the forward movement of the

cell body in the amoeboid movement of nematode sperm. The Journal of cell biology 146, 1087-1096.

Izrayelit, Y., Srinivasan, J., Campbell, S.L., Jo, Y., von Reuss, S.H., Genoff, M.C., Sternberg, P.W., Schroeder, F.C., 2012. Targeted metabolomics reveals a male pheromone and sex-specific ascaroside biosynthesis in Caenorhabditis elegans. ACS chemical biology 7, 1321-1325.

Jaiswal, B.S., Eisenbach, M., 2002. Capacitation, in: DM, H. (Ed.), Fertilization. Academic, San Diego, pp. 57-117.

Jansen, G., Thijssen, K.L., Werner, P., van der Horst, M., Hazendonk, E., Plasterk, R.H., 1999. The complete family of genes encoding G proteins of Caenorhabditis elegans. Nature genetics 21, 414-419.

Jenkins, R.K., Tognelli, M.F., Bowles, P., Cox, N., Brown, J.L., Chan, L., Andreone, F., Andriamazava, A., Andriantsimanarilafy, R.R., Anjeriniaina, M., Bora, P., Brady, L.D., Hantalalaina, E.F., Glaw, F., Griffiths, R.A., Hilton-Taylor, C., Hoffmann, M., Katariya, V., Rabibisoa, N.H., Rafanomezantsoa, J., Rakotomalala, D., Rakotondravony, H., Rakotondrazafy, N.A., Ralambonirainy, J., Ramanamanjato, J.B., Randriamahazo, H., Randrianantoandro, J.C., Randrianasolo, H.H., Randrianirina, J.E., Randrianizahana, H., Raselimanana, A.P., Rasolohery, A., Ratsoavina, F.M., Raxworthy, C.J., Robsomanitrandrasana, E., Rollande, F., van Dijk, P.P., Yoder, A.D., Vences, M., 2014. Extinction risks and the conservation of Madagascar's reptiles. PLoS One 9, e100173.

Kaupp, U.B., Solzin, J., Hildebrand, E., Brown, J.E., Helbig, A., Hagen, V., Beyermann, M., Pampaloni, F., Weyand, I., 2003. The signal flow and motor response controling chemotaxis of sea urchin sperm. Nature cell biology 5, 109-117.

Kim, K., Sato, K., Shibuya, M., Zeiger, D.M., Butcher, R.A., Ragains, J.R., Clardy, J., Touhara, K., Sengupta, P., 2009. Two chemoreceptors mediate developmental effects of dauer pheromone in C. elegans. Science 326, 994-998.

Kubagawa, H.M., Watts, J.L., Corrigan, C., Edmonds, J.W., Sztul, E., Browse, J., Miller, M.A., 2006. Oocyte signals derived from polyunsaturated fatty acids control sperm recruitment in vivo. Nature cell biology 8, 1143-1148.

Kullberg, C., Fransson, T., Hedlund, J., Jonzen, N., Langvall, O., Nilsson, J., Bolmgren, K., 2015. Change in spring arrival of migratory birds under an era of climate change, Swedish data from the last 140 years. Ambio 44 Suppl 1, 69-77.

Kupker, W., Diedrich, K., Edwards, R.G., 1998. Principles of mammalian fertilization. Human reproduction 13 Suppl 1, 20-32.

L'Hernault, S.W., 2006. Spermatogenesis. WormBook : the online review of C. elegans biology, 1-14.

L'Hernault, S.W., Roberts, T.M., 1995. Cell biology of nematode sperm. Methods in cell biology 48, 273-301.

Labrousse, A.M., Zappaterra, M.D., Rube, D.A., van der Bliek, A.M., 1999. C. elegans dynamin-related protein DRP-1 controls severing of the mitochondrial outer membrane. Molecular cell 4, 815-826.

Lackner, M.R., Nurrish, S.J., Kaplan, J.M., 1999. Facilitation of synaptic transmission by EGL-30 Gqalpha and EGL-8 PLCbeta: DAG binding to UNC-13 is required to stimulate acetylcholine release. Neuron 24, 335-346.

Lambert, M., 2005. Lizards used as bioindicators to monitor pesticide contamination in sub-Saharan Africa: A review. Applied Herpetology 2, 99-107.

LaMunyon, C.W., Ward, S., 1998. Larger sperm outcompete smaller sperm in the nematode Caenorhabditis elegans. Proceedings. Biological sciences / The Royal Society 265, 1997-2002.

Langmead, B., Trapnell, C., Pop, M., Salzberg, S.L., 2009. Ultrafast and memory-efficient alignment of short DNA sequences to the human genome. Genome biology 10, R25.

Lessard, C., Siqueira, L.G., D'Amours, O., Sullivan, R., Leclerc, P., Palmer, C., 2011. Infertility in a beef bull due to a failure in the capacitation process. Theriogenology 76, 891-899.

Lishko, P.V., Botchkina, I.L., Kirichok, Y., 2011. Progesterone activates the principal Ca2+ channel of human sperm. Nature 471, 387-391.

Ma, X., Zhu, Y., Li, C., Xue, P., Zhao, Y., Chen, S., Yang, F., Miao, L., 2014. Characterisation of Caenorhabditis elegans sperm transcriptome and proteome. BMC genomics 15, 168.

Malo, A.F., Garde, J.J., Soler, A.J., Garcia, A.J., Gomendio, M., Roldan, E.R., 2005. Male fertility in natural populations of red deer is determined by sperm velocity and the proportion of normal spermatozoa. Biology of reproduction 72, 822-829.

McCarter, J., Bartlett, B., Dang, T., Schedl, T., 1999. On the control of oocyte meiotic maturation and ovulation in Caenorhabditis elegans. Developmental biology 205, 111-128.

McGrath, P.T., Xu, Y., Ailion, M., Garrison, J.L., Butcher, R.A., Bargmann, C.I., 2011. Parallel evolution of domesticated Caenorhabditis species targets pheromone receptor genes. Nature 477, 321-325.

McKnight, K., Hoang, H.D., Prasain, J.K., Brown, N., Vibbert, J., Hollister, K.A., Moore, R., Ragains, J.R., Reese, J., Miller, M.A., 2014. Neurosensory perception of environmental cues modulates sperm motility critical for fertilization. Science 344, 754-757.

Miller, K.G., Emerson, M.D., Rand, J.B., 1999. Goalpha and diacylglycerol kinase negatively regulate the Gqalpha pathway in C. elegans. Neuron 24, 323-333.

Miller, M.A., 2006. Sperm and oocyte isolation methods for biochemical and proteomic analysis. Methods in molecular biology 351, 193-201.

Miller, M.A., Cutter, A.D., Yamamoto, I., Ward, S., Greenstein, D., 2004. Clustered organization of reproductive genes in the C. elegans genome. Current biology : CB 14, 1284-1290.

Moghadam, F.S., Zimmer, M., 2014. Effects of warming and nutrient enrichment on how grazing pressure affects leaf litter-colonizing bacteria. Journal of environmental quality 43, 851-858.

Munire, M., Shimizu, Y., Sakata, Y., Minaguchi, R., Aso, T., 2004. Impaired hyperactivation of human sperm in patients with infertility. Journal of medical and dental sciences 51, 99-104.

Negro-Vilar, A., 1993. Stress and other environmental factors affecting fertility in men and women: overview. Environmental health perspectives 101 Suppl 2, 59-64.

Nelson, G.A., Roberts, T.M., Ward, S., 1982. Caenorhabditis elegans spermatozoan locomotion: amoeboid movement with almost no actin. The Journal of cell biology 92, 121-131.

Nishigaki, T., Chiba, K., Miki, W., Hoshi, M., 1996. Structure and function of asterosaps, sperm-activating peptides from the jelly coat of starfish eggs. Zygote 4, 237-245.

Nurrish, S., Segalat, L., Kaplan, J.M., 1999. Serotonin inhibition of synaptic transmission: Galpha(0) decreases the abundance of UNC-13 at release sites. Neuron 24, 231-242.

Olson, J.H., Xiang, X., Ziegert, T., Kittelson, A., Rawls, A., Bieber, A.L., Chandler, D.E., 2001. Allurin, a 21-kDa sperm chemoattractant from Xenopus egg jelly, is related to mammalian sperm-binding proteins. Proceedings of the National Academy of Sciences of the United States of America 98, 11205-11210.

Pereira, H.M., Leadley, P.W., Proenca, V., Alkemade, R., Scharlemann, J.P., Fernandez-Manjarres, J.F., Araujo, M.B., Balvanera, P., Biggs, R., Cheung, W.W., Chini, L., Cooper, H.D., Gilman, E.L., Guenette, S., Hurtt, G.C., Huntington, H.P., Mace, G.M., Oberdorff, T., Revenga, C., Rodrigues, P., Scholes, R.J., Sumaila, U.R., Walpole, M., 2010. Scenarios for global biodiversity in the 21st century. Science 330, 1496-1501.

Piggott, J.J., Townsend, C.R., Matthaei, C.D., 2015. Climate warming and agricultural stressors interact to determine stream macroinvertebrate community dynamics. Global change biology.

Pimm, S.L., Russell, G.J., Gittleman, J.L., Brooks, T.M., 1995. The future of biodiversity. Science 269, 347-350.

Pizzari, T., Parker, G.A., 2009. Sperm competition and sperm phenotype, in: Birkhead TR, H.D., Pitnick S (Ed.), In Sperm biology: an evolutionary perspective. Academic Press, Oxford, UK, pp. 207–245.

Porta-de-la-Riva, M., Fontrodona, L., Villanueva, A., Ceron, J., 2012. Basic Caenorhabditis elegans methods: synchronization and observation. Journal of visualized experiments : JoVE, e4019.

Publicover, S.J., Giojalas, L.C., Teves, M.E., de Oliveira, G.S., Garcia, A.A., Barratt, C.L., Harper, C.V., 2008. Ca2+ signalling in the control of motility and guidance in mammalian sperm. Front Biosci 13, 5623-5637.

Punjabi, G.A., Chellam, R., Vanak, A.T., 2013. Importance of native grassland habitat for den-site selection of Indian foxes in a fragmented landscape. PLoS One 8, e76410.

Putiri, E., Zannoni, S., Kadandale, P., Singson, A., 2004. Functional domains and temperature-sensitive mutations in SPE-9, an EGF repeat-containing protein required for fertility in Caenorhabditis elegans. Developmental biology 272, 448-459.

Quinn, R.A., Lim, Y.W., Maughan, H., Conrad, D., Rohwer, F., Whiteson, K.L., 2014. Biogeochemical forces shape the composition and physiology of polymicrobial communities in the cystic fibrosis lung. mBio 5, e00956-00913.

Ralt, D., Goldenberg, M., Fetterolf, P., Thompson, D., Dor, J., Mashiach, S., Garbers, D.L., Eisenbach, M., 1991. Sperm attraction to a follicular factor(s) correlates with human egg fertilizability. Proceedings of the National Academy of Sciences of the United States of America 88, 2840-2844.

Ralt, D., Manor, M., Cohen-Dayag, A., Tur-Kaspa, I., Ben-Shlomo, I., Makler, A., Yuli, I., Dor, J., Blumberg, S., Mashiach, S., et al., 1994. Chemotaxis and chemokinesis of human spermatozoa to follicular factors. Biology of reproduction 50, 774-785.

Ribeiro, R., Santos, X., Sillero, N., Carretero, M.A., Llorente, G.A., 2009. Biodiversity and Land uses at a regional scale: Is agriculture the biggest threat for reptile assemblages? Acta Oecologica 35, 327-334.

Rivetti, I., Fraschetti, S., Lionello, P., Zambianchi, E., Boero, F., 2014. Global warming and mass mortalities of benthic invertebrates in the mediterranean sea. PLoS One 9, e115655.

Roberts, T.M., King, K.L., 1991. Centripetal flow and directed reassembly of the major sperm protein (MSP) cytoskeleton in the amoeboid sperm of the nematode, Ascaris suum. Cell motility and the cytoskeleton 20, 228-241.

Roberts, T.M., Ward, S., 1982. Centripetal flow of pseudopodial surface components could propel the amoeboid movement of Caenorhabditis elegans spermatozoa. The Journal of cell biology 92, 132-138.

Rokaya, M.B., Uprety, Y., Poudel, R.C., Timsina, B., Munzbergova, Z., Asselin, H., Tiwari, A., Shrestha, S.S., Sigdel, S.R., 2014. Traditional uses of medicinal plants in gastrointestinal disorders in Nepal. Journal of ethnopharmacology 158 Pt A, 221-229.

Royal, D.C., Royal, M.A., Wessels, D., L'Hernault, S., Soll, D.R., 1997. Quantitative analysis of Caenorhabditis elegans sperm motility and how it is affected by mutants spe11 and unc54. Cell motility and the cytoskeleton 37, 98-110.

Schackwitz, W.S., Inoue, T., Thomas, J.H., 1996. Chemosensory neurons function in parallel to mediate a pheromone response in C. elegans. Neuron 17, 719-728.

Sepsenwol, S., Ris, H., Roberts, T.M., 1989. A unique cytoskeleton associated with crawling in the amoeboid sperm of the nematode, Ascaris suum. The Journal of cell biology 108, 55-66.

Singson, A., Mercer, K.B., L'Hernault, S.W., 1998. The C. elegans spe-9 gene encodes a sperm transmembrane protein that contains EGF-like repeats and is required for fertilization. Cell 93, 71-79.

Smith, H., 2006. Sperm motility and MSP. WormBook : the online review of C. elegans biology, 1-8.

Srinivasan, J., Kaplan, F., Ajredini, R., Zachariah, C., Alborn, H.T., Teal, P.E., Malik, R.U., Edison, A.S., Sternberg, P.W., Schroeder, F.C., 2008. A blend of small molecules regulates both mating and development in Caenorhabditis elegans. Nature 454, 1115-1118.

Stewart, A.D., Phillips, P.C., 2002. Selection and maintenance of androdioecy in Caenorhabditis elegans. Genetics 160, 975-982.

Strunker, T., Goodwin, N., Brenker, C., Kashikar, N.D., Weyand, I., Seifert, R., Kaupp, U.B., 2011. The CatSper channel mediates progesterone-induced Ca2+ influx in human sperm. Nature 471, 382-386.

Suarez, S.S., 2008. Control of hyperactivation in sperm. Human reproduction update 14, 647-657.

Suarez, S.S., Ho, H.C., 2003. Hyperactivation of mammalian sperm. Cellular and molecular biology 49, 351-356.

Trapnell, C., Pachter, L., Salzberg, S.L., 2009. TopHat: discovering splice junctions with RNA-Seq. Bioinformatics 25, 1105-1111.

Trapnell, C., Roberts, A., Goff, L., Pertea, G., Kim, D., Kelley, D.R., Pimentel, H., Salzberg, S.L., Rinn, J.L., Pachter, L., 2012. Differential gene and transcript expression analysis of RNA-seq experiments with TopHat and Cufflinks. Nature protocols 7, 562-578.

Trapnell, C., Williams, B.A., Pertea, G., Mortazavi, A., Kwan, G., van Baren, M.J., Salzberg, S.L., Wold, B.J., Pachter, L., 2010. Transcript assembly and

quantification by RNA-Seq reveals unannotated transcripts and isoform switching during cell differentiation. Nature biotechnology 28, 511-515.

Villanueva-Diaz, C., Vadillo-Ortega, F., Kably-Ambe, A., Diaz-Perez, M.A., Krivitzky, S.K., 1990. Evidence that human follicular fluid contains a chemoattractant for spermatozoa. Fertility and sterility 54, 1180-1182.

Vinagre, C., Leal, I., Mendonca, V., Flores, A.A., 2015. Effect of warming rate on the critical thermal maxima of crabs, shrimp and fish. Journal of thermal biology 47, 19-25.

von Reuss, S.H., Bose, N., Srinivasan, J., Yim, J.J., Judkins, J.C., Sternberg, P.W., Schroeder, F.C., 2012. Comparative metabolomics reveals biogenesis of ascarosides, a modular library of small-molecule signals in C. elegans. Journal of the American Chemical Society 134, 1817-1824.

Vredenburg, V.T., Knapp, R.A., Tunstall, T.S., Briggs, C.J., 2010. Dynamics of an emerging disease drive large-scale amphibian population extinctions. Proceedings of the National Academy of Sciences of the United States of America 107, 9689-9694.

Wake, D.B., Vredenburg, V.T., 2008. Colloquium paper: are we in the midst of the sixth mass extinction? A view from the world of amphibians. Proceedings of the National Academy of Sciences of the United States of America 105 Suppl 1, 11466-11473.

Wang, J., Silva, M., Haas, L.A., Morsci, N.S., Nguyen, K.C., Hall, D.H., Barr, M.M., 2014. C. elegans ciliated sensory neurons release extracellular vesicles that function in animal communication. Current biology : CB 24, 519-525.

Ward, G.E., Brokaw, C.J., Garbers, D.L., Vacquier, V.D., 1985. Chemotaxis of Arbacia punctulata spermatozoa to resact, a peptide from the egg jelly layer. The Journal of cell biology 101, 2324-2329.

Ward, S., Carrel, J.S., 1979. Fertilization and sperm competition in the nematode Caenorhabditis elegans. Developmental biology 73, 304-321.

Wells, I.C., 1952. Antibiotic substances produced by Pseudomonas aeruginosa; syntheses of Pyo Ib, Pyo Ic, and Pyo III. J Biol Chem 196, 331-340.

White, J.Q., Jorgensen, E.M., 2012. Sensation in a single neuron pair represses male behavior in hermaphrodites. Neuron 75, 593-600.

Williams, C.L., Masyukova, S.V., Yoder, B.K., 2010. Normal ciliogenesis requires synergy between the cystic kidney disease genes MKS-3 and NPHP-4. Journal of the American Society of Nephrology : JASN 21, 782-793.

Xiang, X., Burnett, L., Rawls, A., Bieber, A., Chandler, D., 2004. The sperm chemoattractant "allurin" is expressed and secreted from the Xenopus oviduct in a hormone-regulated manner. Developmental biology 275, 343-355.

Xiang, X., Kittelson, A., Olson, J., Bieber, A., Chandler, D., 2005. Allurin, a 21 kD sperm chemoattractant, is rapidly released from the outermost jelly layer of the Xenopus egg by diffusion and medium convection. Mol Reprod Dev 70, 344-360.

Yoshida, M., Murata, M., Inaba, K., Morisawa, M., 2002. A chemoattractant for ascidian spermatozoa is a sulfated steroid. Proceedings of the National Academy of Sciences of the United States of America 99, 14831-14836.

Young, H.S., Dirzo, R., Helgen, K.M., McCauley, D.J., Billeter, S.A., Kosoy, M.Y., Osikowicz, L.M., Salkeld, D.J., Young, T.P., Dittmar, K., 2014. Declines in large wildlife increase landscape-level prevalence of rodent-borne disease in Africa.

Proceedings of the National Academy of Sciences of the United States of America 111, 7036-7041.

Zannoni, S., L'Hernault, S.W., Singson, A.W., 2003. Dynamic localization of SPE-9 in sperm: a protein required for sperm-oocyte interactions in Caenorhabditis elegans. BMC developmental biology 3, 10.

Zatylny, C., Marvin, L., Gagnon, J., Henry, J., 2002. Fertilization in Sepia officinalis: the first mollusk sperm-attracting peptide. Biochemical and biophysical research communications 296, 1186-1193.

FIGURES

DIC + MT

Zone 3: 92% ± 0.6%
Zone 2: 4% ± 0.3%
Zone 1: 4% ± 0.5%
N = 83

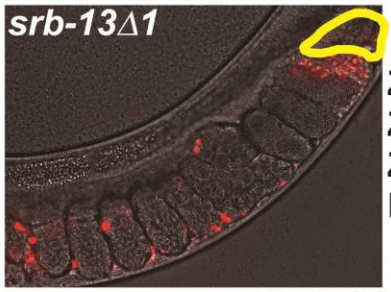

Zone 3: 66% ± 3% *
Zone 2: 13% ± 1%
Zone 1: 20% ± 2%
N = 36

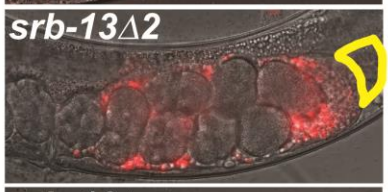

Zone 3: 66% ± 4% *
Zone 2: 17% ± 2%
Zone 1: 17% ± 2%
N = 22

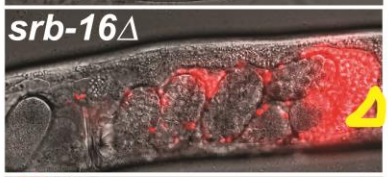

Zone 3: 67% ± 2% *
Zone 2: 14% ± 1%
Zone 1: 20% ± 2%
N = 40

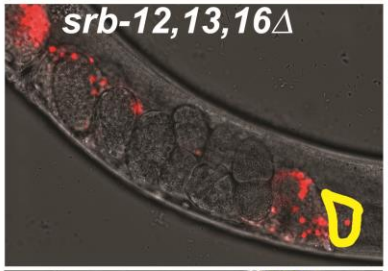

Zone 3: 49% ± 2% * #
Zone 2: 25% ± 1%
Zone 1: 27% ± 2%
N = 57

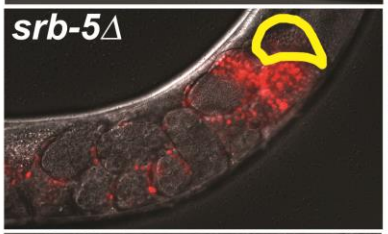

Zone 3: 69% ± 3% *
Zone 2: 11% ± 1%
Zone 1: 21% ± 2%
N = 57

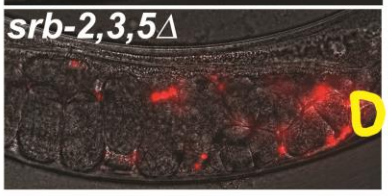

Zone 3: 61% ± 2% * ‡
Zone 2: 19% ± 1%
Zone 1: 21% ± 1%
N = 95

Fig. 1. **Sperm guidance of WT and *srb* mutant males in wild-type hermaphrodites.** Sperm distribution in the hermaphrodite uterus 1 hour after mating wild-type hermaphrodites to wild-type or mutant males. A representative image is shown to the left and average zone distribution ± standard error of the mean is to the right. The zone distribution values for wild-type male sperm are pooled from multiple experiments and used throughout this manuscript for reference. The spermatheca (S) is outlined in yellow. The official allele names for *srb-13Δ1*, *srb-13Δ2*, *srb-16Δ*, *srb-13,12,16Δ*, *srb-5Δ*, and *srb-2,3,4,5Δ* are *ok3126*, *xm1*, *gk774*, *xm3*, *tm5831*, and *xm2*, respectively. Mutant worms were crossed into *fog-2(q71)* mutant background to increase the incidence of males. The control strain is *fog-2(q71),* and wild-type hermaphrodite strain is N2. MT, MitoTracker channel; N, number of gonads quantified; Scale bar, 20 μm. *, statistically different from wild-type ($p<0.000001$). #, statistically different from single mutants *srb-13Δ1*, *srb-13Δ2*, *srb-16Δ* ($p<0.0002$). ‡, statistically different from single mutant *srb-5*$^{\Delta}$ ($p<0.02$). See MATERIALS AND METHODS for zone definitions.

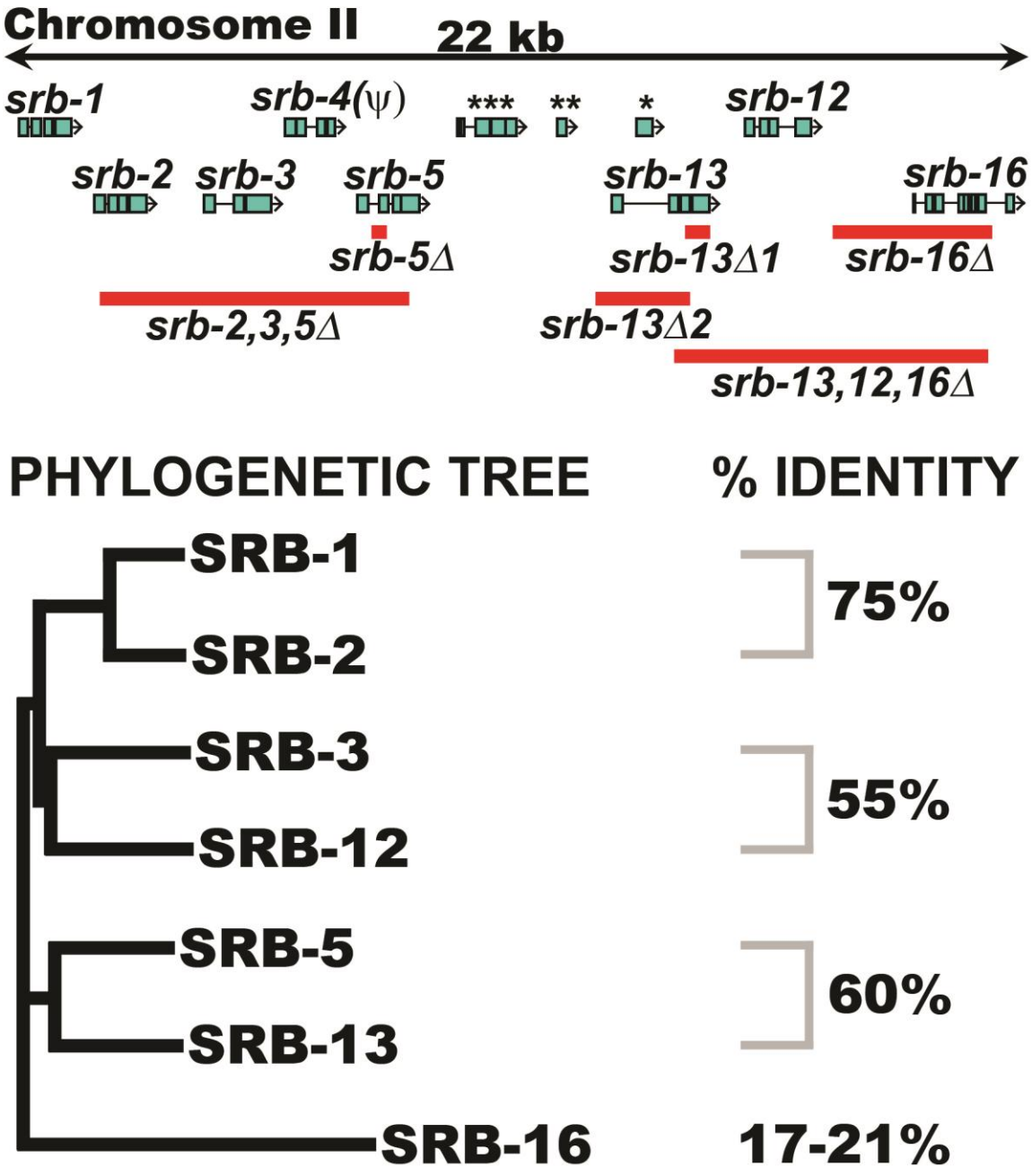

Fig. 2. Diagram of *srb* genomic locus and phylogenetic tree of SRB proteins.

The upper diagram represent *srb* genomic locus chromosome II. Cyan boxes represent coding exons, and red bars represent deleted DNA sequences. All the elements are up to scale. Genes of interest are labeled with names whereas other genes are labeled with asterisks. * & **, two major sperm protein (MSP) coding genes, *msp-45* & *F58A6.9*, respectively; ***, *C27D6.11*, a gene with unknown function. *srb-4* was classified as a

pseudogene. *srb-5Δ (tm5831)* mutant worm was provided by the Japanese worm knock out consortium; *srb-13Δ1(ok3126)* and *srb-16Δ(gk774)* mutant worms were provided by the CGC knock out consortium. *srb-13Δ2* (named *xm1*), *srb-2,3,4,5Δ* (named *xm2*), and *srb-13,12,16Δ* (named *xm3*) alleles were generated in our lab by the MOSDEL technique (Frokjaer-Jensen et al., 2010). The lower diagram depicts the phylogenetic tree of the SRB proteins. Both the tree and the amino acid sequence identity values were generated by ClustalW2, a multiple sequence alignment software from the European Bioinformatics Institute website.

DIC + MT

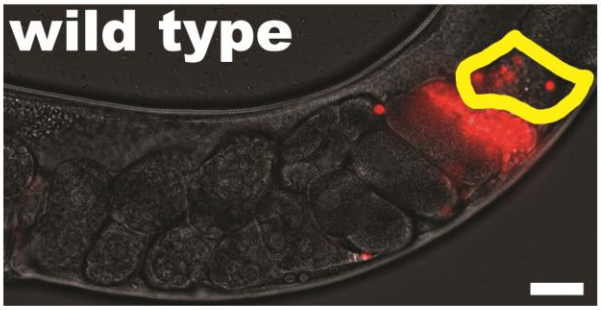

Zone 3: 92% ± 0.6%
Zone 2: 4% ± 0.3%
Zone 1: 4% ± 0.5%
N = 83

Zone 3: 87% ± 3%
Zone 2: 7% ± 2%
Zone 1: 6% ± 2%
N = 18

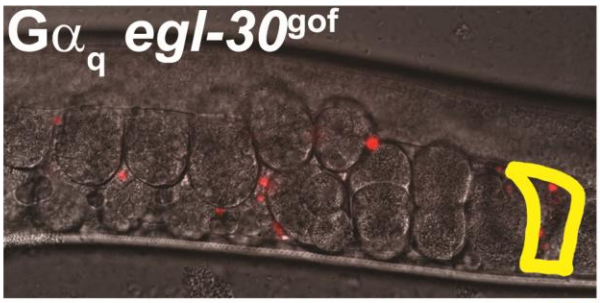

Zone 3: 49% ± 3% *
Zone 2: 26% ± 2%
Zone 1: 25% ± 2%
N = 37

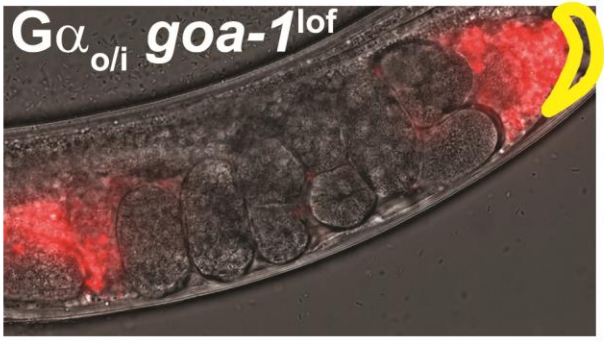

Zone 3: 53% ± 2% *
Zone 2: 25% ± 2%
Zone 1: 22% ± 2%
N = 30

Fig. 3. Sperm guidance of WT and different G-protein mutant males in wild-type hermaphrodites.

Sperm distribution in the hermaphrodite uterus 1 hour after mating wild-type hermaphrodites to wild-type or mutant males. A representative image is shown to the left and average zone distribution ± standard error of the mean is to the right. The zone distribution values for wild-type sperm from Figure 1 are provided for reference. The spermatheca (S) is outlined in yellow. *egl-30*, *goa-1*, and *gsa-1* encode a $G\alpha_q$, $G\alpha_o$, and $G\alpha_s$, respectively. The official allele names for *egl-30*^{gof}, *goa-1*^{lof}, and *gsa-1*^{gof} are *tg26*, *sa734*, and *ce94.* The gain of function mutations in *egl-30* and *gsa-1* were used instead of the loss of function mutations because loss of function in those genes are embryonic lethal (Brundage et al., 1996). Mutant worms were crossed into *fog-2(q71)* mutant background to increase the incidence of males. Wild-type male strain is *fog-2(q71),* and wild-type hermaphrodite strain is N2. MT, MitoTracker channel; N, number of gonads scored; gof, gain of function; lof, loss of function; Scale bar, 20 μm. *, $p<0.000001$. See Materials and Methods for zone definitions.

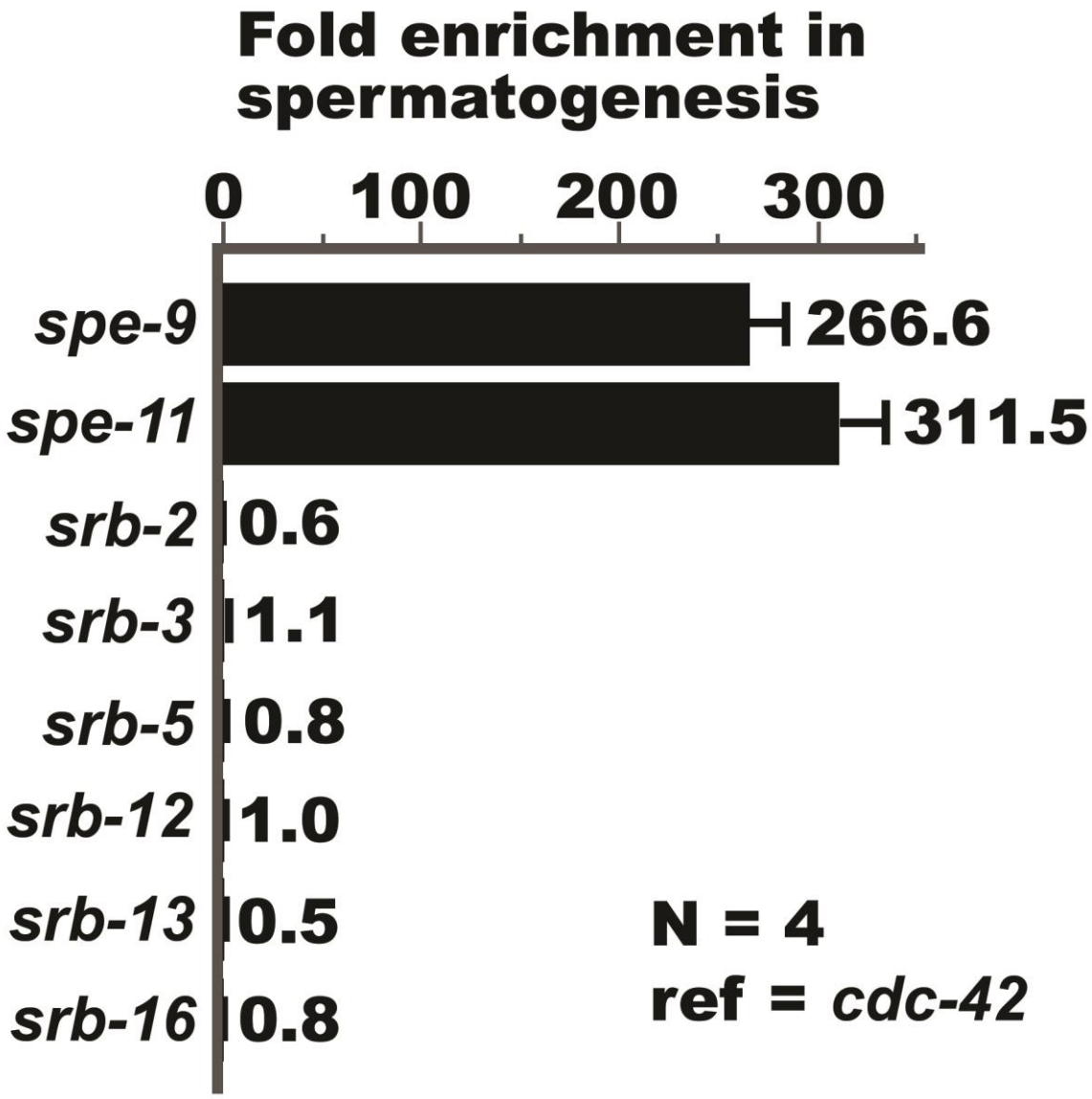

Fig. 4. *srb* gene expression in hermaphrodites undergoing spermatogenesis.

The mutant worm strains were grown at permissive temperature of 16^{o}C and then synchronized at larval stage L1 at 25^{o}C (see methods). Synchronized larval worms were then grown at restrictive temperature for 2-3 days until they became young adults. The worms were then pelleted and total RNA were extracted (Trizol, Invitrogen). Oligo dT primer was used to make cDNA libraries from 1 ug of total RNA (Cloned AMV First-strand cDNA synthesis kit, Invitrogen). Levels of cDNA for different genes were then measured by qPCR. We define fold enrichment in spermatogenesis of a gene as the ratio

of the level of cDNA for that gene in *fem-3(q20)* mutant worms, which make only sperm (Ahringer and Kimble, 1991) to the level of cDNA for that gene in *glp-4(bn2)* mutant worms, which make no sperm nor oocytes (Beanan and Strome, 1992). S*pe-9* and *spe-11* were used as positive control (Browning and Strome, 1996; Putiri et al., 2004; Royal et al., 1997; Singson et al., 1998; Zannoni et al., 2003). All qPCR reactions were run in quadruplicates, and *cdc-42* (a house keeping gene) was used as a reference gene. Fold enrichment was calculated by StepOne™ software version 2.3 (Applied Biosystems). Fold enrichment in spermatogenesis is shown as a bar graph with a numerical value on top of each bar. Error bar represents standard deviation.

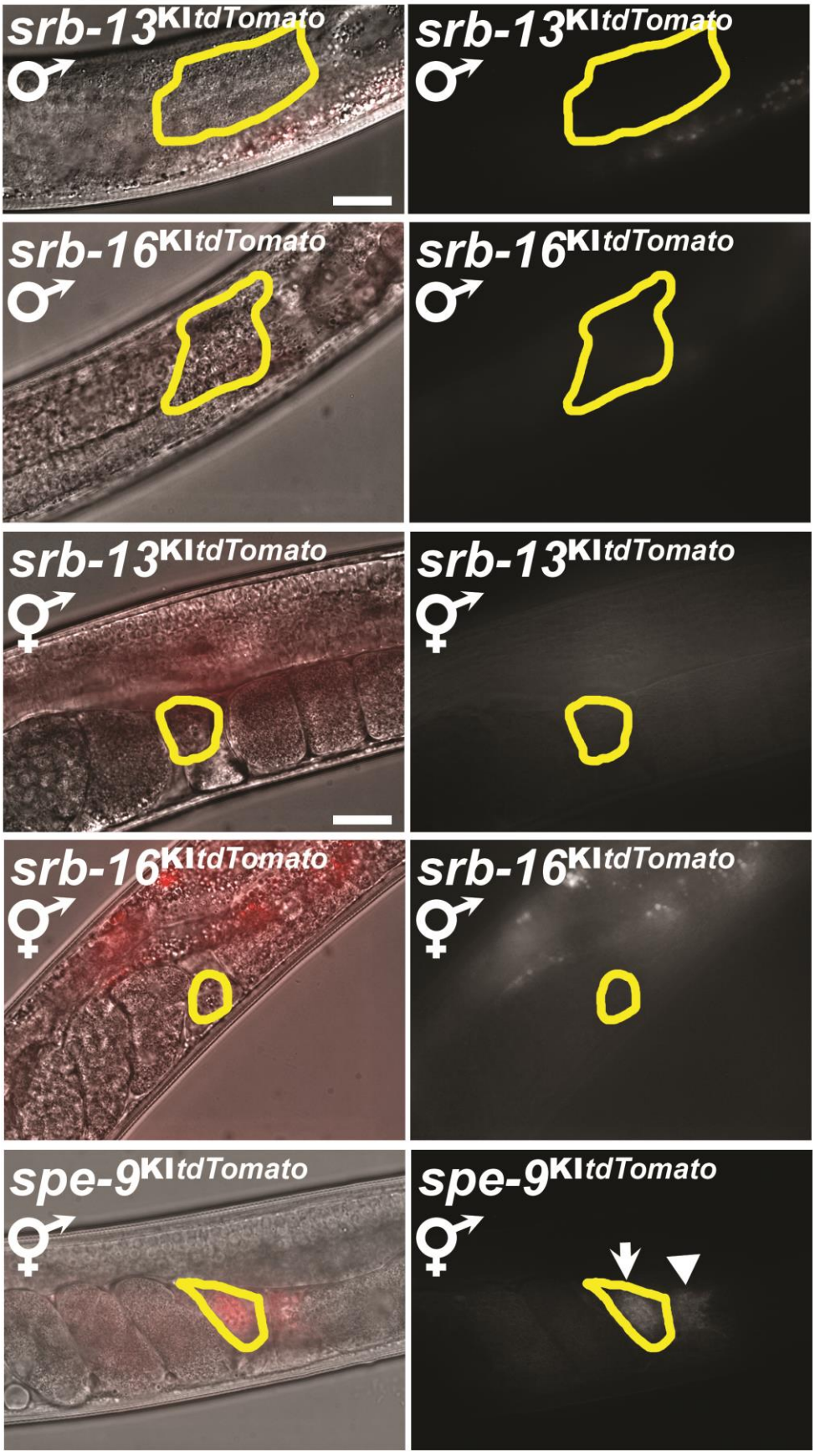
srb-13KItdTomato
srb-13KItdTomato
srb-16KItdTomato
srb-16KItdTomato
srb-13KItdTomato
srb-13KItdTomato
srb-16KItdTomato
srb-16KItdTomato
spe-9KItdTomato
spe-9KItdTomato

Fig. 5. SRB-13 and SRB-16 expression in the gonad.

The generation of the three tdTomato knock-in worm strains is shown in supplementary material Fig. S6-S8. Expression of SRB-13 and SRB-16 in spermatids of male or hermaphrodite worms is not detectable, although expression in head neurons is detectable. *spe-9*$^{\mathrm{KI}tdTomato}$ was generated as a positive control. *spe-9* encodes an EGF domain-containing transmembrane protein required in sperm for fertilization (Fig. 4) (Putiri et al., 2004; Singson et al., 1998; Zannoni et al., 2003). *srb-13*$^{\mathrm{KI}tdTomato}$ and *srb-16*$^{\mathrm{KI}tdTomato}$ male strains are in the *fog-2(q71)* background. Yellow outlines locations of the spermatids and sperm. Images on the right are from the red florescent channel detecting tdTomato signal. Images on the left contain the merged signal from the red fluorescent and Differential Interference Contrast (DIC) channels. The white arrow on the left indicate the mature sperm inside the spermatheca, outlined in yellow. The white arrow on the right indicates sperm residual bodies as by-products of previous spermatogenesis and possibly a few mature sperm. Scale bar, 20 um.

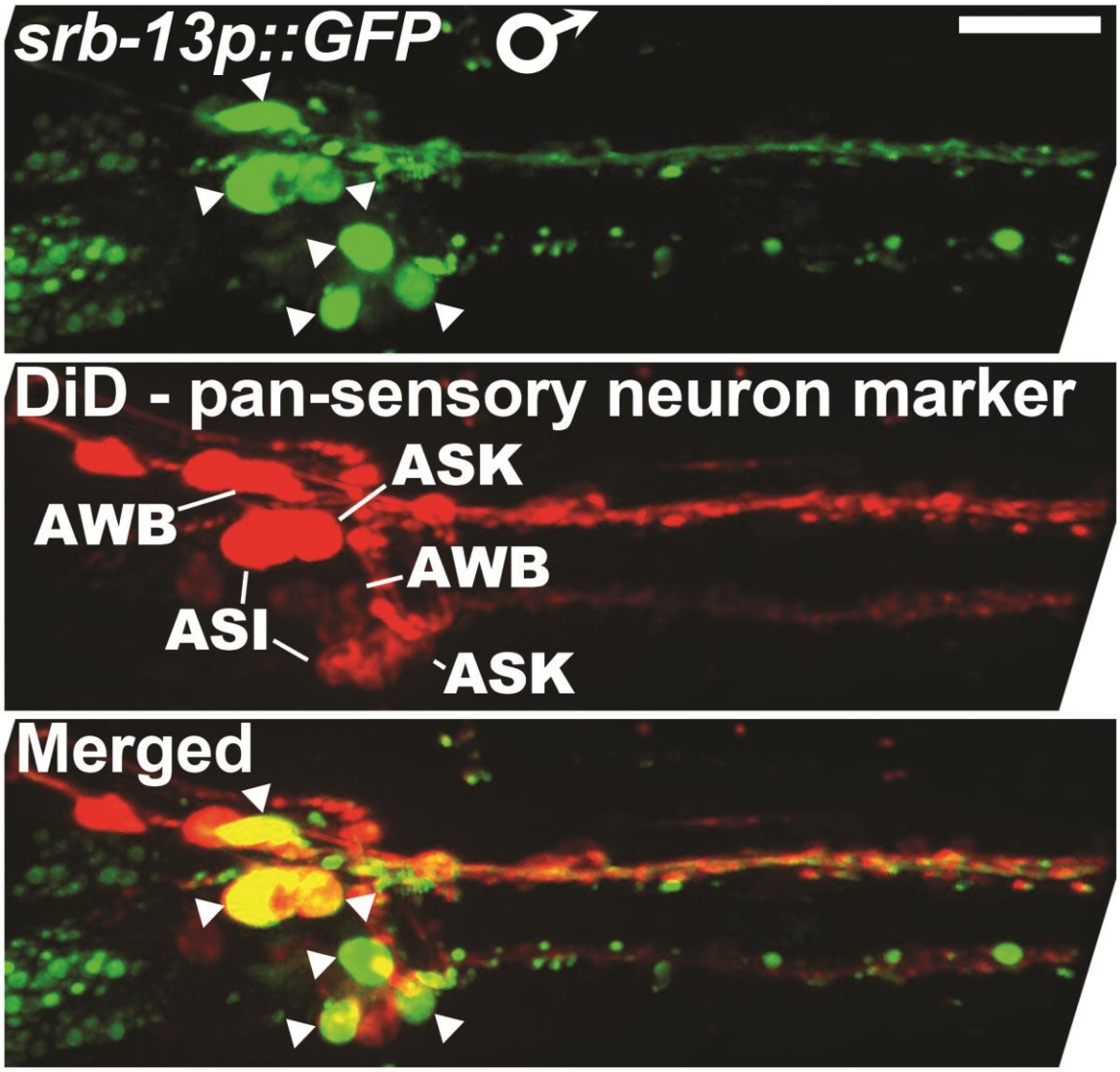

Fig. 6. Predicted *srb-13* promoter expression in males.

The worm strain (*BC14700*) transiently expressing GFP under the predicted *srb-13* promoter (968 bp upstream of the translational start site) was mated with *fog-2 (q71)* males to generate transgenic male animals. The male progeny was then incubated with DiD, a far-red membrane staining fluorescent tag that stains all sensory neurons (see MATERIALS AND METHODS). The images was processed by ImageJ (version 1.48). The images shown were obtained by collapsing all slices by "Z project" function from "Stacks". ASI, Amphid Single-ciliated neuron I with a linear cilium. ASK, Amphid

Single-ciliated neuron K with a linear cilium. AWB, Amphid Wing neuron B with a branched cilium. White arrow heads indicate GFP-positive cell bodies of amphid neurons. Scale bar, 20um.

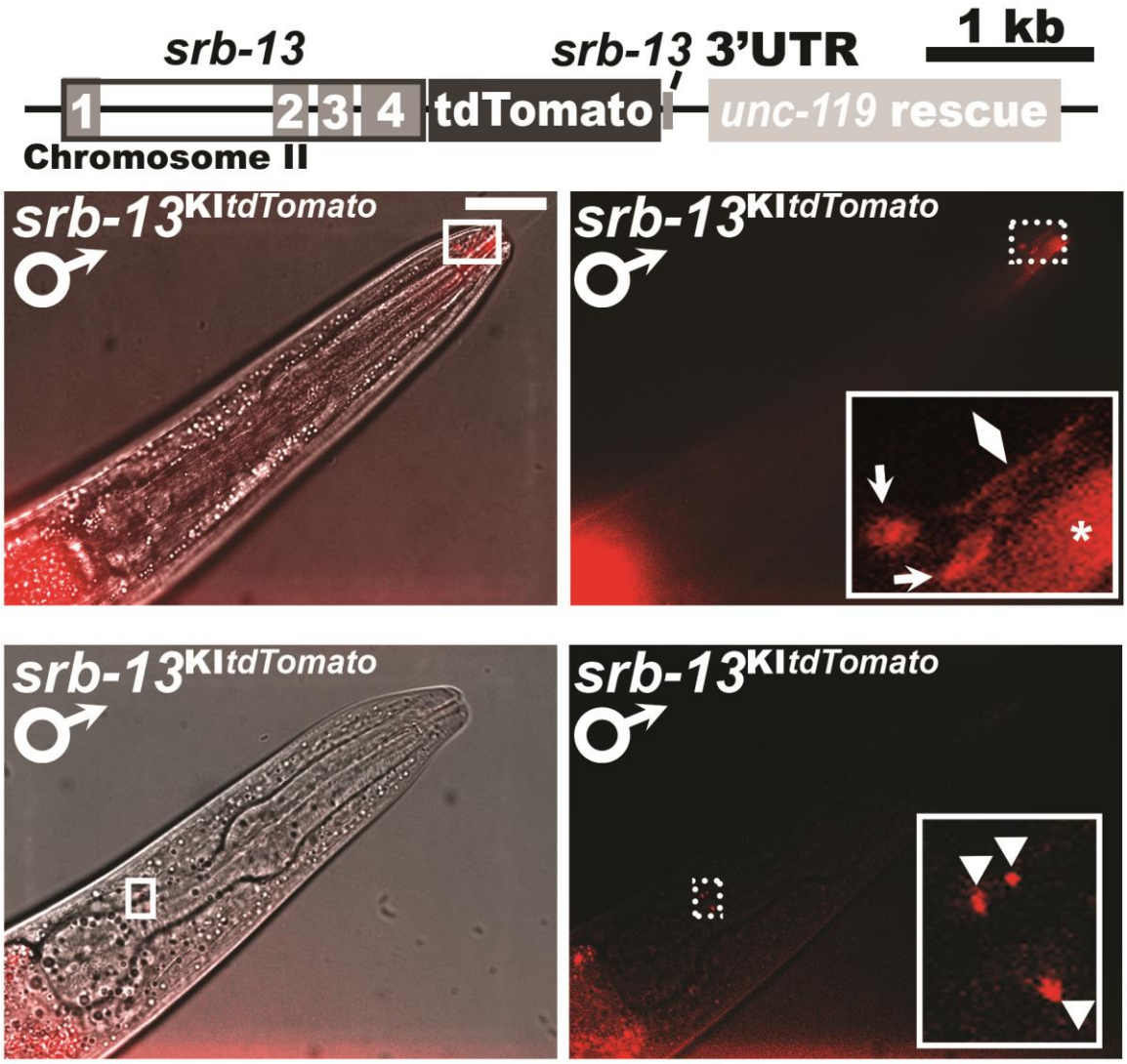

Fig. 7. Endogenous SRB-13 expression pattern in males.

The scheme on the top panel illustrates the position and size of DNA elements in the targeted locus (see supplementary material Fig. S6 for more details). *srb-13*$^{\text{KI}tdTomato}$ mutant hermaphrodites were then crossed into *fog-2(q71)* to increase the incidence of males. The white arrow heads indicate cellular puncta likely associated with neuron cell bodies, and the arrows indicate 2 basal bodies of sensory cilia from which the cilium axoneme-like rays, indicated by white a diamond, extend. The two sensory cilia most

probably belong to single-ciliated ASI and ASK amphid sensory neurons. *, auto-fluorescence of the inner cavity of the mouth. Scale bar, 20 um.

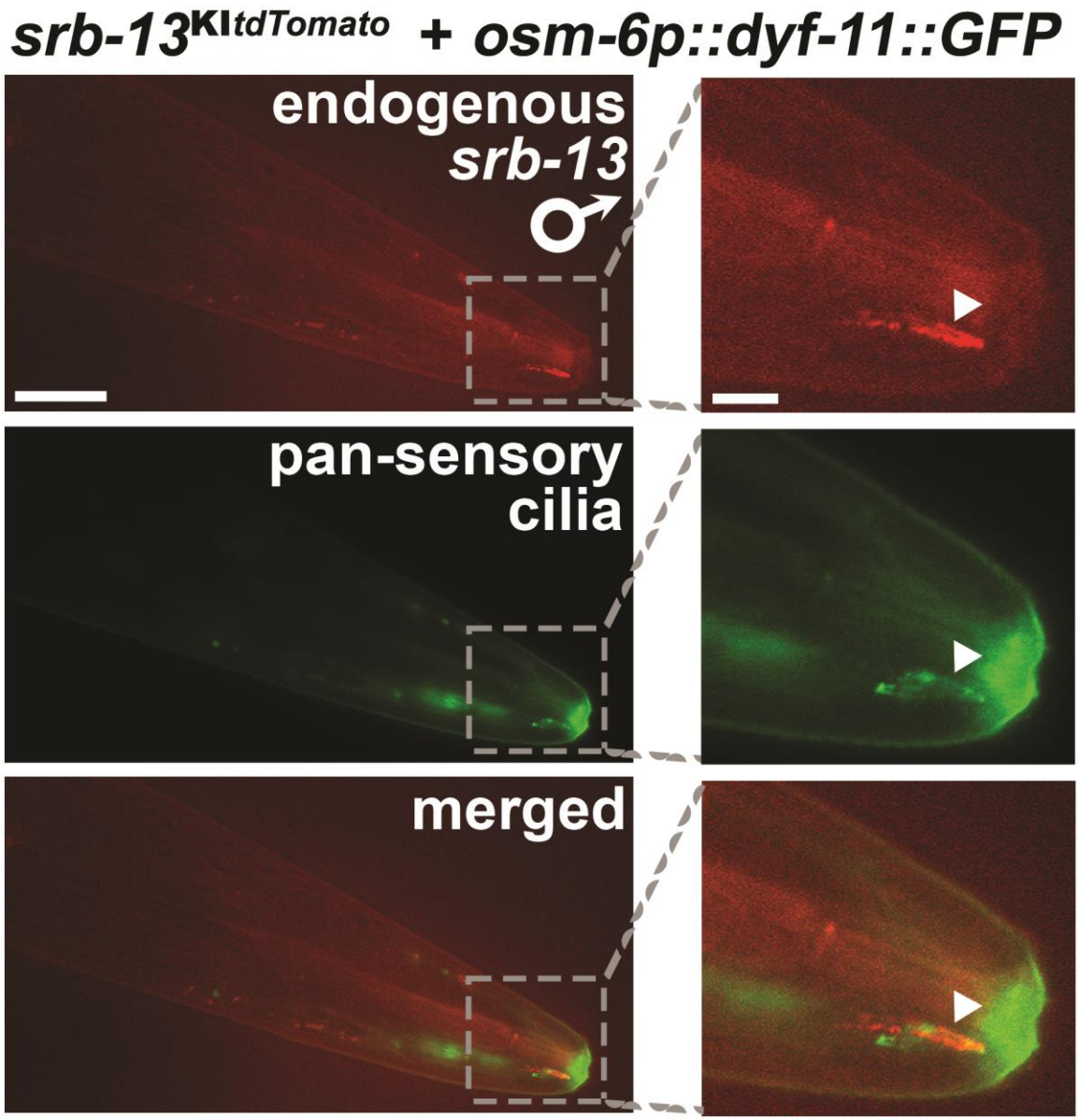

Fig. 8. SRB-13 expression in male sensory cilia.

The *osm-6* predicted promoter (427 bp upstream of translation start site) is known to drive gene expression in all ciliated head and tail sensory neurons (Collet et al., 1998). *dyf-11* encodes for a component of the intraflagellar transport complex B known to be localized throughout the cilium (Bacaj etal., 2008). Together, *osm-6p::dyf-11* drive GFP expression in all sensory cilia. *srb-13*^{KItdTomato} hermaphrodites transiently expressing the pan-sensory cilia marker (*osm-6p::dyf-11::GFP*) were mated to *srb-13*^{KItdTomato}; *fog-2*

(q71) males to generate males of the doubly marked strain. The arrow heads indicate sensory cilia. Left scale bar, 20 um; right scale bar, 5 um.

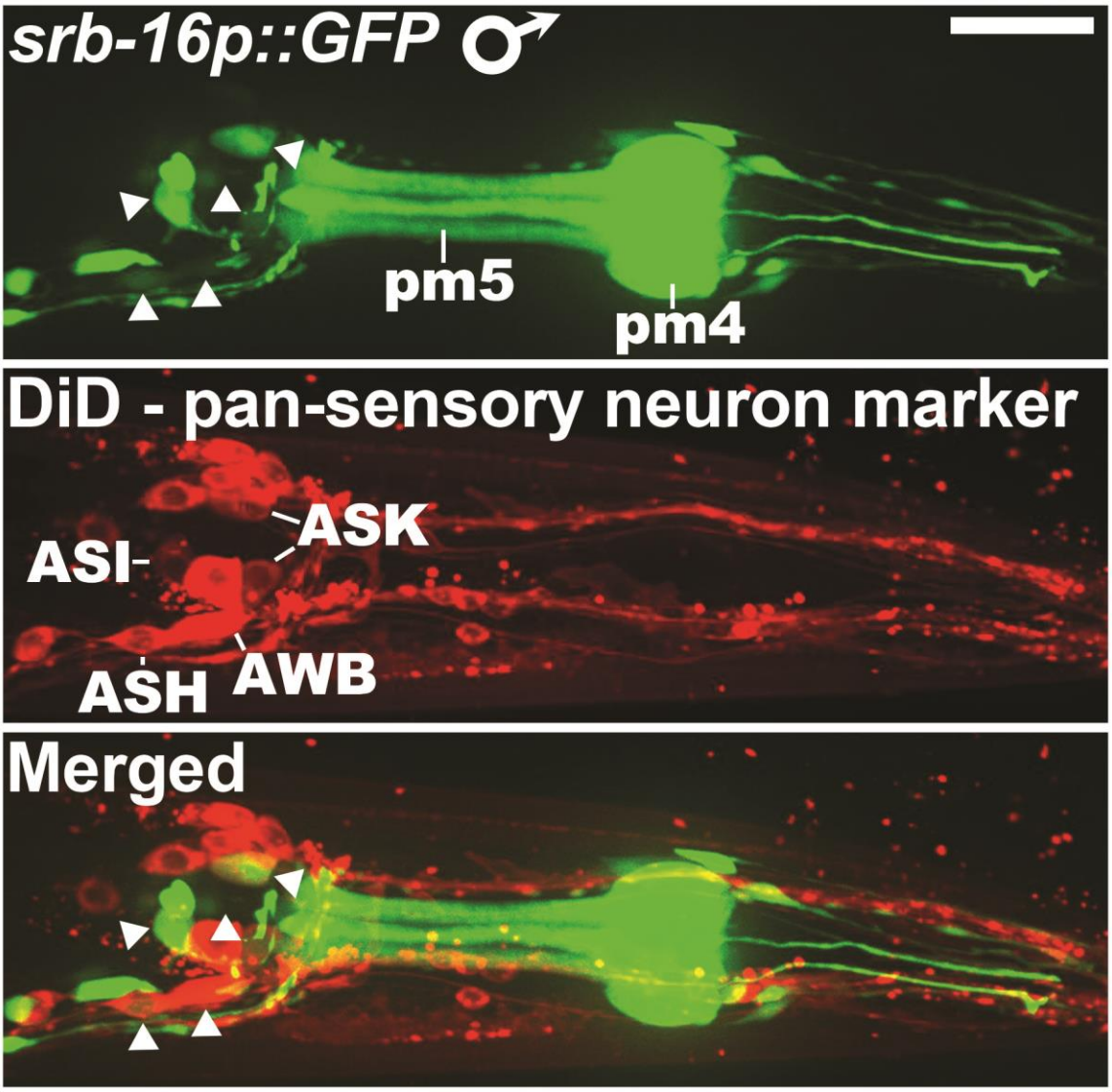

Fig. 9. Predicted *srb-16* promoter expression in males.

The worm strain (*BC14820*) transiently expressing GFP under the predicted *srb-16* promoter (2,127 bp upstream of the translational start site) was mated with *fog-2 (q71)* males to generate transgenic male animals. The male progeny was then incubated with DiD, a far-red membrane staining fluorescent tag that stains all sensory neurons (see MATERIALS AND METHODS). The images was processed by ImageJ (version 1.48). The images shown were obtained by collapsing all slices by "Z project" function from "Stacks". ASH, Amphid Single-ciliated neuron H with a linear cilium. ASI, Amphid

Single-ciliated neuron I with a linear cilium. ASK, Amphid Single-ciliated neuron K with a linear cilium. AWB, Amphid Wing neuron B with a branched cilium. pm4, pharyngeal muscle cells #4. pm5, pharyngeal muscle cells #5. pm4 and pm5 pharyngeal muscles are arranged in three-fold symmetry. White arrow heads indicate GFP-positive cell bodies of amphid neurons. Scale bar, 20um.

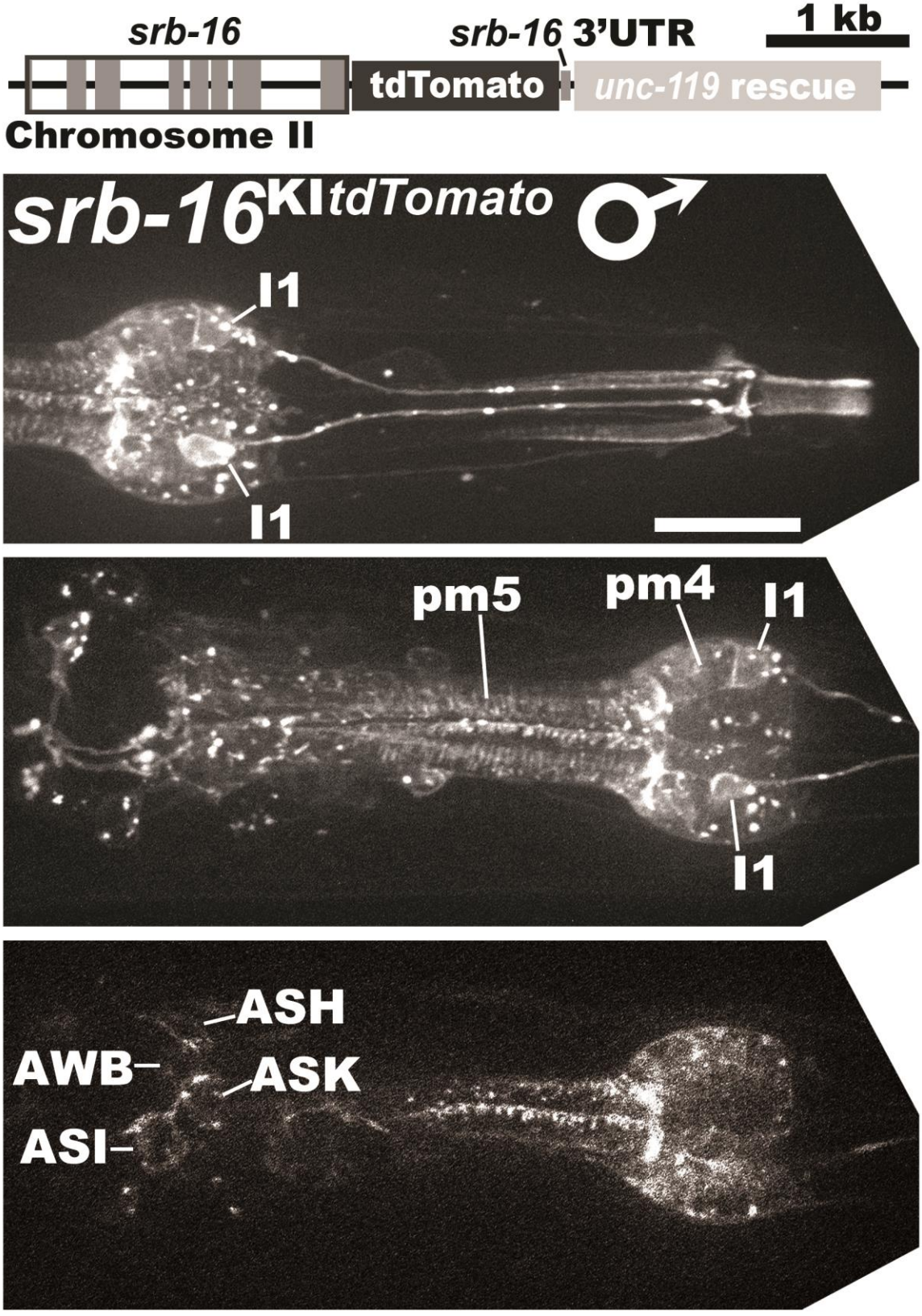

Fig. 10. Endogenous SRB-16 expression pattern in males.

The scheme on the top panel illustrates the position and size of DNA elements in the targeted locus (see supplementary material Fig. S7 for more details). *srb-16*$^{\text{KI}tdTomato}$ mutant was crossed into *fog-2(q71)* to increase the incidence of males. The upper 2 images were obtained by collapsing all slices by "Z project" function from "Stacks" (Image J version 1.48) whereas the lowest image was one slice of the z-stack. I1, pharyngeal Interneuron #1. ASH, Amphid Single-ciliated neuron H with a linear cilium. ASI, Amphid Single-ciliated neuron I with a linear cilium. ASK, Amphid Single-ciliated neuron K with a linear cilium. AWB, Amphid Wing neuron B with a branched cilium. pm4, pharyngeal muscle cells #4. pm5, pharyngeal muscle cells #5. pm4 and pm5 pharyngeal muscles are arranged in three-fold symmetry. Scale bar, 20 um.

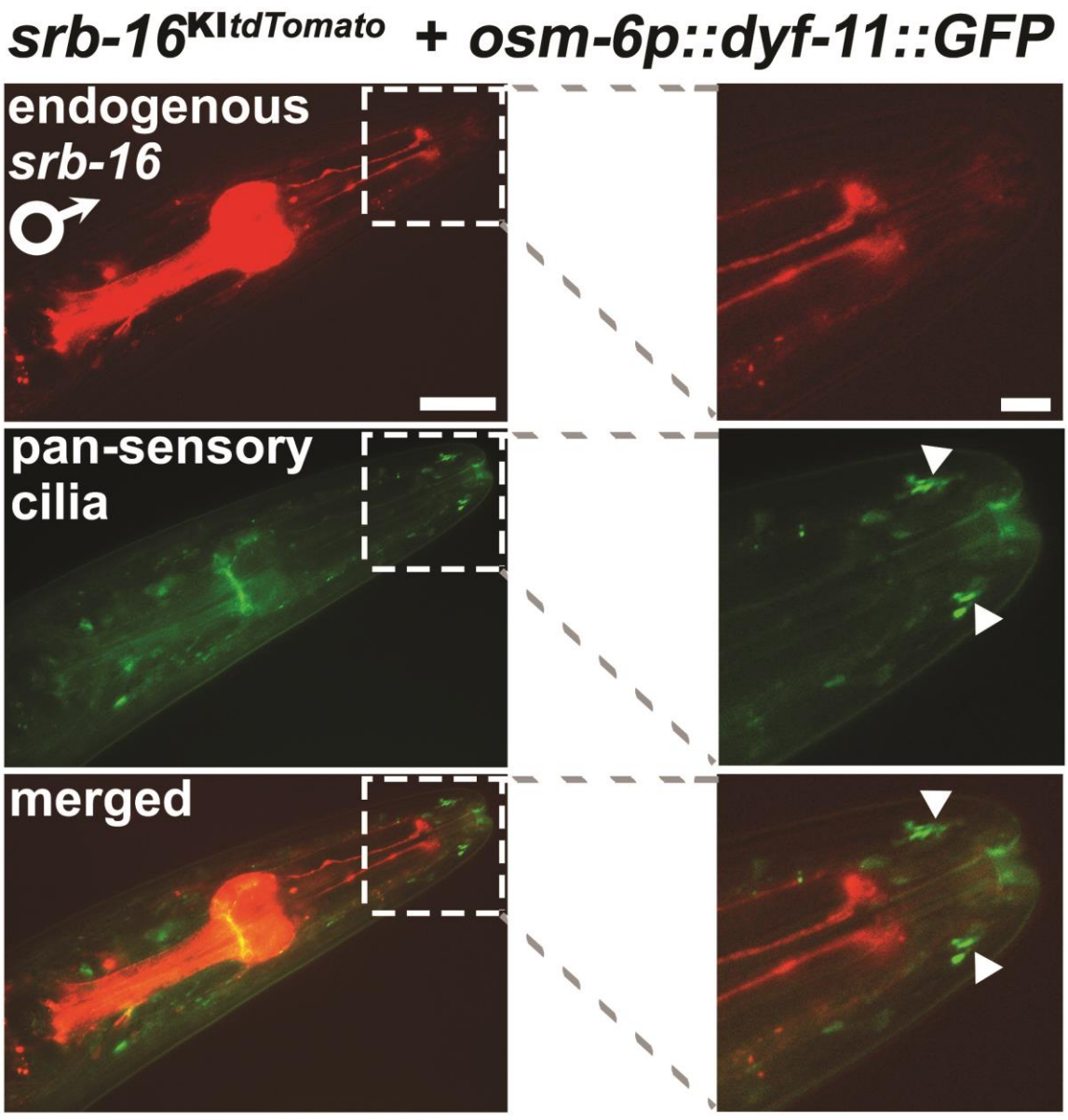

Fig. 11. SRB-16 expression in male sensory neurons.

The *osm-6p::dyf-11* drive GFP expression in all sensory cilia. *srb-16*^{KItdTomato} mutant hermaphrodites transiently expressing *osm-6p::dyf-11::GFP* were mated to *srb-16*^{KItdTomato}; *fog-2 (q71)* males. The arrow heads indicate sensory cilia. Left scale bar, 20 um; right scale bar, 5um.

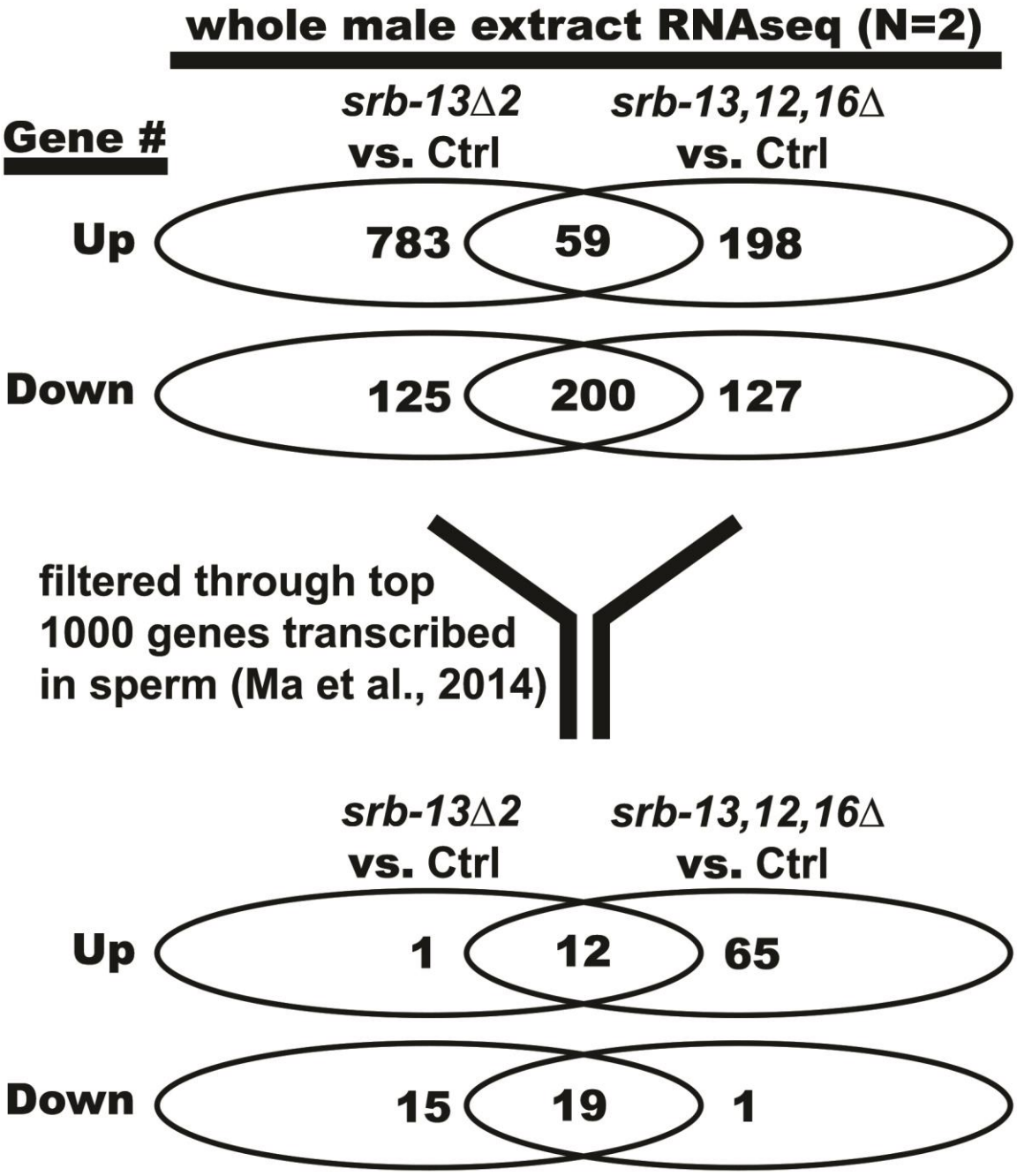

Fig. 12. Venn diagrams of altered gene expression in *srb* mutant and control males. *srb-13Δ2* or *srb-13,12,16Δ* males are in the *fog-2(q71)* background. Control (Ctrl) male genotype is *fog-2(q71)*. Control and *srb* mutant males transcripts were analyzed by high throughput Illumina based sequencing (HiSeq2000). Bioinformatics analysis was performed to map the reads to *C. elegans* reference genome from Ensembl, WBcel235

(ceWS240), release 76. Transcript abundance was measured using Tuxedo suite (Tophat, Bowtie) and differential expression was calculated using Cufflinks. The levels of all transcript isoforms of each gene were pooled together to represent the level of the gene. The average level of transcripts of each gene in mutant males (*srb-13Δ2* or *srb-13,12,16Δ*) was compared with controls to give fold change. p-values of the gene expression differences between mutant and control samples range from $5.0x10^{-5}$ to $3.3x10^{-3}$, and q-values are all under 0.05. 7 genes were excluded from the upper 2 Venn diagrams, including 5 genes up-regulated in *srb-13Δ2* males, but down-regulated in *srb-13,12,16Δ* males and 2 genes down-regulated in *srb-13Δ2* males, but up-regulated in *srb-13,12,16Δ* males (SupplRNAseqData.xlsx Excel sheet 1 and 2). More details on the genes in each category can be found in SupplRNAseqData.xlsx Excel sheet 1 and 2. The gene sets from the upper Venn diagrams are then filtered through a list of 1000 genes whose transcripts are the most abundant in *C. elegans* sperm, as shown in SupplRNAseqData.xlsx Excel sheet 4. More details on the genes shown in the lower 2 Venn diagrams can be found in SupplRNAseqData.xlsx Excel sheet 5 and 6.

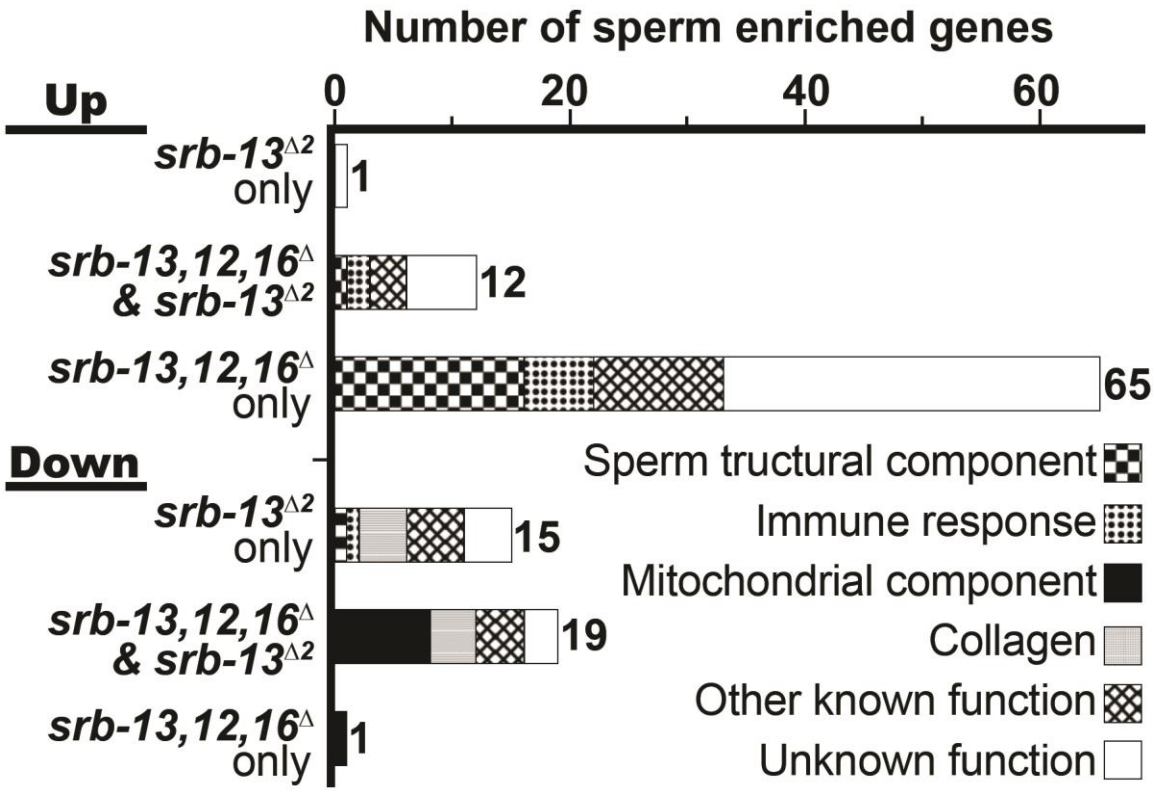

Fig. 13. Sperm-enriched gene categories from *srb* mutant males.

Males are in the *fog-2(q71)* background to increase male incidence. Control male genotype is *fog-2(q71)*. p-values are all < 0.005, and q-values are all < 0.05. All categories were mutually exclusive. More details on the genes in each category can be found in Tables S1, S2, or SupplRNAseqData.xlsx Excel sheet 5 and 6.

SUPPLEMENTARY FIGURES

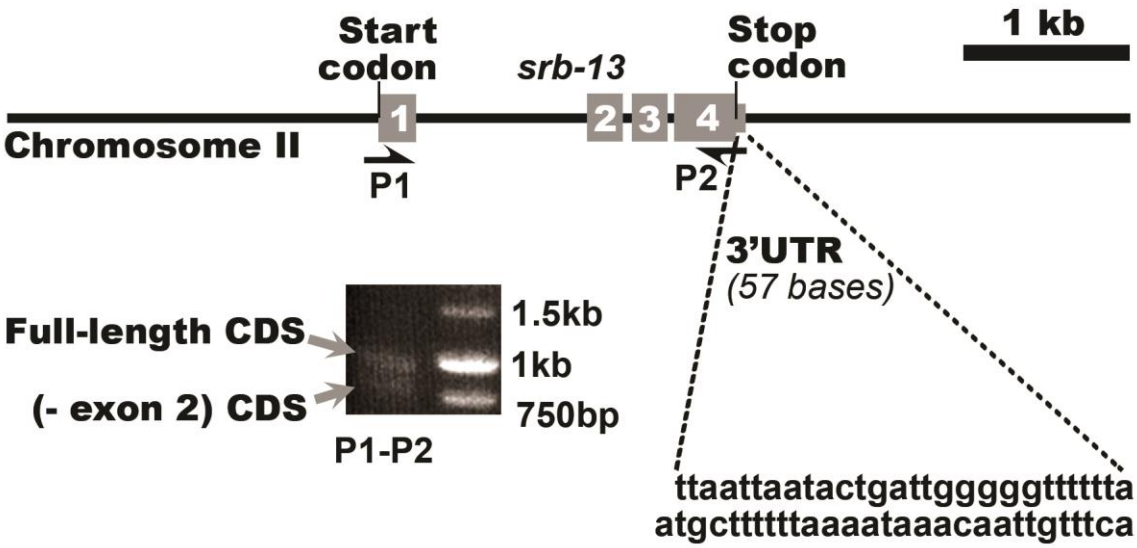

Fig. 1S. Characterization of predicted *srb-13* gene structure.

s*rb-13* coding exons and 3'UTR are up to scale, while the primer (single-barbed arrows) lengths are not. Reverse transcription-polymerase chain reaction (RT-PCR) was performed on a male-enriched *fog-2(q71)* population using the primers *srb-13*P1 and *srb-13*P2, as described in primer table S1. The two PCR products shown in the gel picture were subcloned into pCR2.1 TOPO vector (Invitrogen) and sequenced.

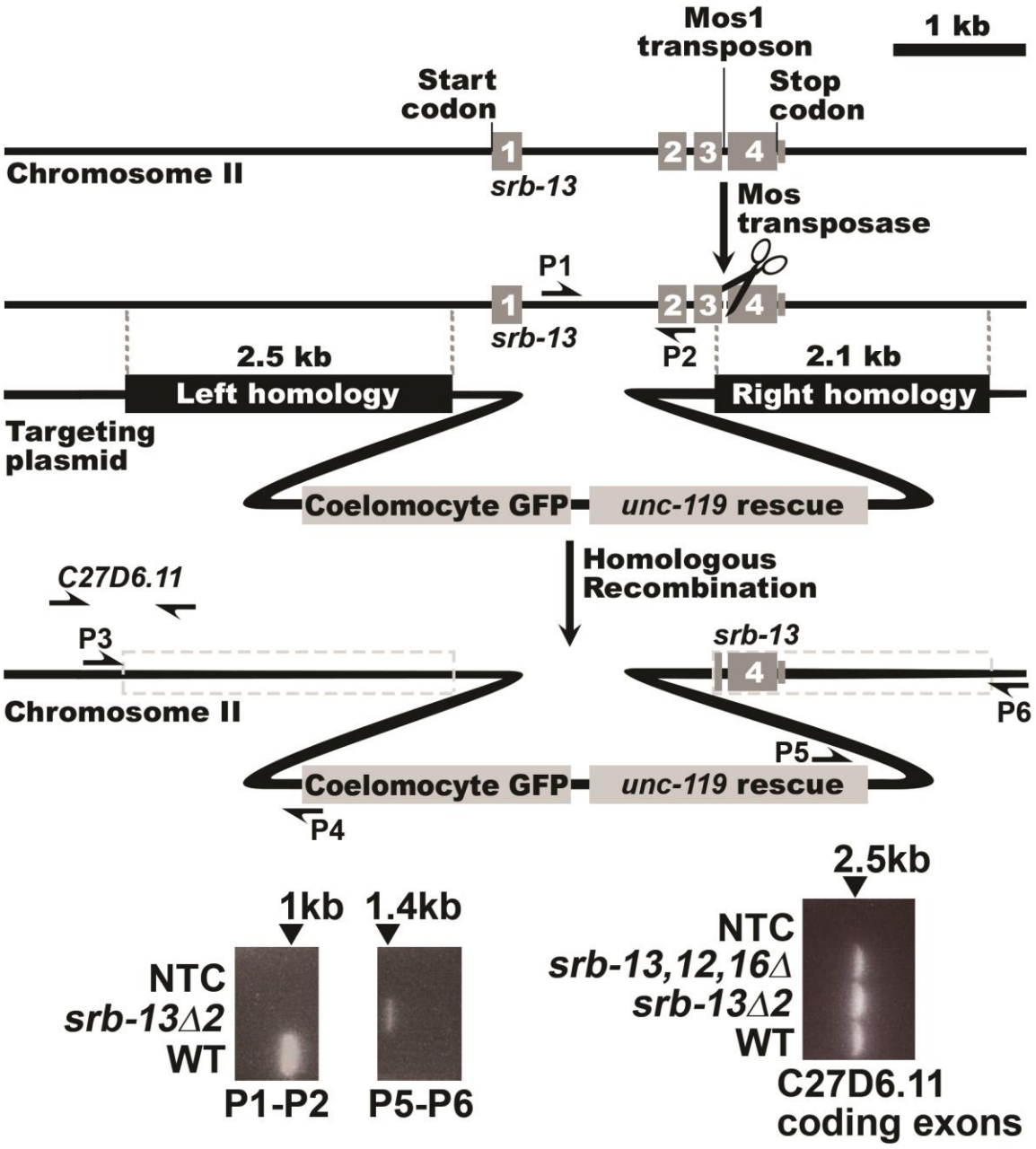

Fig. S2. *srb-13* knock out (*srb-13Δ2* or *xm1* allele) scheme and PCR validation.

srb-13 coding exons (numbered in white) and 3' UnTranslated Region (UTR) on the negative strand of chromosome II were shown up to scale. The targeting plasmid is also shown up to scale. The primers P1 to P6 shown as single-barbed arrows appear longer in the diagram than their relative size. *srb-13* KO was performed using a homologous recombination-based technique called MOSDEL (Frøkjaer-Jensen et al., 2010, see

MATERIALS AND METHODS). Recombination replaced exons 1 and 2 and a part of exon 3 of *srb-13* gene by the *unc-119* rescue fragment and a ceolomocyte expressed GFP marker. The deletion mutant was crossed into *fog-2(q71)* background to generate males. PCR reaction using P1-P2 primers should amplify 1.0 kb of the deleted exons of srb-13. PCR reactions using males with P3-P4 primers or P5-P6 primers should amplify a 2.6 kb or 2.5kb fragment, respectively, from the targeted locus, but not the targeting plasmid or the untargeted locus on chromosome II. The male strain is *fog-2(q71)*. P3-P4 primers PCR reaction failed to give a product from the generated mutant *srb-13Δ2* (data not shown). The coding exons of *C27D6.11*, the gene adjacent to the left homology arm, is intact in the *srb-13Δ2* mutant. A limitation of this mutant is that *msp-45* is also removed. However, the *C. elegans* genome has at least 28 functional copies of major sperm protein (MSP) genes (97-100% identical) (Harris et al., 2010; Smith, 2006). Loss of one *msp* gene is not likely to have a significant impact on sperm performance. The targeting plasmid, named pXM1, was assembled by Multisite Gateway 3-Fragment system (Invitrogen), where the middle fragment came from pCFJ66 plasmid (pDONR221 backbone) (Addgene). pXM1 annotated sequence is provided in pXM1.ape file. The sequences of P1-P6, and C27D6.11 coding sequence primers and primers used for constructing the targeting plasmid are listed in Table S3.

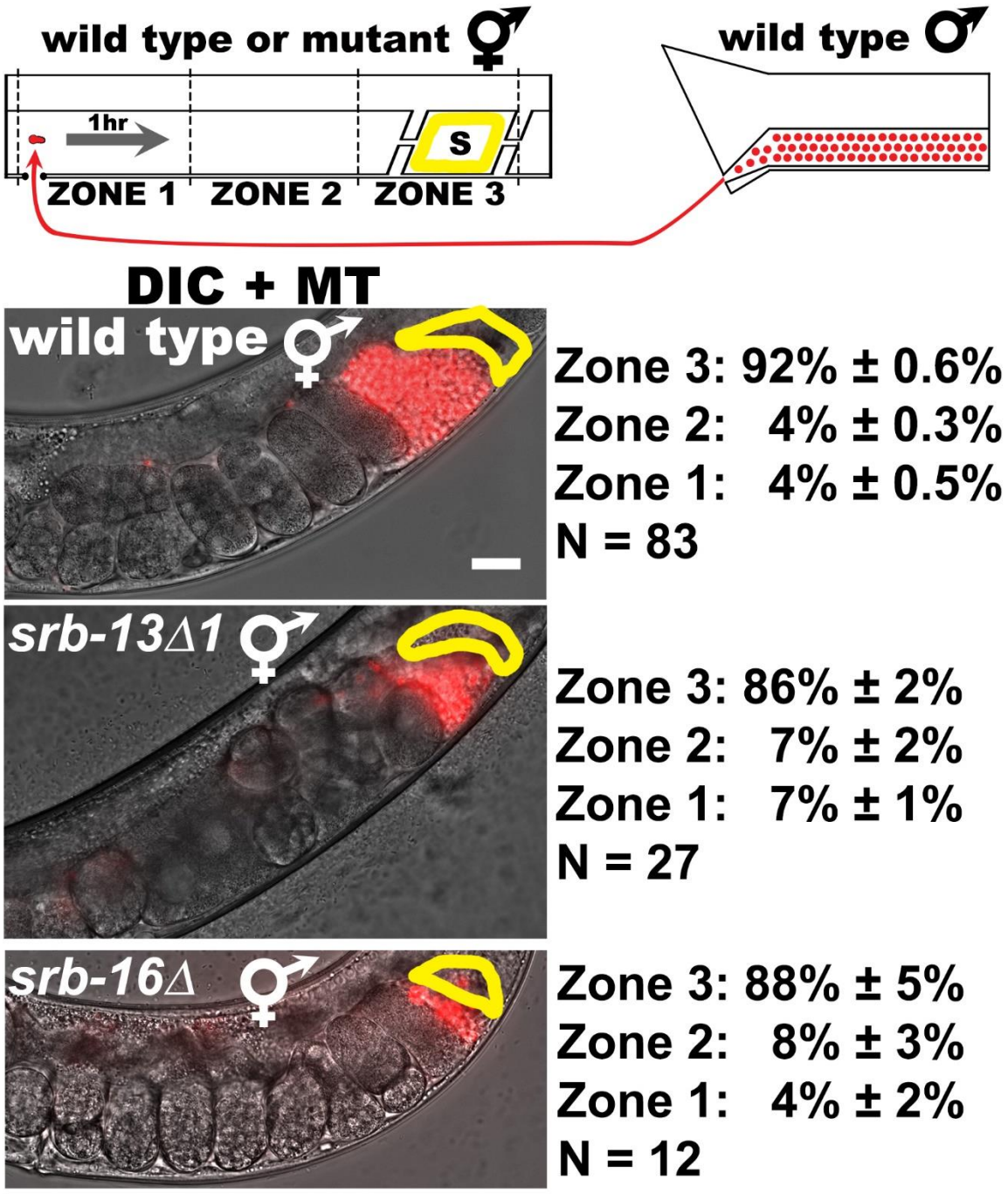

Fig. S3. Sperm guidance of wild-type males in wild-type, *srb-13Δ1*, or *srb-16Δ* mutant hermaphrodites.

Sperm distribution in wild-type or mutant hermaphrodite uterus 1 hour after mating to wild-type males. A representative image is shown to the left and average zone distribution ± standard error of the mean is to the right. The spermatheca (S) is outlined

in yellow. The official allele names for *srb-13*$^{\Delta 1}$ and *srb-16* are *ok3126 and gk774*, respectively. The control male strain is *fog-2(q71)* and wild-type hermaphrodite strain is N2. MT, MitoTracker channel; N, number of gonads quantified; Scale bar, 20 µm. See MATERIALS AND METHODS for zone definitions.

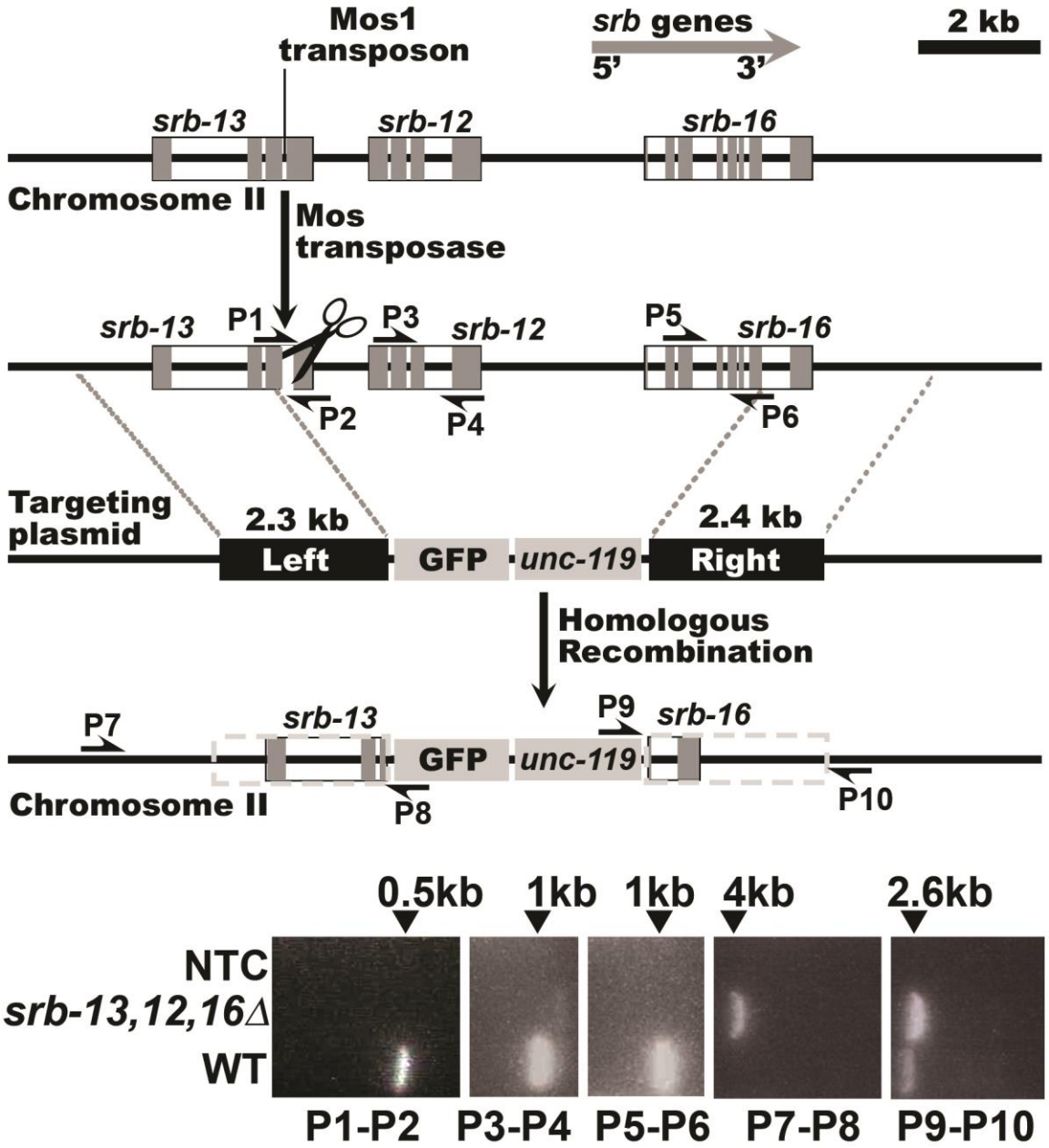

Fig. S4. *srb-13,12,16* knock out scheme and PCR validation.

srb genes models are shown on the negative strand of chromosome II and are up to scale. The targeting plasmid is also shown up to scale. The primers P1 to P10 shown as single-barbed arrows appear longer in the diagram than their relative size. *srb-13,12,16* KO was performed using a homologous recombination-based technique called MOSDEL (Frokjaer-Jensen et al., 2010) (see MATERIALS AND METHODS). Recombination

replaced parts of *srb-13* and *srb-16* genes, and the whole *srb-12* genes by the *unc-119* rescue fragment and a ceolomocyte expressed GFP marker. The deletion mutant was crossed into *fog-2(q71)* background to generate males. PCR reactions using males with P1-P2 primers should amplify about 500 bp of the deleted exons of *srb-13* in wild-type worms, but not targeted worms. Similarly, P3-P4 primers PCR should amplify about 1.0 kb of *srb-12* coding exons only in wild-type worms, but not targeted worms, and P5-P6 primers PCR should amplify 1.0 kb of *srb-16* coding exons only in wild-type worms, but not targeted worms. PCR reactions with P7-P8 primers or P9-P10 primers should amplify a 4.0 kb or 2.6 kb fragment, respectively, from the targeted locus, but not the targeting plasmid or the untargeted locus on chromosome II. PCR with P9-P10 primers generated a correct size (2.6 kb) band in the mutant worm and a larger size (~ 3.0 kb) band in wild-type worm, which is probably a non-specific product. The male strain is *fog-2(q71)*. The targeting plasmid, named pXM3, was assembled by Multisite Gateway 3-Fragment system (Invitrogen), where the middle fragment came from pCFJ66 plasmid (pDONR221 backbone) (Addgene). pXM3 annotated sequence is provided in pXM3.ape file. The sequences of P1-P10 primers and primers used for constructing the targeting plasmid are listed in Table S3.

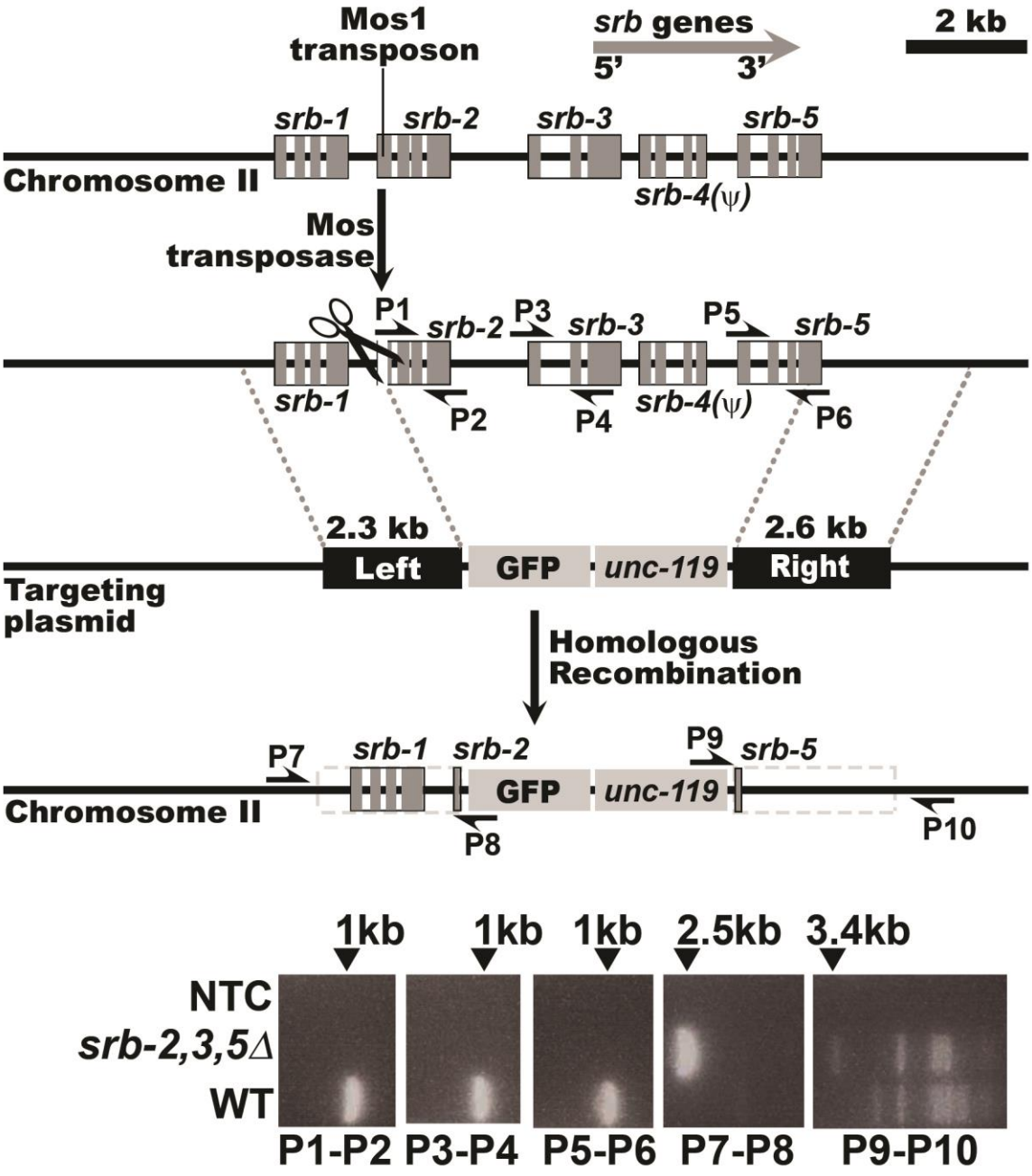

Fig. S5. *srb-2,3,5* knock out scheme and PCR validation.

srb genes models are shown on the negative strand of chromosome II and are up to scale. The targeting plasmid is also shown up to scale. The primers P1 to P10 shown as single-barbed arrows appear longer in the diagram than their relative size. *srb-2,3,5* KO was performed using a homologous recombination-based technique called MOSDEL

(Frokjaer-Jensen et al., 2010) (see MATERIALS AND METHODS). Recombination replaced parts of *srb-2* and *srb-5* genes, and the whole *srb-3* gene by *unc-119* rescue fragment and a ceolomocyte expressed GFP marker. *srb-4* is classified as a pseudogene. The deletion mutant was crossed into *fog-2(q71)* background to generate males. PCR reactions using males with P1-P2 primers should amplify 1.0 kb of the deleted exons of *srb-2* in wild-type worms but not targeted worms. Similarly, P3-P4 primers PCR should amplify 1.0 kb of *srb-3* coding exons only in wild-type worms, but not targeted worms, and P5-P6 primers PCR should amplify 1.0 kb of *srb-5* coding exons only in wild-type worms, but not targeted worms. PCR reactions with P7-P8 primers or P9-P10 primers should amplify a 2.5 kb or 3.4 kb fragment, respectively, from the targeted locus, but not the targeting plasmid or the untargeted locus on chromosome II. PCR with P9-P10 primers generated a correct size (3.4 kb) band in the mutant worm and a smaller size (~ 2.0 kb) band in wild-type worm, which is probably non-specific. The other bands common in both mutant and wild-type are also probably non-specific. The targeting plasmid, named pXM2, was assembled by Multisite Gateway 3-Fragment system (Invitrogen), where the middle fragment came from pCFJ66 plasmid (pDONR221 backbone) (Addgene). pXM2 annotated sequence is provided in pXM2.ape file. The sequences of P1-P10 primers and primers used for constructing the targeting plasmid are listed in Table S3.

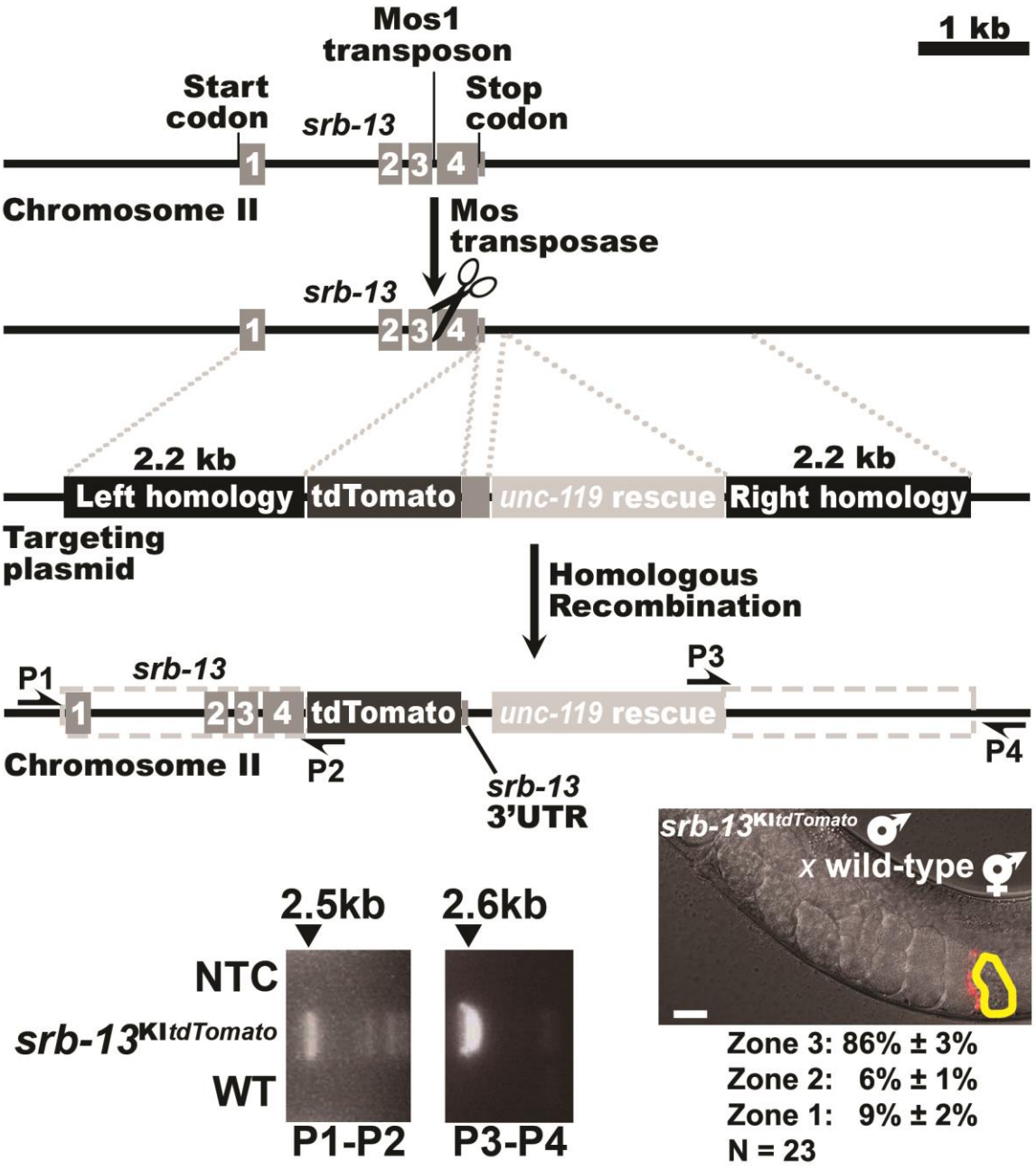

Fig. S6. *srb-13 tdTomato* knock-in scheme and PCR validation.

The *srb-13* locus and the targeting plasmid are shown up to scale. The primers P1 to P4 shown as single-barbed arrows appear longer in the diagram than their relative size. *Srb-13 tdTomato* knock-in was performed using a modification of the MOSDEL method (Frokjaer-Jensen et al., 2010) (see MATERIALS AND METHODS). The targeting plasmid (pXM4) contained a left homology arm (2 kb upstream of *srb-13* stop codon),

tdTomato, 250 bases downstream of *srb-13* stop codon including 57-bp 3'UTR, *unc-119* rescue fragment, and a 2 kb right homology arm. Recombination inserts *tdTomato* right before the *srb-13* stop codon, and inserts the *unc-119* rescue fragment 250bp downstream of *srb-13* stop codon. The tdTomato knock-in mutant was crossed into *fog-2(q71)* background to generate males. PCR reactions with P1-P2 primers or P3-P4 primers should amplify a 2.5 kb or 2.6 kb fragment, respectively, from the targeted locus but not the targeting plasmid or the untargeted locus on chromosome II. PCR reactions were performed on male *fog-2(q71)* worms. The targeting plasmid, called pXM4, was cloned by sequential restriction digest. pXM4 annotated sequence is provided in the pXM4.ape file. The P1-P4 primer sequences and plasmid construction sequences are listed in Table S3. Sperm guidance assay was performed to assess if knocking in tdTomato affects sperm guidance efficiency by mating the mutant males to wild-type hermaphrodites. A representative image is shown, with sperm distribution shown below. Scale bar, 20 um.

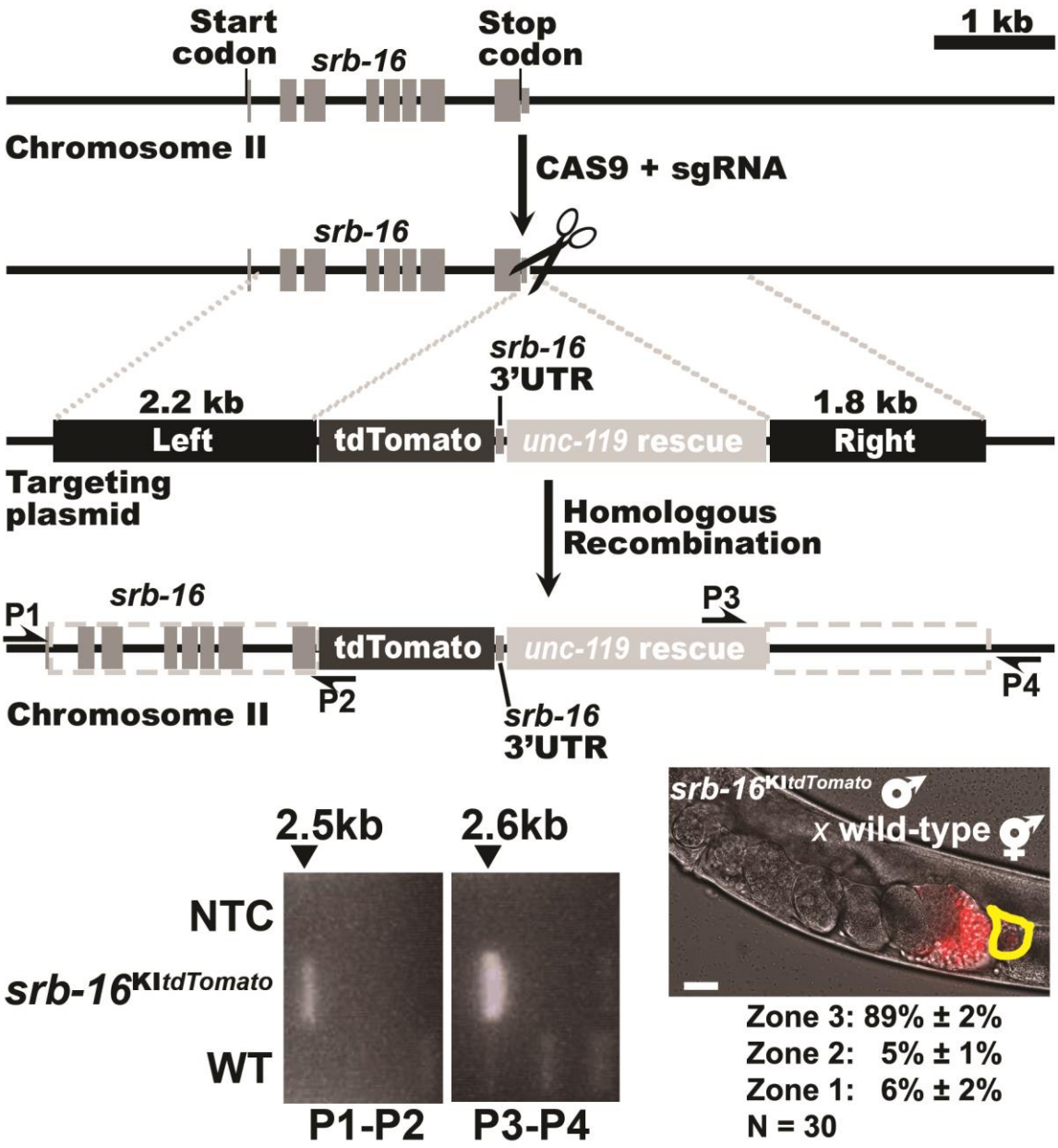

Fig. S7. *srb-16 tdTomato* knock-in scheme and PCR validation.

The *srb-16* locus and the targeting plasmid are shown up to scale. The primers P1 to P4 shown as single-barbed arrows appear longer in the diagram than their relative size. *Srb-16 tdTomato* knock-in was performed using homologous recombination in combination with CRISPR, the double strand break creation technique (Friedland et al., 2013). The

single guide RNA (sgRNA) contained the following 20 bases: gtggttttgggtctgacggg (pSS16 plasmid) which guided CAS9 endonuclease to make a double strand break at about 90 bases downstream from *srb-16* stop codon. Recombination inserts *tdTomato* right before the *srb-16* stop codon, and inserts the *unc-119* rescue fragment 104 bp downstream of *srb-16* stop codon. The tdTomato knock-in mutant was crossed into *fog-2(q71)* background to generate males. PCR reactions with P1-P2 primers or P3-P4 primers should amplify a 2.5 kb or 2.6 kb fragment, respectively, from the targeted locus but not the targeting plasmid or the untargeted locus on chromosome II. The non-specific bands in wild-type (WT) worm using P3-P4 primers could be eliminated in the future by optimizing PCR condition or by using nested primers. PCR reactions were performed on male *fog-2(q71)* worms. The targeting plasmid, pXM10, and the single guide RNA expression plasmids, pSS16, were cloned by Gibson assembly. pXM10 and pSS16 annotated sequences are provided in the pXM10.ape and pSS16 files, respectively. The P1-P4 primer sequences and plasmid construction sequences are listed in Table S3. Sperm guidance assay was performed to assess if knocking in tdTomato affects sperm guidance efficiency by mating the mutant males to wild-type hermaphrodites. A representative image is shown, with sperm distribution shown below. Scale bar, 20 um.

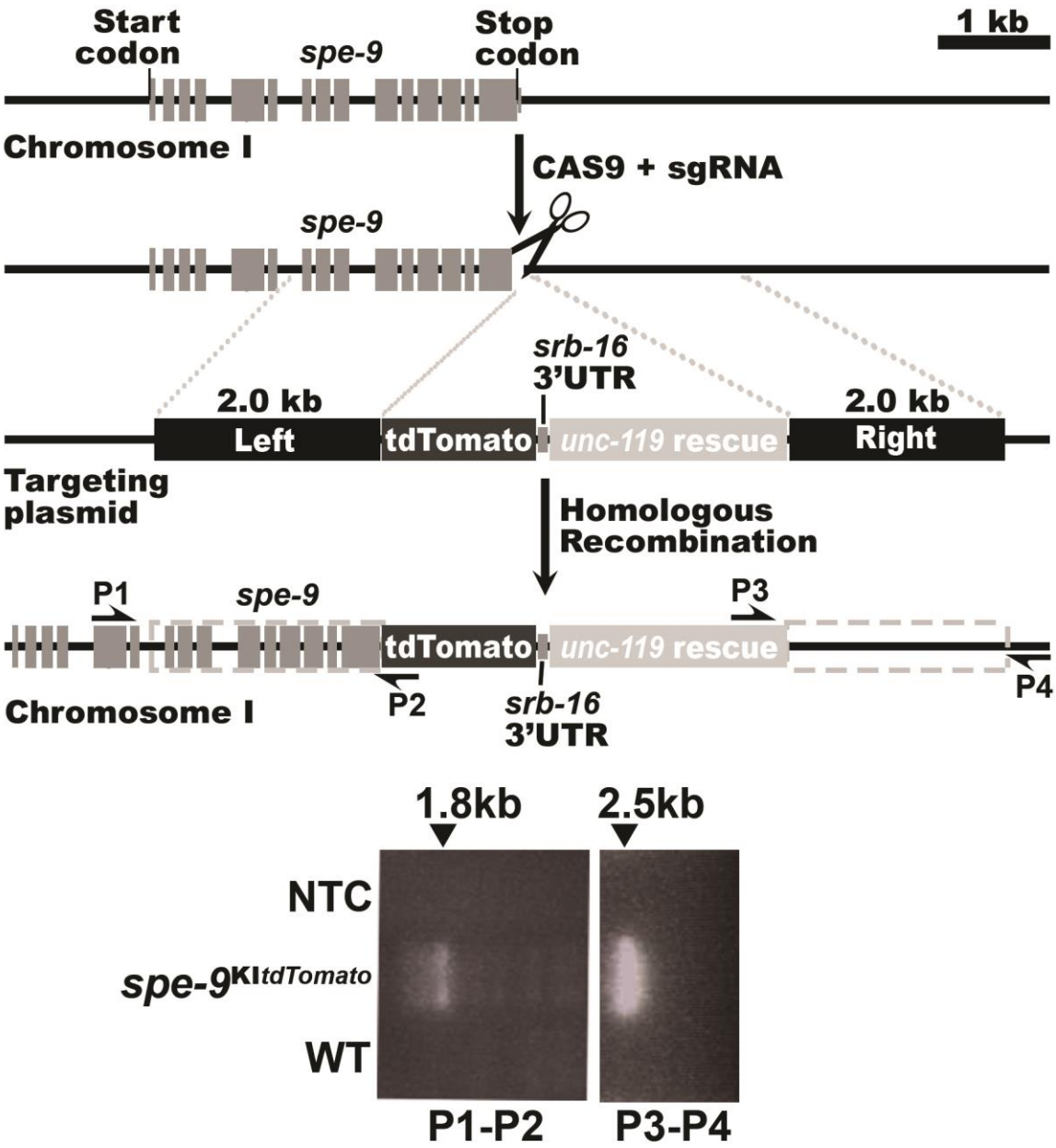

Fig. S8. *spe-9 tdTomato* knock-in scheme and PCR validation.

The *spe-9* locus and the targeting plasmid are shown to scale. The primers P1 to P4 shown as single-barbed arrows appear longer in the diagram than their relative size. *spe-9 tdTomato* knock-in was performed using homologous recombination in combination with CRISPR/Cas9 (Friedland et al., 2013). The single guide RNA contained the following 20 bases: aggaaatgatcggtgacaca (pSS9 plasmid), which guided the Cas 9 endonuclease to

make a double strand break at about 92 bases downstream from *spe-9* stop codon (downstream of *spe-9* predicted 3'UTR). Recombination replaced *spe-9* stop codon and 70 bp downstream by *tdTomato* tag sequence, *srb-16* predicted 3'UTR (104 bp downstream of *srb-16* stop codon), and *unc-119* rescue fragment. *srb-16* predicted 3'UTR was used instead of *spe-9* predicted 3'UTR to simplify cloning. PCR reactions with P1-P2 primers or P3-P4 primers should amplify two 2.5-kb fragments, respectively, from the targeted locus but not the targeting plasmid or the untargeted locus on chromosome I. The P1-P2 primers amplified a strong band slightly below 2 kb raising the possibility a portion of the locus was deleted during recombination or the PCR conditions need optimizing. *spe-9::tdTomato* was functional because *spe-9::tdTomato* is expressed only in sperm and sperm residual bodies (Fig. 5), as expected, and *spe-9*$^{\mathrm{KI}tdTomato}$ hermaphrodites are fertile (Putiri et al., 2004). The sequences of P1-P4 primers are listed in Table S2. The targeting plasmid, pXM14, and the single guide RNA expression plasmid, pSS9, were cloned by Gibson assembly. pXM14 and pSS9 annotated sequences are provided in pXM14.ape and pSS9.ape files, respectively. The P1-P4 primer sequences and plasmid construction primer sequences are listed in Table S3.

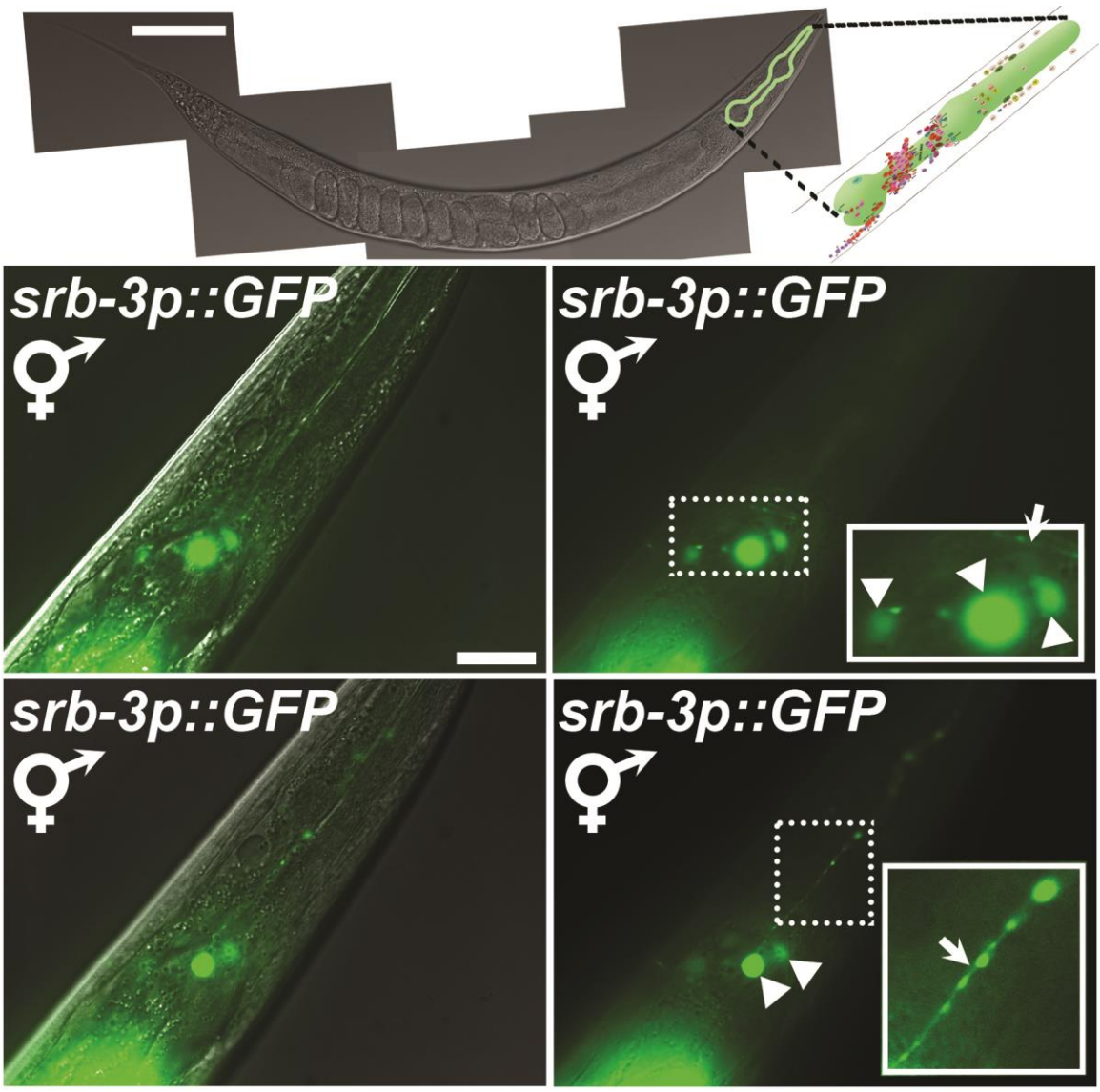

Fig. S9. Predicted *srb-3* promoter expression in hermaphrodites.

The worm strain (*BC12286*) transiently expressing GFP under the predicted *srb-3* promoter (1,156 bp upstream of the translational start site) was kindly provided by the Caenorhabditis Genetics Center. The whole worm image was adapted from Hoang et al. (2013), and the diagram of the pharynx (green tube) and head neuron cell bodies (colorful dots) was adapted from www.wormatlas.org. The arrow heads indicate neuron cell bodies, and the arrows indicate dendrites or axons. Upper and lower GFP images belong to the same worm. Scale bar, 100 um for whole worm image, and 20 um for GFP images.

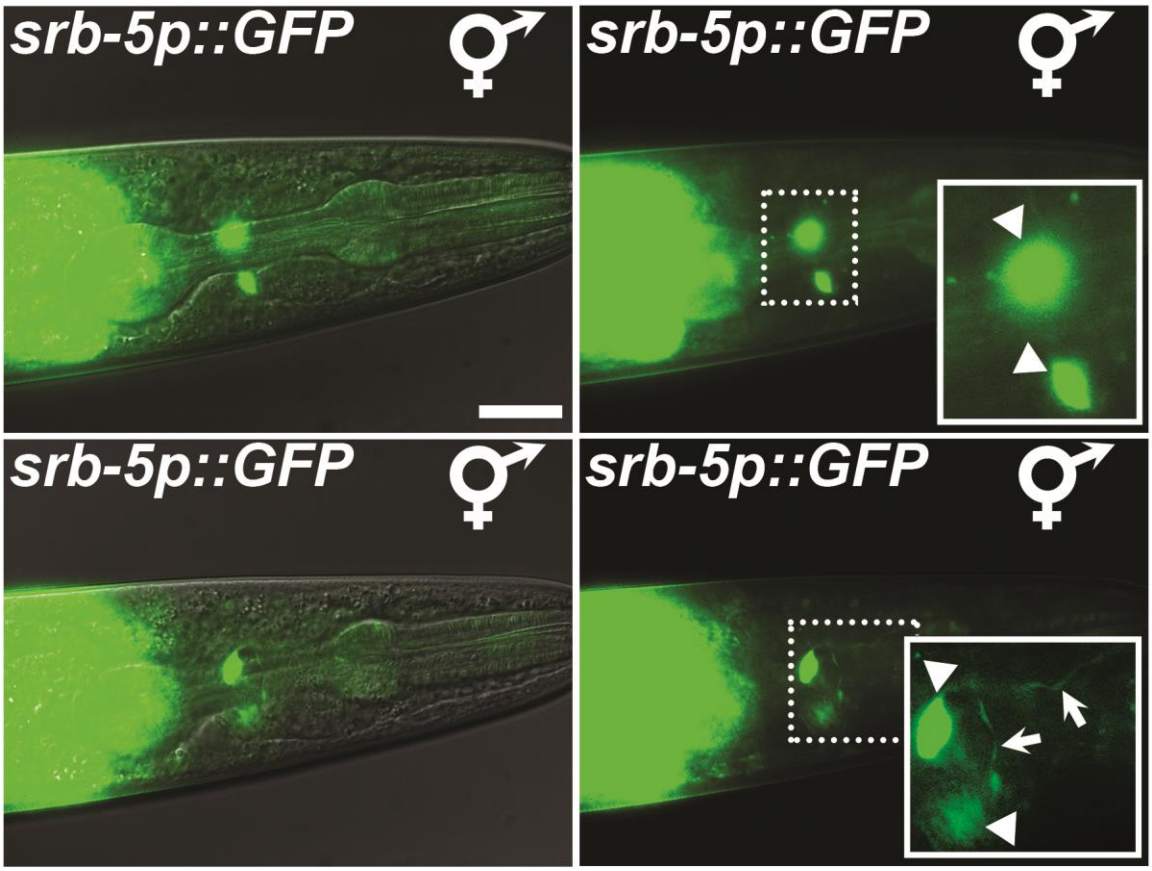

Fig. S10. Predicted *srb-5* promoter expression in hermaphrodites.

The worm strain (*BC12285*) transiently expressing GFP under the predicted *srb-5* promoter (831 bp upstream of the translational start site) was kindly provided by the Caenorhabditis Genetics Center. The arrow heads indicate neuron cell bodies, and the arrows indicate dendrites or axons. Upper and lower GFP images belong to the same worm. Scale bar, 20 um.

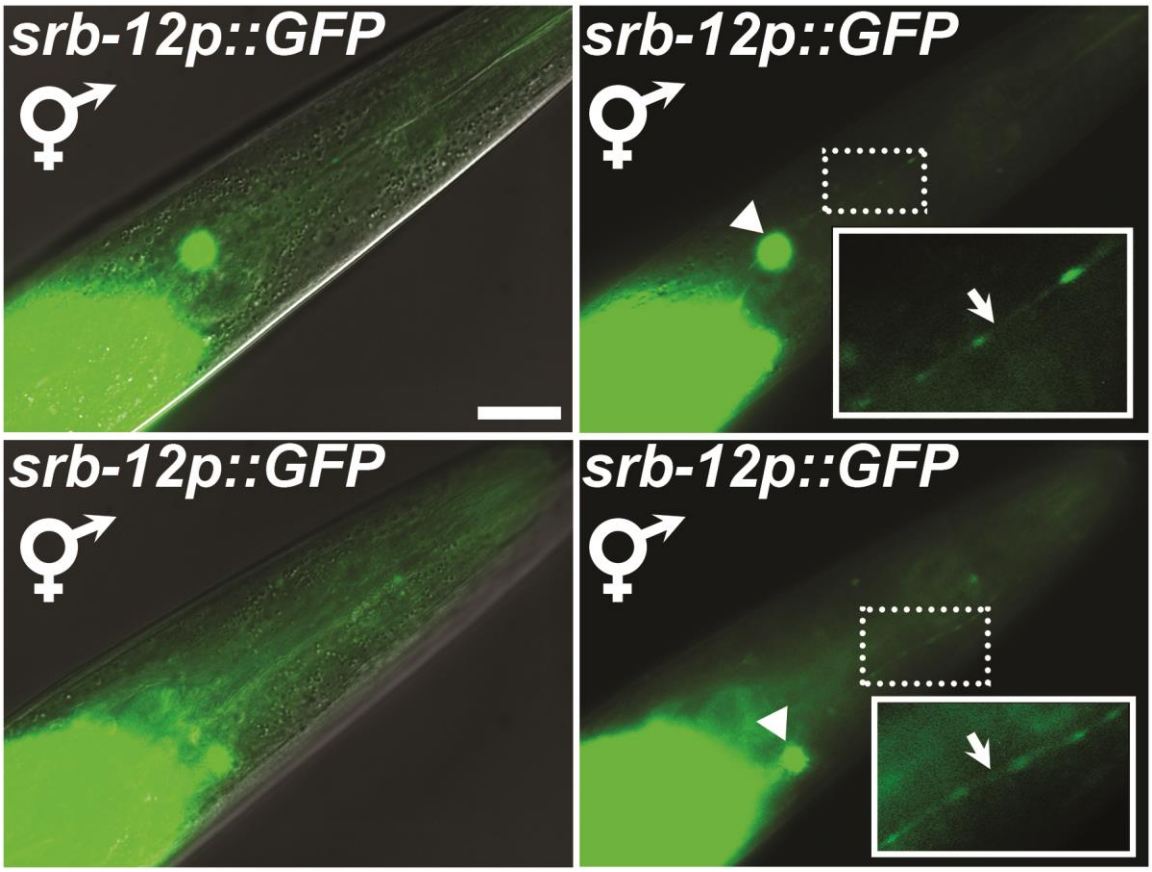

Fig. S11. Predicted *srb-12* promoter expression in hermaphrodites.

The worm strain (*BC12003*) transiently expressing GFP under the predicted *srb-12* promoter (668 bp upstream of the translational start site) was kindly provided by the Caenorhabditis Genetics Center. The arrow heads indicate neuron cell bodies, and the arrows indicate dendrites or axons. Upper and lower GFP images belong to the same worm. Scale bar, 20 um.

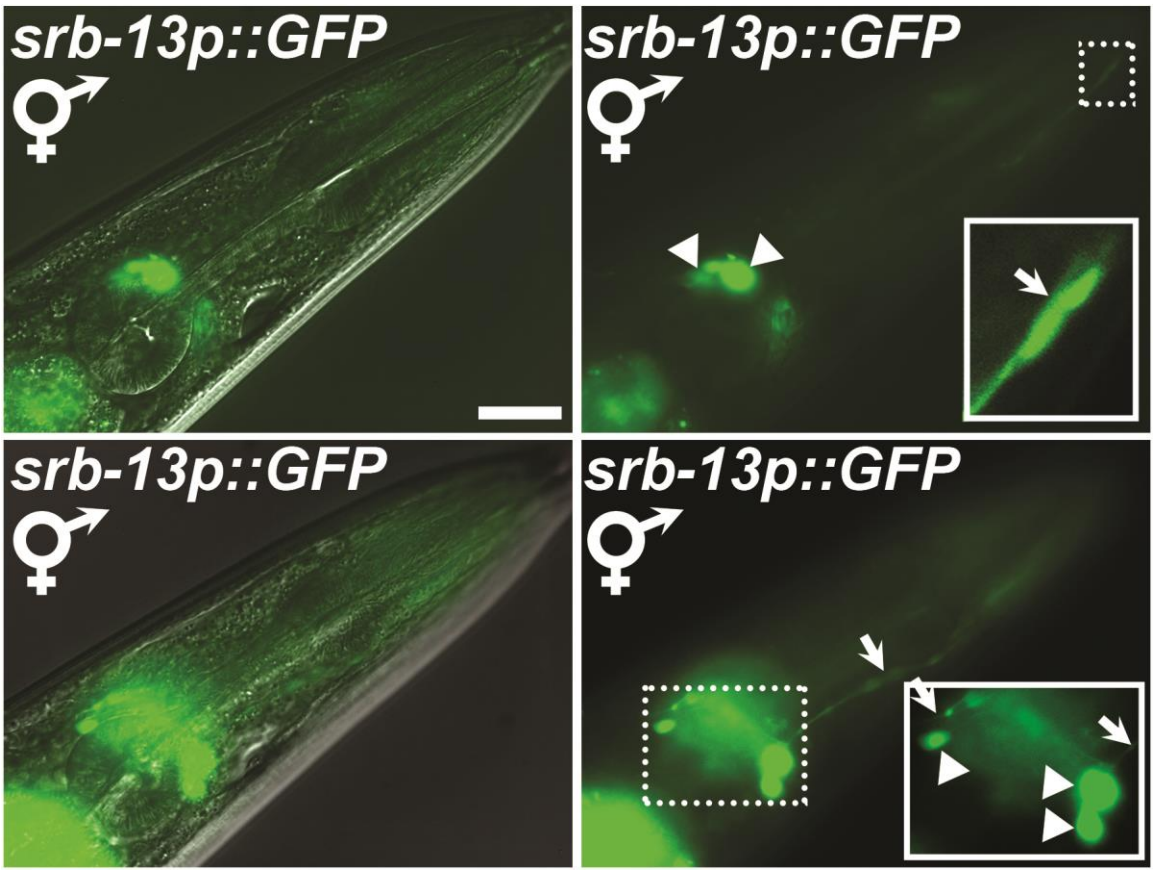

Fig. S12. Predicted *srb-13* promoter expression in hermaphrodites.

The worm strain (*BC14700*) transiently expressing GFP under the predicted *srb-13* promoter (968 bp upstream of the translational start site) was kindly provided by the Caenorhabditis Genetics Center. The arrow heads indicate neuron cell bodies, and the arrows indicate dendrites or axons. Upper and lower GFP images belong to the same worm. Scale bar, 20 um.

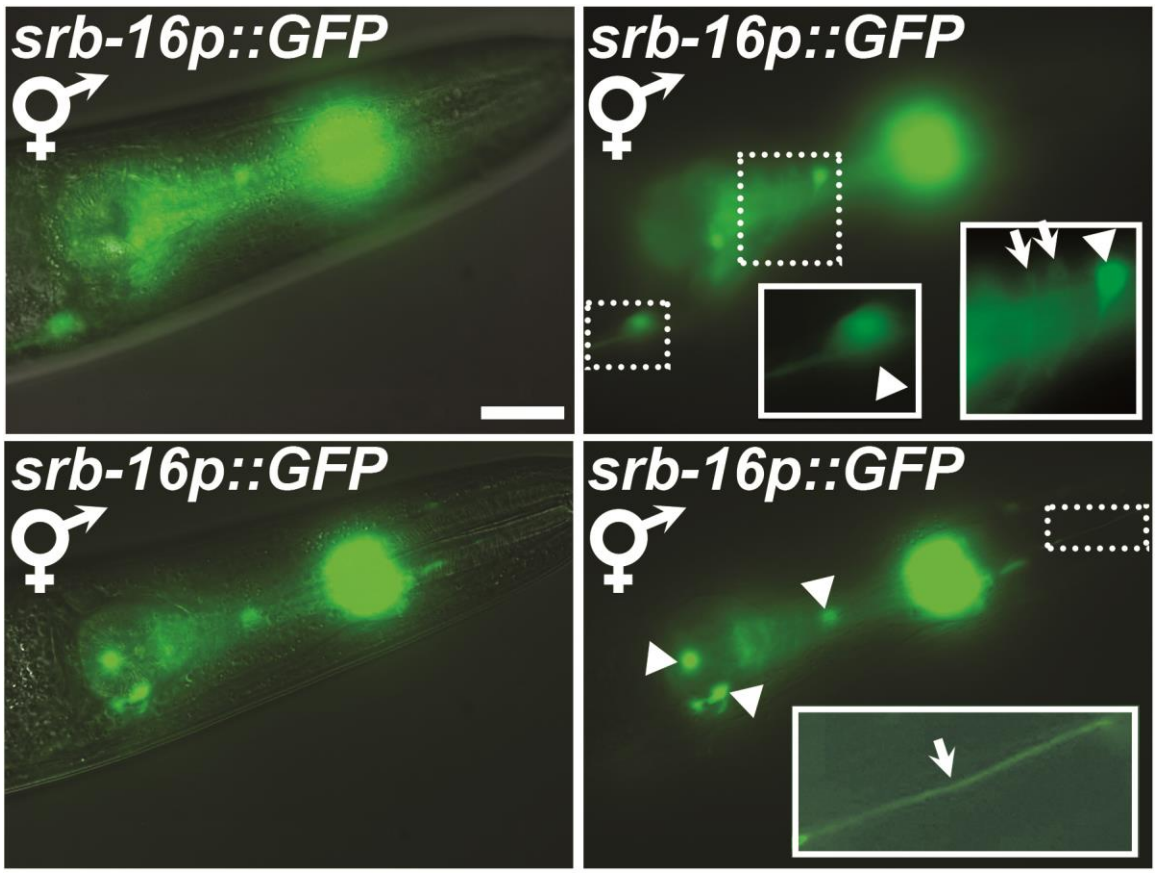

Fig. S13. Predicted *srb-16* promoter expression in hermaphrodites.

The worm strain (*BC14820*) transiently expressing GFP under the predicted *srb-16* promoter (2,127 bp upstream of the translational start site) was kindly provided by the Caenorhabditis Genetics Center. The arrow heads indicate neuron cell bodies, and the arrows indicate dendrites or axons. Upper and lower GFP images belong to the same worm. Scale bar, 20 um.

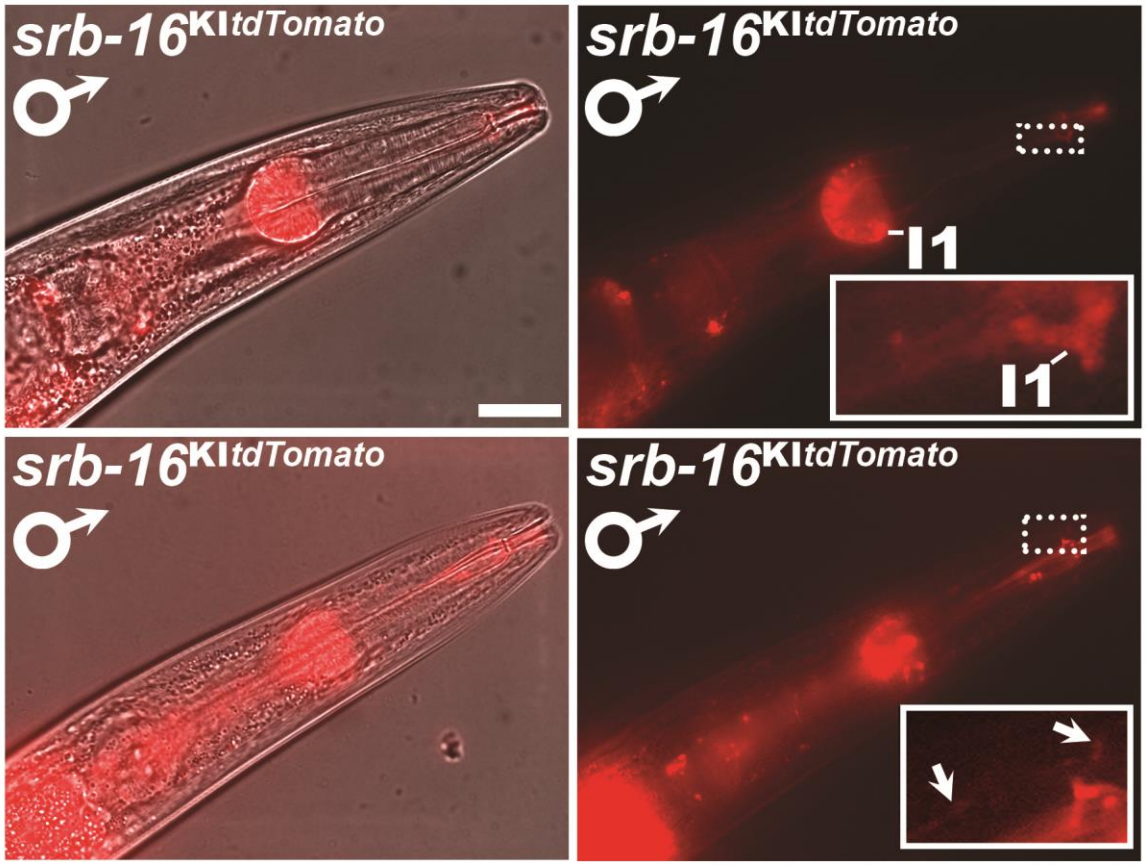

Fig. S14. Endogenous expression pattern of *srb-16* in males.

srb-16$^{KI tdTomato}$ mutant was crossed into *fog-2(q71)* to increase the incidence of males. I1, pharyngeal Interneuron #1 with a crooked-shaped dendritic terminal. The arrows in the lower inset indicate other axon/dendrite- like extension beside that of I1 neurons. Scale bar, 20 um.

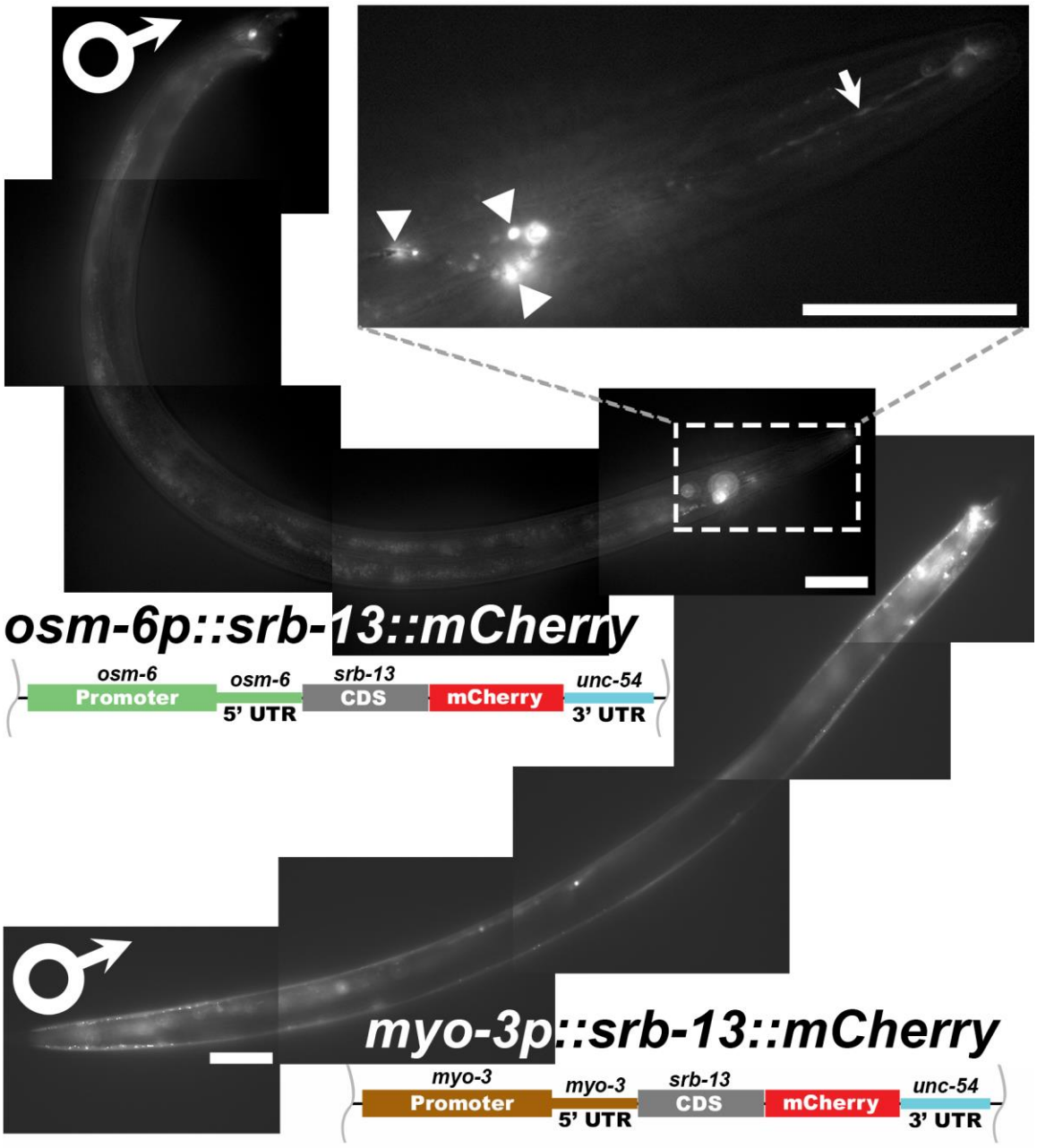

Fig. S15. *osm-6p::srb-13::mCherry* and *myo-3p::srb-13::mCherry* expression in *srb-13Δ1* mutant males.

Upper image shows mCherry signal of *osm-6p::srb-13::mCherry* in several puncta, indicated by white arrow heads, near the first pharyngeal pump where sensory neuron cell bodies are, and in a dendrite, indicated by a white arrow, extending toward the tip of the mouth of worm where the sensory cilia are. Lower image shows mCherry signal of *myo-*

3p::srb-13::mCherry in the outline of the worm where the body wall muscles are located. The diagrams of the transgenes are not to scale. CDS, coding sequence; UTR, untranslated region. Scale bar, 100 um.

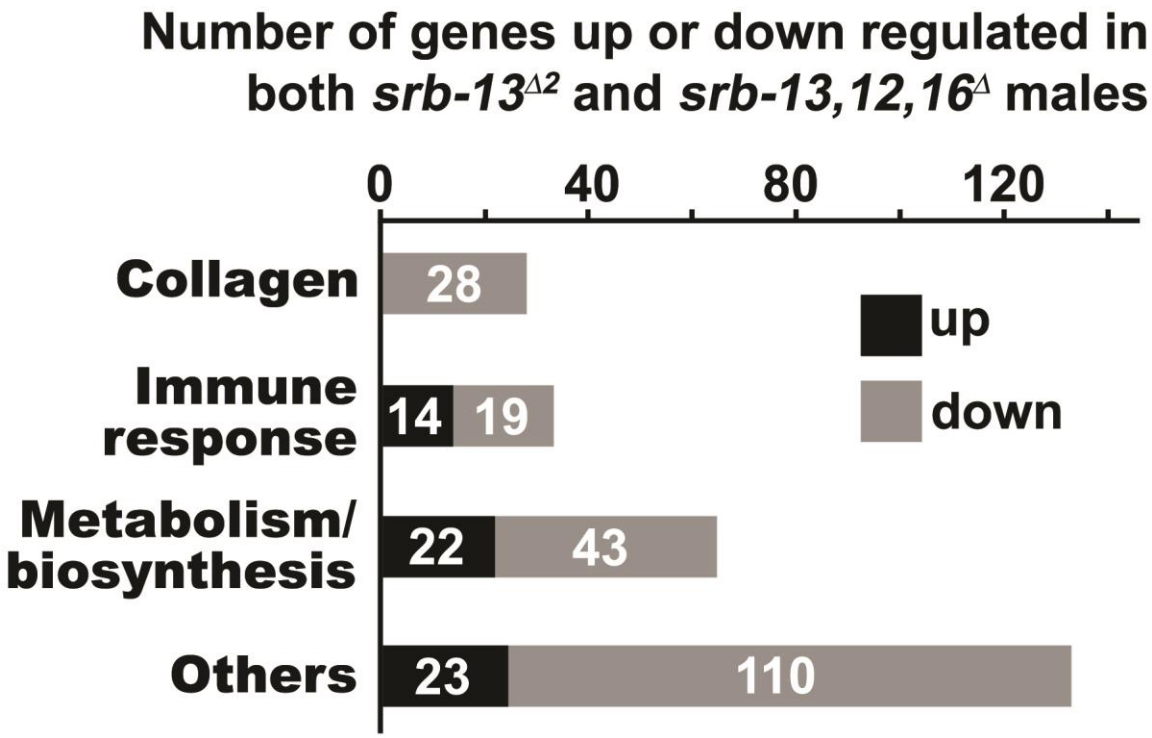

Fig. S16. Categorization of genes up or down regulated in both *srb-13Δ2* and *srb-13,12,16Δ* males compared to control males.

Both mutant and wild type males are in fog-2(q71) background to increase the incidence of males. p-values are all < 0.005, and q-values are all < 0.05. All four categories were all mutually exclusive. More details on the genes in each category can be found in SupplRNAseqData.xlsx Excel sheet 3.

TABLES

Table 1. Sperm distribution in the wild-type hermaphrodite uterus 1 hour after mating wild-type or GPCR mutant males.

Male Genotype	Zone 3	Zone 2	Zone 1	N
wild type	92% ± 0.6%	4% ± 0.3%	4% ± 0.5%	83
sra-11(ok630)	91% ± 1%	6% ± 1%	3% ± 1%	36
sra-13(zh13)	82% ± 2%	7% ± 1%	10% ± 2%	32
srd-1(eh1)	93% ± 1%	4% ± 1%	4% ± 1%	35
srg-4(ok3598)	85% ± 2%	6% ± 1%	9% ± 2%	42
srx-95(ok3415)	89% ± 1%	4% ± 1%	7% ± 1%	39
odr-10(ky225)	85% ± 2%	8% ± 1%	7% ± 1%	36
tkr-3(ok381)	92% ± 2%	4% ± 1%	4% ± 1%	24
gnrr-1(ok238)	85% ± 2%	7% ± 1%	7% ± 2%	39
mig-1(e1787)	89% ± 1%	5% ± 1%	7% ± 1%	48
srb-13Δ1	66% ± 3%	13% ± 1%	20% ± 2%	36

Wild-type or mutant males were mated to wild-type hermaphrodite. Mean ± standard error of the mean (SEM) is shown. See MATERIALS AND METHODS for zone definitions.

srb-13Δ1 refers to *srb-13(ok3126)* allele. *mig-1(e1787)* mutation is a nonsense mutation. Mutations in all other GPCR genes are deletion mutations and are predicted to be loss of function (see wormbase.org). Mutant worms were crossed into *fog-2(q71)* mutant background to increase the incidence of males. The control male strain is *fog-2(q71)* and wild-type hermaphrodite strain is N2.

Table 2. Sperm motility value of wild-type or mutant sperm in wild-type hermaphrodite uteri.

Male Genotype	Average Velocity (um/min)	Reversal Frequency (rev/hr)	Sperm #	Herm. #
Wild type[#]	8.62 ± 0.60	1.81	88	> 12
srb-13Δ1	7.20 ± 0.58 N.S.	4.19	40	4
srb-16Δ	4.84 ± 0.49 *	2.61	40	6
srb-13,12,16Δ	4.95 ± 0.43 *	4.15	40	4
srb-5Δ	4.72 ± 0.45 *	3.23	40	5
srb-2,3,4,5Δ	7.98 ± 0.79 N.S.	6.91	37	4

The average velocity, average directional velocity toward the spermatheca (sperm sac), and average reversal frequency were determined for wild-type and mutant sperm within the uteri of wild-type hermaphrodites. Value ± standard error of the mean (SEM) is shown. N.S., not statistically significant; *, $p<0.00001$. Herm. #, number of hermaphrodite videos used.

[#]Published data from (Edmonds et al., 2010; Hoang et al., 2013; Kubagawa et al., 2006) for reference.

Table 3. Sperm distribution in wild-type hermaphrodite uterus 1 hour after mating to *srb* mutant transgenic males.

Male Genotype		Zone 3	Zone 2	Zone 1	N
Wild type		92% ± 0.6%	4% ± 0.3%	5% ± 0.5%	83
srb-13Δ1	No transgene	66% ± 3%	13% ± 1%	20% ± 2%	36
	unc-119p::srb-13.Line 1	94% ± 1%	3% ± 1%	3% ± 1%	16
	unc-119p::srb-13.Line 2	90% ± 2%	6% ± 1%	4% ± 1%	34
	unc-119p::srb-13.Line 4	81% ± 2%	5% ± 1%	13% ± 2%	38
	osm-6p::srb-13::mCherry.Line 1	85% ± 3%	8% ± 2%	7% ± 2%	24
	osm-6p::srb-13::mCherry.Line 4	87% ± 2%	8% ± 2%	5% ± 1%	27
	myo-3p::srb-13::mCherry.Line 4	70% ± 3%	16% ± 2%	13% ± 2%	26
srb-16Δ	No transgene	67% ± 2%	14% ± 1%	20% ± 2%	40
	unc-119p::srb-16.Line 4	84% ± 4%	7% ± 2%	9% ± 2%	17
	unc-119p::srb-16.Line 7	86% ± 3%	7% ± 2%	7% ± 2%	14
	unc-119p::srb-16.Line 8	87% ± 2%	6% ± 1%	7% ± 1%	22

Wild-type or mutant males with or without transgene were all mated to wild-type hermaphrodites. The control male strain is *fog-2(q71)*, and wild-type hermaphrodite strain is N2. Mean ± standard error of the mean (SEM) is shown. See MATERIALS AND METHODS for zone definition.

The zone distribution values for wild-type sperm, *srb-13Δ1*, and *srb-16Δ* mutant sperm from Figure 1 are provided for reference.

Transgenes *unc-119p::srb*-13, *unc-119p::srb-16*, *osm-6p::srb-13::mCherry*, and *myo-3p::srb-13::mCherry* are carried by pUS13, pUS16, pOS13, and pMS13 plasmids, respectively. The plasmid sequences are provided in annotated ape files pUS13.ape, pUS16.ape, pOS13.ape, and pMS13.ape. Also, see MATERIALS AND METHODS for more details on plasmid construction. *myo-3p::mitoGFP* was used as a co-injection marker to select for worms carrying transgenes (Labrousse et al., 1999). *srb-13Δ1 and srb-16Δ* mutant hermaphrodites expressing one of the transgenes were mated with *srb-13Δ1;fog-2(q71)* or *srb-16Δ;fog-2(q71)* males. *srb* mutant male progenies expressing one of the transgenes were used for sperm guidance assay with wild-type hermaphrodites.

SUPPLEMENTARY TABLES

Table S1. Annotation of sperm enriched genes up-regulated in *srb-13Δ2* or *srb-13,12,16Δ* mutants compared to control males.

	Fold change Versus WT		
Gene Name	***srb-13Δ2***	***srb-13,12,16Δ***	**Annotation**
F16B4.7	3.5	No Diff	unknown protein
C32H11.4	4.9	6.4	unknown protein
scl-2	**6.8**	**5.2**	**sperm coating protein SCP/TAPS family**
R05H10.7	3.7	4.8	unknown protein
spp-17	2.6	4.0	an antimicrobial pore-forming SaPosin-like family member
far-3	3.7	3.9	a Fatty Acid/Retinol binding protein
C17H12.8	2.0	3.5	unknown protein
T05E12.3	3.0	3.1	unknown protein
Y51F10.7	2.9	3.0	unknown protein
asp-14	2.2	2.8	aspartic protease 14
lipl-5	1.7	2.2	a lipase in the intestine induced upon bacterial infection.
C17F4.7	1.8	2.0	unknown protein
cdh-5	2.1	1.8	a homolog of cadherin.
dct-8	No Diff	10.9	DAF-16/FOXO Controlled, germline Tumor affecting
F56D6.8	No Diff	10.9	unknown protein
cnc-2	No Diff	4.6	an antimicrobial caenacin peptide strongly induced in the epidermis upon infection by fungal pathogen
F46C3.6	No Diff	3.4	unknown protein
nlp-30	No Diff	2.8	a predicted antimicrobial neuropeptide-like protein in the hypodermis
pud-4	No Diff	2.7	a nematode-specific gene family *pud* member
fip-6	No Diff	2.5	a Fungus-Induced Protein
nlp-31	No Diff	2.4	an antifungal neuropeptide-like protein in hypodermis
msp-63	**No Diff**	**2.3**	**Major Sperm Protein (MSP) family member**
Y119D3B.21	No Diff	2.3	unknown protein
F15E6.3	No Diff	2.1	unknown protein
C27B7.9	No Diff	2.1	unknown protein
cpz-1	No Diff	1.9	a homolog of cathepsin z-like cysteine protease for normal cuticle and molting
ssp-19	**No Diff**	**1.9**	**Sperm-Specific Protein (ssp) family**

F36D3.8	No Diff	1.9	unknown protein
F32B5.4	No Diff	1.9	unknown protein
msp-77	No Diff	**1.9**	**Major Sperm Protein (MSP) family member**
F21C10.10	No Diff	1.8	unknown protein
F23D12.11	No Diff	1.8	unknown protein
clec-145	No Diff	1.8	C-type LECtin (calcium binding, carbohydrate binding)
msp-3	No Diff	**1.8**	**Major Sperm Protein (MSP) family member**
D2062.7	No Diff	1.8	unknown protein
spp-5	No Diff	1.8	an antimicrobial pore-forming SaPosin-like family member expressed exclusively in the intestine
B0252.5	No Diff	1.8	unknown protein
Y37D8A.5	No Diff	1.8	unknown protein
Y71H2B.4	No Diff	1.8	unknown protein
msp-36	No Diff	**1.7**	**Major Sperm Protein (MSP) family member**
F36D3.4	No Diff	**1.7**	**Major Sperm Protein domain containing protein**
msp-33	No Diff	**1.7**	**Major Sperm Protein (MSP) family member**
Y43F8C.9	No Diff	1.7	unknown protein
R08A2.1	No Diff	1.7	unknown protein
msd-4	No Diff	**1.7**	**Major Sperm Protein domain containing protein**
ssp-31	No Diff	**1.7**	**Sperm-specific class P protein 31**
ssq-3	No Diff	**1.7**	**Sperm-specific family, class Q**
F45D3.4	No Diff	1.6	unknown protein
ZK596.2	No Diff	1.6	unknown protein
msp-142	No Diff	**1.6**	**Major Sperm Protein (MSP) family member**
msp-45	No Diff	**1.6**	**Major Sperm Protein (MSP) family member**
F58A6.9	No Diff	1.6	unknown protein
scrm-5	No Diff	1.6	*scrm-5* encodes a putative phospholipid scramblase
T08B6.9	No Diff	1.6	unknown protein
Y43F8A.2	No Diff	1.6	unknown protein
F08H9.2	No Diff	1.6	unknown protein
nspd-10	No Diff	1.6	Nematode Specific Peptide family, group D
msp-38	No Diff	**1.6**	**Major Sperm Protein (MSP) family member**
fat-2	No Diff	1.6	*fat-2* encodes a delta-12 fatty acyl desaturase that is required for F-series prostaglandins synthesis

ZK484.5	No Diff	1.6	unknown protein
C10G11.9	No Diff	1.6	unknown protein
C33F10.11	No Diff	1.6	unknown protein
K01H12.4	No Diff	1.6	unknown protein
F27C1.1	No Diff	1.6	unknown protein
nspd-9	No Diff	1.6	Nematode Specific Peptide family, group D
C04F12.7	No Diff	1.5	unknown protein
nlp-27	No Diff	1.5	a predicted antimicrobial neuropeptide-like protein
asp-3	No Diff	1.5	an aspartyl protease homolog required for degenerative (necrotic-like) cell death in neurons
T16A9.5	No Diff	1.5	unknown protein
ssp-34	No Diff	**1.5**	**Sperm-specific class P protein 34**
Y106G6G.4	No Diff	1.5	unknown protein
ssq-1	No Diff	**1.5**	**Sperm-specific family, class Q**
Y53H1B.2	No Diff	1.5	unknown protein
R09E10.6	No Diff	1.5	a germline enriched novel protein conserved among nematodes, required for normal germ cell development
Y38C1AA.7	No Diff	1.5	unknown protein
C36H8.1	No Diff	1.5	unknown protein
F58E6.5	No Diff	**1.5**	**a major sperm protein domain containing protein**
F17E9.5	No Diff	1.5	a novel protein conserved among nematodes.

Fold change p-value <0.005, q<0.05. No Diff, no difference between the level of transcripts of mutant and wild type. Rows containing genes coding for sperm structural component are highlighted in gray.

Table S2. Annotation of sperm enriched genes down-regulated in *srb-13Δ2* or *srb-13,12,16Δ* mutants compared to control males.

	Fold change Versus WT		
Gene Name	***srb-13$^{\Delta 2}$***	***srb-13,12,16$^{\Delta}$***	**Annotation**
asp-1	-1.6	No Diff	an aspartic protease in intestine during late embryonic and early larval development
lec-8	-1.7	No Diff	an antimicrobial glycolipid-binding galectinlec-8
asp-5	-1.8	No Diff	Aspartic protease 5
F19C7.1	-1.9	No Diff	unknown protein
col-124	-1.9	No Diff	COLlagen
col-80	-2.0	No Diff	COLlagen
F52E1.14	-2.1	No Diff	unknown protein
col-20	-2.1	No Diff	col-20 encodes a collagen
asp-6	-2.2	No Diff	aspartic protease 6
C49G7.12	-2.3	No Diff	unknown protein
F18E3.13	-2.3	No Diff	unknown protein
col-93	-2.5	No Diff	COLlagen
msp-45	-2.9	No Diff	A major sperm protein family member
F58A6.9	-2.9	No Diff	unknown protein
hsp-16.41	-3.6	No Diff	a 16-kD heat shock protein in intestine and pharynx; prevents unfolded proteins from aggregating.
col-19	-2.1	-1.6	Collagen
lys-1	-2.2	-1.6	*lys-1* encodes a putative lysozyme expressed in neurons and intestine
D1086.3	-2.2	-1.6	unknown protein
F19B2.5	-3.5	-1.7	unknown protein
aldo-1	-2.7	-1.9	a human ALDOLASE A, FRUCTOSE-BISPHOSPHATE homolog
sodh-1	**-2.8**	**-2.0**	**Alcohol dehydrogenase 1, predicted mitochondrial**
MTCE.31	**-2.0**	**-2.0**	**mitochondrial encoded cytochrome c oxidase subunit 2 (ctc-2)**
Y47D7A.11	-2.5	-2.0	unknown protein
MTCE.25	**-2.0**	**-2.0**	**mitochondrial encoded NADH:ubiquinone oxidoreductase (nduo-4)**
gst-7	-2.9	-2.1	gst-7 encodes a predicted glutathione S-transferase.
MTCE.21	**-2.4**	**-2.5**	**Mitochondrial encoded cytochrome b (ctb-1)**
MTCE.23	**-2.4**	**-2.5**	**Mitochondrial encoded subunit 3 of cytochrome c oxidase (ctc-3)**

sqst-2	-3.4	-2.7	SeQueSTosome related, bind polyubiquitin and help protein degradation via proteasome
MTCE.16	**-2.9**	**-2.7**	**Mitochondrial encoded NADH:ubiquinone oxidoreductase (nduo-2)**
MTCE.11	**-3.3**	**-3.1**	**Mitochondrial encoded NADH-ubiquinone oxidoreductase chain 1 (nduo-1)**
MTCE.12	**-3.3**	**-3.1**	**Mitochondrial coded ATP synthase subunit a (atp-6)**
col-139	-4.6	-3.4	COLlagen
col-129	-5.3	-4.2	COLlagen
col-81	-5.7	-5.0	COLlagen
MTCE.26	**No Diff**	**-1.6**	**Mitochondrial encoded subunit 1 of cytochrome c oxidase (ctc-1)**

Fold change p-value <0.005, q<0.05. No Diff, no difference between the level of transcripts of mutant and wild type. Rows containing genes coding for mitochondrial component are highlighted in gray. All MTCE genes are coded by *C. elegans* mitochondrial genome.

Table S3. Primer list.

PRIMER NAME	SEQUENCE
*srb-13*P1	ATGGCGGGAATTAATCAAACAA
*srb-13*P2	TTAGAATCCTATCTGAGTAATTGTAGCCC
*xm1*P1	cgtgaaatgacctcacgttg
*xm1*P2	TGGAGAATCCCAATGGAAAC
*xm1*P5	TTGGGTCAATTTGAGCATGA
*xm1*P6	catgttgtgttttgtccgaaag
*C27D6.11*cdsF	ATGGTAAAAGAAGAAAGCACTGGT
*C27D6.11*cdsR	ccttcTTATGCATGTTGTCTCTTG
*xm2*P1	TCCTGCCTCTTCCATTTCAT
*xm2*P2	CGCGACACAAAATTCCAATA
*xm2*P3	CAACTCGCCTATCACCCAGT
*xm2*P4	CTTGCCGTAGTCGATGGAAC
*xm2*P5	CGCTTTGGTTTTATGCTTTGA
*xm2*P6	CGGAACTGCACAATTTACACC
*xm2*P7	gcctgagtatcccgcctaat
*xm2*P8	ATGAGGGAAACTGCGTGTCT
*xm2*P9	GAGTTGAAAAGGGCGATGAA
*xm2*P10	gggcgttgaatgtgaaaact
*xm3*P1	TTCATATCATTCCTCATGCTTCC
*xm3*P2	TCCTTGCTCCTTCTTTTCCA
*xm3*P3	gcagGGCTATCACTTCTTCG
*xm3*P4	GAAAGAAATCAGGGCCAACA
*xm3*P5	GCACAGCTCAATTGCATGTT
*xm3*P6	GCCAATGCTGGCTGATTATT
*xm3*P7	CGTCCAACCTACAAGGCAAT
*xm3*P8	AGTCATTTCCGTGGGGTTTT
*xm3*P9	CAATTCATCCCGGTTTCTGT
*xm3*P10	tcggtgtagccagagagtaaaa
*xm4*P1	tcagcgcaaaatttcagaca
*xm4*P2	ACCTTGAAGCGCATGAACTC
*xm4*P3	TTCGCTGTCCTGTCACACTC
*xm4*P4	tgcgtcaaaaagcaacaaag
*xm10*P1	agctaaatgagggcgaatca
*xm10*P2	GCGCATGAACTCTTTGATGA
*xm10*P3	GGACGACATGATCAACAATCC
*xm10*P4	tggtgaagccagagagtgaa
*xm14*P1	GGGAGCAATTAATGCGACTG
*xm14*P2	CCTTGGTCACCTTCAGCTTG

*xm14*P3	CTCGTCATGCACAACAAAGC
*xm14*P4	attcttctcgtccgcaatgt
*srb-13*qpcrF	GTTTTGCCGTTCCAGGATTGA
*srb-13*qpcrR	TCACAGTTGGATTTGATGAAGAAAGG
*srb-16*qpcrF	TGGTCCCGTATGCTATTGTGC
*srb-16*qpcrR	CAGCGTCTTGGTAAGCCCAAA
*srb-12*qpcrF	CAAGAGAAGTTTGACAAGCCGTTCA
*srb-12*qpcrR	TGATACATTCTTGCGGCGGTA
*srb-5*qpcrF	CGGGTATTATTGCTCCCATTTCA
*srb-5*qpcrR	TGACGTCATGTGACCGCATTT
*srb-3*qpcrF	TTTCCATGGCATTGTGTTTTGC
*srb-3*qpcrR	CATTTCCCAATGCAACAAATCG
*srb-2*qpcrF	GCCTTTGGGTTTTTCCATCG
*srb-2*qpcrR	ATGGCTGAGGTCTCAGGGACA
*spe-9*qpcrF	TTGTTTGGGCAGAGGCAAGG
*spe-9*qpcrR	CAGGTGGCAGTGACGGTTTT
*spe-11*qpcrF	CGGGAAAGGAGCGGCTATGA
*spe-11*qpcrR	CACGTTGTCGTTCCCATTCG
*cdc-42*qpcrF	TGCCTGAAATTTCGCATCATTG
*cdc-42*qpcrR	TGTTGTGGTGGGTCGAGAGC
*pXM1*attB4.PLI.ttTi4405	ggggacaactttgtatagaaaagttgTTTGGGAGACCCAAGTTGAA
*pXM1*attB1r.PLI.ttTi4405	ggggactgctttttgtacaaacttgTGCATCGGAAATTTAAAAGGA
*pXM1*attB2r.DRe.ttTi4405	ggggacagctttcttgtacaaagtggCCAGAGATCTGCCGGAATTA
*pXM1*attB3.DRe.ttTi4405	ggggacaactttgtataataaagttgGCAGCGCTCATGGTTAGTTT
*pXM2*attB4.s5DL.4953	ggggacaactttgtatagaaaagttgTGGCTATGTCGCTTGATTTG
*pXM2*attB1r.s5DL.4953	ggggactgctttttgtacaaacttgGGCAGGAAGGTGCTAGGAAT
*pXM2*attB2r.s2PR.4953	ggggacagctttcttgtacaaagtggTGCAGGAATAGCGAGAATTG
*pXM2*attB3.s2PR.4953	ggggacaactttgtataataaagttgCCGAAGAAAGATCTCCCACA
*pXM3*attB4.s16DL.4405	ggggacaactttgtatagaaaagttgTGAAGCCAGAGAGTTTGGTG
*pXM3*attB1r.s16DL.4405	ggggactgctttttgtacaaacttgGTGAGTTTGGAGGGGTTTTT
*pXM3*attB2r.s13PR.4405	ggggacagctttcttgtacaaagtggCATCATAGGTTTCGTGTTGGAA
*pXM3*attB3.s13PR.4405	ggggacaactttgtataataaagttgTTATAACCGGGGGATGTTGA

*pXM4*pSpe11HindIIIF	cttggaaatgaaataagcttgagcagtggtcgacagaaca
*pXM4*pSpe11XbaINoS	cttgactgatattctagatttatctagtcggtttgcgaaataatc
*pXM4*xm4LHXbaIF2	ggggacaacttttctagaATGGCGGGAATTAATCAA ACAA
*pXM4*xm4LHBamHIR2	ggggactgctttggatccGAATCCTATCTGAGTAATT GTAGCCC
*pXM4*tdTomatoBamHIF	attggggcttgggcggatccATGGTGAGCAAGGGCGA GGA
*pXM4*tdTomatoEcoRIR	gggcttgggcgaattcCTTGTACAGCTCGTCCATGC
*pXM4*Srb13UTREcoRIF	gggcttgggcgaattcttaattaatactgattgggggttttt
*pXM4*Srb13UTRSpeIR	gggctgggagggactagtttgagatgtttttgacattatgaaac
*pXM4*cepUnc119SpeIF	gggagtccgggactagtGAGCCAATTTATCCAAGTC CTTG
*pXM4*cbUnc119UTRSpeIR	gggagtccgggccactagtCGGCCGCCTAGTTCTA GAC
*pXM4*xm4RHSpeIF2	ggggacaactttactagtTTTTGTATGACGGTTTGA AAGTTTTAG
*pXM4*xm4RHApaIR2	ggggactgctttgggcccTTTCAGATTCCCATGCC TTT
*pXM10*xm10LHFpgem5	GCCATGGCCGCGGGATATCAttccacaccgttca gacaaaaaaa
*pXM10*xm10LHRtdTom	CTCGCCCTTGCTCACCATcttaagaaaatgttgagtc cattgatcatg
*pXM10*tdTomFxm10LH	ggactcaacattttcttaagATGGTGAGCAAGGGCG AGGA
*pXM10*tdTomRs16UTR	gagtccattgatcatgaagcTTACTTGTACAGCTCG TCCATGC
*pXM10*s16UTRFtdTom	TGGACGAGCTGTACAAGTAAgcttcatgatcaa tggactcaacatt
*pXM10*s16UTRRu119res	GGACTTGGATAAATTGGCTCtaaaaaaaggcc gccacgagtt
*pXM10*u119resFs16UTR	ctcgtggcggccttttttaGAGCCAATTTATCCAAG TCCTTGTAA
*pXM10*u119resRxm10RH	ggccgccacgagttaatagaCGCCTAGTTCTAGACA TTCTCTAATGAA
*pXM10*xm10RHFu119res	GAGAATGTCTAGAACTAGGCGtctattaactcgt ggcggcctt
*pXM10*xm10RHRpgem5	CCTGCAGGCGGCCGCACTAGtgaagccagagag tttggtgaagt
*pSS16*srb16sgRNA1F	gtggttttgggtctgacgggGTTTTAGAGCTAGAAAT AGCAAGTTAAAATAAGG
*pSS16*srb16sgRNA1R	cccgtcagacccaaaaccacAAACATTTAGATTTGC AATTCAATTATATAGGG
*pXM14*xm14LHFpGem5	aggtcgaccatatgggagagctcagagggtctagagaaatgttggg
*pXM14*xm14LHRtdTo	CTCGCCCTTGCTCACCATTGGATTCTCAGT TTTCACTTCTGAC

*pXM14*tdToFxm14LH	GAAGTGAAAACTGAGAATCCAATGGTGAGCAAGGGCGAGG
*pXM14*unc54UTRRxm14RH	gtgtgtcaccgatcatttccCGCCTAGTTCTAGACATTCTCTAATGA
*pXM14*xm14RHFU54U	AGAGAATGTCTAGAACTAGGCGggaaatgatcggtgacacacg
*pXM14*xm14RHRpGem5	ctatgcatccaacgcgttgggatgcagccgacaccgatct
*pSS9*spe9sgRNAF	TaggaaatgatcggtgacacaGTTTTAGAGCTAGAAATAGCAAGTTAAAATAAGG
*pSS9*spe9sgRNAR	CtgtgtcaccgatcatttcctAAACATTTAGATTTGCAATTCAATTATATAGGG
*pO6D11GFP*pOsm6FpGem5	Ggtcgaccatatgggagagctaattttataattgcttatatgtagtagttatattttc
*pO6D11GFP*pOsm6RDyf11cds	CGAGTTTCCTCAACGCTCATagatgtatactaatgaaggtaatagcttgaa
*pO6D11GFP*Dyf11cdsFpOsm6	accttcattagtatacatctATGAGCGTTGAGGAAACTCGGG
*pO6D11GFP*Dyf11cdsRGFP	AAGTTCTTCTCCTTTACTCATAACATTGGAAATGAATAGTTGAATGCG
*pO6D11GFP*GFPFDyf11cds	TCAACTATTCATTTCCAATGTTATGAGTAAAGGAGAAGAACTTTTCACTG
*pO6D11GFP*Unc54UTRRpGem5	ctatgcatccaacgcgttgggCCCGTACGGCCGACTAGTAG
*pMS13*pMyo3FpGem5	Aggtcgaccatatgggagagctggctataataagttcttgaataaaataattttcccg
*pMS13*pMyo3RSrb13cds	ATTTTGTTTGATTAATTCCCGCCATttctagatggatctagtggtcgt
*pMS13*Srb13cdsFpMyo3	gaccactagatccatctagaaATGGCGGGAATTAATCAAACAAAATGC
*pMS13*Srb13cdsRmCherry	TCTTCACCCTTTGAGACCATGAATCCTATCTGAGTAATTGTAGCCCA
*pMS13*mCherryFSrb13cds	GCTACAATTACTCAGATAGGATTCATGGTCTCAAAGGGTGAAGAAGATAA
*pMS13*Unc54UTRRpGem5	ctatgcatccaacgcgttgggCCCGTACGGCCGACTAGTAG
*pOS13*pOsm6FpGem5	Ggtcgaccatatgggagagctaattttataattgcttatatgtagtagttatattttc
*pOS13*pOsm6RSrb13cds	TTTGTTTGATTAATTCCCGCCATagatgtatactaatgaaggtaatagctt
*pOS13*Srb13cdsFpOsm6	ttcaagctattaccttcattagtatacatctATGGCGGGAATTAATCAAACAAAATGC
*pOS13*Srb13cdsRmCherry	TCTTCACCCTTTGAGACCATGAATCCTATCTGAGTAATTGTAGCCCA
*pOS13*mCherryFSrb13cds	GCTACAATTACTCAGATAGGATTCATGGTCTCAAAGGGTGAAGAAGATAA
*pOS13*Unc54UTRRpGem5	ctatgcatccaacgcgttgggCCCGTACGGCCGACTAGTAG

*pUS13*U119FpGem5	gccgcgggatatcactagtgcAAGCTTCAGTAAAAGAAGTAGAATTTTATAGTTTT
*pUS13*U119Rsrb13Ex1	AATTCCCGCCATttcagaTAATGGGGGTCGTCCGTAATGATT
*pUS13*srb13FU119	ATTACGGACGACCCCCATTAtctgaaATGGCGGGAATTAATCAAACA
*pUS13*srb13UTRRpGem5	tggtcgacctgcaggcggccgttttgccctgcataagctatatttataac
*pUS16*U119FpGem5	gccgcgggatatcactagtgcAAGCTTCAGTAAAAGAAGTAGAATTTTATAGTTTT
*pUS16*U119Rsrb16Ex1	TTCTCGATCCATattttcTAATGGGGGTCGTCCGTAATGATT
*pUS16*srb16FU119	ATTACGGACGACCCCCATTAgaaaatATGGATCGAGAATTGATTGAAATTTGTAA
*pUS16*srb16UTRRpGem5	tggtcgacctgcaggcggccaataaaaaaaggccgccacgagt

CHAPTER 4

DISCUSSION

A Model for Sperm Chemotaxis in *C. elegans*

The work in this thesis, together with work from prior studies, supports the following model. PUFAs are transferred from the intestine to oocytes in lipoprotein complexes called yolk (Edmonds et al., 2010; Grant and Hirsh, 1999; Kubagawa et al., 2006). In Chapter two, we showed that oocytes convert 20-carbon PUFAs into at least ten structurally related F-series prostaglandins (PGFs), independent of cyclooxygenase enzymes. PGF precursors include DGLA (for PGF1 class), AA (for PGF2 class), omega-3 AA (for PGF2 class), and EPA (for PGF3 class). The PGF1 class includes CePGF1, which is either PGF1α or a co-eluting stereoisomer. The PGF2 class includes CePGF2, which is primarily the enantiomer of PGF2α.

Oocytes and their precursors release F-series prostaglandins into the reproductive tract. The PGF mixture promotes sperm velocity and provides directional cues, allowing sperm to locate oocytes and maintain their place in the spermatheca, despite the obstruction of passing fertilized eggs (Figure 1). Whether PGFs act as classical chemoattractants in a gradient or as position-instructive signals is not clear. Immediately after fertilization, a

cytochrome P450 CYP-31A2 enzyme catabolizes PGFs to prevent PGF synthesis in already fertilized eggs.

Previous and contemporary studies have shown that endocrine signals such as insulin and TGF-beta, as well as signals from somatic gonadal cells transduced by gap junctions regulate ovarian PGF metabolism (Edmonds et al., 2011; Edmonds et al., 2010; McKnight et al., 2014; Whitten and Miller, 2007). Together, these mechanisms allow hermaphrodite worms to coordinate nutritional status, population density signals, and oocyte development with reproductive output.

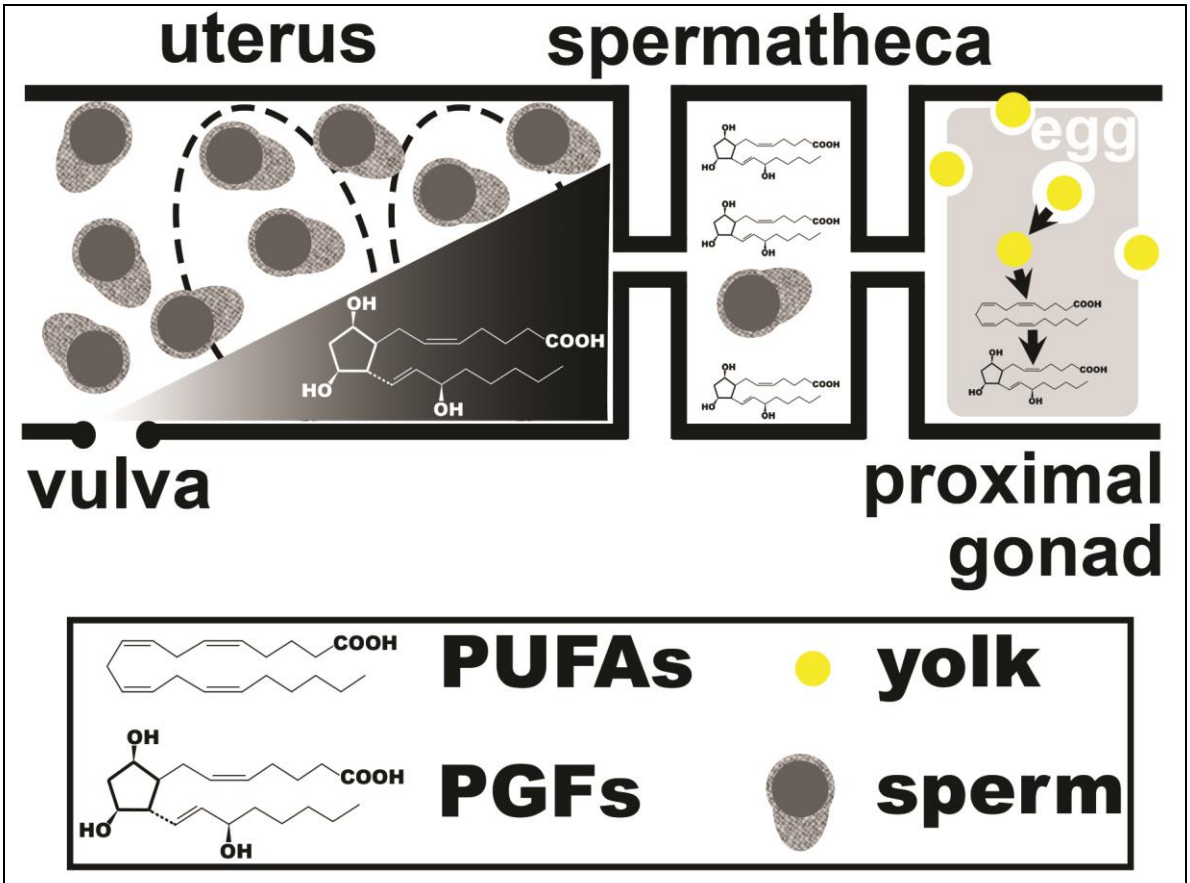

Figure 1. Current model of PGF synthesis and function in sperm guidance

Oocytes uptake polyunsaturated fatty acids (PUFAs) including DGLA, AA, O3AA, and EPA from intestine-derived yolk and convert them into F-series prostaglandins (PGFs)

including cePGF1, cePGF2, and other PGF1, PGF2, and PGF3 stereoisomers. cePGF2 is primarily the enantiomer of $PGF_{2\alpha}$ (ent-$PGF_{2\alpha}$). Structure of AA and ent-$PGF_{2\alpha}$ are used to illustrate PUFAs and PGFs. PGFs defuse out towards the spermatheca and the uterus creating a PGF gradient. Activated sperm perceive the PGF gradient and crawl toward the spermatheca to fertilize oocytes. Bulky fertilized eggs, outlined with broken gray lines, make the sperm's journey more challenging.

In Chapter three, the focus is on males. We show that s*rb-13* and other *srb* chemoreceptor genes are expressed and function in neurons, e.g. amphid sensory neurons, where they directly or indirectly sense environmental cues (e.g. male-derived ascarosides, molecules within exosomes, etc.). In favorable environments, SRBs GPCRs signal through the $G\alpha_{i/o}$ protein GOA-1, which is thought to trigger a neuroendocrine mechanism(s) affecting transcription of spermatogenic genes. Spermatogenic transcription changes (e.g. in cytoskeletal and metabolic genes) generate more competitive sperm that can better sense PGF guidance cues (Figure 2). Results from this chapter challenge conventional wisdom that males maximize their reproductive success by abundantly producing competitive sperm. Instead, *C. elegans* males appear to coordinate sperm quality with the external environment. Higher quality sperm have increased motility in the oviduct and are more efficient at finding the fertilization site. Below I discuss this model further, providing additional published and unpublished results.

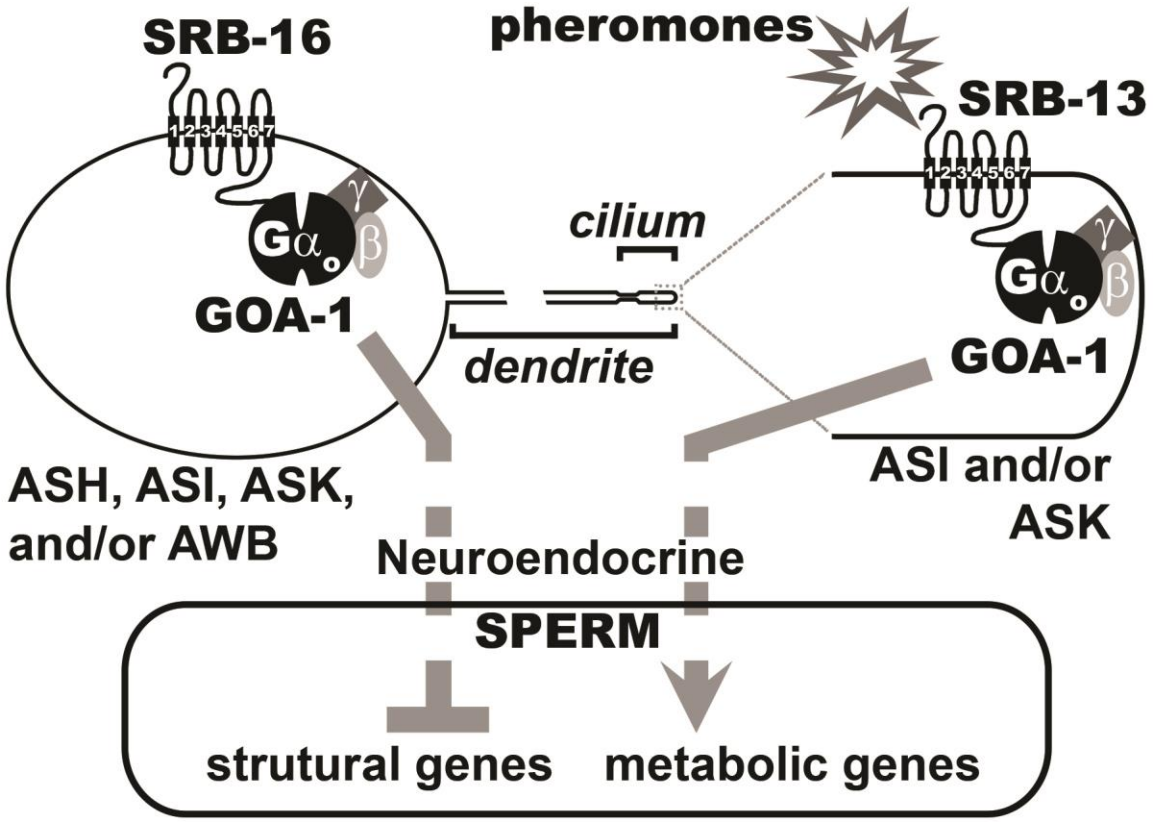

Figure 2. Current model of chemosensory neurons promoting sperm guidance

SRB GPCRs function in sensory neuron cell bodies or cilia to signal via $G\alpha_o$ GOA-1. GOA-1 signaling triggers a neuroendocrine mechanism(s) to suppress expression of sperm structural genes and promote expression of sperm metabolic genes. ASH, amphid single ciliated sensory neuron H; ASI, amphid single ciliated sensory neuron I; ASK, amphid single ciliated sensory neuron K; and AWB, amphid winged sensory neuron B. The environmental cues that bind SRB-13 are hypothesized to be pheromones because ASI and ASK sensory neurons are previously implicated in pheromone signaling (Bargmann and Horvitz, 1991; Gray et al., 2005; Kim et al., 2009; McKnight et al., 2014; White and Jorgensen, 2012).

COX-Independent Prostaglandin Synthesis

Results from chapter two show that adult mice tissues (e.g. kidney, heart, and liver) produce PGFs that co-elute with *C. elegans* PGF1 and PGF2 isomers. These PGF isomers are in different stereochemical configurations than that generated through the COX pathway. These data led to the hypothesis that mice generate PGFs independent of COX enzymes.

We obtained control, *Cox-1* single KO, and *Cox-1,2* double KO neonatal mice delivered at term from our collaborators in Dr. Jeff Reese's laboratory at Vanderbilt University. PG levels were measured in lipid extracts using liquid chromatography tandem mass spectrometry operated in multiple reaction monitoring (MRM) mode. MRM is a highly specific method for detecting and quantifying PGs. The level of 6-keto PGF1α, the stable metabolite of prostacyclin, is reduced to the limit of detection in the *Cox-1,2* double KO neonatal mice, consistent with the known role of COX enzymes in prostacyclin synthesis (Figure 3) (McKnight et al., 2014). On the other hand, PGF2α and/or co-eluting ent-PGF2α is reduced by about two fold (Figure 3) (McKnight et al., 2014). Two other PGF2α stereoisomers are unaffected (Figures 3-4) (McKnight et al., 2014). These COX-independent PGF2 isomers co-elute with *C. elegans* PGF2 stereoisomers (Figure 3) (McKnight et al., 2014). In addition, brain and several other tissues of a rare six-month-old adult *Cox* double KO also contained the same PGF2 isomers (Figure 5) (McKnight et al., 2014). Together, these results suggest that COX-independent PGF synthesis is conserved between *C. elegans* and mouse. Further work is needed to determine if the metabolic pathway is conserved. Nevertheless, there are two important implications of these findings.

First, an alternative and possibly evolutionarily ancient COX-independent PG synthesis pathway exists. Second, the *C. elegans* model might contribute to our understanding of human diseases or disorders involving prostaglandin dysregulation.

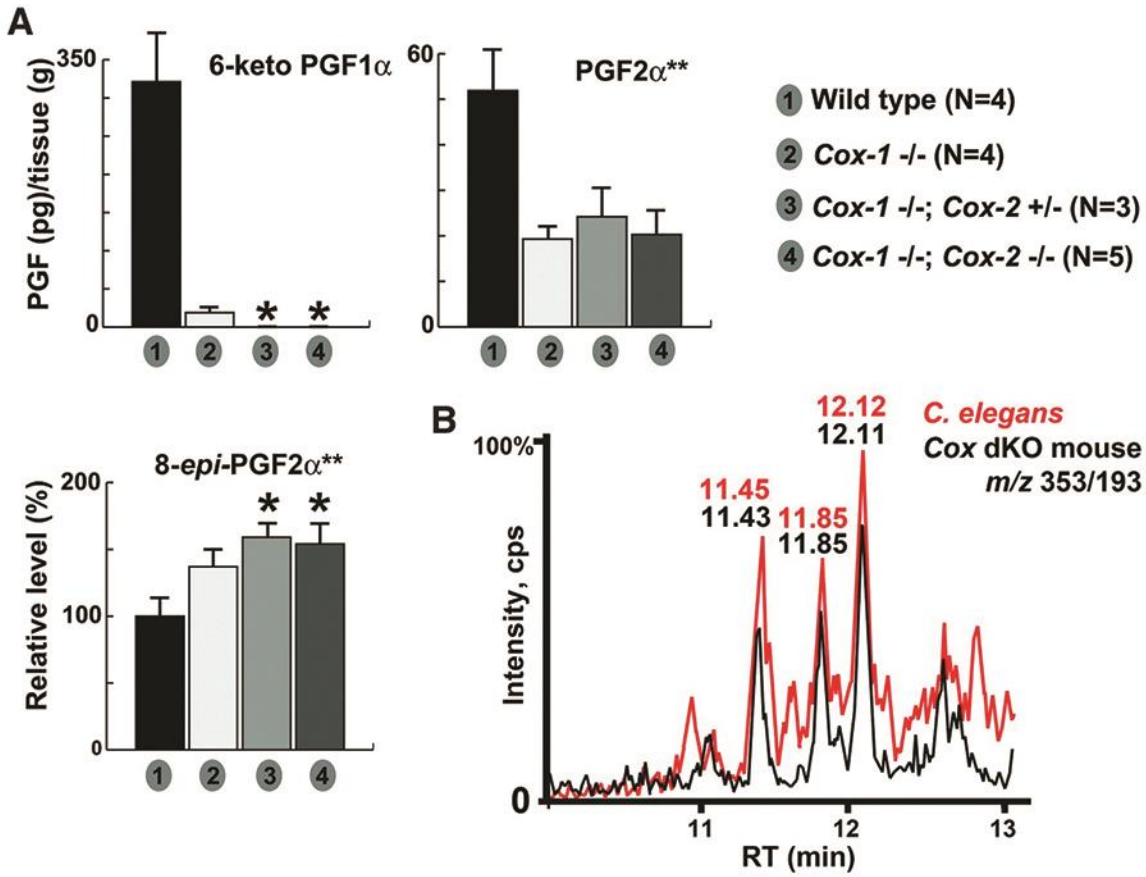

Figure 3. Prostaglandins in WT and Cox knockout mouse extracts

(A) Quantification of selected prostaglandins. Error bars denote SEM. (B) MRM chromatograms showing PGF2α isomer retention times in *C. elegans* (red) and Cox dKO (black) extracts. 8-epi-PGF2α eluting at RT = 11.4 and PGF2α eluting at RT = 11.8 are shown. The *C. elegans* isomer at RT = 12.1 is CePGF2β, a PGF2α stereoisomer (7). *P < 0.05. ** indicates that PGF2α and ent-PGF2α co-elute, as do 8-epi-PGF2α and 8-epi-15(R)

PGF2α. This figure is adapted from (McKnight et al., 2014). No permission is required from Science journal for thesis reprinting.

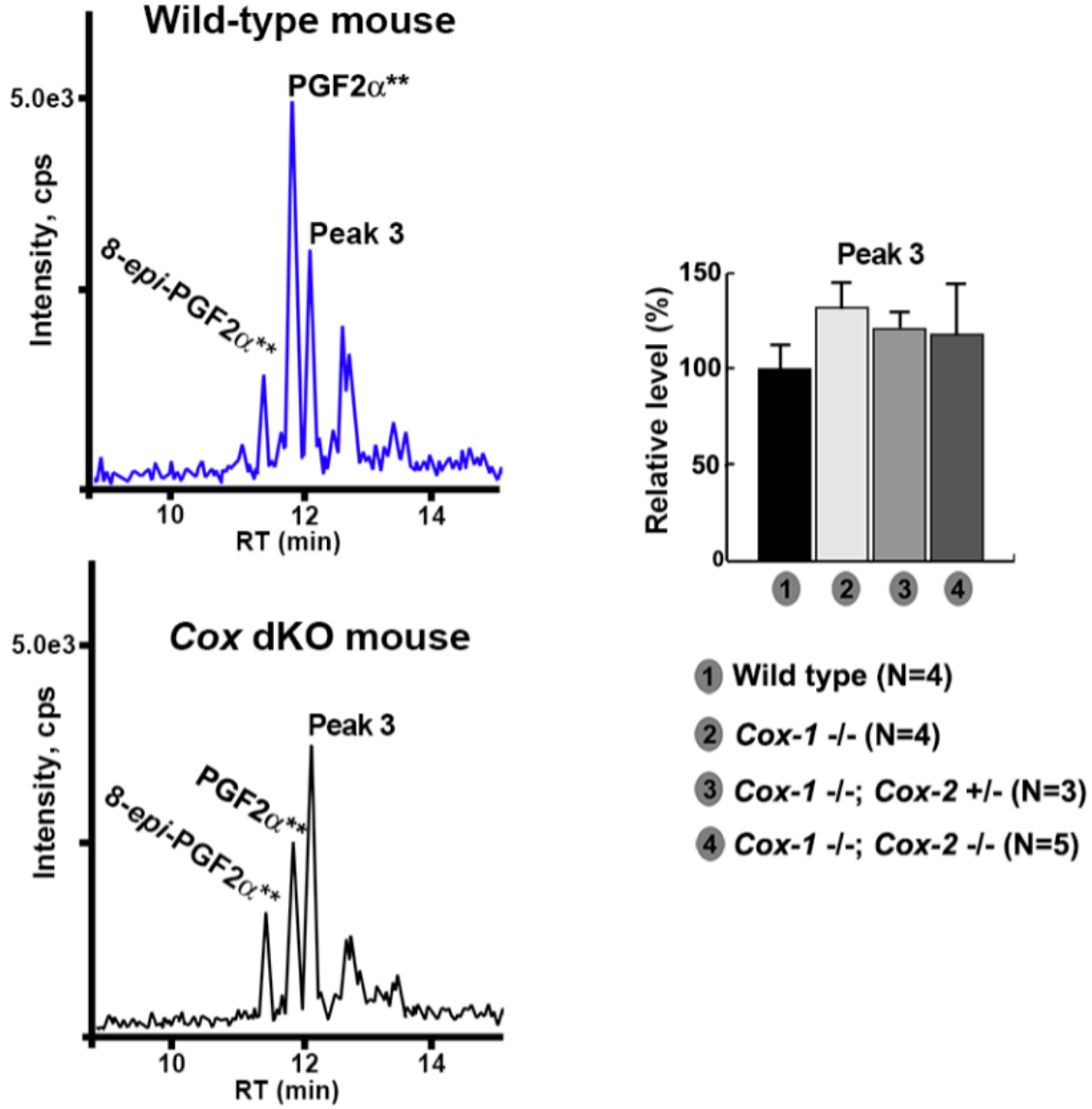

Figure 4. MRM chromatograms of wild-type and Cox double mutant pup extracts, focusing on PGF2α isomers (mass transition m/z 353/193).

**, PGF2α and ent-PGF2α standards co-elute (RT=11.8), as do 8-epi-PGF2α and 8-epi-15(R) PGF2αstandards (RT=11.4). Peak 3 is an unidentified PGF2α isomer that does not

co-elute with commercially available standards. Peak 3 does co-elute with CePGF2b. No permission is required from Science journal for thesis reprinting.

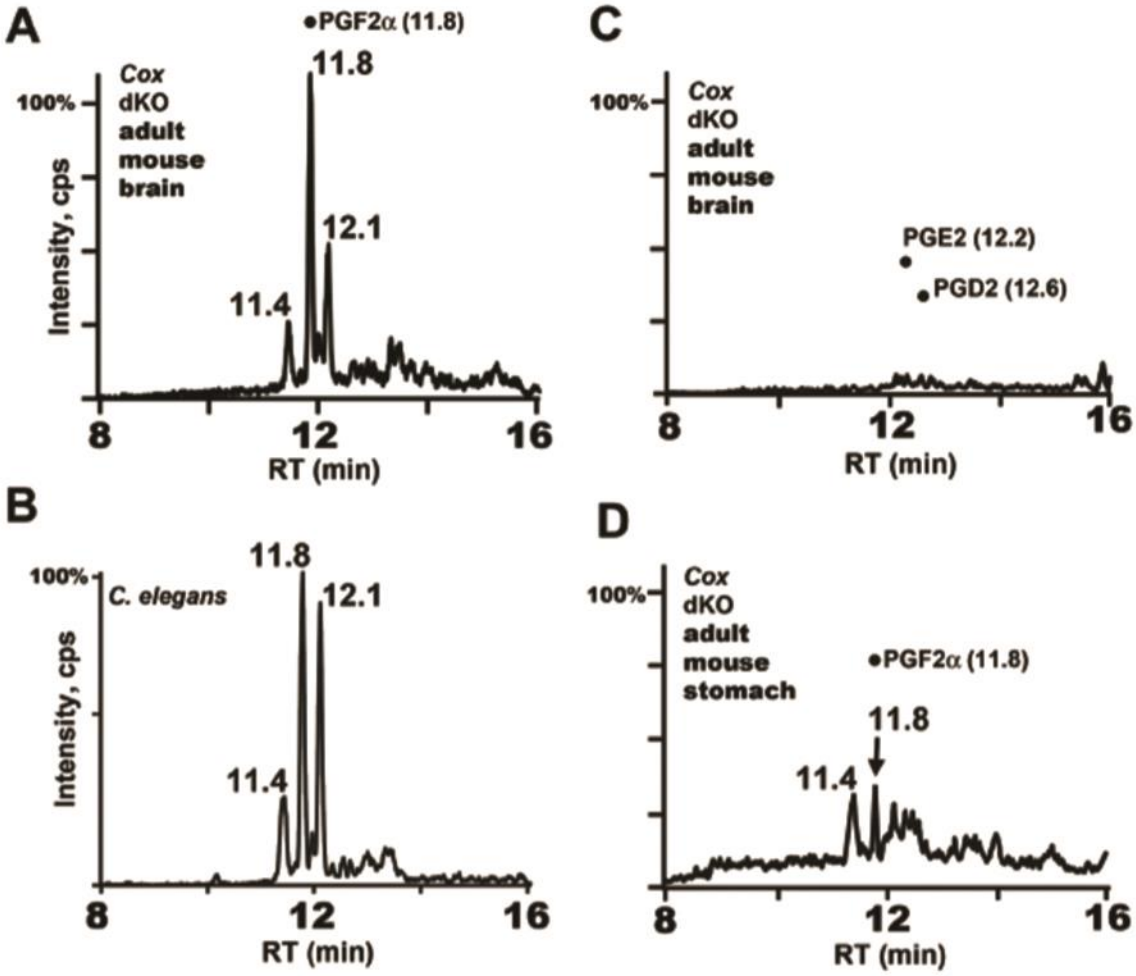

Figure 5. MRM chromatograms of *Cox* double mutant adult and *C. elegans* extracts. (A) MRM chromatogram of adult brain tissue using mass transition m/z 353/193, which detects PGF2α isomers. The three prominent peaks have identical retention times as *C. elegans* PGF2α isomers derived from arachidonic acid (B, published chromatogram from Hoang et al. 2013 shown for reference) (15). The peak at RT=11.4 is 8-iso PGF2α and/or

8-iso 15(R) PGF2α, the peak at RT=11.8 is PGF2α and/or ent-PGF2α, and the peak at RT=12.1 is an unidentified PGF2α stereoisomer that does not match commercially available standards (15). (C) MRM chromatogram of adult brain tissue using mass transition m/z 351/189, which detects PGD2 and PGE2 isomers. (D) MRM chromatogram of adult stomach tissue using mass transition m/z 353/193, which detects PGF2α isomers. Similar results were observed for the small intestine. PGF2α isomers were not detected in the large intestine (not shown), although degradation could be a factor. These Cox dKO adult tissues were from a very rare mouse that escaped postnatal lethality and lived to 6 months of age before being sacrificed. Only small amounts of tissue were available that was stored at -80°C for 9 months. A wild-type comparison was not included for this experiment because mutant tissue was limited and stored, which causes prostaglandin breakdown over time. No permission is required from Science journal for thesis reprinting.

COX Pathway Enzymes in COX-Independent PGF Synthesis

Although the *C. elegans* genome does not encode COX homologs, it does encode enzymes that are similar in sequence to human prostaglandin synthases acting downstream of COX. We previously identified several of these putative PG synthases (Edmonds et al., 2010). Mutations in Glutathione S Transferase (*gst-4*) or Prostaglandin E synthase 2 homolog (*pges-2* or R11A8.5) genes in hermaphrodites resulted in modest to mild sperm distribution defects. Gene knockdown by RNA-mediated interference of *gst-1* and *Y39G8B.2* (another aldo-keto reductase) also resulted in sperm distribution

defects (Edmonds et al., 2010). By homology, we selected four other candidate genes, including *pges-3* (or *ZC395.10*), *gst-2*, *gst-3*, and *Y39G8B.1*. Hermaphrodite strains containing deletions in *gst-4*, *pges-2*, *pges-3*, or *Y39G8B.1* were kindly provided by the *Caenorhabditis* Genetics Center, Minnesota, USA. Hermaphrodite strains containing both the *gst-4* deletion and *pges-2* deletion, or the *pges-3* deletion were kindly provided by Dr. Horikawa and Dr. Antebi from the Max Planck Institute for Biology of Ageing, Cologne, Germany.

Using genome-editing techniques, we generated knockout (KO) mutations in *Y39G8B.2*, *gst-1*, and a double KO mutation in *gst-2* and *gst-3* (Figures S1, S2). Homozygous *gst-1* KO mutant hermaphrodites are sterile, and the mutation has to be maintained in a heterozygous state. Therefore, mass spectrometry analysis on this mutant strain is currently not possible because a large amount of homozygous KO worms are needed. We will focus instead on the other genes.

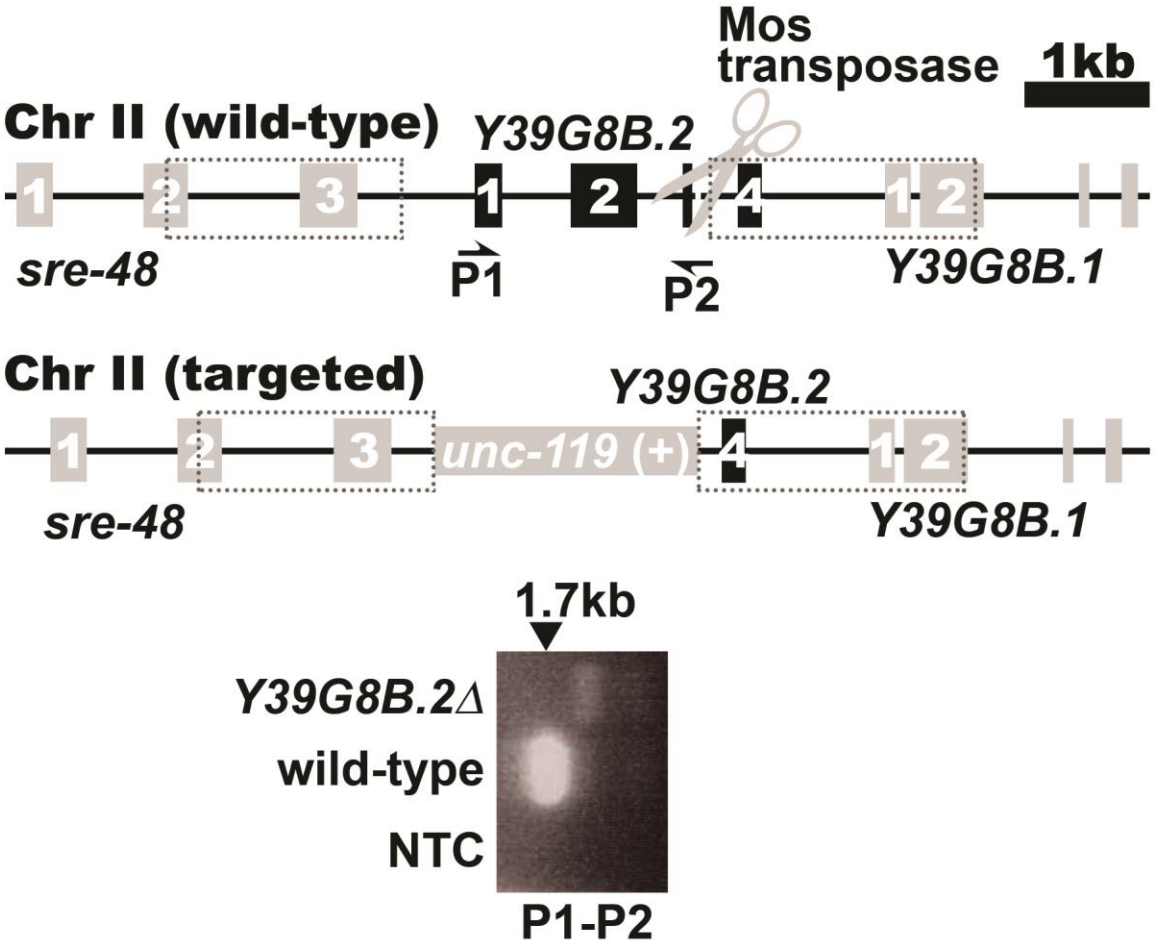

Figure S1. *Y39G8B.2* knock out (*Y39G8B.2Δ* or *xm9* allele) scheme and PCR validation

Y39G8B.2 coding exons (numbered in white) on the negative strand of chromosome II were shown up to scale. The primers P1 to P2 shown as single-barbed arrows appear longer in the diagram than their relative size. *Y39G8B.2* KO was performed using a homologous recombination based technique called MOSDEL (Frokjaer-Jensen et al., 2010). Briefly, a mutant worm carrying a Mos1 transposon in *Y39G8B.2* third intron (*cxTi10385* allele) was crossed into the *unc-119* loss of function background (*ed3* allele) to facilitate positive selection. Recombination replaced exons 1, 2, and 3 by the *unc-119* rescue fragment. PCR reaction using P1-P2 primers should amplify 1.7 kb of *Y39G8B.2* coding sequences only

in wild type. The targeting plasmid, pXM9, was assembled by Gibson assembly (New England Biolab). Annotated sequence of pXM9 plasmid is provided in pXM9.ape file. The sequences of P1, P2 primers and primers used for constructing the targeting plasmid are listed in Table S1.

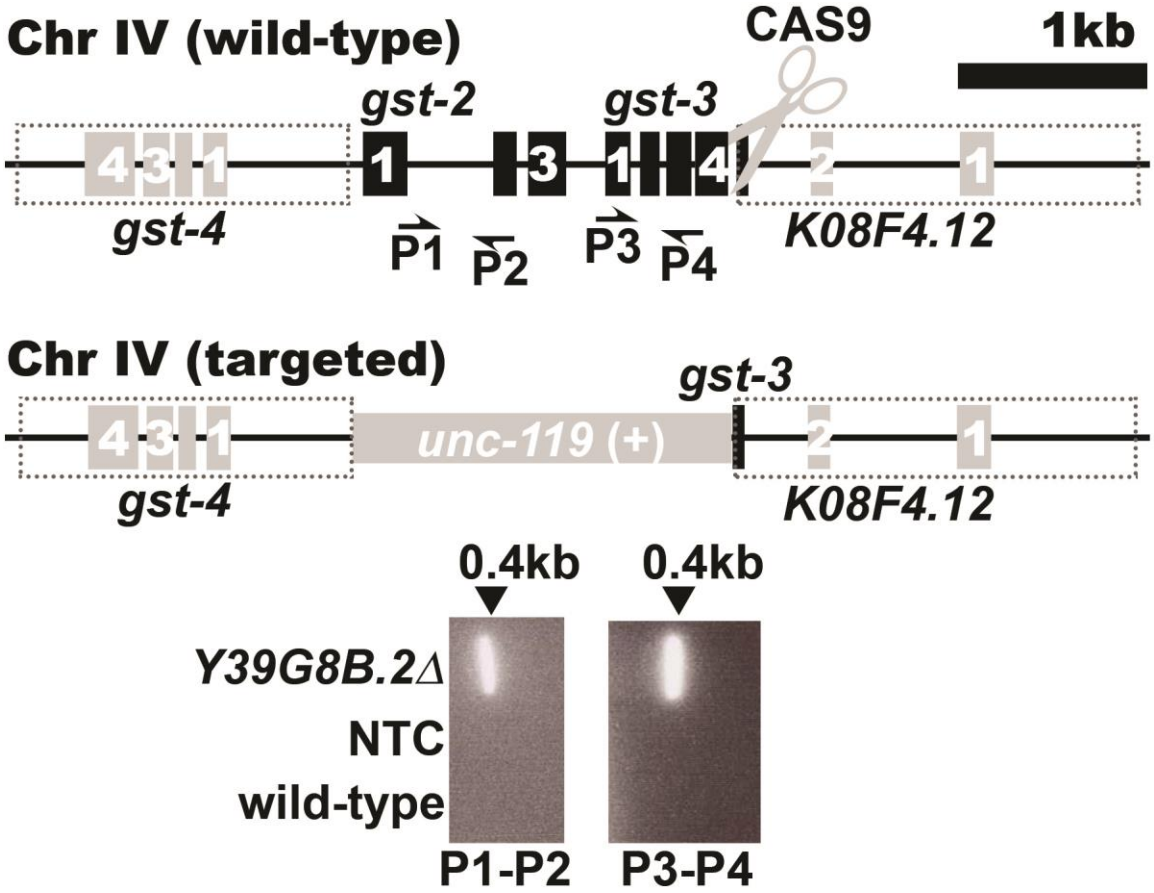

Figure S2. *gst-2* and *gst-3* double knock out (*Y39G8B.2Δ* or *xm9* allele*)* scheme and PCR validation

gst-2 and *gst-3*coding exons (numbered in white) on the negative strand of chromosome IV were shown up to scale. The primers P1 to P4 shown as single-barbed arrows appear longer in the diagram than their relative size. *gst-2* and *gst-3* double KO was performed using a combination of CRISPR technique and homologous recombination (Friedland et

al., 2013). Briefly, a single-guide RNA and CAS9 cleave near 3' end of the last exon of *gst-3* to make a DNA double strand break. *unc-119* loss of function (*ed3* allele) worms was used to facilitate positive selection. Recombination replaced all *gst-2* coding exons and most *gst-3* coding exons by the *unc-119* rescue fragment. PCR reaction using P1-P2 primers should amplify 426 bp of *gst-2* coding exons only in wild type. PCR reaction using P1-P2 primers should amplify 414 bp of *gst-3* coding exons only in wild type. The targeting plasmid, pXM7, and the single-guide RNA expression plasmid, pSG3, were assembled by Gibson assembly (New England Biolab). Annotated sequence of pXM7 andpSG3 plasmids are provided in pXM7.ape and pGS3.ape files. The sequences of P1 to P4 primers and the plasmids constructing primers are listed in Table S1.

Table S1. Primer list.

PRIMER NAME	SEQUENCE
*xm9*P1	ACTCAACTCGGGCTACGAGA
*xm9*P2	TGGATTCGGAAGATTTCACC
*xm7*P2	tgcatttcttcagtcggtgt
*xm7*P1	ccgttagtttcacccagcat
*xm7*P4	ggaaagtacggcaatcacaaa
*xm7*P3	attttaatgcacgcggactt
*pXM7*LHFpgem5	GCCATGGCCGCGGGATATCAttacgtggcacagctgaaactct
*pXM7*LHRu119	CTTGGATAAATTGGCTCgagactccgaaattgaaggaatggtt
*pXM7*u119resFLH	ccttcaatttcggagtctcGAGCCAATTTATCCAAGTCCTTG TAA
*pXM7*u119resRRH	gaatgggttggtcgataCGCCTAGTTCTAGACATTCTCTAA TG AA
*pXM7*RHFu119	ATGTCTAGAACTAGGCGtatcgaccaacccattcacacttc
*pXM7*RHRpgem5	CCTGCAGGCGGCCGCACTAGgcaagaaccttccaatcgagtaca
*pXM9*LHFpgem5	GCCATGGCCGCGGGATATCAgagcgatgttgtgcctgttattttc
*pXM9*LHRu119	ACTTGGATAAATTGGCTCgcacacctttttgcatctgacaaa
*pXM9*u119resFxm9LH	agatgcaaaaaggtgtgcGAGCCAATTTATCCAAGTCCTTG TAAA
*pXM9*u119resRxm9RH	tgatttttcagcggttccCGCCTAGTTCTAGACATTCTCTAAT GAA
*pXM9*RHFu119	GAATGTCTAGAACTAGGCGgaaccgctgaaaaatcaaaaaaaccg

*pXM9*RHRpgem5	CCTGCAGGCGGCCGCACTAGttcggatctccatccttacgga
*pSG3*gst3sgRNAF	TTgttgattaatgccgagttgtGTTTTAGAGCTAGAAATAGCAAG TTAAAATAAGGC
*pSG3*gst-3sgRNAR	ACacaactcggcattaatcaacAAACATTTAGATTTGCAATTCA ATTATATAGGGACC

Table 1. Sperm distribution in wild-type or mutant hermaphrodite uterus 1 hour after mating wild-type males.

Hermaphrodite Genotype	Zone 3	Zone 2	Zone 1	N
wild type	91% ± 1%	4% ± 1%	4% ± 1%	20
pges-2Δ	90% ± 2%	3% ± 1%	7% ± 1%	18
gst-4Δ	75% ± 3%	11% ± 1%	15% ± 2%	24
pges-2Δ gst-4Δ	95% ± 1%	2% ± 1%	3% ± 1%	20
pges-3Δ	70% ± 3%	17% ± 2%	13% ± 2%	17
Y39G8B.1Δ	81% ± 2%	10% ± 1%	8% ± 1%	42
Y39G8B.2Δ	45% ± 4%	10% ± 2%	45% ± 5%	16
gst-2,3Δ	72% ± 5%	7% ± 3%	21% ± 4%	13

Control males were mated to wild-type or mutant hermaphrodite. Mean ± standard error of the mean (SEM) is shown. See MATERIALS AND METHODS section of chapter 2 or 3 for zone definitions.

gst-4Δ (allele *ok2358*) mutation deletes all coding exons of *gst-4* and a small part of *msp-38*. *pges-2Δ* (allele *ok3316*) mutation deletes a part of exon 2 and 5, and all exons in between. *pges-3Δ* (allele *ok3052*) mutation deletes all coding exons of *pges-3* gene. *Y39G8B.1Δ* (allele *ok1682*) mutation deletes a part of exon 2 and intron 2, causing incorrect splicing and frameshift (see wormbase.org). *Y39G8B.2Δ* (allele *xm9*) mutation deletes the first three coding exons of *Y39G8B.2* gene (Figure 1). *gst-2,3Δ* (allele *xm7*) mutation deletes all coding exons of *gst-2* gene, and the first three coding exons and a part of exon 4 of *gst-3* gene (Figure 2).

pges-2Δ and *gst-4Δ* mutant worms were outcrossed 3 and 4 times, respectively. *Y39G8B.2Δ* and *gst-2,3Δ* mutant worms were generated by genome-editing. See figure Figures S1 and S2 for more details.

Wild-type male strain is *fog-2(q71)*, and wild-type hermaphrodite strain is N2.

The sperm guidance assay was performed by mating wild-type males to wild-type or mutant hermaphrodites (Table 1). *Y39G8B.2Δ*, *pges-3Δ*, *gst-2,3Δ*, and *gst-4Δ* mutant hermaphrodites had significant sperm distribution defects, which ranged from (zone 3)

45% to 75%, compared to 91% in wild-type controls (Table 1). The rest of the mutant hermaphrodites appear to have no gross sperm distribution defects. We measured PGF levels of the mutant hermaphrodites by LC-MS/MS analysis, as previously described (Edmonds et al., 2010; Hoang et al., 2013; Prasain et al., 2013). We found that none of the mutants are strongly deficient in PGF classes (e.g. PGF1, PGF2, or PGF3) (Figure 6). Therefore, we conclude that none of the tested candidate genes are essential for COX-independent PG synthesis. The mutant hermaphrodites with sperm guidance defects (e.g. *Y39G8B.2Δ*, *pges-3Δ*, *gst-2,3Δ*, and *gst-4Δ*) have no major changes in PGF levels (e.g. CePGF1 and CePGF2), suggesting that these enzymes act either downstream of or in a parallel pathway with respect to PGF synthesis and signaling (Figure 6).

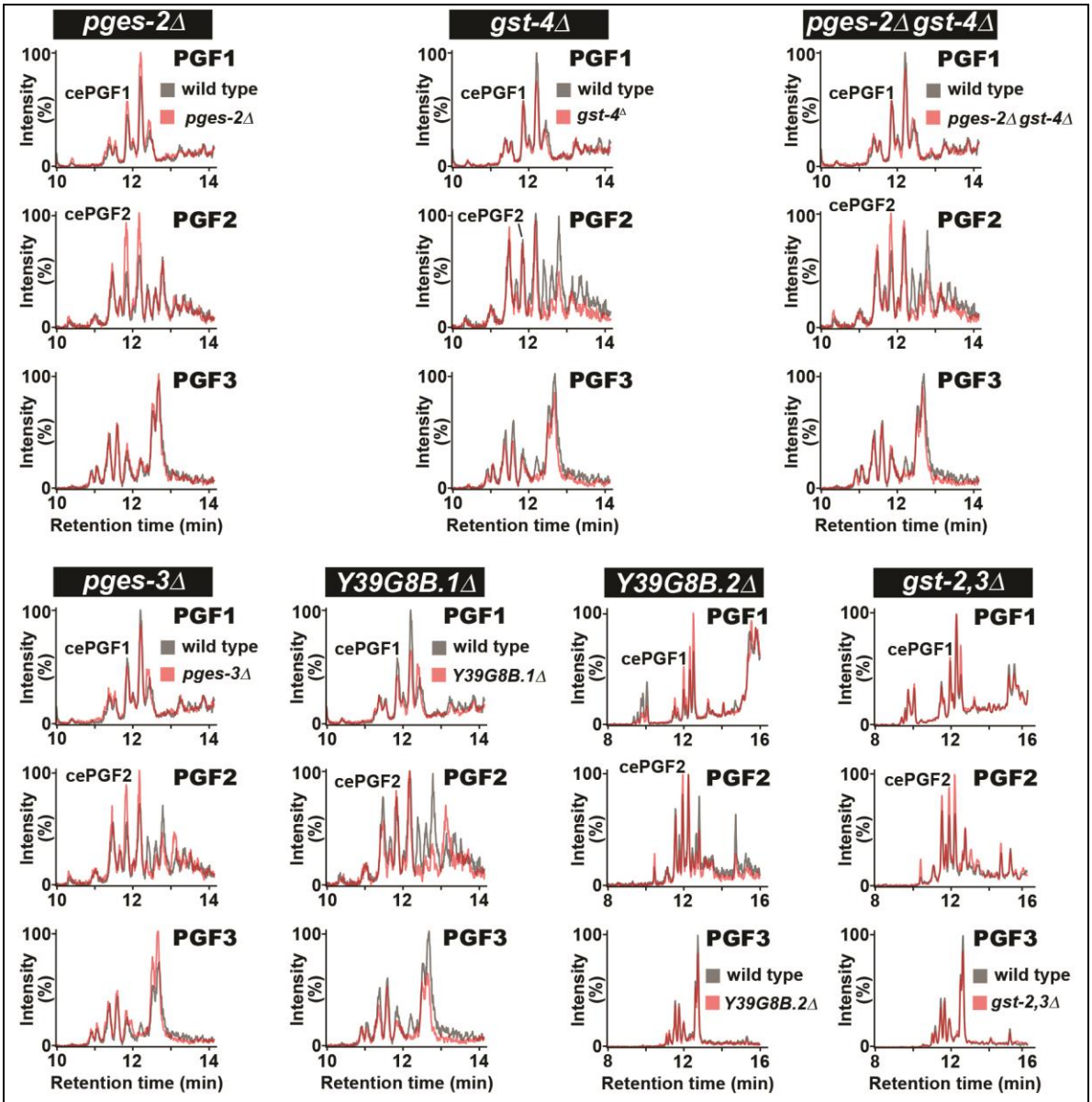

Figure 6. Prostaglandins in wild-type and candidate PG synthase mutant extracts

MRM chromatograms of wild-type and candidate PG synthase mutant extracts analyzed by LC-MS/MS. cps, counts per second. The mass transitions for PGF1s, PGF2s, and PGF3s species are 355.0/311.1, 353.2/193.0, and 351.0/193.0, respectively. Lipid extraction and mass spectrometry conditions were previously published (Prasain et al., 2013). The same wild-type hermaphrodite lipid extract was analyzed together with pges-2Δ, gst-4Δ, pges-2Δ gst-4Δ, pges-3Δ, and Y39G8B.1Δ hermaphrodite lipid extracts.

Therefore, the same wild-type chromatograms are repeated used as references for these mutant chromatograms.

These data, together with previous results (Kubagawa et al., 2006; Edmonds et al., 2010; Hoang et al., 2013), indicate that homology based searches to identify enzymes important for PG metabolism are unlikely to be fruitful. Instead, the large majority of genes with sequence similarity to COX pathway genes do not play a role in the COX-independent pathway. In the future, we need to use unbiased screening approaches. The results are consistent with the model that the COX-independent PG pathway is novel.

What are the Ligands of SRB-13 or Other SRB Chemoreceptors?

In Chapter three, we discuss several possible ligands of SRB-13 and other SRB chemoreceptors: hermaphrodite-derived ascaroside pheromones, male-derived ascarosides pheromones, or signals from exosome-like vesicles. An alternative possibility is that unligated SRB GPCRs modulate the activity of other receptors. While SRB-13 appears expressed in the cilia of pheromone-sensing ASI and ASK neurons, SRB-16 does not localize to cilia. Thus, SRB receptors may bind different ligands or function as modulators. Numerous male-derived and hermaphrodite-derived ascaroside pheromones have been identified (Izrayelit et al., 2012; Srinivasan et al., 2008), but there is great complexity in their structures. However, signals from exosome-like vesicles released from male sensory cilia are unknown (Wang et al., 2014). It is therefore possible to test for direct interactions between SRB-13 and specific ascarosides, but not exosome-associated ligands.

Recent studies support the model that chemoreceptors are ascaroside receptors. Four serpentine receptors, SRBC-64, SRBC-66, SRG-36, and SRG-37 function in either ASK or ASI sensory cilia to perceive different ascaroside pheromones (Kim et al., 2009; McGrath et al., 2011). Expression of SRBC-64 and SRBC-66 together confer ascaroside-mediated signaling in cultured cells (Kim et. al, 2009). Moreover, ascarosides induced calcium transients in ASH neurons ectopically expressing *srg-36* or *srg-37* (McGrath et al., 2011). The SRB-13 amino acid sequence is considerably different than the SRBC and SRG class receptors (Figure 7). At present, whether SRB-13 is a strong candidate for another ascaroside receptor is an open question. Driving the calcium sensor GCAMP 3.0 under the *srb-13* predicted promoter in wild-type or *srb-13Δ1* males can help test if SRB-13 signals via calcium. If calcium signaling is involved, similar approaches could be used to screen for SRB-13 ligands.

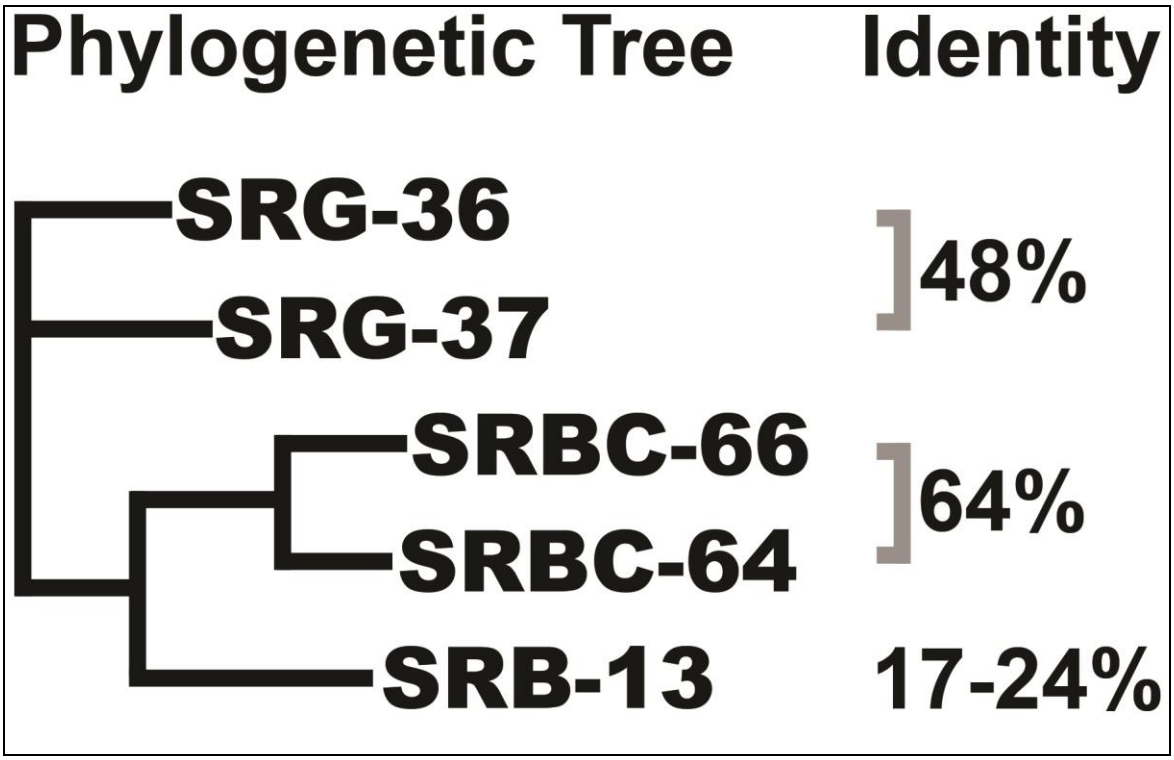

Figure 7. Phylogenetic tree and percent identity of selected serpentine receptors

Multiple sequence alignment, percent identity matrix, and phylogenetic analysis was computed by ClustalO version 1.2.1. The sequence of the SRG-37 longest isoform (e.g. isoform C) was used. Note that SRBC-64 and SRBC-66 function in ASK cilia to receive ascaroside hormone #2 and #3, whereas SRG-36 and SRG-37 function in ASI cilia to receive ascaroside hormone #5 (Kim et al., 2009; McGrath et al., 2011).

SRB GPCR Signaling and Sperm Quality

Hermaphrodite larva perceive ascaroside pheromones as cues for high population density and food scarcity by ASK amphid sensory neurons and other sensory neurons (Kim et al., 2009; Ludewig and Schroeder, 2013). Pheromones at high concentration inhibit DAF-7/TGF-β release from ASI sensory neurons, which in turn down-regulate R-SMAD activity. This pathway helps promote dauer entry. We have recently shown that this mechanism also operates in adult hermaphrodites. In adults, DAF-7 signals are transduced by DAF-1 and DAF-4 receptors expressed in developing oocytes and head interneurons (McKnight et al., 2014). SMAD transcriptional activity regulates the expression of a gene(s) essential for oocyte PGF synthesis. This neuroendocrine mechanism provides an example of how pheromones can influence sperm motility.

In Chapter 3, we identified SRB GPCRs that function in male sensory neurons to promote sperm quality, or more specifically sperm guidance efficiency. RNAseq studies suggest that these GPCRs modulate gene expression in the male gonad and other tissues.

Hence, it is possible that SRBs stimulate neuroendocrine signaling. Males have been shown to be able to sense ascarosides secreted by hermaphrodites. Both ASK sensory neurons and CEM male-specific sensory neurons are required for hermaphrodite-derived pheromone detection (Srinivasan et al., 2008). However, the molecular mechanisms that mediate pheromone signaling are not well understood in males, which are much less studied compared to hermaphrodites. Genetic ablation of ASI or ASK sensory neurons in males could help test whether these sensory neurons are required for efficient sperm guidance (Chelur and Chalfie, 2007). Hermaphrodite neuroendocrine systems such as DAF-7/TGF-beta and insulin pathways can be investigated in males to test for roles in sperm quality. Nevertheless, future work is needed to identify the signaling pathway(s) acting downstream of SRB GPCRs.

What are the PGF Receptors in *C. elegans* Sperm?

Mammalian PGF receptors are GPCRs (Funk, 2001). Several GPCRs, including the chemokine receptor CCR6 and olfactory receptor OR1D2, are thought to be expressed in human sperm (Caballero-Campo et al., 2014; Kang and Koo, 2012; Ottaviano et al., 2013). However, the *C. elegans* genome does not encode homologs of mammalian prostaglandin receptors or CCR6/OR1D2 receptors.

Recent studies show that a calcium channel expressed in human sperm called CatSper specifically binds to prostaglandins, such as PGE1 and PGF1α. CatSper is essential for sperm hyperactivation and fertilization and is thought to play a role in chemotaxis (Brenker et al., 2012; Lishko et al., 2011; Publicover et al., 2008; Strunker et al., 2011; Suarez, 2008). The *C. elegans* genome does not encode CatSper homologs.

Based on these data, we hypothesize that PGF signals are transduced by a novel pathway. Calcium signaling could be downstream, as *C. elegans* sperm express multiple calcium channels. The one identified sperm calcium channel is *spe-41*, but *spe-41* mutants do not have sperm guidance defects (Singaravelu et al., 2012). Unfortunately, we know very little about the mechanisms of PGF signal transduction in *C. elegans*. A genetic screen in males could be used to identify genes required for efficient sperm guidance (Nelson et al., 2011). Alternatively, biochemical strategies could be used to identify sperm membrane proteins that bind to PGFs. An advantage of the latter approach is that sperm can be purified in large quantity.

Concluding Remarks

Data presented in this thesis addresses the question of how *C. elegans* oocytes attract sperm. On the hermaphrodite end, we identified a mixture of PGFs with partially overlapping functions in promoting sperm guidance. The PGF precursors were identified and metabolic pathways investigated. Strong evidence was provided for COX-independent PGF synthesis in *C. elegans* and mice. On the male end, we identified chemosensory GPCRs and a downstream G-protein that function in male sensory neurons to promote efficient sperm guidance. These GPCRs appear to couple the perception of environmental cues to sperm gene expression important for PGF signal transduction.

These studies highlight the value of animal model system like *C. elegans* for unanticipated discoveries. Conventional wisdom was that PGs are made solely through the COX metabolic pathway. The hermaphrodite gonad told a different story. Similarly, males were thought to maximize their reproductive success by producing vast amounts of

competitive sperm. Male worms are telling us that this may be true, but only in certain environments.

Addressing the one question of how *C. elegans* oocytes attract sperm has led me to many more exciting and unexpected questions. This the beauty of biological research: the same beauty that fascinated me during my first biology course in college, and committed me to doctoral training. I hope to devote my future career to further understanding how the nervous system communicates with other organ systems to coordinate development and maintain physiology.

GENERAL LIST OF REFERENCES

Abramovitz, M., Boie, Y., Nguyen, T., Rushmore, T.H., Bayne, M.A., Metters, K.M., Slipetz, D.M., Grygorczyk, R., 1994. Cloning and expression of a cDNA for the human prostanoid FP receptor. The Journal of biological chemistry 269, 2632-2636.

Ahmed, S.R., McGettrick, H.M., Yates, C.M., Buckley, C.D., Ratcliffe, M.J., Nash, G.B., Rainger, G.E., 2011. Prostaglandin D2 regulates CD4+ memory T cell trafficking across blood vascular endothelium and primes these cells for clearance across lymphatic endothelium. Journal of immunology 187, 1432-1439.

Anderson, J.L., Morran, L.T., Phillips, P.C., 2010. Outcrossing and the maintenance of males within C. elegans populations. The Journal of heredity 101 Suppl 1, S62-74.

Asemota, O.A., Klatsky, P., 2015. Access to infertility care in the developing world: the family promotion gap. Semin Reprod Med 33, 17-22.

Barbera-Cremades, M., Baroja-Mazo, A., Gomez, A.I., Machado, F., Di Virgilio, F., Pelegrin, P., 2012. P2X7 receptor-stimulation causes fever via PGE2 and IL-1beta release. FASEB J 26, 2951-2962.

Bargmann, C.I., 2006. Chemosensation in C. elegans. WormBook : the online review of C. elegans biology, 1-29.

Bargmann, C.I., Hartwieg, E., Horvitz, H.R., 1993. Odorant-selective genes and neurons mediate olfaction in C. elegans. Cell 74, 515-527.

Bargmann, C.I., Horvitz, H.R., 1991. Chemosensory neurons with overlapping functions direct chemotaxis to multiple chemicals in C. elegans. Neuron 7, 729-742.

Barnosky, A.D., Matzke, N., Tomiya, S., Wogan, G.O., Swartz, B., Quental, T.B., Marshall, C., McGuire, J.L., Lindsey, E.L., Maguire, K.C., Mersey, B., Ferrer, E.A., 2011. Has the Earth's sixth mass extinction already arrived? Nature 471, 51-57.

Bentley, J.K., Tubb, D.J., Garbers, D.L., 1986. Receptor-mediated activation of spermatozoan guanylate cyclase. J Biol Chem 261, 14859-14862.

Bhattacharya, M., Peri, K., Ribeiro-da-Silva, A., Almazan, G., Shichi, H., Hou, X., Varma, D.R., Chemtob, S., 1999. Localization of functional prostaglandin E2 receptors EP3 and EP4 in the nuclear envelope. J Biol Chem 274, 15719-15724.

Bhattacharya, M., Peri, K.G., Almazan, G., Ribeiro-da-Silva, A., Shichi, H., Durocher, Y., Abramovitz, M., Hou, X., Varma, D.R., Chemtob, S., 1998. Nuclear localization of prostaglandin E2 receptors. Proceedings of the National Academy of Sciences of the United States of America 95, 15792-15797.

Birkhead, T.R., Martinez, J.G., Burke, T., Froman, D.P., 1999. Sperm mobility determines the outcome of sperm competition in the domestic fowl. Proceedings. Biological sciences / The Royal Society 266, 1759-1764.

Blacque, O.E., Reardon, M.J., Li, C., McCarthy, J., Mahjoub, M.R., Ansley, S.J., Badano, J.L., Mah, A.K., Beales, P.L., Davidson, W.S., Johnsen, R.C., Audeh, M., Plasterk, R.H., Baillie, D.L., Katsanis, N., Quarmby, L.M., Wicks, S.R., Leroux, M.R., 2004. Loss of C. elegans BBS-7 and BBS-8 protein function results in cilia defects and compromised intraflagellar transport. Genes & development 18, 1630-1642.

Bohmer, M., Van, Q., Weyand, I., Hagen, V., Beyermann, M., Matsumoto, M., Hoshi, M., Hildebrand, E., Kaupp, U.B., 2005. Ca2+ spikes in the flagellum control chemotactic behavior of sperm. The EMBO journal 24, 2741-2752.

Brenker, C., Goodwin, N., Weyand, I., Kashikar, N.D., Naruse, M., Krahling, M., Muller, A., Kaupp, U.B., Strunker, T., 2012. The CatSper channel: a polymodal chemosensor in human sperm. The EMBO journal 31, 1654-1665.

Brenner, S., 1974. The genetics of Caenorhabditis elegans. Genetics 77, 71-94.

Buck-Louis, G.M., Sundaram, R., Schisterman, E.F., Sweeney, A., Lynch, C.D., Kim, S., Maisog, J.M., Gore-Langton, R., Eisenberg, M.L., Chen, Z., 2014a. Semen quality and time to pregnancy: the Longitudinal Investigation of Fertility and the Environment Study. Fertility and sterility 101, 453-462.

Buck-Louis, G.M., Sundaram, R., Sweeney, A.M., Schisterman, E.F., Maisog, J., Kannan, K., 2014b. Urinary bisphenol A, phthalates, and couple fecundity: the Longitudinal Investigation of Fertility and the Environment (LIFE) Study. Fertility and sterility 101, 1359-1366.

Burnett, L.A., Sugiyama, H., Bieber, A.L., Chandler, D.E., 2011. Egg jelly proteins stimulate directed motility in Xenopus laevis sperm. Mol Reprod Dev 78, 450-462.

Caballero-Campo, P., Buffone, M.G., Benencia, F., Conejo-Garcia, J.R., Rinaudo, P.F., Gerton, G.L., 2014. A role for the chemokine receptor CCR6 in mammalian sperm motility and chemotaxis. Journal of cellular physiology 229, 68-78.

Campbell, N.A., Reece, J.B., 2005. The tree of life: an introduction to biological diversity, in: Wilbur, B. (Ed.), Biology, 7th ed. Pearson, San Fracisco, pp. 512-531.

Ceballos, G., Ehrlich, P.R., 2002. Mammal population losses and the extinction crisis. Science 296, 904-907.

Chelur, D.S., Chalfie, M., 2007. Targeted cell killing by reconstituted caspases. Proceedings of the National Academy of Sciences of the United States of America 104, 2283-2288.

Chen, N., Pai, S., Zhao, Z., Mah, A., Newbury, R., Johnsen, R.C., Altun, Z., Moerman, D.G., Baillie, D.L., Stein, L.D., 2005. Identification of a nematode chemosensory gene family. Proceedings of the National Academy of Sciences of the United States of America 102, 146-151.

Claar, D., Hartert, T.V., Peebles, R.S., Jr., 2015. The role of prostaglandins in allergic lung inflammation and asthma. Expert review of respiratory medicine 9, 55-72.

Clermont, Y., Oko, R., Hermo, L., 1990. Immunocytochemical localization of proteins utilized in the formation of outer dense fibers and fibrous sheath in rat spermatids: an electron microscope study. Anat Rec 227, 447-457.

Cohen-Dayag, A., Tur-Kaspa, I., Dor, J., Mashiach, S., Eisenbach, M., 1995. Sperm capacitation in humans is transient and correlates with chemotactic responsiveness to follicular factors. Proceedings of the National Academy of Sciences of the United States of America 92, 11039-11043.

Curtin, S.C., Abma J.C, Ventura, S.J., Statistics, N.C.f.H., Henshaw, S.K., Institute, G., 2013. Pregnancy rates for U.S. women continue to drop. NCHS Data Brief.

Cutter, A.D., Dey, A., Murray, R.L., 2009. Evolution of the Caenorhabditis elegans genome. Molecular biology and evolution 26, 1199-1234.

Cutter, A.D., Payseur, B.A., 2003. Rates of deleterious mutation and the evolution of sex in Caenorhabditis. Journal of evolutionary biology 16, 812-822.

Denk, A.G., Holzmann, A., Peters, A., Vermeirssen, E.L.M., Kempenaer, B., 2005. Paternity in mallards: effects of sperm quality, and female sperm selection for inbreeding avoidance. Behavioral Ecology 16, 825-833.

Dirzo, R., Raven, P.H., 2003. Global state of biodiversity and loss. Annu. Rev. Environ. Resour. 28, 137-167.

Donnelly, E.T., Lewis, S.E., McNally, J.A., Thompson, W., 1998. In vitro fertilization and pregnancy rates: the influence of sperm motility and morphology on IVF outcome. Fertility and sterility 70, 305-314.

Donoghue, A.M., 1999. Prospective approaches to avoid flock fertility problems: predictive assessment of sperm function traits in poultry. Poultry science 78, 437-443.

Dubois, R.N., Abramson, S.B., Crofford, L., Gupta, R.A., Simon, L.S., Van De Putte, L.B., Lipsky, P.E., 1998. Cyclooxygenase in biology and disease. FASEB J 12, 1063-1073.

Dwyer, N.D., Troemel, E.R., Sengupta, P., Bargmann, C.I., 1998. Odorant receptor localization to olfactory cilia is mediated by ODR-4, a novel membrane-associated protein. Cell 93, 455-466.

Edmonds, J.W., McKinney, S.L., Prasain, J.K., Miller, M.A., 2011. The gap junctional protein INX-14 functions in oocyte precursors to promote C. elegans sperm guidance. Developmental biology 359, 47-58.

Edmonds, J.W., Prasain, J.K., Dorand, D., Yang, Y., Hoang, H.D., Vibbert, J., Kubagawa, H.M., Miller, M.A., 2010. Insulin/FOXO signaling regulates ovarian prostaglandins critical for reproduction. Developmental cell 19, 858-871.

Fawcett, D.W., 1975. The mammalian spermatozoon. Developmental biology 44, 394-436.

Fielenbach, N., Antebi, A., 2008. C. elegans dauer formation and the molecular basis of plasticity. Genes & development 22, 2149-2165.

Friedland, A.E., Tzur, Y.B., Esvelt, K.M., Colaiacovo, M.P., Church, G.M., Calarco, J.A., 2013. Heritable genome editing in C. elegans via a CRISPR-Cas9 system. Nature methods 10, 741-743.

Frokjaer-Jensen, C., Davis, M.W., Hollopeter, G., Taylor, J., Harris, T.W., Nix, P., Lofgren, R., Prestgard-Duke, M., Bastiani, M., Moerman, D.G., Jorgensen, E.M., 2010. Targeted gene deletions in C. elegans using transposon excision. Nature methods 7, 451-453.

Funk, C.D., 2001. Prostaglandins and leukotrienes: advances in eicosanoid biology. Science 294, 1871-1875.

Gage, M.J., Macfarlane, C.P., Yeates, S., Ward, R.G., Searle, J.B., Parker, G.A., 2004. Spermatozoal traits and sperm competition in Atlantic salmon: relative sperm

velocity is the primary determinant of fertilization success. Current biology : CB 14, 44-47.

Garbers, D.L., Bentley, J.K., Dangott, L.J., Ramarao, C.S., Shimomura, H., Suzuki, N., Thorpe, D., 1986. Peptides associated with eggs: mechanisms of interaction with spermatozoa. Adv Exp Med Biol 207, 315-357.

Grant, B., Hirsh, D., 1999. Receptor-mediated endocytosis in the Caenorhabditis elegans oocyte. Mol Biol Cell 10, 4311-4326.

Gray, J.M., Hill, J.J., Bargmann, C.I., 2005. A circuit for navigation in Caenorhabditis elegans. Proceedings of the National Academy of Sciences of the United States of America 102, 3184-3191.

Guerrero, A., Wood, C.D., Nishigaki, T., Carneiro, J., Darszon, A., 2010. Tuning sperm chemotaxis. Biochem Soc Trans 38, 1270-1274.

Guo, Y., Weck, J., Sundaram, R., Goldstone, A.E., Louis, G.B., Kannan, K., 2014. Urinary concentrations of phthalates in couples planning pregnancy and its association with 8-hydroxy-2'-deoxyguanosine, a biomarker of oxidative stress: longitudinal investigation of fertility and the environment study. Environmental science & technology 48, 9804-9811.

Gupta, R.A., Tan, J., Krause, W.F., Geraci, M.W., Willson, T.M., Dey, S.K., DuBois, R.N., 2000. Prostacyclin-mediated activation of peroxisome proliferator-activated receptor delta in colorectal cancer. Proceedings of the National Academy of Sciences of the United States of America 97, 13275-13280.

Gurke, S., Barroso, J.F., Gerdes, H.H., 2008. The art of cellular communication: tunneling nanotubes bridge the divide. Histochem Cell Biol 129, 539-550.

Hall, D.H., Russell, R.L., 1991. The posterior nervous system of the nematode Caenorhabditis elegans: serial reconstruction of identified neurons and complete pattern of synaptic interactions. The Journal of neuroscience : the official journal of the Society for Neuroscience 11, 1-22.

Hamberg, M., Svensson, J., Wakabayashi, T., Samuelsson, B., 1974. Isolation and structure of two prostaglandin endoperoxides that cause platelet aggregation. Proceedings of the National Academy of Sciences of the United States of America 71, 345-349.

Han, S.M., Cottee, P.A., Miller, M.A., 2010. Sperm and oocyte communication mechanisms controlling C. elegans fertility. Dev Dyn 239, 1265-1281.

Harizi, H., Corcuff, J.B., Gualde, N., 2008. Arachidonic-acid-derived eicosanoids: roles in biology and immunopathology. Trends Mol Med 14, 461-469.

Harvey, R.J., Depner, U.B., Wassle, H., Ahmadi, S., Heindl, C., Reinold, H., Smart, T.G., Harvey, K., Schutz, B., Abo-Salem, O.M., Zimmer, A., Poisbeau, P., Welzl, H., Wolfer, D.P., Betz, H., Zeilhofer, H.U., Muller, U., 2004. GlyR alpha3: an essential target for spinal PGE2-mediated inflammatory pain sensitization. Science 304, 884-887.

Hauser, R., 2006. The environment and male fertility: recent research on emerging chemicals and semen quality. Semin Reprod Med 24, 156-167.

Hayaishi, O., 2000. Molecular mechanisms of sleep-wake regulation: a role of prostaglandin D2. Philosophical transactions of the Royal Society of London. Series B, Biological sciences 355, 275-280.

Hilliard, M.A., Bergamasco, C., Arbucci, S., Plasterk, R.H., Bazzicalupo, P., 2004. Worms taste bitter: ASH neurons, QUI-1, GPA-3 and ODR-3 mediate quinine avoidance in Caenorhabditis elegans. The EMBO journal 23, 1101-1111.

Himes, J.E., Riffell, J.A., Zimmer, C.A., Zimmer, R.K., 2011. Sperm chemotaxis as revealed with live and synthetic eggs. The Biological bulletin 220, 1-5.

Hoang, H.D., Prasain, J.K., Dorand, D., Miller, M.A., 2013. A heterogeneous mixture of F-series prostaglandins promotes sperm guidance in the Caenorhabditis elegans reproductive tract. PLoS genetics 9, e1003271.

Hobert, O., 2010. Neurogenesis in the nematode Caenorhabditis elegans. WormBook : the online review of C. elegans biology, 1-24.

Hoffmann, M., Hilton-Taylor, C., Angulo, A., Bohm, M., Brooks, T.M., Butchart, S.H., Carpenter, K.E., Chanson, J., Collen, B., Cox, N.A., Darwall, W.R., Dulvy, N.K., Harrison, L.R., Katariya, V., Pollock, C.M., Quader, S., Richman, N.I., Rodrigues, A.S., Tognelli, M.F., Vie, J.C., Aguiar, J.M., Allen, D.J., Allen, G.R., Amori, G., Ananjeva, N.B., Andreone, F., Andrew, P., Aquino Ortiz, A.L., Baillie, J.E., Baldi, R., Bell, B.D., Biju, S.D., Bird, J.P., Black-Decima, P., Blanc, J.J., Bolanos, F., Bolivar, G.W., Burfield, I.J., Burton, J.A., Capper, D.R., Castro, F., Catullo, G., Cavanagh, R.D., Channing, A., Chao, N.L., Chenery, A.M., Chiozza, F., Clausnitzer, V., Collar, N.J., Collett, L.C., Collette, B.B., Cortez Fernandez, C.F., Craig, M.T., Crosby, M.J., Cumberlidge, N., Cuttelod, A., Derocher, A.E., Diesmos, A.C., Donaldson, J.S., Duckworth, J.W., Dutson, G., Dutta, S.K., Emslie, R.H., Farjon, A., Fowler, S., Freyhof, J., Garshelis, D.L., Gerlach, J., Gower, D.J., Grant, T.D., Hammerson, G.A., Harris, R.B., Heaney, L.R., Hedges, S.B., Hero, J.M., Hughes, B., Hussain, S.A., Icochea, M.J., Inger,

R.F., Ishii, N., Iskandar, D.T., Jenkins, R.K., Kaneko, Y., Kottelat, M., Kovacs, K.M., Kuzmin, S.L., La Marca, E., Lamoreux, J.F., Lau, M.W., Lavilla, E.O., Leus, K., Lewison, R.L., Lichtenstein, G., Livingstone, S.R., Lukoschek, V., Mallon, D.P., McGowan, P.J., McIvor, A., Moehlman, P.D., Molur, S., Munoz Alonso, A., Musick, J.A., Nowell, K., Nussbaum, R.A., Olech, W., Orlov, N.L., Papenfuss, T.J., Parra-Olea, G., Perrin, W.F., Polidoro, B.A., Pourkazemi, M., Racey, P.A., Ragle, J.S., Ram, M., Rathbun, G., Reynolds, R.P., Rhodin, A.G., Richards, S.J., Rodriguez, L.O., Ron, S.R., Rondinini, C., Rylands, A.B., Sadovy de Mitcheson, Y., Sanciangco, J.C., Sanders, K.L., Santos-Barrera, G., Schipper, J., Self-Sullivan, C., Shi, Y., Shoemaker, A., Short, F.T., Sillero-Zubiri, C., Silvano, D.L., Smith, K.G., Smith, A.T., Snoeks, J., Stattersfield, A.J., Symes, A.J., Taber, A.B., Talukdar, B.K., Temple, H.J., Timmins, R., Tobias, J.A., Tsytsulina, K., Tweddle, D., Ubeda, C., Valenti, S.V., van Dijk, P.P., Veiga, L.M., Veloso, A., Wege, D.C., Wilkinson, M., Williamson, E.A., Xie, F., Young, B.E., Akcakaya, H.R., Bennun, L., Blackburn, T.M., Boitani, L., Dublin, H.T., da Fonseca, G.A., Gascon, C., Lacher, T.E., Jr., Mace, G.M., Mainka, S.A., McNeely, J.A., Mittermeier, R.A., Reid, G.M., Rodriguez, J.P., Rosenberg, A.A., Samways, M.J., Smart, J., Stein, B.A., Stuart, S.N., 2010. The impact of conservation on the status of the world's vertebrates. Science 330, 1503-1509.

Hughes, J.B., Daily, G.C., Ehrlich, P.R., 1997. Population diversity: its extent and extinction. Science 278, 689-692.

Inglis, P.N., Ou, G., Leroux, M.R., Scholey, J.M., 2007. The sensory cilia of Caenorhabditis elegans. WormBook : the online review of C. elegans biology, 1-22.

Inoue, T., Thomas, J.H., 2000a. Suppressors of transforming growth factor-beta pathway mutants in the Caenorhabditis elegans dauer formation pathway. Genetics 156, 1035-1046.

Inoue, T., Thomas, J.H., 2000b. Targets of TGF-beta signaling in Caenorhabditis elegans dauer formation. Developmental biology 217, 192-204.

Italiano, J.E., Jr., Stewart, M., Roberts, T.M., 1999. Localized depolymerization of the major sperm protein cytoskeleton correlates with the forward movement of the cell body in the amoeboid movement of nematode sperm. The Journal of cell biology 146, 1087-1096.

Izrayelit, Y., Srinivasan, J., Campbell, S.L., Jo, Y., von Reuss, S.H., Genoff, M.C., Sternberg, P.W., Schroeder, F.C., 2012. Targeted metabolomics reveals a male pheromone and sex-specific ascaroside biosynthesis in Caenorhabditis elegans. ACS chemical biology 7, 1321-1325.

Jaiswal, B.S., Eisenbach, M., 2002. Capacitation, in: DM, H. (Ed.), Fertilization. Academic, San Diego, pp. 57-117.

Jansen, G., Thijssen, K.L., Werner, P., van der Horst, M., Hazendonk, E., Plasterk, R.H., 1999. The complete family of genes encoding G proteins of Caenorhabditis elegans. Nature genetics 21, 414-419.

Jansen, G., Weinkove, D., Plasterk, R.H., 2002. The G-protein gamma subunit gpc-1 of the nematode C.elegans is involved in taste adaptation. The EMBO journal 21, 986-994.

Kang, N., Koo, J., 2012. Olfactory receptors in non-chemosensory tissues. BMB reports 45, 612-622.

Kaupp, U.B., Kashikar, N.D., Weyand, I., 2008. Mechanisms of sperm chemotaxis. Annu Rev Physiol 70, 93-117.

Kaupp, U.B., Solzin, J., Hildebrand, E., Brown, J.E., Helbig, A., Hagen, V., Beyermann, M., Pampaloni, F., Weyand, I., 2003. The signal flow and motor response controling chemotaxis of sea urchin sperm. Nature cell biology 5, 109-117.

Kelly, W.G., Schaner, C.E., Dernburg, A.F., Lee, M.H., Kim, S.K., Villeneuve, A.M., Reinke, V., 2002. X-chromosome silencing in the germline of C. elegans. Development 129, 479-492.

Kim, K., Sato, K., Shibuya, M., Zeiger, D.M., Butcher, R.A., Ragains, J.R., Clardy, J., Touhara, K., Sengupta, P., 2009. Two chemoreceptors mediate developmental effects of dauer pheromone in C. elegans. Science 326, 994-998.

Kirichok, Y., Navarro, B., Clapham, D.E., 2006. Whole-cell patch-clamp measurements of spermatozoa reveal an alkaline-activated Ca2+ channel. Nature 439, 737-740.

Kiriyama, M., Ushikubi, F., Kobayashi, T., Hirata, M., Sugimoto, Y., Narumiya, S., 1997. Ligand binding specificities of the eight types and subtypes of the mouse prostanoid receptors expressed in Chinese hamster ovary cells. Br J Pharmacol 122, 217-224.

Kitanaka, J., Hasimoto, H., Sugimoto, Y., Negishi, M., Aino, H., Gotoh, M., Ichikawa, A., Baba, A., 1994. Cloning and expression of a cDNA for rat prostaglandin F2 alpha receptor. Prostaglandins 48, 31-41.

Kliewer, S.A., Lenhard, J.M., Willson, T.M., Patel, I., Morris, D.C., Lehmann, J.M., 1995. A prostaglandin J2 metabolite binds peroxisome proliferator-activated receptor gamma and promotes adipocyte differentiation. Cell 83, 813-819.

Koljak, R., Jarving, I., Kurg, R., Boeglin, W.E., Varvas, K., Valmsen, K., Ustav, M., Brash, A.R., Samel, N., 2001. The basis of prostaglandin synthesis in coral: molecular cloning and expression of a cyclooxygenase from the Arctic soft coral Gersemia fruticosa. J Biol Chem 276, 7033-7040.

Kubagawa, H.M., Watts, J.L., Corrigan, C., Edmonds, J.W., Sztul, E., Browse, J., Miller, M.A., 2006. Oocyte signals derived from polyunsaturated fatty acids control sperm recruitment in vivo. Nature cell biology 8, 1143-1148.

Kunzle, R., Mueller, M.D., Hanggi, W., Birkhauser, M.H., Drescher, H., Bersinger, N.A., 2003. Semen quality of male smokers and nonsmokers in infertile couples. Fertility and sterility 79, 287-291.

L'Hernault, S.W., 2006. Spermatogenesis. WormBook : the online review of C. elegans biology, 1-14.

L'Hernault, S.W., Roberts, T.M., 1995. Cell biology of nematode sperm. Methods in cell biology 48, 273-301.

LaMunyon, C.W., Ward, S., 1998. Larger sperm outcompete smaller sperm in the nematode Caenorhabditis elegans. Proceedings. Biological sciences / The Royal Society 265, 1997-2002.

Lessard, C., Siqueira, L.G., D'Amours, O., Sullivan, R., Leclerc, P., Palmer, C., 2011. Infertility in a beef bull due to a failure in the capacitation process. Theriogenology 76, 891-899.

Lewis, J.A., Hodgkin, J.A., 1977. Specific neuroanatomical changes in chemosensory mutants of the nematode Caenorhabditis elegans. The Journal of comparative neurology 172, 489-510.

Lishko, P.V., Botchkina, I.L., Kirichok, Y., 2011. Progesterone activates the principal Ca2+ channel of human sperm. Nature 471, 387-391.

Ludewig, A.H., Schroeder, F.C., 2013. Ascaroside signaling in C. elegans. WormBook : the online review of C. elegans biology, 1-22.

Malo, A.F., Garde, J.J., Soler, A.J., Garcia, A.J., Gomendio, M., Roldan, E.R., 2005. Male fertility in natural populations of red deer is determined by sperm velocity and the proportion of normal spermatozoa. Biology of reproduction 72, 822-829.

Marei, W.F., Abayasekara, D.R., Wathes, D.C., Fouladi-Nashta, A.A., 2014. Role of PTGS2-generated PGE2 during gonadotrophin-induced bovine oocyte maturation and cumulus cell expansion. Reproductive biomedicine online 28, 388-400.

Martine, G., Chandra, A., Febo-Vazq, I., Mosher, W., Statistics, D.o.V., 2013. Use of Family Planning and Related Medical Services Among Women Aged 15–44 in the United States: National Survey of Family Growth, 2006–2010. DHHS publication: National Health Statistics Reports, 1-16.

Matsumoto, M., Solzin, J., Helbig, A., Hagen, V., Ueno, S., Kawase, O., Maruyama, Y., Ogiso, M., Godde, M., Minakata, H., Kaupp, U.B., Hoshi, M., Weyand, I., 2003. A sperm-activating peptide controls a cGMP-signaling pathway in starfish sperm. Developmental biology 260, 314-324.

McGrath, P.T., Xu, Y., Ailion, M., Garrison, J.L., Butcher, R.A., Bargmann, C.I., 2011. Parallel evolution of domesticated Caenorhabditis species targets pheromone receptor genes. Nature 477, 321-325.

McKnight, K., Hoang, H.D., Prasain, J.K., Brown, N., Vibbert, J., Hollister, K.A., Moore, R., Ragains, J.R., Reese, J., Miller, M.A., 2014. Neurosensory perception of

environmental cues modulates sperm motility critical for fertilization. Science 344, 754-757.

Miao, L., Vanderlinde, O., Stewart, M., Roberts, T.M., 2003. Retraction in amoeboid cell motility powered by cytoskeletal dynamics. Science 302, 1405-1407.

Miller, L.M., Plenefisch, J.D., Casson, L.P., Meyer, B.J., 1988. xol-1: a gene that controls the male modes of both sex determination and X chromosome dosage compensation in C. elegans. Cell 55, 167-183.

Mittendorf, R., Herbst, A.L., 1994. DES exposure: an update. Contemporary Pediatrics 11, 59-62.

Moncada, S., Vane, J.R., 1979. Arachidonic acid metabolites and the interactions between platelets and blood-vessel walls. N Engl J Med 300, 1142-1147.

Munire, M., Shimizu, Y., Sakata, Y., Minaguchi, R., Aso, T., 2004. Impaired hyperactivation of human sperm in patients with infertility. Journal of medical and dental sciences 51, 99-104.

Nelson, G.A., Roberts, T.M., Ward, S., 1982. Caenorhabditis elegans spermatozoan locomotion: amoeboid movement with almost no actin. The Journal of cell biology 92, 121-131.

Nelson, M.D., Zhou, E., Kiontke, K., Fradin, H., Maldonado, G., Martin, D., Shah, K., Fitch, D.H., 2011. A bow-tie genetic architecture for morphogenesis suggested by a genome-wide RNAi screen in Caenorhabditis elegans. PLoS genetics 7, e1002010.

Niklas, K.J., Newman, S.A., 2013. The origins of multicellular organisms. Evolution & development 15, 41-52.

Nishigaki, T., Chiba, K., Miki, W., Hoshi, M., 1996. Structure and function of asterosaps, sperm-activating peptides from the jelly coat of starfish eggs. Zygote 4, 237-245.

Olson, J.H., Xiang, X., Ziegert, T., Kittelson, A., Rawls, A., Bieber, A.L., Chandler, D.E., 2001. Allurin, a 21-kDa sperm chemoattractant from Xenopus egg jelly, is related to mammalian sperm-binding proteins. Proceedings of the National Academy of Sciences of the United States of America 98, 11205-11210.

Ombelet, W., Campo, R., 2007. Affordable IVF for developing countries. Reproductive biomedicine online 15, 257-265.

Ottaviano, G., Zuccarello, D., Menegazzo, M., Perilli, L., Marioni, G., Frigo, A.C., Staffieri, A., Foresta, C., 2013. Human olfactory sensitivity for bourgeonal and male infertility: a preliminary investigation. European archives of oto-rhino-laryngology : official journal of the European Federation of Oto-Rhino-Laryngological Societies 270, 3079-3086.

Peden, E.M., Barr, M.M., 2005. The KLP-6 kinesin is required for male mating behaviors and polycystin localization in Caenorhabditis elegans. Current biology : CB 15, 394-404.

Pereira, H.M., Leadley, P.W., Proenca, V., Alkemade, R., Scharlemann, J.P., Fernandez-Manjarres, J.F., Araujo, M.B., Balvanera, P., Biggs, R., Cheung, W.W., Chini, L., Cooper, H.D., Gilman, E.L., Guenette, S., Hurtt, G.C., Huntington, H.P., Mace, G.M., Oberdorff, T., Revenga, C., Rodrigues, P., Scholes, R.J., Sumaila, U.R., Walpole, M., 2010. Scenarios for global biodiversity in the 21st century. Science 330, 1496-1501.

Perkins, L.A., Hedgecock, E.M., Thomson, J.N., Culotti, J.G., 1986. Mutant sensory cilia in the nematode Caenorhabditis elegans. Developmental biology 117, 456-487.

Pimm, S.L., Russell, G.J., Gittleman, J.L., Brooks, T.M., 1995. The future of biodiversity. Science 269, 347-350.

Prasain, J.K., Hoang, H.D., Edmonds, J.W., Miller, M.A., 2013. Prostaglandin extraction and analysis in C. elegans. J. Vis. Exp. 76, e50447.

Publicover, S.J., Giojalas, L.C., Teves, M.E., de Oliveira, G.S., Garcia, A.A., Barratt, C.L., Harper, C.V., 2008. Ca2+ signalling in the control of motility and guidance in mammalian sperm. Front Biosci 13, 5623-5637.

Ralt, D., Goldenberg, M., Fetterolf, P., Thompson, D., Dor, J., Mashiach, S., Garbers, D.L., Eisenbach, M., 1991. Sperm attraction to a follicular factor(s) correlates with human egg fertilizability. Proceedings of the National Academy of Sciences of the United States of America 88, 2840-2844.

Ralt, D., Manor, M., Cohen-Dayag, A., Tur-Kaspa, I., Ben-Shlomo, I., Makler, A., Yuli, I., Dor, J., Blumberg, S., Mashiach, S., et al., 1994. Chemotaxis and chemokinesis of human spermatozoa to follicular factors. Biology of reproduction 50, 774-785.

Ramarao, C.S., Garbers, D.L., 1985. Receptor-mediated regulation of guanylate cyclase activity in spermatozoa. J Biol Chem 260, 8390-8396.

Riddle, D.L., Blackburn, T.M., Meyer, B.J., Priess, J.R., 1997. C. elegans II. Cold Spring Harbor, New York

Riffell, J.A., Krug, P.J., Zimmer, R.K., 2002. Fertilization in the sea: the chemical identity of an abalone sperm attractant. J Exp Biol 205, 1439-1450.

Roayaie, K., Crump, J.G., Sagasti, A., Bargmann, C.I., 1998. The G alpha protein ODR-3 mediates olfactory and nociceptive function and controls cilium morphogenesis in C. elegans olfactory neurons. Neuron 20, 55-67.

Roberts, T.M., King, K.L., 1991. Centripetal flow and directed reassembly of the major sperm protein (MSP) cytoskeleton in the amoeboid sperm of the nematode, Ascaris suum. Cell motility and the cytoskeleton 20, 228-241.

Roberts, T.M., Ward, S., 1982. Centripetal flow of pseudopodial surface components could propel the amoeboid movement of Caenorhabditis elegans spermatozoa. The Journal of cell biology 92, 132-138.

Robertson, H.M., 1998. Two large families of chemoreceptor genes in the nematodes Caenorhabditis elegans and Caenorhabditis briggsae reveal extensive gene duplication, diversification, movement, and intron loss. Genome research 8, 449-463.

Robertson, H.M., 2001. Updating the str and srj (stl) families of chemoreceptors in Caenorhabditis nematodes reveals frequent gene movement within and between chromosomes. Chemical senses 26, 151-159.

Robertson, H.M., Thomas, J.H., 2006. The putative chemoreceptor families of C. elegans. WormBook : the online review of C. elegans biology, 1-12.

Rowley, A.F., Vogan, C.L., Taylor, G.W., Clare, A.S., 2005. Prostaglandins in non-insectan invertebrates: recent insights and unsolved problems. J Exp Biol 208, 3-14.

Sakamoto, K., Ezashi, T., Miwa, K., Okuda-Ashitaka, E., Houtani, T., Sugimoto, T., Ito, S., Hayaishi, O., 1994. Molecular cloning and expression of a cDNA of the bovine prostaglandin F2 alpha receptor. The Journal of biological chemistry 269, 3881-3886.

Schackwitz, W.S., Inoue, T., Thomas, J.H., 1996. Chemosensory neurons function in parallel to mediate a pheromone response in C. elegans. Neuron 17, 719-728.

Sengupta, P., Chou, J.H., Bargmann, C.I., 1996. odr-10 encodes a seven transmembrane domain olfactory receptor required for responses to the odorant diacetyl. Cell 84, 899-909.

Sepsenwol, S., Ris, H., Roberts, T.M., 1989. A unique cytoskeleton associated with crawling in the amoeboid sperm of the nematode, Ascaris suum. The Journal of cell biology 108, 55-66.

Shibata-Nozaki, T., Ito, H., Mitomi, H., Akaogi, J., Komagata, T., Kanaji, T., Maruyama, T., Mori, T., Nomoto, S., Ozaki, S., Yamada, H., 2011. Endogenous prostaglandin E2 inhibits aberrant overgrowth of rheumatoid synovial tissue and the development of osteoclast activity through EP4 receptor. Arthritis and rheumatism 63, 2595-2605.

Shimomura, H., Dangott, L.J., Garbers, D.L., 1986. Covalent coupling of a resact analogue to guanylate cyclase. J Biol Chem 261, 15778-15782.

Shukla, K.K., Mahdi, A.A., Rajender, S., 2012. Ion channels in sperm physiology and male fertility and infertility. Journal of andrology 33, 777-788.

Simmons, D.L., Botting, R.M., Hla, T., 2004. Cyclooxygenase isozymes: the biology of prostaglandin synthesis and inhibition. Pharmacol Rev 56, 387-437.

Singaravelu, G., Chatterjee, I., Rahimi, S., Druzhinina, M.K., Kang, L., Xu, X.Z., Singson, A., 2012. The sperm surface localization of the TRP-3/SPE-41 Ca2+ -permeable channel depends on SPE-38 function in Caenorhabditis elegans. Developmental biology 365, 376-383.

Smith, H., 2006. Sperm motility and MSP. WormBook : the online review of C. elegans biology, 1-8.

Smith, W.L., Lands, W.E., 1972. Oxygenation of polyunsaturated fatty acids during prostaglandin biosynthesis by sheep vesicular gland. Biochemistry 11, 3276-3285.

Srinivasan, J., Kaplan, F., Ajredini, R., Zachariah, C., Alborn, H.T., Teal, P.E., Malik, R.U., Edison, A.S., Sternberg, P.W., Schroeder, F.C., 2008. A blend of small molecules regulates both mating and development in Caenorhabditis elegans. Nature 454, 1115-1118.

Stein, L.D., Bao, Z., Blasiar, D., Blumenthal, T., Brent, M.R., Chen, N., Chinwalla, A., Clarke, L., Clee, C., Coghlan, A., Coulson, A., D'Eustachio, P., Fitch, D.H., Fulton, L.A., Fulton, R.E., Griffiths-Jones, S., Harris, T.W., Hillier, L.W., Kamath, R., Kuwabara, P.E., Mardis, E.R., Marra, M.A., Miner, T.L., Minx, P., Mullikin, J.C., Plumb, R.W., Rogers, J., Schein, J.E., Sohrmann, M., Spieth, J., Stajich, J.E., Wei, C., Willey, D., Wilson, R.K., Durbin, R., Waterston, R.H., 2003. The genome sequence of Caenorhabditis briggsae: a platform for comparative genomics. PLoS biology 1, E45.

Stewart, A.D., Phillips, P.C., 2002. Selection and maintenance of androdioecy in Caenorhabditis elegans. Genetics 160, 975-982.

Strunker, T., Goodwin, N., Brenker, C., Kashikar, N.D., Weyand, I., Seifert, R., Kaupp, U.B., 2011. The CatSper channel mediates progesterone-induced Ca2+ influx in human sperm. Nature 471, 382-386.

Suarez, S.S., 2008. Control of hyperactivation in sperm. Human reproduction update 14, 647-657.

Sugimoto, Y., Hasumoto, K., Namba, T., Irie, A., Katsuyama, M., Negishi, M., Kakizuka, A., Narumiya, S., Ichikawa, A., 1994. Cloning and expression of a

cDNA for mouse prostaglandin F receptor. The Journal of biological chemistry 269, 1356-1360.

Sulston, J.E., Albertson, D.G., Thomson, J.N., 1980. The Caenorhabditis elegans male: postembryonic development of nongonadal structures. Developmental biology 78, 542-576.

Tholl, N., Naqvi, S., McLaughlin, E., Boyles, S., Bieber, A.L., Chandler, D.E., 2011. Swimming of Xenopus laevis sperm exhibits multiple gears and its duration is extended by egg jelly constituents. The Biological bulletin 220, 174-185.

Thomas, J.H., Kelley, J.L., Robertson, H.M., Ly, K., Swanson, W.J., 2005. Adaptive evolution in the SRZ chemoreceptor families of Caenorhabditis elegans and Caenorhabditis briggsae. Proceedings of the National Academy of Sciences of the United States of America 102, 4476-4481.

Tootle, T.L., Spradling, A.C., 2008. Drosophila Pxt: a cyclooxygenase-like facilitator of follicle maturation. Development 135, 839-847.

Troemel, E.R., Chou, J.H., Dwyer, N.D., Colbert, H.A., Bargmann, C.I., 1995. Divergent seven transmembrane receptors are candidate chemosensory receptors in C. elegans. Cell 83, 207-218.

Turner, R.M., 2006. Moving to the beat: a review of mammalian sperm motility regulation. Reprod Fertil Dev 18, 25-38.

Villanueva-Diaz, C., Vadillo-Ortega, F., Kably-Ambe, A., Diaz-Perez, M.A., Krivitzky, S.K., 1990. Evidence that human follicular fluid contains a chemoattractant for spermatozoa. Fertility and sterility 54, 1180-1182.

Vredenburg, V.T., Knapp, R.A., Tunstall, T.S., Briggs, C.J., 2010. Dynamics of an emerging disease drive large-scale amphibian population extinctions. Proceedings

of the National Academy of Sciences of the United States of America 107, 9689-9694.

Wake, D.B., Vredenburg, V.T., 2008. Colloquium paper: are we in the midst of the sixth mass extinction? A view from the world of amphibians. Proceedings of the National Academy of Sciences of the United States of America 105 Suppl 1, 11466-11473.

Wang, J., Silva, M., Haas, L.A., Morsci, N.S., Nguyen, K.C., Hall, D.H., Barr, M.M., 2014. C. elegans ciliated sensory neurons release extracellular vesicles that function in animal communication. Current biology : CB 24, 519-525.

Ward, G.E., Brokaw, C.J., Garbers, D.L., Vacquier, V.D., 1985. Chemotaxis of Arbacia punctulata spermatozoa to resact, a peptide from the egg jelly layer. The Journal of cell biology 101, 2324-2329.

Ward, S., 1973. Chemotaxis by the nematode Caenorhabditis elegans: identification of attractants and analysis of the response by use of mutants. Proceedings of the National Academy of Sciences of the United States of America 70, 817-821.

Ward, S., Carrel, J.S., 1979. Fertilization and sperm competition in the nematode Caenorhabditis elegans. Developmental biology 73, 304-321.

Ward, S., Thomson, N., White, J.G., Brenner, S., 1975. Electron microscopical reconstruction of the anterior sensory anatomy of the nematode Caenorhabditis elegans.?2UU. The Journal of comparative neurology 160, 313-337.

Ware, R.W., Clark, D., Crossland, K., Russell, R.L., 1975. The nerve ring of the nematode Caenorhabditis elegans: Sensory input and motor output. Journal of Comparative Neurology 162, 71-110.

White, J.G., Southgate, E., Thomson, J.N., Brenner, S., 1986. The structure of the nervous system of the nematode Caenorhabditis elegans. Philosophical transactions of the Royal Society of London. Series B, Biological sciences 314, 1-340.

White, J.Q., Jorgensen, E.M., 2012. Sensation in a single neuron pair represses male behavior in hermaphrodites. Neuron 75, 593-600.

White, J.Q., Nicholas, T.J., Gritton, J., Truong, L., Davidson, E.R., Jorgensen, E.M., 2007. The sensory circuitry for sexual attraction in C. elegans males. Current biology : CB 17, 1847-1857.

Whitten, S.J., Miller, M.A., 2007. The role of gap junctions in Caenorhabditis elegans oocyte maturation and fertilization. Developmental biology 301, 432-446.

Xiang, X., Burnett, L., Rawls, A., Bieber, A., Chandler, D., 2004. The sperm chemoattractant "allurin" is expressed and secreted from the Xenopus oviduct in a hormone-regulated manner. Developmental biology 275, 343-355.

Xiang, X., Kittelson, A., Olson, J., Bieber, A., Chandler, D., 2005. Allurin, a 21 kD sperm chemoattractant, is rapidly released from the outermost jelly layer of the Xenopus egg by diffusion and medium convection. Mol Reprod Dev 70, 344-360.

Xue, L., Salimi, M., Panse, I., Mjosberg, J.M., McKenzie, A.N., Spits, H., Klenerman, P., Ogg, G., 2014. Prostaglandin D2 activates group 2 innate lymphoid cells through chemoattractant receptor-homologous molecule expressed on TH2 cells. J Allergy Clin Immunol 133, 1184-1194.

Yoshida, M., Murata, M., Inaba, K., Morisawa, M., 2002. A chemoattractant for ascidian spermatozoa is a sulfated steroid. Proceedings of the National Academy of Sciences of the United States of America 99, 14831-14836.

Young, H.S., Dirzo, R., Helgen, K.M., McCauley, D.J., Billeter, S.A., Kosoy, M.Y., Osikowicz, L.M., Salkeld, D.J., Young, T.P., Dittmar, K., 2014. Declines in large wildlife increase landscape-level prevalence of rodent-borne disease in Africa. Proceedings of the National Academy of Sciences of the United States of America 111, 7036-7041.

Yu, K., Bayona, W., Kallen, C.B., Harding, H.P., Ravera, C.P., McMahon, G., Brown, M., Lazar, M.A., 1995. Differential activation of peroxisome proliferator-activated receptors by eicosanoids. J Biol Chem 270, 23975-23983.

Zamaria, N., 2004. Alteration of polyunsaturated fatty acid status and metabolism in health and disease. Reprod Nutr Dev 44, 273-282.

Zatylny, C., Marvin, L., Gagnon, J., Henry, J., 2002. Fertilization in Sepia officinalis: the first mollusk sperm-attracting peptide. Biochemical and biophysical research communications 296, 1186-1193.

Zenzes, M.T., Bielecki, R., Reed, T.E., 1999. Detection of benzo(a)pyrene diol epoxide-DNA adducts in sperm of men exposed to cigarette smoke. Fertility and sterility 72, 330-335.

Zhang, M., Feigenson, M., Sheu, T.J., Awad, H.A., Schwarz, E.M., Jonason, J.H., Loiselle, A.E., O'Keefe, R.J., 2015. Loss of the PGE2 receptor EP1 enhances bone acquisition, which protects against age and ovariectomy-induced impairments in bone strength. Bone 72, 92-100.